

Development of a cell flux model and its application to nitrogen fixers

by

Keisuke Inomura

B.S., Kyushu University (2009)

Submitted to the Department of Earth, Atmospheric, and Planetary Science

in partial fulfillment of the requirements for the degree of

Doctor of Philosophy

at the

MASSACHUSETTS INSTITUTE OF TECHNOLOGY

September 2016

© Massachusetts Institute of Technology 2016. All rights reserved.

Signature redacted

Author

Department of Earth, Atmospheric, and Planetary Sciences

June 24, 2016

Signature redacted

Certified by

.....

Michael J. Follows

Associate professor

Thesis Supervisor

Signature redacted

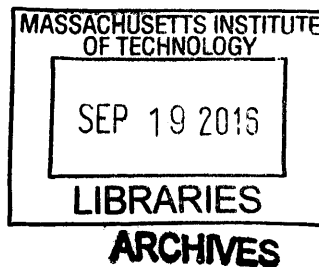
Accepted by

.....

Robert D. van der Hilst

Schlumberger Professor of Earth and Planetary Sciences

Head of Department



Development of a cell flux model and its application to nitrogen fixers

by

Keisuke Inomura

Submitted to the Department of Earth, Atmospheric, and Planetary Science

on June 24, 2016, in partial fulfillment of the

requirements for the degree of

Doctor of Philosophy

Abstract

Quantifying and modeling the macroscopic ecological and biogeochemical effects of cellular physiology and metabolism is a challenge: most quantitative “systems biology” models are focused at the metabolic and individual scale. In this study, we develop and apply a simplified metabolic model at the individual scale, which we call “the cell flux model”, in order to quantify costs and benefits of nitrogen fixers.

In Chapter 2, we develop the cell flux model for heterotrophic nitrogen fixers in order to examine and quantify the direct and indirect energy costs of nitrogen fixation. We have tested the model using data from *Azotobacter vinelandii* grown in continuous culture. The model indicates that the direct energy cost of nitrogen fixation is relatively small, whereas oxygen management to protect nitrogenase becomes dominant as the oxygen concentration increases.

In Chapter 3, we have adapted the cell flux model of *Azotobacter vinelandii* to consider the organisms’ response to the presence of ammonium in the environment. The model shows that even under high oxygen concentrations and with high ambient concentrations of fixed nitrogen, nitrogen fixation occurs if there is sufficient carbohydrate resource available to fully consume intracellular oxygen.

Most nitrogen fixers in the ocean are photoautotrophic. Thus, in Chapter 4, we extend the cell flux model to resolve phototrophy and use it to simulate and study light and nutrient co-limitation of *Synechococcus* spp. as observed in published continuous culture studies. In order to capture the observed variations in elemental composition with light and resource availability, we resolve the macromolecular composition of the cells. The highly simplified model is able to simulate key aspects of the laboratory cultures including explicit prediction of the average elemental composition and maximum growth rates under different environmental limitations.

In Chapter 5, we have applied the cell flux model to simulate laboratory studies, and interpreted the ecological costs for the photoautotrophic nitrogen fixer *Crocospaera watsonii*. Our model suggests that these organisms also utilize multiple oxygen protection strategies, including scavenging oxygen with excess respiration, changing their size, and using extracellular polymeric substances as a barrier to the invasion of oxygen into the cell.

Thesis Supervisor: Michael J. Follows

Title: Associate professor

Massachusetts Institute of Technology

Acknowledgments

The help of many people has contributed to this thesis, and I would like to acknowledge those who have influenced on this thesis. First and foremost, I would like to thank my advisor Michael Follows for his guidance, sharing his brilliant ideas, and knowledge. I also thank him for his continuously encouraging me in research and development of the cell flux model and beyond. I thank my thesis committee members Sallie Chisholm, Stephanie Dutkiewicz, and Mak Saito for their comments and suggestions on this thesis work. Specifically, I thank Sallie Chisholm for her pin-point suggestions on the models, and for encouraging me to study biological sciences, Stephanie Dutkiewicz for her ideas in ecological sciences and global ocean models of ecosystems, and Mak Saito for his ideas in biochemistry and nitrogen fixing organisms.

During the Ph.D. program, I have also spent time discussing the thesis related subjects and here I would like to acknowledge people I have frequently discussed science with. Each discussion has stimulated my scientific brain and quite often those people provided important tips for the thesis work. I thank Jason Bragg, co-author of Chapter 2, for his ideas from a biologist's view point through discussion. I am grateful to Hedy Kling for sharing the information about *Synechococcus* spp. I would like to express my gratitude to Joseph Vallino, since discussing with him has made me realize important things; we are expanding knowledge of the natural world, and there are multiple ways to interpret one phenomena. I would like to thank David Talmy for a series of discussion on microbiology and its modeling. Our discussion of previously developed cell-growth models have been helpful to understand what approach people made in the past. I would also like to thank Rogier Braakman for his help and discussion on metabolic pathways, and biochemistry in cells.

In addition, I would like to thank the people who spent time privately teaching me subjects related to the thesis work. First, I would like to thank Yuwei Gu for sharing deep knowledge in both organic and inorganic chemistry, and for answering all my detailed questions. Each interaction with him was fun and enlightening. I thank Tanja Bosak for her help and encouragement in studying microbiology. Also, I would like to show my appreciation to Mark Sullivan for sharing his ideas in what is happening in the cell from biochemical view point. Eric Stansifer spent a large amount of time sharing his refined programming skills with me, and I am grateful for all his help and ideas. I thank Martin Singh for his being my mentor giving me advice on every aspect of academic life, during the early years of the Ph.D. program. I am thankful to Teachers and TAs for teaching and clarifying my questions in all the classes I took. I would like to thank members of the Writing and Communication Center at MIT for their help in English writing throughout the Ph.D. program.

I also would like to show my appreciation to people who supported my academic life during the Ph.D. program from various directions. I thank the support staff at the Green Building at MIT who has been great help in various tasks, such as computer maintenance, moving offices, and educational and financial administration. Also, I also thank the staff at the MIT libraries for their help on finding resources and teaching me rules in citation. I thank all my current and previous officemates for their help in creating environments conducive to research and all the people in Mick Follows' group for stimulating discussion and useful feedback during group meeting and beyond. I would also like to thank yoga instructors at Body & Brain for helping me relax and refresh throughout the Ph.D. program. Many good ideas come to me during the yoga classes. I thank my family in Japan for all their support for my academic life.

Finally I thank support for this work from the Japan Student Service Organization and corresponding staff at Kyushu University. I am also grateful for support from the Gordon and

Betty Moore Foundation (GBMF#3778), the Simons Foundation (Simons Collaboration on Ocean Processes and Ecology, Award 329108, Follows).

Contents

Chapter 1 Introduction	10
1.1 The cell flux model as a studying tool for cell physiology and function	10
1.2 Nitrogen fixation in the context of climate.....	17
1.3 Nitrogen fixation in the context of ecosystems.....	17
1.4 What controls the rate of nitrogen fixation?	19
1.5 Oxygen management of nitrogen fixers	20
1.6 Thesis goals and outline.....	22
1.7 References.....	25
Chapter 2 A quantitative analysis of the direct and indirect costs of nitrogen fixation: a model based on <i>Azotobacter vinelandii</i>	30
2.1 Abstract.....	30
2.2 Introduction.....	31
2.3 Materials and Methods	35
2.4 Results and discussion.....	43
2.5 Broader Context	48
2.6 Conclusions.....	51
2.7 References.....	52
Supplementary Material	55
S2.1 Evaluation of yields.....	55
S2.2 Oxygen diffusion through alginate layer and cost of alginate production.....	60
S2.3 Other parameterizations	63
S2.4 Equations and reactions	64
S2.5 Nomenclature	68
S2.6 References.....	74
Chapter 3 On microbial nitrogen fixation in the presence of fixed nitrogen	76
3.1 Abstract.....	76

3.2 Introduction	77
3.3 Model description.....	81
3.4 Results and discussion	85
3.5 Implication for nitrogen fixation under various oxygen-and-ammonium-existing environments.....	99
3.6 Summary and conclusions	102
3.7 References.....	104
Supplementary Material	107
3.S1 Model details: carbohydrate limiting case	107
3.S2 Model details-ammonium limiting case	107
3.S3 Model details: nitrogen fixing case	108
3.S4 Determining which case to apply	110
3.S5 How to optimize f value.....	111
Chapter 4 A macromolecular model of phytoplankton growth under light and nutrient co-limitation	112
4.1 Abstract.....	112
4.2 Introduction.....	113
4.3 Methods	120
4.4 Results and discussions.....	138
4.5 Summary and conclusions	149
4.6 References.....	152
4.7 Supplementary material: model parameterization.....	157
4.8 References for Supplementary Material	167
Chapter 5 The cell flux model indicates multiple oxygen management strategies in <i>Crocospaera watsonii</i>	169
5.1 Abstract.....	169
5.2 Introduction.....	169
5.3 Methods: A metabolic model of <i>Crocospaera watsonii</i>	172
5.3.1 Model overview:.....	173

5.3.2 Parameterizations and Algorithms.....	179
5.4 Results and Discussion: Oxygen management strategies in <i>Crocospaera</i>	184
5.5 Implication of these oxygen management mechanisms to the ecosystem.....	194
5.6 Summary and conclusions	195
5.7 References.....	195
Supplementary Material	199
5.S1 Computation of carbon, nitrogen, and oxygen metabolism.....	199
5.S2 Computation of iron metabolism.....	205
5.S3 Parameterization.....	209
5.S4 Nomenclature	213
5.S5 References.....	218
Chapter 6 Summary and future directions	220
6.1 Chapter Summary.....	221
6.2 Future directions.....	224
6.3 References.....	232

Chapter 1

Introduction

We have developed a macromolecular model of microbial cells (the “cell flux model”) in order to study and connect cellular physiology and ecosystems. In this thesis, we have applied the model to nitrogen fixers (diazotrophs) to examine the costs and benefits of nitrogen fixation and their ecological implications. In this chapter, we first motivate the model development, and then briefly review nitrogen fixation related topics. Then we consider nitrogen fixation in the context of climate and ecosystems and narrow down to discuss the physiology of nitrogen fixers, more specifically, their oxygen management strategies. At the end of this chapter, we provide goals and outline of the thesis.

1.1 The cell flux model as a studying tool for cell physiology and function

Cell biologists study how cells function. Biochemists study chemical processes in biological system. Geneticists study genes. Molecular biologists study molecules in biology. These disciplines complement each other and have achieved great progress for understanding what is happening in the cells. Deeper understanding of the cell leads to developing effective drugs, effective production of agricultural products, and many other contributions in human society.

Currently, in biology text books (e.g. Neidhard *et al.*, 1990; Madigan *et al.*, 2000; Kim and Gadd, 2008; Berg *et al.*, 2010; Lodish *et al.*, 2012) there are schematic depictions of the cell organelles, chemical processes, biomass synthesis, DNA reproductions, cell divisions, etc. However, we rarely encounter model diagrams with numbers. How much of each process is happening? For example, in our daily lives, we eat a variety of foods. They are broadly

categorized as proteins, carbohydrates, fat, and vitamins. Biochemistry has answered what they can potentially become after they are absorbed into cells. However, the quantity of the each fate has yet to become clear or well represented. For example, we still have questions about how much of fat eaten really becomes fat? Does it mostly become body fat or is most of the fat actually used for energy production or does it become a part of other macromolecules, such as carbohydrate, proteins, or even DNA?

Similar issues hold true in microbiology. A wide range of genes, proteins, lipids, carbohydrates, and organelles, have been studied and the understanding of how they function and where in the cells they exist has been increasing significantly especially since the 20th century. However, we still have limited quantitative understanding of the rates of each process, and the fate of acquired nutrients become what, in a given physical and chemical environment. One of the reasons for this limited quantitative understanding is the limited development of the computational models of the whole cell system. To understand biology as a system, recently, computational approaches have been developed and created a new discipline, Systems Biology, the study of biological systems by systematic perturbation (Ideker, *et al.*, 2001). However, this approach is mainly used for understanding detailed functions or metabolic pathways (Kitano, 2002), and faces a challenge in scaling up to the whole cell metabolism in a simple manner. One Systems Biology approach towards expressing the whole cell metabolism is Flux Balance Analysis (FBA) (Kauffman *et al.*, 2003; Palsson, 2005; Schuster and Fell, 2007; Orth *et al.*, 2010). FBA resolves a whole cell metabolic flux network, with a large number of reactions, and obtain a single solution based on the optimization of an objective functions (Kauffman *et al.*, 2003; Orth *et al.*, 2010). In many cases, the single solution is obtained based on maximizing biomass production (e.g. Lee *et al.*, 2007; Orth *et al.*, 2010). However, the assumption that

organisms work to this end does not always apply (Schuster, *et al.*, 2008). Another challenge is that FBA does not calculate concentration of each molecule since fluxes are solved based on the steady state and the concentrations of metabolites or enzymes are not resolved. Also, since the model resolves a large number of reactions, FBA often fails to provide bird's-eye view of the cell functions, thus intuitive quantitative understanding of the metabolic fluxes may not be obtained easily. How could we obtain such simple and intuitive quantitative view of the cell and concentration of each molecule?

We can obtain a hint from earth science. In earth science, the idealized, at the same time, very intuitive quantitative understanding of ocean basin, atmospheric layers, etc. can often be obtained through the box model. Figure 1.1 shows one example from Vaughan and Lenton (2012). While the model is highly idealized, it provides an intuitive view of the carbon cycles on the earth, not only representing the fluxes, but also it computes the magnitude of each carbon pool. In appropriate circumstances, such models can be parameterized sufficiently well to accurately represent sensitivities and observed trends (Figure 1.2). They are then used to predict future temperature and atmospheric CO₂ concentrations under different scenarios (Figure 1.3).

In this thesis, we take the philosophy of this idealized, box-model approach to modeling the simplified metabolism of a microbial cell. For example, we model the fate of nutrient through different chemical reactions in the cell. We use multiple boxes to represent cytoplasm, extracellular environments, and chemical pools, such as the inorganic nutrients and organic components (Figure 1.4). Each box is connected with other boxes or boundaries with fluxes (Figure 1.4). The fluxes are parameterized according to known processes where possible.

Similar modeling approaches have been taken in the past (e.g. Geider *et al.*, 1996, 1997, 1998; Flynn *et al.*, 2001, Pahlow and Oschlies, 2009); see Chapter 4 for more details. However,

those models tend to resolve the cellular quotas of each element instead of resolving the quotas of the macro-molecules. Here, we hypothesize that key differences between various functional types of microorganisms can be more faithfully and dynamically captured by a model which accounts for key macromolecular pools, simple metabolic fluxes, uptake of nutrient, cell sizes, and internal biochemical balances.

With the model we develop in this thesis, we will provide the intuitive pictures of metabolic fluxes and the relative sizes of each pool. The model can be used for interpolating the available experimental data, predicting unknown parameters, and simulating the growth of the cells in the laboratory and the ecosystems. In this thesis, we name the model “the cell flux model”, and apply the model to study nitrogen fixation and nitrogen fixing organisms.

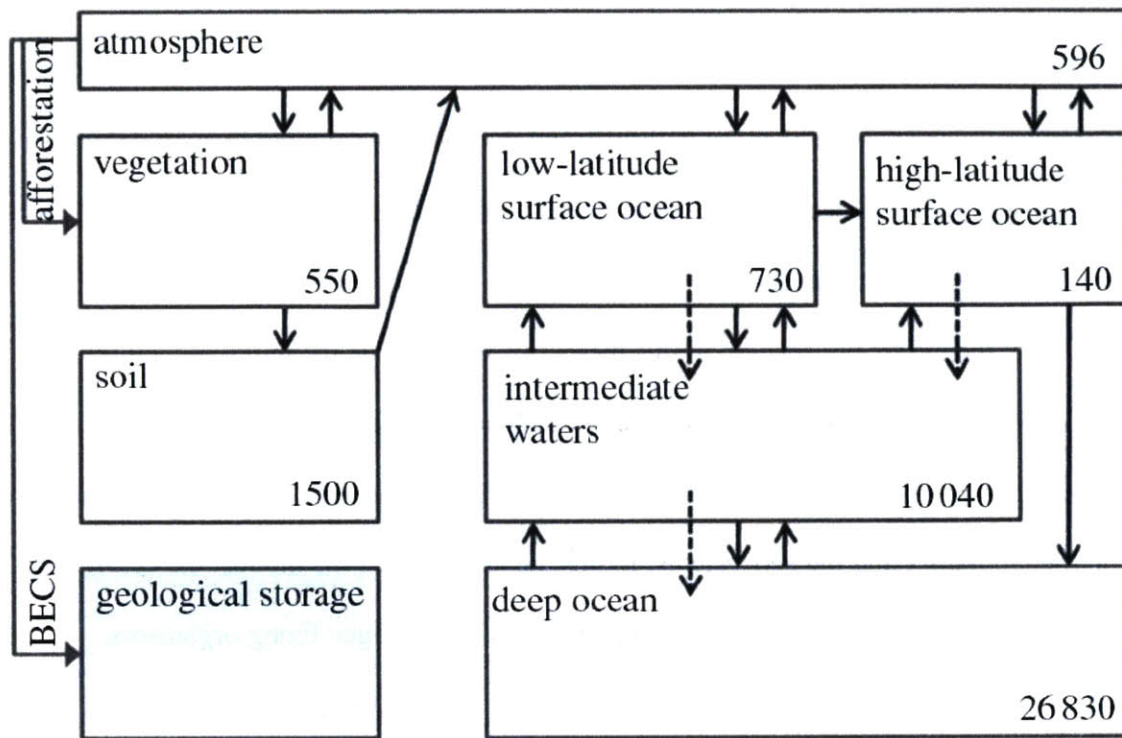


Figure 1.1 Example of a box model from Vaughan and Lenton (2012). In this example, pre-industrial steady state global carbon cycle is computed. Each box shows major carbon inventories in the earth system with concentration in numbers. Arrows represent carbon fluxes. For the ocean boxes, solid arrows are carbon fluxes due to water flows, and dashed arrows are carbon fluxes due to sinking particles. The figure is from Vaughan and Lenton (2012) with permission.

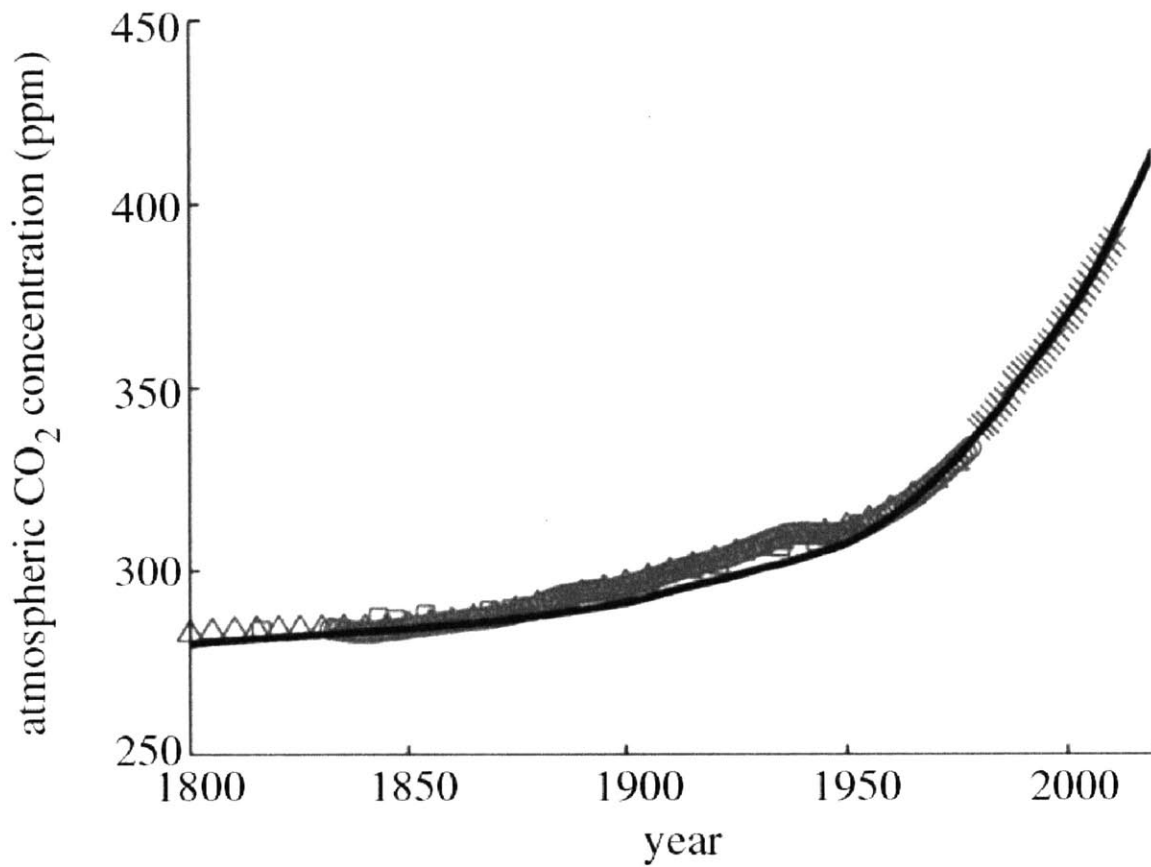


Figure 1.2 Model output of atmospheric CO₂ (black) compared to values obtained from ice core data and direct atmospheric measurements (gray). The model is calibrated to represent the ice core data and direct measurements. The figure is from Vaughan and Lenton (2012) with permission.

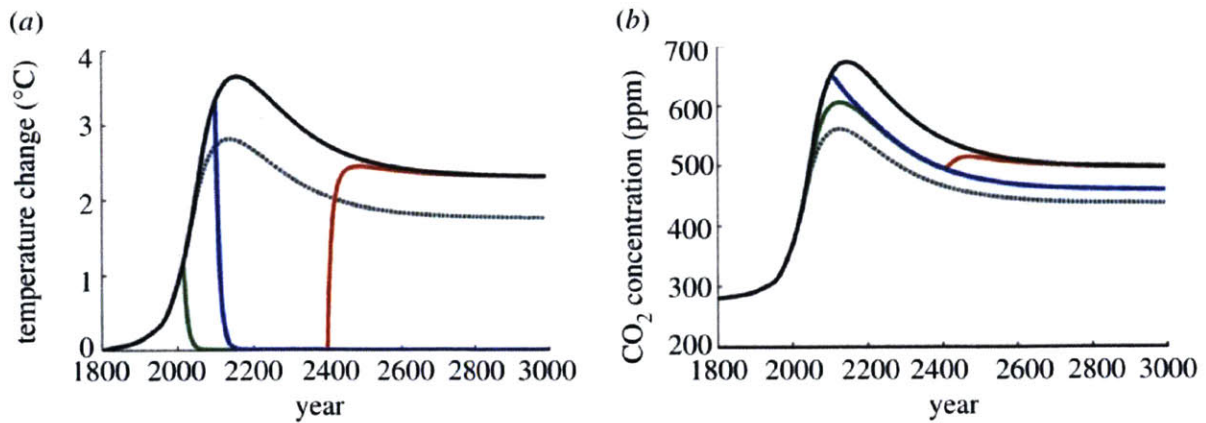


Figure 1.3 Prediction of temperature change and atmospheric CO₂ concentrations for various scenarios with the box model. The figure is from Vaughan and Lenton (2012) with permission.

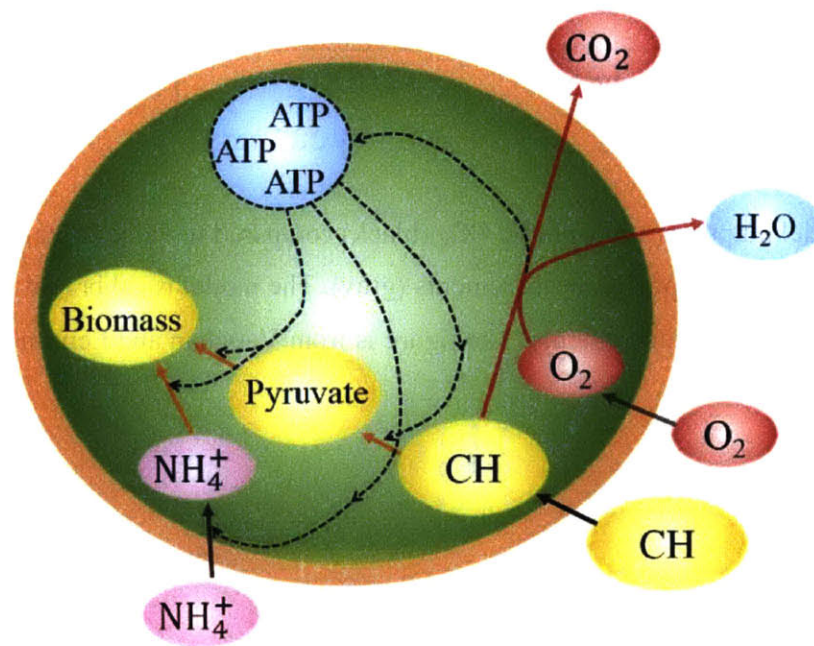


Figure 1.4 Schematic depiction of the cell flux model. Green part represent cytoplasm, and the outer orange layer is cell membrane layers. Black solid arrows represent nutrient uptake, orange arrows represent biosynthesis, red arrows show respiration, and black dashed arrows are energy flow. CH represents carbohydrate.

1.2 Nitrogen fixation in the context of climate

Nitrogen fixation has an indirect but significant impact on climate, since nitrogen fixation is a major source of bio-available nitrogen, and nitrogen and carbon cycles (including CO₂, the major greenhouse gas) are tightly coupled (Gruber and Galloway, 2008). There are two types of nitrogen fixation: anthropogenic and natural. Both types of nitrogen fixation have a similar order of magnitude (Gruber and Galloway, 2008), thus, equally important for the ecosystem.

Anthropogenic nitrogen fixation has the largest contribution to the terrestrial ecosystems where synthesized fertilizer is used. However, it has a certain impact in the ocean since 10~30% of nitrogen is discharged into the ocean (Galloway *et al.*, 1995). Natural nitrogen fixation has a large impact on both in the terrestrial and oceanic ecosystems. The nitrogen and carbon cycles are closely coupled as they are tied together in the formation and destruction of living biomass (Gruber and Galloway, 2008). Nitrogen is often the growth limiting factor in the ocean (e.g. Moore *et al.*, 2013), and provides bioavailable nitrogen for cellular carbon fixation. Carbon fixation in turn impacts the abundance of atmospheric CO₂, a major greenhouse gas which influences climate. Falkowski (1997) argues that a slight change in nitrogen fixation to denitrification ratio can alter atmospheric CO₂ concentrations significantly in the timescale of glacial-to-interglacial periods. Thus, in order to predict climate change, it is important to predict the rate of nitrogen fixation accurately, which has been challenging.

1.3 Nitrogen fixation in the context of ecosystems

Nitrogen fixation has important implications for ecosystem functions since all organisms need nitrogen for key macromolecules, such as proteins and nucleic acids. Nitrogen fixation also supplies “new nitrogen” to the system which is passed to other organisms through excretion,

grazing, sharing and symbiosis. In the terrestrial systems, fixed nitrogen is used by plants influencing the plant growth. In the ocean, nitrogen fixation mainly impacts the microbial ecology since oceans are much more dominated by micro-organisms than plants (Pomeroy, *et al.*, 2007).

Depending on the ecosystem, the dominant nitrogen fixers are different. In terrestrial ecosystems, the dominant type is heterotrophic bacteria (e.g. Cleveland *et al.*, 1999) while in the ocean, photoautotrophic bacteria (cyanobacteria) are more significant (e.g. Sohm *et al.*, 2011). The major difference is that heterotrophic bacteria have to obtain organic carbon from external sources, while cyanobacteria can synthesize organic carbon from inorganic carbon through photosynthesis. Most of the chapters of this thesis are focused on models of nitrogen fixers, using laboratory data to inform and constrain simulations, and the models to interpret the data. Chapter 2, and 3 focus on a heterotrophic nitrogen fixer and Chapter 5 on a photoautotrophic nitrogen fixer. In order to achieve the latter, we needed to develop a suitable model of photoautotrophy, so Chapter 4 is focused exclusively on modeling a non-nitrogen fixing phytoplankton.

In the ocean, nitrogen fixation is predicted in regions (Moore *et al.*, 2004; Monteiro *et al.*, 2010, 2011; Ward *et al.*, 2013; Stukel *et al.*, 2014; Dutkiewicz *et al.*, 2014), where Fe/N and P/N resource supply ratios are high, based on the assumption that nitrogen fixers have low maximum growth rates. While this simple assumption leads to a general picture of biogeography of nitrogen fixers, physiological controls on them have yet to become well constrained. In the next section, we will elaborate on the controls on nitrogen fixation.

1.4 What controls the rate of nitrogen fixation?

The viability and rate of nitrogen fixation is controlled by many factors which can be categorized on five scales: molecular controls, physiological controls, ecological controls, ecosystem level constraints, and regional/global level constraints (Vitousek, *et al.*, 2002). Molecular controls include genetic control, enzyme synthesis, and other detailed cellular mechanisms (Vitousek, *et al.*, 2002). Physiological controls include whole cell level controls, such as the impact of intracellular concentration of oxygen or the cellular level of molybdenum on nitrogen fixation (Vitousek, *et al.*, 2002). Next are the ecological controls, such as colonization, competition, predation and nutrient availability (Vitousek, *et al.*, 2002). Ecosystem level constraints include the nutrient inputs to and outputs from the system. Finally, regional/global level constraints include patterns of land cover, biome distribution, climate, and nitrogen deposition (Vitousek *et al.*, 2002).

These controls are highly interactive, influencing each other. For example, increasing cellular oxygen concentration leads to inactivation of nitrogen fixing enzyme, nitrogenase (Gallon, 1981; Wang *et al.*, 1985; Poole and Hill, 1997). Also, expressions of different respiratory enzymes influence the cellular oxygen concentration (Poole and Hill, 1997; Oelze 2000). A high concentration of heterotrophic organisms might lead to depletion of oxygen in the environment, promoting nitrogen fixation (e.g. Steunou *et al.*, 2008). In addition, nitrogen fixation contributes the fixed nitrogen input to the ecosystem (e.g. Peoples *et al.*, 1995), which in turn influences CO₂ fixation. Nitrogen fixation, which occurs at the molecular level, may influence climate on long time scales (e.g. Falkowski, 1997; Broecker and Henderson, 1998).

In a global scale ecosystem models, large scale constraints are relatively well resolved. For example, models consider global-scale dust deposition, ocean circulation, regional light

intensities, and temperatures (e.g. Monteiro *et al.*, 2010, 2011; Ward *et al.*, 2013; Stukel *et al.*, 2014; Dutkiewicz *et al.*, 2014). Also, they resolve key ecological controls, such as predation and nutrient competition. However, the bottom-level controls such as physiology and molecular level controls have yet to be well constrained and are not represented. For example, growth of the microorganisms are often expressed as Monod kinetics (Monod, 1949), which connects environmental nutrient concentration to the growth rate, bypassing the physiology and molecular scale phenomena (Follows and Dutkiewicz 2011). In order to predict the rate of nitrogen fixation as a function of any particular environment, it is necessary to incorporate quantitative descriptions of the physiology and molecular scale controls into the large-scale ecosystem models.

Among all the physiological and molecular scale controls, in this study, we will particularly address oxygen management of nitrogen fixers since oxygen directly influences the nitrogen fixation rate (e.g. Wang *et al.*, 1985) and the cost for oxygen management in terms of growth efficiency (addressed in Chapter 2 and 3). Despite the importance of oxygen management, ecosystem models have not yet resolved the underlying mechanisms. In the following section, we will briefly discuss different oxygen management mechanisms employed by nitrogen fixers.

1.5 Oxygen management of nitrogen fixers

There are multiple ways to keep the intracellular oxygen concentration low enough for nitrogen fixation. We explain the oxygen management in detail in Chapter 2, 3 and 5, but here we provide a brief overview. The simplest form of oxygen management can be represented by the following equation:

$$[O_2]_C = [O_2] - \frac{r^2 R_C}{3D_{O_2}}. \quad (1.1)$$

where intracellular oxygen concentration $[O_2]_C$ (mol m^{-3}) is influenced by, $[O_2]$ (mol m^{-3}), the environmental oxygen concentration, r (m), the cell radius, R_C ($\text{mol s}^{-1} \text{m}^{-3}$), the cellular net oxygen consumption rate (oxygen consumption rate minus oxygen production rate) per volume ($\text{mol s}^{-1} \text{m}^{-3}$), and D_{O_2} ($\text{m}^2 \text{s}^{-1}$), the effective diffusion coefficient for oxygen. Based on the four parameters on the right hand side of the equation, there are four potential oxygen management strategies; (i) living in low oxygen environment; decreasing $[O_2]$, (ii) increasing cell size; increasing r , (iii) increasing respiration/other oxygen consumption; increasing R_C , (iv) decreasing the diffusivity of oxygen; decreasing D_{O_2} .

Strategy (i) is employed by multiple types of nitrogen fixers. For example, rhizobium lives in the root of plants where oxygen concentration is limited (e.g. Tjepkema and Yocum, 1974; Tjepkema 1983). Also, in marine sediments, benthic nitrogen fixers can take advantage of the low oxygen environment (e.g. Revsbech *et al.*, 1980; Herbert, 1999). Strategy (ii) can be seen in multiple types of nitrogen fixers as well. For example, *Azotobacter vinelandii*, soil dwelling heterotrophic bacteria, increase in size under a high oxygen environment (Post *et al.*, 1982). Heterocystous cyanobacteria have specialized cells for nitrogen fixation, and have a larger cells than other non-nitrogen fixers (e.g. Liu and Golden, 2002; Khudyakov and Golden, 2004). Strategy (iii) is well studied in *Azotobacter vinelandii*. Since they have significantly higher respiration rates than other heterotrophic bacteria, and respiration rate increases with oxygen concentration, it is hypothesized that they increase respiration in order to scavenge oxygen (Dalton and Postgate, 1969; Poole and Hill, 1997). In addition, it is hypothesized that *Trichodesmium*, a filamentous cyanobacterium, use the Mehler reaction for scavenging oxygen (Kana, 1992, 1993; Berman-Frank *et al.*, 2001). Finally, strategy (iv) is most clear in

heterocystous cyanobacteria; the heterocysts are specialized nitrogen fixing cells in a colony, which have an envelope of multiple layers of thick cell wall, regulating passive uptake of oxygen (e.g. Fay, 1992; Walsby 2007; Nicolaisen *et al.*, 2009). This strategy is also hypothesized in *Azotobacter*, which produces extra polymeric substrate, whose composition varies with oxygen concentration, possibly preventing oxygen diffusion (Sabra *et al.*, 2000). In this study, we will address strategy (ii)~(iv) since those strategies have been described at the physiological and cellular scale.

1.6 Thesis goals and outline

The goal of the thesis is to develop the cell flux model, and to investigate the physiological and cellular controls of nitrogen fixation, and its costs and benefits using the model. In Chapter 2 and 3, we develop the cell flux model for heterotrophic nitrogen fixers. While Chapter 2 addresses the nitrogen fixers under conditions with no sources of fixed nitrogen, Chapter 3 explores the nitrogen fixation rates and growth of nitrogen fixers with the presence of ammonium. In Chapter 4, we have developed the cell flux model for phytoplankton and studied light-nutrient co-limitation of phytoplankton growth. Finally, in Chapter 5, we develop the cell flux model for photoautotrophic nitrogen fixers and examine their oxygen management. We present the outline of each chapter as follows.

Chapter 2: A quantitative analysis of the direct and indirect costs of nitrogen fixation

Both heterotrophic and photoautotrophic nitrogen fixers grow more slowly and less efficiently than non-nitrogen fixers of the same types. What makes the growth of nitrogen fixers inefficient? In order to answer this question, we developed the cell flux model for heterotrophic nitrogen

fixers, and analyzed direct and indirect costs of nitrogen fixation. We have chosen chemostat culture data of *Azotobacter vinelandii* (Kuhla and Oelze, 1988) on which to base and calibrate the model, but its implications applies to other nitrogen fixers: both heterotrophic and autotrophic.

Chapter 3: Maximizing population provides mechanistic explanation of the physiology of nitrogen fixing microbes growing in ammonium present environment

Ammonium and other forms of fixed nitrogen are known to inhibit nitrogen fixation. However, the magnitude of inhibition varies depending on the level of oxygen and availability of carbohydrate sources. How do ammonium, oxygen and carbohydrate co-limit the rate of nitrogen fixation and population of nitrogen fixers? To address this question, we have adapted the cell flux model developed in Chapter 2 into ammonium existing environment, in particular chemostat culture of *Azotobacter vinelandii* with ammonium input into the culture (Buhler *et al.*, 1987a, 1987b). With the model, we made a simple assumption that the metabolism of the cell is constrained to maximize biomass concentration. With this assumption, we have predicted nitrogen fixation rate, population and other physiological rates, for various ammonium, oxygen and carbohydrate environments.

Chapter 4: Macromolecular model for studying light-nutrient co-limitation of phytoplankton growth

The majority of nitrogen fixers in the ocean are phytoplankton. Not only do they contribute to global photosynthesis, they account for a large fraction nitrogen fixation in the world.

Phytoplankton are often co-limited by the availability of light and nutrients. However, most

ocean ecosystem models use highly idealized methods to predict growth rate without sufficiently considering the physiology and molecular scale constraints which control this co-limitation. Resolving such detailed scale in the model is necessary to predict the growth of phytoplankton, which in turn influence the ecosystem and biogeochemistry in global scale. In this chapter, we develop a macromolecular scale phytoplankton model “the cell flux model for phytoplankton” to study light-nutrient co-limitation of phytoplankton. In this model we have considered various macromolecules which vary differently with light-nutrient availability and growth of phytoplankton. For the model calibration, we have used the data of *Synechococcus* sp. Although this chapter exclusively addresses non-nitrogen fixers, it provides basis for modeling photoautotrophic nitrogen fixers.

*Chapter 5: The cell flux model indicates multiple oxygen management strategies by *Crocospaera watsonii**

Nitrogen fixers in the ocean account for about a half of fixed nitrogen input into the ocean (Gruber and Galloway, 2008), influencing the nitrogen cycle and coupled carbon cycle. A considerable fraction of nitrogen fixation in the ocean may be done by unicellular nitrogen fixers (e.g. Zehr *et al.*, 2001; Montoya *et al.*, 2004; Moisander *et al.*, 2010). Thus, understanding the physiological control of nitrogen fixation by unicellular organisms may contribute to the prediction of the elemental cycles in the ocean. One of the major unicellular nitrogen fixers is *Crocospaera watsonii*, which fixes nitrogen during the night time in order to avoid photosynthetically produced oxygen (e.g. Mohr *et al.*, 2010; Saito, *et al.*, 2011; Großkopf and LaRoche, 2012). However, even during the night time, the oxygen concentration in the ocean is nearly saturated (ex. Robertson *et al.*, 1993; Fransson *et al.*, 2004; de Boyer Montégut, *et al.*,

2004; Yates *et al.*, 2007). Under such high oxygen concentration, how do *Crocospaera* manage to fix nitrogen? In order to address this question, we have developed the cell flux model for photoautotrophic unicellular nitrogen fixers. The model resolves diurnal cycles of metabolisms and iron movement within the cell (Saito *et al.*, 2011). We hypothesize that *Crocospaera* adopt similar oxygen management strategies to that of *Azotobacter*, and examine each strategy with the model. Our simulations suggest that *Crocospaera* does indeed employ analogous strategies.

1.7 References

- Berg JM, Tymoczko JL, Stryer L. (2010). Biochemistry, 7th edition. W. H. Freeman and Company: New York.
- Berman-Frank I, Lundgren P, Chen Y-B, Küpper H, Kolber Z, Bergman B, *et al.* (2001). Segregation of nitrogen fixation and oxygenic photosynthesis in the marine cyanobacterium *Trichodesmium*. *Science* **294**: 1534–1537.
- de Boyer Montégut C, Madec G, Fischer AS, Lazar A, Iudicone D. (2004). Mixed layer depth over the global ocean: An examination of profile data and a profile-based climatology. *J Geophys Res* **109**: C12003, doi:10.1029/2004JC002378.
- Broecker WS, Henderson GM. (1998). The sequence of events surrounding termination II and their implications for the cause of glacial interglacial CO₂ changes. *Paleoceanography* **13**: 352–364.
- Cleveland CC, Townsend AR, Schimel DS, Fisher H, Howarth RW, Hedin LO, *et al.* (1999). Global patterns of terrestrial biological nitrogen (N₂) fixation in natural ecosystems. *Global Biogeochem Cycles* **13**: 623–646.
- Dalton H, Postgate JR. (1969). Effect of oxygen on growth of *Azotobacter chroococcum* in batch and continuous cultures. *J Gen Microbiol* **54**: 463–473.
- Dutkiewicz S, Ward BA, Scott JR, Follows MJ. (2014). Understanding predicted shifts in diazotroph biogeography using resource competition theory. *Biogeosciences Discuss* **11**: 7113–7149.
- Falkowski PG. (1997). Evolution of the nitrogen cycle and its influence on the biological sequestration of CO₂ in the ocean. *Nature* **387**: 272–275.
- Fay P. (1992). Oxygen relations of nitrogen fixation in cyanobacteria. *Microbiol Rev* **56**: 340–373.
- Flynn KJ. (2001). A mechanistic model for describing dynamic multi-nutrient, light, temperature interactions in phytoplankton. *J Plankton Res* **23**: 977–997.

- Follows MJ, Dutkiewicz S. (2011). Modeling diverse communities of marine microbes. *Ann Rev Mar Sci* **3**: 427–451.
- Fransson A, Chierici M, Anderson LG. (2004). Diurnal variability in the oceanic carbon dioxide system and oxygen in the Southern Ocean surface water. *Deep Res Part II Top Stud Oceanogr* **51**: 2827–2839.
- Gallon JR. (1981). The oxygen sensitivity of nitrogenase: a problem for biochemists and microorganisms. *Trends Biochem Sci* **6**: 19–23.
- Galloway JN, Schlesinger WH, Levy H, Michaels A, Schnoor JL. (1995). Nitrogen fixation: Anthropogenic enhancement-environmental response. *Global Biogeochem Cycles* **9**: 235–252.
- Geider RJ, Macintyre HL, Kana TM. (1996). A dynamic model of photoadaptation in phytoplankton. *Limnol Oceanogr* **41**: 1–15.
- Geider RJ, Macintyre HL, Kana TM. (1998). A dynamic regulatory model of phytoplanktonic acclimation to light, nutrients, and temperature. *Limnol Oceanogr* **43**: 679–694.
- Geider RJ, Macintyre HL, Kana TM. (1997). Dynamic model of phytoplankton growth and acclimation: responses of the balanced growth rate and the chlorophyll a: carbon ratio to light, nutrient-limitation and temperature. *Mar Ecol Prog Ser* **148**: 187–200.
- Großkopf T, LaRoche J. (2012). Direct and indirect costs of dinitrogen fixation in *Crocospaera watsonii* WH8501 and possible implications for the nitrogen cycle. *Front Microbiol* **3**: doi: 10.3389/fmicb.2012.00236.
- Gruber N, Galloway JN. (2008). An Earth-system perspective of the global nitrogen cycle. *Nature* **451**: 293–296.
- Herbert RA. (1999). Nitrogen cycling in coastal marine ecosystems. *FEMS Microbiol Rev* **23**: 563–590.
- Ideker T, Galitski T, Hood L. (2001). A new approach to decoding life: Systems biology. *Annu Rev Genomics Hum Genet* **2**: 343–372.
- Kana TM. (1992). Oxygen cycling in cyanobacteria with specific reference to oxygen protection in *Trichodesmium* spp. In: E. J. Carpenter et al. (eds.). *Marine Pelagic Cyanobacteria: Trichodesmium and other diazotrophs*. Kluwer Academic publishers. *Mar Pelagic Cyanobacteria Trichodesmium other Diazotrophs* 29–41.
- Kana TM. (1993). Rapid oxygen cycling in *Trichodesmium thiebautii*. *Limnol Oceanogr* **38**: 18–24.
- Kauffman KJ, Prakash P, Edwards JS. (2003). Advances in flux balance analysis. *Curr Opin Biotechnol* **14**: 491–496.
- Khudyakov IY, Golden JW. (2004). Different functions of HetR, a master regulator of heterocyst differentiation in *Anabaena* sp. PCC 7120, can be separated by mutation. *Proc Natl Acad Sci USA* **101**: 16040–16045.
- Kim GH, Gadd GM. (2008). *Bacterial physiology and metabolism*. Cambridge University Press: Cambridge.

- Kitano H. (2002). Computational systems biology. *Nature* **420**: 206–210.
- Kuhla J, Oelze J. (1988). Dependency of growth yield, maintenance and K_s -values on the dissolved oxygen concentration in continuous cultures of *Azotobacter vinelandii*. *Arch Microbiol* **149**: 509–514.
- Lee TJ, Tu D, Tan CM, You L. (2006). Modeling cellular networks. Bioinformatics: An Engineering Case-Based Approach. G. Alterovitz and M. F. Ramoni, editors. Artech House: Boston. *Constr Anal Kenetic Model* 151–178.
- Liu D, Golden JW. (2002). *hetL* overexpression stimulates heterocyst formation in *Anabaena* sp. Starin PCC 7120. *J Bacteriol* **184**: 6873–6881.
- Lodish H, Berk A, Kaiser CA, Krieger M, Scott MP, Bretscher A, et al. (2012). Molecular Cell Biology. 7th edition. W. H. Freeman: New York.
- Madigan MT, Martinko JM, Parker J. (2000). Brock Biology of Microorganisms. 9th edition. Prentice-Hall, inc.: Upper Saddle River, New jersey.
- Mohr W, Intermaggio MP, LaRoche J. (2010). Diel rhythm of nitrogen and carbon metabolism in the unicellular, diazotrophic cyanobacterium *Crocospaera watsonii* WH8501. *Environ Microbiol* **12**: 412–421.
- Moisander PH, Beinart RA, Hewson I, White AE, Johnson KS, Carlson CA, et al. (2010). Unicellular cyanobacterial distributions broaden the oceanic N_2 fixation domain. *Science* **327**: 1512–1514.
- Monod J. (1949). The growth of bacterial cultures. *Ann Rev Mar Sci* **3**: 371–394.
- Monteiro FM, Dutkiewicz S, Follows MJ. (2011). Biogeographical controls on the marine nitrogen fixers. *Global Biogeochem Cycles* **25**: GB2003, doi:10.1029/2010GB003902.
- Monteiro FM, Follows MJ, Dutkiewicz S. (2010). Distribution of diverse nitrogen fixers in the global ocean. *Global Biogeochem Cycles* **24**: GB3017, doi:10.1029/2009GB003731.
- Montoya JP, Holl CM, Zehr JP, Hansen A, Villareal TA, Capone DG. (2004). High rates of N_2 fixation by unicellular diazotrophs in the oligotrophic Pacific Ocean. *Nature* **430**: 1027–1031.
- Moore CM, Mills MM, Arrigo KR, Berman-Frank I, Bopp L, Boyd PW, et al. (2013). Processes and patterns of oceanic nutrient limitation. *Nat Geosci* **6**: 701–710.
- Moore JK, Doney SC, Lindsay K. (2004). Upper ocean ecosystem dynamics and iron cycling in a global three-dimensional model. *Global Biogeochem Cycles* **18**: 1–21.
- Neidhards FC, Ingraham JL, Schaechter M. (1990). Physiology of the Bacterial Cell: a Molecular Approach. Sinauer Associate, Inc.: Sunderland, Massachusetts.
- Nicolaisen K, Hahn A, Schleiff E. (2009). The cell wall in heterocyst formation by *Anabaena* sp. PCC 7120. *J Basic Microbiol* **49**: 5–24.
- Oelze J. (2000). Respiratory protection of nitrogenase in *Azotobacter* species: is a widely held hypothesis unequivocally supported by experimental evidence? *FEMS Microbiol Rev* **24**: 321–333.
- Orth JD, Thiele I, Palsson BØ. (2010). What is flux balance analysis? *Nat Biotechnol* **28**: 245–

248.

- Pahlow M, Oschlies A. (2009). Chain model of phytoplankton P, N and light colimitation. *Mar Ecol Prog Ser* **376**: 69–83.
- Palsson BØ. (2006). *Systems Biology: Properties of Reconstructed Networks*. Cambridge University Press, New York.
- Peoples MB, Herridge DF, Ladha JK. (1995). Biological nitrogenfixation: An efficient source of nitrogen for sustainable agricultural production. *Plant Soil* **174**: 3–28.
- Pomeroy LP, Williams PL, Azam WF, Hobbie JE. (2007). The microbial loop. *Oceanography* **20**: 28–33.
- Poole RK, Hill S. (1997). Respiratory protection of nitrogenase activity in *Azotobacter vinelandii*: Roles of the terminal oxidases. *Biosci Rep* **17**: 303–317.
- Post E, Golecki JR, Oelze J. (1982). Morphological and ultrastructural variations in *Azotobacter vinelandii* growing in oxygen-controlled continuous culture. *Arch Microbiol* **133**: 75–82.
- Revsbech NP, Srensen J, Blackburn TH, Lomholt JP. (1980). Distribution of oxygen in marine sediments measured with microelectrodes. *Limnol Oceanogr* **25**: 403–411.
- Robertson JE, Watson AJ, Langdon C, Ling RD, Wood JW. (1993). Diurnal variation in surface pCO₂ and O₂ at 60°N, 20°W in the North Atlantic. *Deep Res Part II* **40**: 409–422.
- Sabra W, Zeng AP, Lünsdorf H, Deckwer WD. (2000). Effect of oxygen on formation and structure of *Azotobacter vinelandii* alginate and its role in protecting nitrogenase. *Appl Environ Microbiol* **66**: 4037–4044.
- Saito MA, Bertrand EM, Dutkiewicz S, Bulygin VV, Moran DM, Monteiro FM, *et al.* (2011). Iron conservation by reduction of metalloenzyme inventories in the marine diazotroph *Crocospaera watsonii*. *Proc Natl Acad Sci USA* **108**: 2184–2189.
- Schuster S, Fell D. (2007). Modeling and simulating metabolic networks. In: Lengauer, T. (Ed.), *Bioinformatics: From Genomes to Therapies*. Wiley-VCH: Weinheim. **2**: 755–805.
- Schuster S, Fell DA, Pfeiffer T. (2008). Is maximization of molar yield in metabolic networks favoured by evolution? *J Theor Biol* **252**: 497–504.
- Sohm JA, Webb EA, Capone DG. (2011). Emerging patterns of marine nitrogen fixation. *Nat Rev Microbiol* **9**: 499–508.
- Steunou A-S, Jensen SI, Brecht E, Becraft ED, Bateson MM, Kilian O, *et al.* (2008). Regulation of nif gene expression and the energetics of N₂ fixation over the diel cycle in a hot spring microbial mat. *ISME J* **2**: 364–378.
- Stukel MR, Coles VJ, Brooks MT, Hood RR. (2014). Top-down, bottom-up and physical controls on diatom-diazotroph assemblage growth in the Amazon River plume. *Biogeosciences* **11**: 3259–3278.
- Tjepkema J. (1983). Oxygen concentration within the nitrogen-fixing root nodules of *Myrica gale* L. *Am J Bot* **70**: 59–63.
- Tjepkema JD, Yocum CS. (1974). Measurement of oxygen partial pressure within soybean

nodules by oxygen microelectrodes. *Planta (Berl.)* **119**: 351–360.

Vaughan NE, Lenton TM. (2012). Interactions between reducing CO₂ emissions, CO₂ removal and solar radiation management. *Philos Trans R Soc A Math Phys Eng Sci* **370**: 4343–4364.

Vitousek PM, Cassman K, Cleveland C. (2002). Towards an ecological understanding of biological nitrogen fixation. *Biogeochemistry* **57/58**: 1–45.

Walsby AE. (2007). Cyanobacterial heterocysts: terminal pores proposed as sites of gas exchange. *Trends Microbiol* **15**: 340–349.

Walsby AE. (1985). The permeability of heterocysts to the gases nitrogen and oxygen. *Proc R Soc B Biol Sci* **226**: 345–366.

Wang ZC, Burns A, Watt GD. (1985). Complex formation and O₂ sensitivity of *Azotobacter vinelandii* nitrogenase and its component proteins. *Biochemistry* **24**: 214–221.

Ward BA, Dutkiewicz S, Moore CM, Follows MJ. (2013). Iron, phosphorus, and nitrogen supply ratios define the biogeography of nitrogen fixation. *Limnol Oceanogr* **58**: 2059–2075.

Yates KK, Dufore C, Smiley N, Jackson C, Halley RB. (2007). Diurnal variation of oxygen and carbonate system parameters in Tampa Bay and Florida Bay. *Mar Chem* **104**: 110–124.

Zehr JP, Waterbury JB, Turner PJ, Montoya JP, Omoregie E, Steward GF, *et al.* (2001). Unicellular cyanobacteria fix N₂ in the subtropical North Pacific Ocean. *Nature* **412**: 635–638.

Chapter 2

A quantitative analysis of the direct and indirect costs of nitrogen fixation: a model based on *Azotobacter vinelandii*

The chapter is reproduced from the article “A quantitative analysis of the direct and indirect costs of nitrogen fixation: a model based on *Azotobacter vinelandii*” by Inomura K, Bragg J, Follows MJ, recently accepted to The ISME Journal.

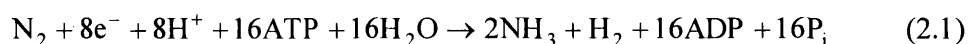
2.1 Abstract

Nitrogen fixation is advantageous in microbial competition when bioavailable nitrogen is scarce, but has substantial costs for growth rate and growth efficiency. To quantify these costs, we have developed a model of a nitrogen-fixing bacterium that constrains mass, electron and energy flow at the scale of the individual. When tested and calibrated with laboratory data for the soil bacterium *Azotobacter vinelandii*, the model reveals that the direct energetic cost of nitrogen fixation is small relative to the cost of managing intra-cellular oxygen. It quantifies the costs and benefits of several potential oxygen protection mechanisms present in nature including enhanced respiration (respiratory protection) as well as the production of extra-cellular polymers as a barrier to O₂ diffusion, and increasing cell size. The latter mechanisms lead to higher growth efficiencies relative to respiratory protection alone. This simple, yet mechanistic framework provides a quantitative model of nitrogen fixation which can be applied in ecological simulations.

2.2 Introduction

All organisms need nitrogen for the synthesis of important molecules including nucleic acids and proteins. Nitrogen pervades the environment in the form of N₂ gas, yet it is often a limiting resource on land and in aquatic environments. Nitrogen fixation provides some marine and terrestrial prokaryotes with an ecological advantage but is typically associated with low growth efficiencies and rates (Kuhla and Oelze, 1988a, 1988b; LaRoche and Breitbarth, 2005; Berman-Frank *et al.*, 2007; Goebel *et al.*, 2007) placing significant constraints on the relative fitness of nitrogen fixers and their biogeography. Here we address the question of what underpins the low growth efficiency of nitrogen fixers and develop a quantitative analysis which forms the basis for trait-based ecological and biogeochemical models.

One contribution to the low growth rate/efficiency of nitrogen fixers is the direct cost of reducing dinitrogen. Nitrogen fixation is catalyzed by the nitrogenase enzyme, and uses 8 electrons and at least 16 molecules of ATP to reduce each N₂ molecule to two molecules of NH₃ (Sohm *et al.*, 2011).



Although the energetic expense of breaking the dinitrogen triple bond is high this direct cost may not necessarily be the greatest challenge faced by nitrogen fixing cells. Nitrogenase consists of an Fe-protein and a Mo-Fe-protein and other metal co-factors whose activity is decreased upon exposure to oxygen (Gallon, 1981). Thus aerobic nitrogen fixers have developed numerous strategies to protect nitrogenase from oxygen, particularly in oxygenic phototrophs. For example, in *Anabaena* and *Nostoc* the nitrogen fixing cells also become heterocysts, losing the ability to fix carbon and building a thick cell coating which is less permeable to oxygen (Neilson *et al.*, 1971; Wolk, 1996; Golden and Yoon, 2003) demanding an exchange of

metabolites between cells, as do nitrogen fixers in symbiotic relationships with other species. Free living, unicellular aerobic nitrogen fixers use other strategies, including the separation of oxygenic photosynthesis and nitrogen fixation between day and night (e.g. Colón-López *et al.*, 1997; Misra, 1999; Tucker *et al.*, 2001; Berman-Frank *et al.*, 2003; Saito *et al.*, 2011; Großkopf and Laroche, 2012b). Heterotrophic, soil dwelling nitrogen-fixers, such as *Azotobacter vinlandii*, use elevated rates of respiration to deplete intra-cellular oxygen (Poole and Hill, 1997). They also produce an extra-cellular polymeric substance that impedes oxygen invasion (Sabra *et al.*, 2000), and maintain larger cell sizes (Post *et al.*, 1982), which likely also reduces the specific oxygen invasion rate.

Each of these strategies demands that the organism invest resources in nitrogen fixation that could otherwise be used for other activities, such as carbon fixation or biosynthesis, offsetting the ecological advantage of nitrogen fixation. The resulting reduction in growth rate and/or efficiency is key to understanding the biogeography of nitrogen fixation in the environment (e.g. Staal *et al.*, 2003; Monteiro *et al.*, 2010; Dutkiewicz *et al.*, 2012). In current ecological and biogeochemical simulations, this cost is typically empirically imposed (e.g. Krishnamurthy *et al.*, 2007; Dutkiewicz *et al.*, 2012; Stukel *et al.*, 2013). Here we present a mechanistic and quantitative approach to modeling the cost of nitrogen fixation and its associated oxygen management. Though the model represents a generalized approach, we focus on the heterotrophic, nitrogen-fixing soil bacterium, *Azotobacter vinelandii*, for which extensive, quantitative laboratory characterizations have been published (e.g. Post *et al.*, 1982, 1983a, 1983b; Kuhla and Oelze, 1988a, 1988b; Allman *et al.*, 1990; Poole and Hill, 1997; Oelze, 2000; Dixon and Kahn, 2004).

Laboratory cultures of *Azotobacter* (e.g. Kuhla and Oelze, 1988a, 1988b) have demonstrated a decrease in growth efficiency at all growth rates as the ambient concentration of oxygen in the medium was increased. This was manifested as an increased carbohydrate cost, which has been interpreted as enhanced energetically uncoupled respiration (exceeding the level required for biosynthesis) (Nagai and Aiba, 1972; Kuhla and Oelze, 1988b) to manage intracellular oxygen concentration and maintain functional nitrogenase; hereafter termed ‘respiratory protection’ (Dalton and Postgate, 1969; Poole and Hill, 1997). This is illustrated in Figure 2.1A (data in circles; lines represent a model discussed later), in which the specific sucrose consumption rate increased with oxygen concentration. The sensitivity to oxygen manifests largely as a “maintenance” effect, increasing overall carbohydrate consumption (Figure 2.1A) because the cell must be equally clear of oxygen even at very low growth and nitrogen fixation rates. *Azotobacter* encodes and expresses cytochrome bd, which has high oxygen consumption relative to ATP production (Poole and Hill, 1997). The reduction of growth efficiency with increasing oxygen concentration was also reflected in a lower standing stock of protein (Kuhl and Oelze, 1988b) in Figure 2.1B. At the lowest oxygen concentration (12 μM) there was a sharp change in the slope at a dilution rate of about 0.1 day^{-1} .

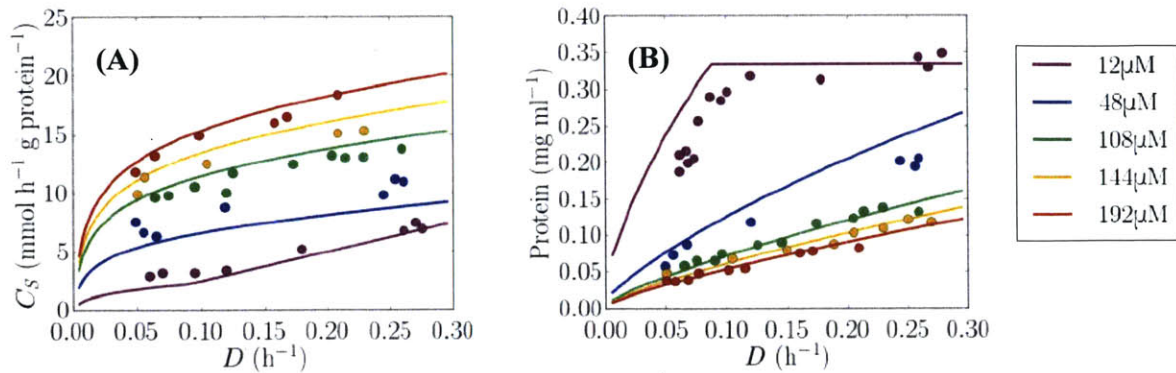


Figure 2.1 Continuous cultures of *Azotobacter vinelandii* with observed data (circles) redrawn from Kuhla and Oelze (1988b). Solid lines are the corresponding simulations from this work. (A) Protein specific sucrose consumption rate, (B) standing stock of protein, all with respect to dilution (and growth) rate, D (x-axis) and oxygen concentration (colored points/lines). The legend indicates oxygen concentration.

However, it was noted that the increase in maintenance carbohydrate consumption and respiration are not linear with oxygen concentration, increasing less rapidly at concentrations above 70 μM (Oelze, 2000) (Figure 2.1A and 2.1B respectively), suggesting other protection mechanisms must also be at play. *Azotobacter vinelandii* is also observed to increase in cell size in more oxygenated cultures (Post *et al.*, 1982) and to form an external alginate capsule as a barrier to oxygen diffusion, which increases in molecular weight and glucuronic acid content with higher oxygen conditions (Sabra *et al.*, 2000).

The thorough characterization of the energetics of *Azotobacter vinelandii* in the laboratory (e.g. Post *et al.*, 1982; Bühler, *et al.*, 1987a, 1987b; Kuhla and Oelze, 1988a, 1988b, Oelze 2000) provides an excellent opportunity to develop a quantitative, mechanistic model of nitrogen fixer physiology which we can employ both as a diagnostic tool and in dynamic ecological simulations. Shortly, we will present such a model, but first we consider the general principle which underpins it.

2.3 Materials and Methods

Intra-cellular oxygen balance

Oxygen management is a key cost for nitrogen fixers that we seek to quantitatively model. First consider the rate of change of the intra-cellular oxygen, Q_{O_2} (mol O₂ cell⁻¹), in a spherical microbe:

$$\frac{dQ_{O_2}}{dt} = P_{O_2} + 4\pi r \kappa_{O_2} ([O_2] - [O_2]_C) - (R_S + R_m + R_p) \quad (2.2)$$

Here, $[O_2]$ and $[O_2]_C$ are the environmental and intra-cellular oxygen concentrations respectively (mol O₂ m⁻³). The first term on the right, P_{O_2} (mol O₂ cell⁻¹ s⁻¹) represents a source from oxygenic photosynthesis. The second term is a source due to transfer across the membrane of cell with the cytoplasmic radius r (m cell⁻¹), governed by the oxygen gradient and the effective diffusivity across the membrane and external molecular boundary layer, κ_{O_2} (m² s⁻¹). The third term, in parentheses, represents consumption of intra-cellular oxygen by respiration associated with synthesis (R_S) including the direct cost of nitrogen fixation, maintenance (R_m) and respiratory protection (R_p) (mol O₂ cell⁻¹ s⁻¹). R_S is related to the growth rate of the population, μ (s⁻¹) by

$$R_S = \mu Q_C Y_S^{O_2: BIO} \quad (2.3)$$

where Q_C is the carbon quota (mol C cell⁻¹) of the species in question and $Y_S^{O_2: BIO}$ is the growth yield with respect to oxygen (mol O₂ consumed per mol C biomass synthesized) which can be evaluated from the overall stoichiometry of the reactions (Heijnen and Roels, 1981; Rittmann and McCarty, 2001; see Supplementary Material 2.S1).

Since reducing intra-cellular oxygen concentration is critical for nitrogen fixers, consider the solution for the intra-cellular oxygen concentration $[O_2]_C$ at steady state ($dQ_{O_2}/dt \approx 0$):

$$[O_2]_C = [O_2] + \frac{P_{O_2} - (\mu Q_C Y_S^{O_2: BIO} + R_m + R_P)}{4\pi r \kappa_{O_2}} \quad (2.4)$$

Oxygenic photosynthesis, P_{O_2} , always acts to increase intra-cellular oxygen concentration along with invasion from the environment, if the external concentration is higher. In contrast there are numerous strategies to reduce intra-cellular oxygen levels and protect nitrogenase, as mentioned in the introduction: living in a low oxygen environment, reducing $[O_2]$; increasing the efficiency of respiratory oxygen consumption, $Y_S^{O_2: BIO}$; creating thick membranes or mucus layers to reduce the effective diffusivity of oxygen, κ_{O_2} into the cell. Since carbon quota, Q_C , increases with cell volume (r^3), increasing cell radius will increase R_S and reduce $[O_2]_C$, as increasing growth rate μ also increases the respiratory oxygen demand. A high maintenance respiration or deliberate respiratory protection, R_P , consumes oxygen. The investment in respiratory protection to reduce the intra-cellular oxygen concentration to very low levels can be estimated by setting $[O_2]_C = 0$ in (2.4) and re-arranging:

$$R_P = 4\pi r \kappa_{O_2} [O_2] + P_{O_2} - (\mu Q_C Y_S^{O_2: BIO} + R_m) \quad (2.5)$$

The required R_P is the difference between sources due to oxygenesis and diffusive invasion, and the demand from growth and maintenance.

A model of Azotobacter vinelandii

Azotobacter vinelandii employs several of the strategies encapsulated in (2.4): It employs respiratory protection (see Figure 2.1). Its radius increases with the environmental oxygen concentration (Post *et al.*, 1982, 1983b; Poole and Hill, 1997). If respiration rate is proportional to the cell volume, i.e. the rate is influenced by r^3 (which is approximately the case for

prokaryotes; Glazier, 2009), then the cell radius impacts intra-cellular oxygen concentration in a quadratic manner according to equation (2.4). Thus, the influence of the cell radius on oxygen management can be significant. *Azotobacter* also creates an alginate barrier, as the environmental oxygen concentration increases, and the amount of intracytoplasmic membrane increased with environmental oxygen concentration (Post *et al.*, 1982).

Here we extend the simple model of the previous section to develop a more complete representation of a heterotrophic nitrogen fixer (the cell flux model) that we interface with published data on *Azotobacter vinelandii* cultures. This constrains key parameters and the model, in turn, provides a quantitative interpretation of the cultures. Extending the simple model of (2.3), we consider carbon nitrogen, electron and energy flow in a simplified cell. We combine an idealized biochemical model (Rittmann and McCarty, 2001) which guides the evaluation of growth efficiencies such as $Y_S^{O_2: BIO}$, with a diffusive representation of the transport of oxygen and other substrates through the cell membrane and surrounding molecular boundary layer (Staal *et al.*, 2003).

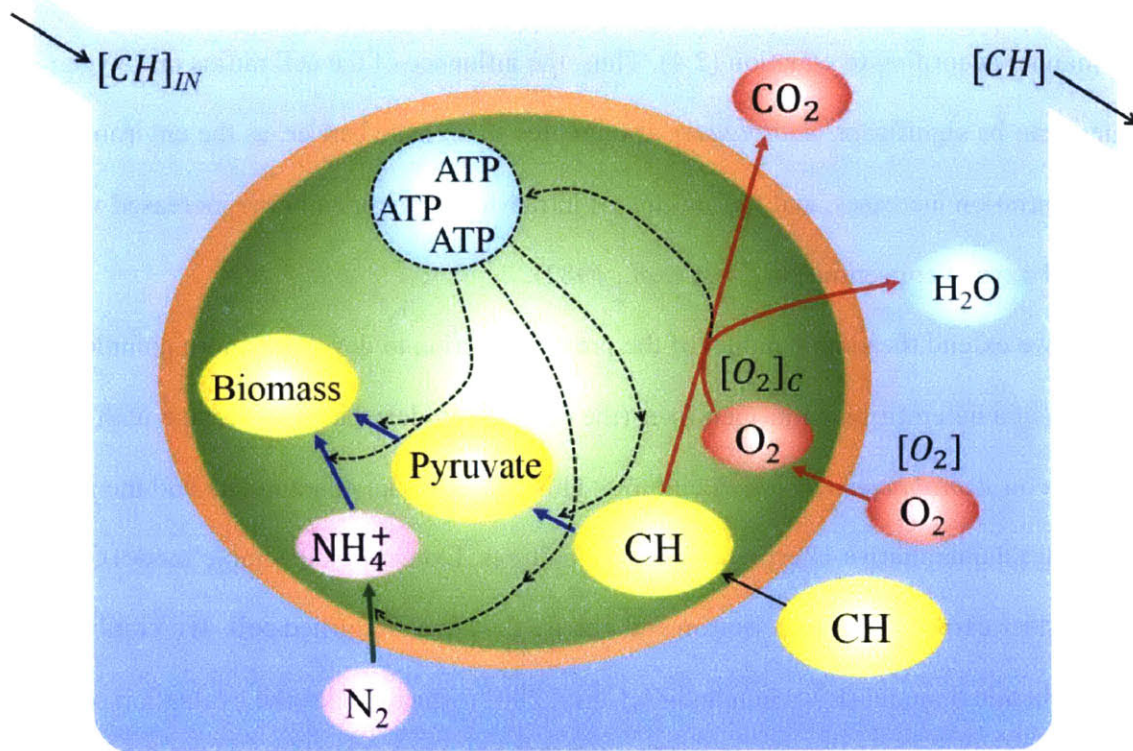


Figure 2.2 Schematic depiction of the cell flux model in continuous culture. $[CH]_{IN}$ is the incoming carbohydrate concentration. $[CH]$ and $[O_2]$ are the concentrations of carbohydrate and oxygen in the medium. $[O_2]_c$ represents the intra-cellular oxygen concentration. Red arrows represent the energy production pathways and blue arrows represent the biomass synthesis pathways. The green arrow represents nitrogen fixation. The black dashed lines represent energy flow. Orange shading indicates the cell membrane layers. See main text for details.

Ultimately the model has two free parameters: ϵ , the energetic efficiency of cellular metabolism, and ϵ_m , the efficiency of diffusion of oxygen through the cell membrane. We constrain these parameters using the laboratory data for *Azotobacter* illustrated in Figure 2.1, and use the model to infer the cost of nitrogen fixation and the relative effect of different protection mechanisms. Though we focus on *Azotobacter*, for which systematic data is available, the model is potentially applicable to a broad range of nitrogen-fixing microbes, and we discuss the broader implications in later sections.

Table 2.1 Fundamental relationships of the cell flux model. Supplementary Material 2.S5 provides the definition of each parameter.

Cellular conservation of carbon (mol C cell ⁻¹ s ⁻¹)	$\frac{dQ_{CH}}{dt} = V_{CH} - \frac{DQ_C Y_S^{CH: BIO}}{P_V} - mQ_C - \frac{R_P}{Y_{N-S}^{O_2: CH}} \quad (2.6)$
Cellular conservation of oxygen (mol O ₂ cell ⁻¹ s ⁻¹)	$\frac{dQ_{O_2}}{dt} = V_{O_2} - \frac{DQ_C Y_S^{O_2: BIO}}{P_V} - mQ_C Y_{N-S}^{O_2: CH} - R_P \quad (2.7)$
Cellular oxygen uptake (mol O ₂ cell ⁻¹ s ⁻¹)	$V_{O_2} = 4\pi r \kappa_{O_2} ([O_2] - [O_2]_C) \quad (2.8)$
Effective diffusivity of oxygen (m ² s ⁻¹)	$\kappa_{O_2} = \kappa_{O_2}^0 \frac{L_g + r}{L_s/\epsilon_m + r} \quad (2.9)$
Conservation of carbon in the reactor (mol C m ⁻³ s ⁻¹)	$\frac{d[CH]}{dt} = D([CH]_{IN} - [CH]) - V_{CH} X P_V \quad (2.10)$

The model, depicted schematically in Figure 2.2, conserves mass, energy (when $R_P=0$) and electron flow at the individual scale and in the simulated reactor vessel and assumes that cultures are in steady state. Key rate equations (2.6), (2.7) and (2.10) (Table 2.1) describe the cellular-scale conservation of carbohydrate and oxygen, as well as conservation of carbohydrate in the reactor vessel.

For a steady state, conservation of carbohydrate at the cellular scale, equation (2.6), balances uptake of the carbohydrate (CH) substrate, V_{CH} , against synthesis into “biomass” at dilution rate D (s⁻¹), respiration to support that synthesis (included in the second term),

maintenance respiration mQ_C , and additional respiration associated with respiratory protection $R_P / Y_{N-S}^{O_2:CH}$ (all mol C cell⁻¹ s⁻¹).

An expression for the specific carbohydrate uptake rate, C_S (mol C in carbohydrate s⁻¹ / mol C in biomass) = V_{CH}/Q_C , can be found by rearrangement of (2.6):

$$C_S = \frac{Y_S^{CH: BIO} D}{P_V} + m + \frac{R_P}{Q_C Y_{N-S}^{O_2:CH}} \quad (2.11)$$

Here $Y_S^{CH: BIO}$ is the cellular rate of CH consumption required to supply the balanced electron, carbon and energy for biomass synthesis including nitrogen fixation. Q_C is the cellular quota of carbon (mol C cell⁻¹) which is determined as a function of cell volume V (Bratbak *et al.*, 1984).

$Y_{N-S}^{O_2:CH}$ is the ratio in which oxygen is consumed relative to carbohydrate for non-synthesis related respiration (i.e. maintenance and respiratory protection). We evaluate $Y_S^{CH: BIO}$ and $Y_{N-S}^{O_2:CH}$ using the method described by Rittmann and McCarty (2001), balancing mass, electron and energy flow at the individual scale (outlined in Supplementary Material 2.S1). The simple model for C_S in equation (2.11) suggests a linear relationship with dilution rate (average growth rate), D , and additional costs due to minimal maintenance and respiratory protection. If the latter is neglected ($R_P=0$) then equation (2.11) represents the classical Pirt model (Pirt, 1982), where $Y_S^{CH: BIO}$ is constrained by exact energy balance. In this study, however, we assume the maintenance rate m is negligible, since it is typically small relative to respiratory protection in most instances explored here. We note that $Y_S^{CH: BIO}$ is a function of the energy transfer efficiency, ϵ , which characterizes unresolved details of metabolic adaptations (see Results and Discussion, and Supplementary Material 2.S1) and, as such, is a tunable parameter of this model.

The vitality ratio, P_V represents the fraction of active cells in the culture. Under unfavorable conditions, such as nutrient depletion, cells can survive in dormancy with low metabolic rate (Lennon and Jones, 2011). In continuous culture, there are also dormant or non-vital cells (Postgate, 1973), possibly due to nutrient limitation, and the division rate reflects the average from growing and non-growing cells. The vitality ratio has a significant impact on the growth efficiency since the respiration rate of the non-vital cells is observed to be low (Postgate, 1973). Here we parameterize the fraction of non-vital cells as a function of growth rate based on empirical data of Postgate (1973) for cultures of *Klebsiella aerogenes*:

$$P_V = 0.18547 \ln(D) + 2.75176 . \quad (2.12)$$

At present there is no explicit data on the viability rate of *Azotobacter* but incorporating this effect as calibrated for *Klebsiella* significantly improves the simulation. Specifically, this mechanism reduces the effective yield of the simulation with dilution rate (i.e. increases the slopes of the C_S vs D curves).

Respiratory protection appears as an additional “maintenance” term in equation (2.11), consistent with observed as oxygen stress increases in *Azotobacter vinelandii* (increasing the total carbohydrate consumption and respiration rates with oxygen in data on Figure 2.1A and 2.1B). Higher environmental oxygen concentrations increase the invasion rate, requiring more vigorous respiratory protection and reducing the overall growth efficiency. In order to fix nitrogen, the cell must keep the intra-cellular oxygen concentration very low (i.e. $[O_2]_C \approx 0$) at all rates of growth (dilution). Thus, we can constrain R_P by estimating the rate of oxygen invasion into the cell using equation (2.13), derived from (2.7) and (2.8) from Table 1 under the steady state assumption.

$$\frac{R_P}{Q_C} = \frac{4\pi r \kappa_{O_2} [O_2]}{Q_C} - \frac{D Y_S^{O_2: BIO}}{P_V} - m Y_{N-S}^{O_2: CH} \quad (2.13)$$

Here $Y_S^{O_2: BIO}$ represents moles of oxygen gas consumed per mole of carbon biomass production for synthesis. Though energy balance can provide some constraint, the realized efficiency of energy transfer depends upon unresolved details of the specific metabolic pathways utilized by the organism and is encapsulated by the energy efficiency parameter, ε (see Supplementary Material 2.S1).

The diffusive transfer of oxygen from the ambient environment into the cell is described by equation (2.8) and (2.9), following Staal *et al.* (2003), where the effective diffusivity, κ_{O_2} , depends on the diffusivity in water, the cytoplasmic radius, r , and the thickness and relative diffusivity of the cell membrane layers (L_g and ε_m). We impose a positive correlation between the cell radius of *Azotobacter* and the ambient oxygen concentration as well as a fixed ratio between cell membrane thickness and radius, based on the empirical data of Post *et al.* (1982). Since the diffusivity of oxygen in water is well known, we are left with a second control parameter, ε_m . When the invasion of oxygen exceeds the minimum energy demand, the model invokes respiratory protection sufficient to consume all the excess oxygen flux.

Substituting for R_P in (2.11) with (2.13) provides a quantitative, mechanistic model for the growth efficiency of nitrogen fixing *Azotobacter* that incorporates both direct and indirect costs. Using conservation of carbohydrate in the reactor vessel, equation (2.10) in Table 2.1, and assuming that at steady state the carbohydrate is drawn down to a low, subsistence concentration (i.e. $[CH] \ll [CH]_{IN}$), we find an expression for the standing concentration of protein in the reactor:

$$[PR] = \frac{D[CH]_{IN}}{C_S P_V} Y^{PRBIO} \quad (2.14)$$

where Y^{PRBIO} is the ratio of carbon in protein to carbon in total biomass. We have used 1/1.32 for this ratio based on the laboratory study of Bühler, *et al.* (1987a).

Considerations of mass, electron and energy balance at the individual and reactor scales, along with an estimate of the rate of invasion of oxygen through the cell wall, allowed us to fully describe the system and predict the specific carbohydrate consumption rate, C_S and concentration of protein in the reactor, $[PR]$.

2.4 Results and discussion

Direct and indirect costs of nitrogen fixation

The model described above was brought into consistency with the data of Kuhla and Oelze (1988b) (data points in Figure 2.1) by tuning the two control parameters (i.e. $\epsilon_m = 7.9 \times 10^{-4}$ and $\epsilon = 0.22$) and approximating the energetics of one sucrose molecule as that of two glucose molecules. The simulations qualitatively and quantitatively capture the key features of the laboratory cultures. It identifies the transition between energy limited and oxygen controlled regimes in the experiment, confirms that *Azotobacter* is using several strategies to manage oxygen, quantifies their relative contributions, and quantifies the allocation of carbon resources, showing that indirect cost of oxygen management far exceeds the direct cost of nitrogen fixation.

i. Transition between energy limitation and oxygen management regimes

The solid curves in Figure 2.1 depict the optimized model solutions for carbohydrate consumption rate and protein concentration against dilution rate for different oxygen

concentration along with laboratory data in (Kuhla and Oelze, 1988b). In most cases, the diffusive oxygen supply exceeds the demand for synthesis and respiratory protection is present, increasing specific sucrose consumption at all dilution rates. However, at higher dilution rates and low ambient oxygen concentrations ($[O_2]=12 \mu\text{M}$) respiratory protection is no longer necessary. There, growth is oxygen limited (see equation (2.3)), and the minimum respiration limit is appropriate. This leads to a sharp transition in the appropriate curves on Figure 2.1 particularly so for the protein standing stock (Figure 2.1B); it represents the transition between energy limited and oxygen management regimes. The model captures and explains this transition.

ii. Multiple oxygen protection strategies

The simulations capture the trend of increasing carbohydrate consumption rate both with dilution rate and oxygen concentration (Figure 2.1A, solid lines). When oxygen management is not a major control, for example the minimum respiration case at $[O_2] = 12 \mu\text{M}$, the increase of carbohydrate consumption rate with dilution rate is caused by increasing biomass production, nitrogen fixation and balanced respiration. At higher oxygen concentrations, there is an overall increase in carbohydrate consumption due to respiratory protection (i.e. appears as a “maintenance” effect). High dilution rates also increase carbohydrate consumption due to the increased proportion of viable cells, which need respiratory protection for fixing nitrogen while non-viable cells do not.

Figure 2.3 shows data and model solutions for C_S as a function of oxygen concentration at a fixed dilution rate. The dotted black line indicates the required specific sucrose consumption rate if the cells respond only by respiratory protection to increasing ambient oxygen

concentrations. As Oelze (2000) pointed out, this linear response is inconsistent with the data (Figure 2.3, circles) and demands additional mechanisms. This non-linearity is captured by the model if the specific invasion rate of oxygen is reduced by an increase in cell radius ($r+L_g$) or a reduction in the effective diffusivity of oxygen invasion (κ_{O_2}) under higher oxygen concentrations, either by thickening the cell membrane or developing an alginate capsule at higher oxygen concentrations (as observed by Post *et al.*, 1982; Sabra *et al.*, 2000). A relatively minor change in effective cell diameter is sufficient. In the solid grey line of Figure 2.3 an increase in cell diameter of a factor of 1.4 (1.76 μm to 2.41 μm) as oxygen concentration increased from 12 μM to 192 μM , brought the model into consistency with the observed data. This is consistent with the increase in size by a factor of 1.6 observed by Post *et al.* (1982) over a similar range of oxygen concentration in the lab.

Azotobacter can also produce an alginate capsule, which decreases the diffusivity on the cell boundary layer (Sabra *et al.*, 2000), though this phenomenon is not always reported in the laboratory studies. We represent the development of an alginate capsule by altering the effective diffusivity and thickness of alginate capsule, and imposing a carbohydrate cost for alginate production (dashed black line in Figure 2.3; for details see Supplementary Material 2.S2). Though sucrose expenditure is increased in order to achieve larger cell radius or alginate layer, the model clearly shows these strategies to significantly improve growth efficiency at higher oxygen concentrations, relative to pure respiratory protection (i.e. the solid grey and dashed black are significantly lower than the dotted black line in Figure 2.3).

The model confirms that multiple oxygen protection strategies must be at play in *Azotobacter vinelandii*. At higher oxygen concentrations, changes in cell volume and/or alginate

production supplement respiratory protection and significantly increase growth efficiency, while at lower concentrations, respiratory protection alone is as effective.

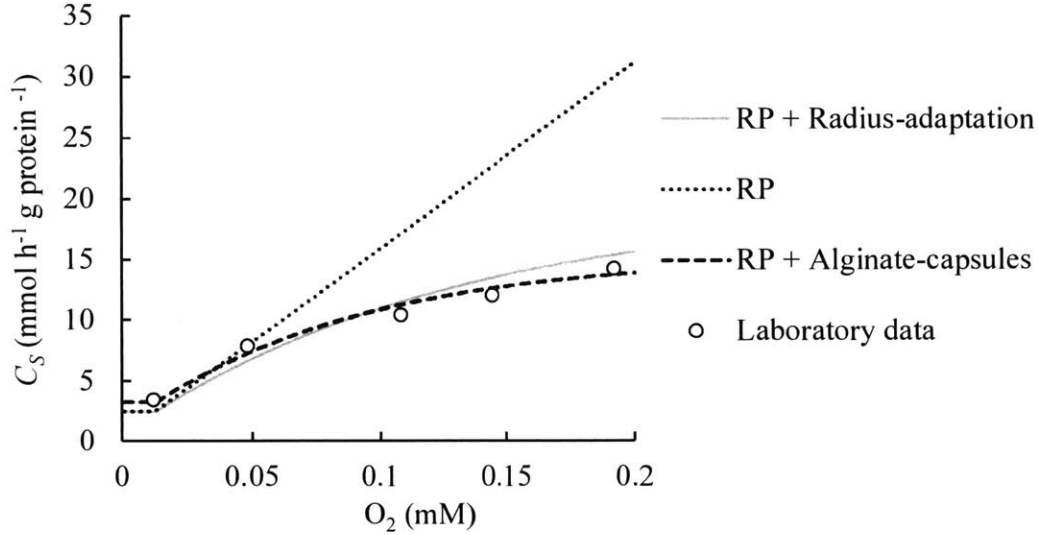


Figure 2.3 Simulated specific carbohydrate consumption rate as a function of oxygen concentrations for different scenarios: gray solid line, respiratory protection (RP) and radius-adaptation. Black dotted line, respiratory protection only. Black dashed line, respiratory protection and alginate layer formation. Open circles are linearly interpolated values from Kuhla and Oelze (1988b).

iii. Allocation of resources

The qualitative and quantitative fit to the laboratory data suggest that the model is a suitable tool for quantitative interpretation of resource allocation by *Azotobacter vinelandii* in different oxygen environments. The analysis, shown in Figure 2.4, reveals that in low ambient oxygen concentrations, the major respiratory cost is synthesis (Figure 2.4A). In an oxygenated environment, the greatest carbohydrate cost is for respiratory protection (Figure 2.4B), and the direct costs of nitrogen fixation are quite small (yellow and red portions, Figure 2.4B).

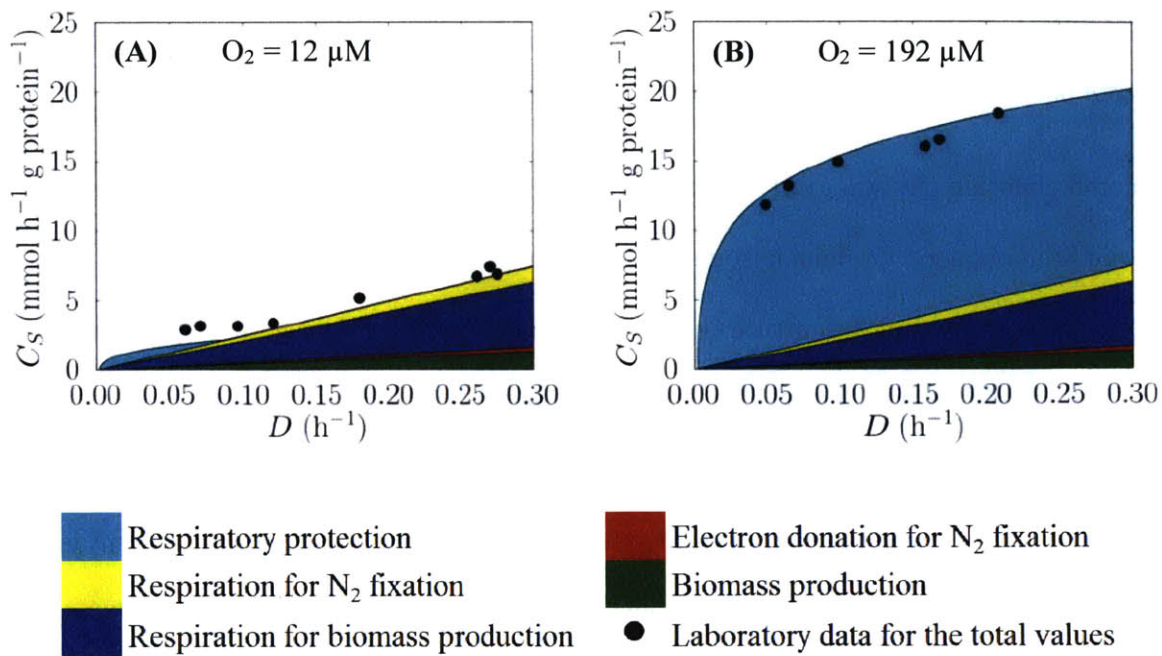


Figure 2.4 Allocation of carbohydrate resource (as measured by the contribution to specific carbohydrate consumption rate) at (A) 12 μM O_2 and (B) 192 μM O_2 . Solid circles indicate data from (Kuhla and Oelze, 1988b).

We note that the whole-cell energy transfer efficiency for *Azotobacter*, $\epsilon = 0.22$, inferred from the model fit is rather low relative to comparable simulations of other organisms growing on ammonium and glucose, where $\epsilon = 0.54$, using data from Heijnen and Roels (1981). Even when oxygen is low and respiratory protection is not in play (Figure 2.4A), the efficiency of carbohydrate utilization for synthesis remains relatively low. *Azotobacter vinelandii* expresses cytochrome bd, which has high oxygen consumption relative to ATP production (Poole and Hill, 1997), trading off low energy efficiency against the ability to manage oxygen for nitrogen fixation. There may also be a high cost in protein turnover, since nitrogenase is so sensitive to even low oxygen concentrations.

2.5 Broader Context

Nitrogen fixation and oxygen management

The comprehensive physiological and energetic data sets characterizing *Azotobacter vinelandii* have not been obtained for most nitrogen fixers. However, the model indicates that other types of nitrogen fixers may employ similar oxygen management strategies despite their differences in their sizes and physiology (Table 2.2). The model has two free parameters that were constrained by minimizing model-data differences: ϵ reflects the efficiency of energy production and ϵ_m encapsulates the permeability of the cell membrane layers to oxygen. Assuming that this low energy transfer efficiency is common amongst nitrogen fixers, we can apply the cell flux model to consider the oxygen management strategies of other nitrogen fixers. Table 2.2 illustrates the variety of strategies and their occurrence amongst several nitrogen fixing species; terrestrial and aquatic, heterotrophic and phototrophic. We note that several of these species are phototrophic, so the energetic constraints may be rather different during the day. However, in the dark (when some are fixing nitrogen) the cell flux model as developed for *Azotobacter* may be informative.

Crocospaera is a free living, unicellular marine nitrogen fixer with a typical cell radius of 1 μm (estimated from Dron *et al.*, 2012). Großkopf and LaRoche (2012) found that about 60% of respiration by *Crocospaera* is non-essential (i.e. respiratory protection) at 186 μM O_2 . We applied the cell flux model framework to a simulation of *Crocospaera* in the dark (they fix nitrogen at night) with a growth rate of 0.23 d^{-1} (Großkopf and LaRoche, 2012) and 100% vitality. To balance the books, the model suggests that *Crocospaera* must have a very low effective diffusivity for oxygen (i.e. a low ϵ_m), about 1/57th that of the cell membrane layer of *Azotobacter vinelandii* (in the absence of alginate). Such a low O_2 permeability could result from either a thickened cell wall or extra-cellular polymer layer analogous to alginate in *Azotobacter*.

The latter is consistent with the significant amounts of extracellular polymeric substances observed in association with *Crocospaera* (Dron *et al.*, 2012).

Table 2.2 The list of oxygen management strategies employed by each species. References: ^aPost, *et al.* (1982), ^bSabra, *et al.*, (2000) ^cPool and Hill (1997), ^dKumar, *et al.* (2010), ^eMaldener and Muro-Pastor (2010), ^fDron, *et al.* (2012), ^gGroßkopf and LaRoche (2012), ^hCapone *et al.* (1997), ⁱYang, *et al.* (2007), ^jBerman-Frank, *et al.* (2001).

Strategy	Size change	Extra cellular polymeric substrate	Respiratory protection
<i>Azotobacter</i>	^a Yes	^b Alginate	^c Yes
<i>Anabaena</i> and <i>Nostoc</i>	^d Yes: Heterocysts	^e Highly likely: Polysaccharide layer	-
<i>Crocospaera</i>	-	^f Possible: EPS	^g Possible
<i>Trichodesmium</i>	^h Possible: Colony	ⁱ Possible: Envelope-Related Genes	^j Possible

Other organisms use specialized heterocyst cells with very thick cell membranes to exclude oxygen. The cell wall of heterocysts of *Anabaena* have an effective diffusivity of about $1.18 \times 10^{-12} \text{ m}^2 \text{ s}^{-1}$ for oxygen (Walsby 1985). Simulations with the cell flux model assuming this diffusivity, along with a cell radius of 2.89 (estimated from Walsby 1985) and 100% vitality, we find that at typical saturated oxygen concentrations of 225 $\mu\text{M O}_2$ (Post *et al.*, 1982), this organism should not require respiratory protection for growth rates above about 0.10 d^{-1} . Its maximum growth rate is about 0.75 d^{-1} (Fogg, 1944).

One strategy of *Azotobacter vinelandii* is to increase cell size, therefore reducing surface to volume ratio and the specific invasion rate of oxygen. Forming rafts, with strands of cells bundled together, as seen in the aquatic species *Trichodesmium* and *Aphanizomenon*, may have

the same effect. Under saturated oxygen concentrations $225 \mu\text{M O}_2$ (Post *et al.*, 1982), cell radius of $2.17 \mu\text{m}$, (Bidle and Falkowski, 2004), growth rate of 0.23 d^{-1} (Prufert-Bebout *et al.*, 1993), and 100% vitality our model suggests that for an isolated trichome, about 97% of total respiration would be required for respiratory protection. However, if the colony radius triples due to bundling, the central trichomes are shielded from oxygen with an analogy to increasing the radius of individual cells. Exposed surface area is reduced such as to increase efficiency with about 75% of respiration expended on oxygen management. With colony radius 6 times that of a single cell, no respiratory protection is needed for the central trichomes. Hence the formation of bundles may provide a significant enhancement of growth efficiency for *Trichodesmium* and other marine nitrogen fixers.

Finally, we note that recent studies find heterotrophic nitrogen fixers in various ocean environments (reviewed in Zehr *et al.*, 2003; Riemann *et al.*, 2010), though the exact manner of their lifestyle is yet to be determined. Such organisms might be considered marine analogs of *Azotobacter*. It might seem surprising that such organisms could thrive in the open ocean: given the energetic cost of oxygen management it is logical that most marine nitrogen fixers would be photoautotrophic or photoheterotrophic. The high cost of oxygen management in the highly aerobic surface ocean, along with the potential paucity of sufficiently rich organic carbon substrates in dissolved form, makes it hard to envisage heterotrophic nitrogen fixation as a viable strategy for a free-living cell. However, heterotrophic nitrogen fixation can be favored in certain oxygen conditions. With growth rate of 1 d^{-1} , our *Azotobacter* study suggests a sweet spot of about 3% O_2 saturation at which the organisms are neither oxygen limited nor poisoned. Such conditions may occur in regions of low oxygen near Oxygen Minimum Zones, or on the microscale in organic particles creating viable habitats. Also, even under much higher oxygen

pressure, given sufficient quantities of carbohydrate substrates, aquatic heterotrophic organisms may carry out nitrogen fixation, as observed recently in *Pseudomonas stutzeri* (Bentzon-Tilia *et al.*, 2015). Alternatively, symbiosis may lead to fruitful sources of high energy substrates. While the precise nature and biogeography of heterotrophic marine nitrogen fixers remains elusive at present, we suggest that the cell flux model developed here may prove a useful tool for understanding and modeling these organisms.

2.6 Conclusions

To examine the growth efficiency of nitrogen-fixing bacteria, we have developed a “cell flux model”, constrained by mass, redox and energy balance, to simulate *Azotobacter vinelandii* in nitrogen-fixing conditions. The model qualitatively and quantitatively captures the trends in specific carbohydrate consumption, respiration, and the standing stock of protein as a function of growth rate and ambient oxygen concentration. It indicates that in oxygenated conditions the direct cost of nitrogen fixation has a limited impact on the growth efficiency of *Azotobacter*, relative to the major investment in respiratory protection. *Azotobacter* also employs other strategies to protect nitrogenase from oxygen including an increase in cell radius and the production of an alginate capsule, both of which increase efficiency relative to respiratory protection alone. The strategies for oxygen management employed by *Azotobacter* are common with many nitrogen fixers; aquatic and terrestrial, heterotrophic and autotrophic. The model has sufficient detail to quantitatively capture many aspects of the energetics and lifestyle of *Azotobacter* and other nitrogen fixers, yet it remains simple, transparent and computationally cheap. We suggest that it can form the basis for a general physiological model with which to

simulate and interpret the relative fitness of microbes of a variety of functionality in biogeochemical and ecological simulations.

2.7 References

- Allman R, Hann AC, Phillips AP, Martin KL, Lloyd D. (1990). Growth of *Azotobacter vinelandii* with correlation of coulter cell size, flow cytometric parameters, and ultrastructure. *Cytometry* **11**: 822–831.
- Bentzon-Tilia M, Severin I, Hansen LH, Riemann L. (2015). Genomics and ecophysiology of heterotrophic nitrogen-fixing bacteria isolated from estuarine surface water. *mBio* **6**: e00929–15. doi:10.1128/mBio.00929–15.
- Berman-Frank I, Lundgren P, Chen Y-B, Küpper H, Kolber Z, Bergman B, *et al.* (2001). Segregation of nitrogen fixation and oxygenic photosynthesis in the marine cyanobacterium *Trichodesmium*. *Science* **294**: 1534–1537.
- Berman-Frank I, Lundgren P, Falkowski P. (2003). Nitrogen fixation and photosynthetic oxygen evolution in cyanobacteria. *Res Microbiol* **154**: 157–164.
- Berman-Frank I, Quigg A, Finkel ZV, Irwin AJ, Liti H. (2007). Nitrogen-fixation strategies and Fe requirements in cyanobacteria. *Limnol Oceanogr* **52**: 2260–2269.
- Bidle KD, Falkowski PG. (2004). Cell death in planktonic, photosynthetic microorganisms. *Nat Rev Microbiol* **2**: 643–655.
- Bratbak G, Dundas I. (1984). Bacterial dry matter content and biomass estimations. *Appl Environ Microbiol* **48**: 755–757.
- Bühler T, Monter U, Sann R, Kuhla J, Dingier C, Oelze J. (1987a). Control of respiration and growth yield in ammonium-assimilating cultures of *Azotobacter vinelandii*. *Arch Microbiol* **148**: 242–246.
- Bühler T, Sann R, Monter U, Dingier C, Kuhla J, Oelze J. (1987b). Control of dinitrogen fixation in ammonium-assimilating cultures of *Azotobacter vinelandii*. *Arch Microbiol* **148**: 247–251.
- Capone DG, Zehr JP, Paerl HW, Bergman B, Carpenter EJ. (1997). *Trichodesmium*, a globally significant marine cyanobacterium. *Science* **276**: 1221–1229.
- Colón-López MS, Sherman DM, Herman LA. (1997). Transcriptional and translational regulation of nitrogenase in light-dark- and continuous-light-grown cultures of the unicellular cyanobacterium *Cyanothece* sp. strain ATCC 51142. *J Bacteriol* **179**: 4319–4327.
- Dalton H, Postgate JR. (1969). Effect of oxygen on growth of *Azotobacter chroococcum* in batch and continuous cultures. *J Gen Microbiol* **54**: 463–473.
- Dixon R, Kahn D. (2004). Genetic regulation of biological nitrogen fixation. *Nat Rev Microbiol* **2**: 621–631.
- Dron A, Rabouille S, Claquin P, Chang P, Raimbault V, Talec A, *et al.* (2012). Light:dark (12:12

- h) quantification of carbohydrate fluxes in *Crocospaera watsonii*. *Aquat Microb Ecol* **68**: 43–55.
- Dutkiewicz S, Ward BA, Monteiro F, Follows MJ. (2012). Interconnection of nitrogen fixers and iron in the Pacific Ocean: Theory and numerical simulations. *Global Biogeochem Cycles* **26**: GB1012, doi:10.1029/2011GB004039.
- Fogg GE. (1944). Growth and heterocyst production in *Anabaena cylindrica* lemm. *New Phytol* **43**: 164–175.
- Gallon JR. (1981). The oxygen sensitivity of nitrogenase: a problem for biochemists and microorganisms. *Trends Biochem Sci* **6**: 19–23.
- Glazier DS. (2009). Metabolic level and size scaling of rates of respiration and growth in unicellular organisms. *Funct Ecol* **23**: 963–968.
- Goebel NL, Edwards CA, Church MJ, Zehr JP. (2007). Modeled contributions of three types of diazotrophs to nitrogen fixation at Station ALOHA. *ISME J* **1**: 606–619.
- Golden JW, Yoon H-S. (2003). Heterocyst development in *Anabaena*. *Curr Opin Microbiol* **6**: 557–563.
- Großkopf T, LaRoche J. (2012). Direct and indirect costs of dinitrogen fixation in *Crocospaera watsonii* WH8501 and possible implications for the nitrogen cycle. *Front Microbiol* **3**: doi: 10.3389/fmicb.2012.00236.
- Heijnen JJ, Roels JA. (1981). A macroscopic model describing yield and maintenance relationships in aerobic fermentation processes. *Biotechnol Bioeng* **23**: 739–763.
- Inomura K, Bragg J, Follows MJ. A quantitative analysis of the direct and indirect costs of nitrogen fixation: a model based on *Azotobacter vinelandii*. *ISME J*. accepted
- Krishnamurthy A, Moore JK, Zender CS, Luo C. (2007). Effects of atmospheric inorganic nitrogen deposition on ocean biogeochemistry. *J Geophys Res* **112**: doi:10.1029/2006JG000334.
- Kuhla J, Oelze J. (1988a). Dependence of nitrogenase switch-off upon oxygen stress on the nitrogenase activity in *Azotobacter vinelandii*. *J Bacteriol* **170**: 5325–5329.
- Kuhla J, Oelze J. (1988b). Dependency of growth yield, maintenance and K_s -values on the dissolved oxygen concentration in continuous cultures of *Azotobacter vinelandii*. *Arch Microbiol* **149**: 509–514.
- Kumar K, Mella-Herrera RA, Golden JW. (2010). Cyanobacterial Heterocysts. *Cold Spring Harb Perspect Biol* **2**: a000315.
- LaRoche J, Breitbarth E. (2005). Importance of the diazotrophs as a source of new nitrogen in the ocean. *J Sea Res* **53**: 67–91.
- Lennon JT, Jones SE. (2011). Microbial seed banks: the ecological and evolutionary implications of dormancy. *Nat Rev Microbiol* **9**: 119–130.
- Maldener I, Muro-Pastor AM. (2010). Cyanobacterial Heterocysts. In: *Encyclopedia of Life Sciences (ELS)*. John Wiley & Sons, Ltd: Chichester. doi: 10.1002/9780470015902.a0000306.pub2.

- Misra HS. (1999). Oxygen implication in the diazotrophic growth of *Plectonema boryanum* in dark–light cycles. *Plant Sci* **143**: 135–142.
- Monteiro FM, Follows MJ, Dutkiewicz S. (2010). Distribution of diverse nitrogen fixers in the global ocean. *Global Biogeochem Cycles* **24**: GB3017, doi:10.1029/2009GB003731.
- Nagai S, Aiba S. (1972). Reassessment of maintenance and energy uncoupling in the growth of *Azotobacter vinelandii*. *J Gen Microbiol* **73**: 531–538.
- Neilson A, Rippka R, Kunisawa R. (1971). Heterocyst formation and nitrogenase synthesis in *Anabaena* sp. *Arch Mikrobiol* **76**: 139–150.
- Oelze J. (2000). Respiratory protection of nitrogenase in *Azotobacter* species: is a widely held hypothesis unequivocally supported by experimental evidence? *FEMS Microbiol Rev* **24**: 321–333.
- Pirt SJ. (1982). Maintenance energy: a general model for energy-limited and energy-sufficient growth. *Arch Microbiol* **133**: 300–302.
- Poole RK, Hill S. (1997). Respiratory protection of nitrogenase activity in *Azotobacter vinelandii*-Roles of the terminal oxidases. *Biosci Rep* **17**: 303–317.
- Post E, Golecki JR, Oelze J. (1982). Morphological and ultrastructural variations in *Azotobacter vinelandii* growing in oxygen-controlled continuous culture. *Arch Microbiol* **133**: 75–82.
- Post E, Kleiner D, Oelze J. (1983a). Whole cell respiration and nitrogenase activities in *Azotobacter vinelandii* growing oxygen controlled continuous culture. *Arch Microbiol* **134**: 68–72.
- Post E, Vakalopoulou E, Oelze J. (1983b). On the relationship of intracytoplasmic to cytoplasmic membranes in nitrogen-fixing *Azotobacter vinelandii*. *Arch Microbiol* **134**: 265–269.
- Postgate JR. (1973). The viability of very slow-growing populations: A model for the natural ecosystem. *Bull Ecol Res Comm* **17**: 287–292.
- Prufert-Bebout L, Paerl HW, Lassen C. (1993). Growth, nitrogen fixation, and spectral attenuation in cultivated *Trichodesmium* species. *Appl Environ Microbiol* **59**: 1367–1375.
- Riemann L, Farnelid H, Steward GF. (2010). Nitrogenase genes in non-cyanobacterial plankton: Prevalence, diversity and regulation in marine waters. *Aquat Microb Ecol* **61**: 235–247.
- Rittmann BE, McCarty PL. (2001). Stoichiometry and bacterial energetics. In: *Environmental Biotechnology: Principles and Applications*. McGraw-Hill: New York. 126–164.
- Sabra W, Zeng AP, Lünsdorf H, Deckwer WD. (2000). Effect of oxygen on formation and structure of *Azotobacter vinelandii* alginate and its role in protecting nitrogenase. *Appl Environ Microbiol* **66**: 4037–4044.
- Saito MA, Bertrand EM, Dutkiewicz S, Bulygin VV, Moran DM, Monteiro FM, *et al.* (2011). Iron conservation by reduction of metalloenzyme inventories in the marine diazotroph *Crocospaera watsonii*. *Proc Natl Acad Sci USA* **108**: 2184–2189.
- Sohm JA, Webb EA, Capone DG. (2011). Emerging patterns of marine nitrogen fixation. *Nat*

Rev Microbiol **9**: 499–508.

Staal M, Meysman FJR, Stal LJ. (2003). Temperature excludes N₂-fixing heterocystous cyanobacteria in the tropical oceans. *Nature* **425**: 504–507.

Stukel MR, Coles VJ, Brooks MT, Hood RR. (2014). Top-down, bottom-up and physical controls on diatom-diazotroph assemblage growth in the Amazon River plume. *Biogeosciences* **11**: 3259–3278.

Tucker DL, Hirsh K, Li H, Boardman B, Sherman LA. (2001). The manganese stabilizing protein (MSP) and the control of O₂ evolution in the unicellular, diazotrophic cyanobacterium, *Cyanothece* sp. ATCC 51142. *Biochim Biophys Acta* **1504**: 409–422.

Walsby AE. (1985). The permeability of heterocysts to the gases nitrogen and oxygen. *Proc R Soc B Biol Sci* **226**: 345–366.

Wolk CP. (1996). Heterocyst formation. *Annu Rev Genet* **30**: 59–78.

Yang Y, Qin S, Zhao F, Chi X, Zhang X. (2007). Comparison of envelope-related genes in unicellular and filamentous cyanobacteria. *Comp Funct Genomics* 2007: Article ID 25751, 10 pages doi:10.1155/2007/2575.

Zehr JP, Jenkins BD, Short SM, Steward GF. (2003). Nitrogenase gene diversity and microbial community structure: a cross-system comparison. *Environ Microbiol* **5**: 539–554.

Supplementary Material

This supplementary material provides detailed information about the cell flux model, and nomenclature.

S2.1 Evaluation of yields

The efficiency of the modeled metabolism are determined by assuming balanced mass, electron and energy flow at the individual scale following Rittmann and McCarty (2001). Though highly simplified, such approaches have proven useful (Heijnen and Roels, 1981; Xiao and VanBriesen, 2005; McCarty, 2007). A set of balanced half-reactions represent key metabolic transformations, each reflecting the flow of one unit of electrons. A respiratory electron acceptor half-reaction is paired with an appropriate electron donor, which supports the synthesis of biomass of specific stoichiometry, $C_nH_aO_bN_c$; $C_6H_{10.8}O_{2.9}N_{1.5}$ is used based on Bühler *et al.*, (1987), which refers to van Verseveld (1979). Biomass synthesis, in turn is represented by a second electron donor-

acceptor pair which consumes energy. The resulting bio-synthetic and respiratory reactions are combined in such a way as to balance the energy budget and maintain balanced electron and mass flow. An important factor is the efficiency of energy transfer, represented by ϵ , which modifies the pairing. To represent heterotrophic nitrogen fixation and to reflect the experimental setup simulated, we choose the following reactions in Table 2.S1:

Table 2.S1 Half reactions used for the cell flux model adapted from Rittmann and McCarty (2001).

Reaction	Chemical equation	Free energy change
Respiratory electron acceptor, R_a	$\frac{1}{4}O_2 + H^+ + e^- \rightarrow \frac{1}{2}H_2O$	$-\Delta G_a$
Synthesis of biomass including N_2 fixation, R_{CN}	$\left(\frac{n-c}{d}\right)CO_2 + \left(\frac{c}{d}\right)HCO_3^- + \left(\frac{c}{2d}\right)N_2 + \left(\frac{c+d}{d}\right)H^+ + e^- \rightarrow$ $\left(\frac{1}{d}\right)C_nH_aO_bN_c + \left(\frac{2n-b+c}{d}\right)H_2O + \left(\frac{c}{2d}\right)H_2$	$-\Delta G_{CN}$
where, $d = 4n + a - 2b + c$.		
Electron donor, R_d	$\frac{1}{24}C_6H_{12}O_6 + \frac{1}{4}H_2O \rightarrow \frac{1}{4}CO_2 + H^+ + e^-$	$+\Delta G_d$
Synthesis of pyruvate, R_{py}	$\frac{1}{5}CO_2 + \frac{1}{10}HCO_3^- + H^+ + e^- \rightarrow \frac{1}{10}CH_3COCOO^- + \frac{2}{5}H_2O$	$-\Delta G_{py}$

To form a balanced equation for whole cell synthesis, we use the following procedure (Rittmann and McCarty, 2001): form a respiration equation and its associated energy source:

$$R_e = R_d + R_a, \quad \Delta G_e = \Delta G_d - \Delta G_a. \quad (2.S1)$$

From R_e , $Y_{N-S}^{O_2:CH}$ is defined. Similarly, form an equation representing synthesis of biomass with given stoichiometry: here including nitrogen fixation.

$$R_s = R_d + R_{CN}, \quad \Delta G_s = \Delta G_d - \Delta G_{CN}. \quad (2.S2)$$

The whole cell formula is produced by a linear combination of the energy and synthesis equations:

$$R_{cell} = f_s R_s + f_e R_e \quad (2.S3)$$

Assuming unit electron flow,

$$f_s + f_e = 1. \quad (2.S4)$$

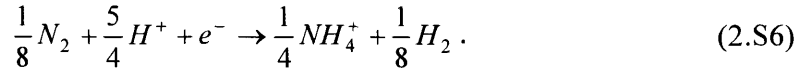
Finally, in order to close equations, we invoke energy balance allowing us to solve for f_s and f_e , and write the balance equation R_{cell} . First we must account for the less than perfect efficiency of energy transfer, via intermediates such as ATP, in the metabolic network. If $0 < \varepsilon < 1$ is the efficiency of energy transfer, and we assume the formation of an intermediate carbon compound, pyruvate, between uptake and synthesis, then the actual free energy transfer can be expressed in terms of

$$\Delta G_n = \Delta G_{2ATP} - \varepsilon \Delta G_d, \quad \Delta G_s^l = \frac{\Delta G_{py}}{\varepsilon^j} + \frac{\Delta G_{pc}}{\varepsilon} \quad \text{and} \quad \Delta G_e^l = \varepsilon \Delta G_e \quad (2.S5)$$

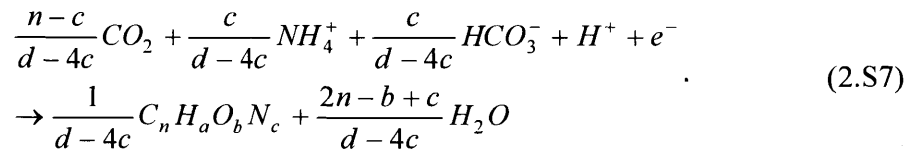
Here ΔG_n is the energy required for nitrogen fixation and electron donation. ΔG_{2ATP} is the energy produced by 2 ATP consumptions for fixing $1/8N_2$. We have assumed that $\Delta G_{2ATP}=100$ (kJ) based on Falkowski and Raven (2007), which refers to Alberts *et al.* (1983). ΔG_s^l is the energy required for biomass production with ammonium as the nitrogen source. The superscript j on ε is the modifier for the energy transfer efficiency, depending on the sign of ΔG_{py} ; when ΔG_{py} is negative, $j = -1$, and when it is positive, $j = +1$. By introducing the term j , we avoid amplifying ΔG_{py} when it is negative. ΔG_{pc} represents energy consumption for biomass production with pyruvate as a carbohydrate source and ammonium as a nitrogen source. To obtain ΔG_{pc} , we have used the estimated value of 3.33 kJ per gram cells (McCarty, 1971; Rittmann and McCarty, 2001). ΔG_e^l is the available energy from respiration. Other details and

values can be found in the section 2.7 in Rittmann and McCarty (2001) with $\Delta G_r = \Delta G_e$ and $\Delta G_p = \Delta G_{py}$.

Once we obtain ΔG_n , ΔG_s^l , and ΔG_e^l , the next step toward solving for f_s and f_e is to determine the balance among these values. In order to compute the ratio of ΔG_n and ΔG_s^l , we consider how much nitrogen has to be fixed in order to support a certain biomass production. The half reaction for nitrogen fixation, R_N , is described as follows:



Here, we have replaced the NH_3 with NH_4^+ in equation (2.1), since at the pH of typical cytoplasm, most ammonia exists in the form of NH_4^+ . Also, we have removed the reaction related to ATP since we compute the energy separately. The NH_4^+ produced in R_N has to be balanced by the NH_4^+ consumption by biomass production in R_B , the half reaction for NH_4^+ based biomass production (Rittmann and McCarty, 2001, with a different definition of d):



In order to obtain the half reaction for biomass production based on nitrogen fixation (thus R_{CN} in Table 2.S1), we assume that all the fixed nitrogen is used for biomass production, and we multiply R_N by $4c/d$ and R_B by $(d-4c)/d$ and add the together. We apply the same calculation to the energy as well; the energy requirement for biomass synthesis including nitrogen fixation per electron ΔG_{BN} is computed as follows:

$$\Delta G_{BN} = \frac{4c}{d} \Delta G_n + \frac{d-4c}{d} \Delta G_s^l. \quad (2.S8)$$

ΔG_{BN} has to be balanced by the available energy from respiration with the electron based biosynthesis-respiration ratio of $f_s : f_e$, thus:

$$f_e \Delta G_e^l + f_s \Delta G_{BN} = 0. \quad (2.S9)$$

Finally with this equation and (2.S4), we obtain f_s and f_e as follows:

$$f_s = \left(1 - \frac{\Delta G_{BN}}{\Delta G_e^l} \right)^{-1}, \quad f_e = \left(1 - \frac{\Delta G_e^l}{\Delta G_{BN}} \right)^{-1}. \quad (2.S10)$$

With f_s and f_e obtained, from (2.S3), the whole cell equation R_{cell} can be written and the stoichiometry and yields, $Y_S^{O2:BIO}$ and $Y_S^{CH:BIO}$ are defined.

S2.2 Oxygen diffusion through alginate layer and cost of alginate production

To incorporate the alginate influence on diffusivity of oxygen, we have added an alginate layer right outside of the cell membrane. This addition influences the effective diffusion coefficient of oxygen κ_{O_2} in equation (2.S11), which we restate here:

$$V_{O_2} = 4\pi r \kappa_{O_2} ([O_2] - [O_2]_C). \quad (2.S11)$$

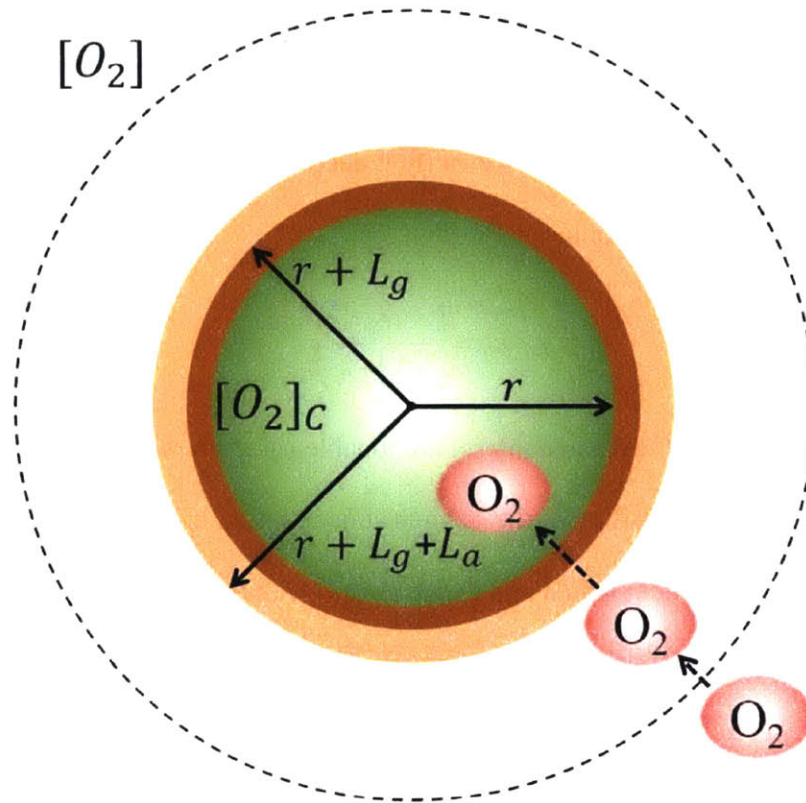


Figure 2.S1 The schematic diagram of the oxygen uptake by diffusion adapted from Staal *et al.* (2003). The green part is the bacterial cell where the concentration of oxygen is $[O_2]_c$ (mol m^{-3}), the brown part is the glycolipid layer, the peach part is the alginate layer, and the white part inside the dashed circle is the boundary layer where the concentration of oxygen is $[O_2]$ (mol m^{-3}). The transport of oxygen through different layers is driven by oxygen concentration gradient.

To incorporate the alginate layer, κ_{O_2} is modified as follows:

$$\kappa_{O_2} = \frac{\kappa_{O_2}^0}{r} \left(\frac{1}{\varepsilon_m} \left(\frac{1}{r} - \frac{1}{r+L_g} \right) - \frac{1}{\varepsilon_a} \left(\frac{1}{r+L_g+L_a} - \frac{1}{r+L_g} \right) + \frac{1}{r+L_g+L_a} \right)^{-1} \quad (2.S12)$$

where ε_a is the alginate-layer/water diffusivity ratio and L_a is the thickness of the alginate layer (m cell⁻¹). Sabra *et al.* (2000) suggests that the diffusivity of the alginate layer decreases with oxygen concentration. However, the how exactly it decreases has yet to be known. Here, we have applied the following equation:

$$\varepsilon_a = \left(\frac{l_1}{[O_2] + l_1} \right)^{l_2} \quad (2.S13)$$

where l_1 (mol O₂ m⁻³), and l_2 (dimensionless) are tunable parameters. This equation express continuously decreasing diffusivity as the oxygen concentration increases as reported in (Sabra *et al.*, 2000) and represent data in Kuhla and Oelze (1988) with $l_1=1.81 \times 10^{-3}$ (mol O₂ m⁻³) and $l_2=1.26$ (dimensionless).

We have assumed that the cost of alginate production is 1.75 times of biomass production based on the average ratio of exopolysaccharide and cell biomass production for various dilution rates in Jarman *et al.*, (1978). The energetic cost for alginate production is assumed to be small, based on the metabolic pathway of alginate production from sucrose described in Sabra *et al* (1999).

S2.3 Other parameterizations

We have used 100 mol m^{-3} for $[CH]_{IN}$ based on Kuhla and Oelze (1988). In order to calculate the cell volume V ($\text{m}^3 \text{ cell}^{-1}$), we have used $r+L_g$ for the cell radius:

$$V = \frac{4}{3}\pi(r+L_g)^3. \quad (2.S14)$$

$r + L_g$ (m cell^{-1}) is approximated from the linear regression of the cell width W (m cell^{-1}) and length L (m cell^{-1}) from Fig. 4a in Post *et al.* (1982), based on the following equation:

$$r+L_g = \frac{L/2+W}{3}. \quad (2.S15)$$

For the ratio $r : L_g$, we have used 29 : 1 based on the microscopic picture in FIG. 2 of Oppenheim and Marcus (1970). In order to obtain the oxygen diffusivity $\kappa_{O_2}^0$ at 30 °C to represent the experimental environment in Kuhla and Oelze (1988), we have converted the oxygen diffusivity of 2.12×10^{-9} at 20 °C in MacDougall and McCabe (1967) by using Walden's rule (Fernandez and Phillis, 1983) and the viscosity of water for each temperature (Kestin *et al.*, 1978).

S2.4 Equations and reactions

Table 2.S4A Model solutions with equation numbers. Equations are listed in order of appearance.

$$[O_2]_C = [O_2] + \frac{P_{O_2} - (\mu Q_C Y_S^{O_2: BIO} + R_m + R_p)}{4\pi r \kappa_{O_2}} \quad (2.4)$$

$$V_{O_2} = 4\pi r \kappa_{O_2} ([O_2] - [O_2]_C) \quad (2.8)$$

$$\kappa_{O_2} = \kappa_{O_2}^0 \frac{L_g + r}{L_g/\varepsilon_m + r} \quad (2.9)$$

$$C_S = \frac{Y_S^{CH: BIO} D}{P_V} + m + \frac{R_p}{Q_C Y_{N-S}^{O_2: CH}} \quad (2.11)$$

$$P_V = 0.18547 \ln(D) - 0.28576 \quad (2.12)$$

$$\frac{R_p}{Q_C} = \frac{4\pi r \kappa_{O_2} [O_2]}{Q_C} - \frac{D Y_S^{O_2: BIO}}{P_V} - m Y_{N-S}^{O_2: CH} \quad (2.13)$$

$$[PR] = \frac{D[CH]_{IN}}{C_S P_V} Y^{PR: BIO} \quad (2.14)$$

$$R_e = R_d + R_a, \quad \Delta G_e = \Delta G_d - \Delta G_a \quad (2.S1)$$

$$R_s = R_d + R_{CN}, \quad \Delta G_s = \Delta G_d - \Delta G_{CN} \quad (2.S2)$$

$$R_{cell} = f_s R_s + f_e R_e \quad (2.S3)$$

$$\Delta G_n = \Delta G_{2ATP} - \varepsilon \Delta G_d, \quad \Delta G_s^l = \frac{\Delta G_{py}}{\varepsilon^j} + \frac{\Delta G_{pc}}{\varepsilon} \quad \text{and} \quad \Delta G_e^l = \varepsilon \Delta G_e \quad (2.S5)$$

$$\Delta G_{BN} = \frac{4c}{d} \Delta G_n + \frac{d-4c}{d} \Delta G_s^l \quad (2.S8)$$

$$f_s = \left(1 - \frac{\Delta G_{BN}}{\Delta G_e^l}\right)^{-1}, \quad f_e = \frac{\Delta G_{BN}}{\Delta G_e^l} \left(\frac{\Delta G_{BN}}{\Delta G_e^l} - 1\right)^{-1} \quad (2.S10)$$

$$V_{O_2} = 4\pi r \kappa_{O_2} ([O_2] - [O_2]_C). \quad (2.S11)$$

$$\kappa_{O_2} = \frac{\kappa_{O_2}^0}{r} \left(\frac{1}{\varepsilon_m} \left(\frac{1}{r} - \frac{1}{r+L_g} \right) - \frac{1}{\varepsilon_a} \left(\frac{1}{r+L_g+L_a} - \frac{1}{r+L_g} \right) + \frac{1}{r+L_g+L_a} \right)^{-1} \quad (2.S12)$$

$$\varepsilon_a = \left(\frac{l_1}{[O_2] + l_1} \right)^{1/2} \quad (2.S13)$$

$$V = \frac{4}{3} \pi (r+L_g)^3 \quad (2.S14)$$

$$r+L_g = \frac{L/2+W}{3} \quad (2.S15)$$

Table 2.S4B Other equations in the main text and Supplementary Material listed in order of their appearance.

$$\frac{dQ_{O_2}}{dt} = P_{O_2} + 4\pi r \kappa_{O_2} ([O_2] - [O_2]_C) - (R_S + R_m + R_P) \quad (2.2)$$

$$R_S = \mu Q_C Y_S^{O_2: BIO} \quad (2.3)$$

$$R_P = 4\pi r \kappa_{O_2} [O_2] + P_{O_2} - (\mu Q_C Y_S^{O_2: BIO} + R_m) \quad (2.5)$$

$$\frac{dQ_{CH}}{dt} = V_{CH} - \frac{D Q_C Y_S^{CH: BIO}}{P_V} - m Q_C - \frac{R_P}{Y_{N-S}^{O_2: CH}} \quad (2.6)$$

$$\frac{dQ_{O_2}}{dt} = V_{O_2} - \frac{D Q_C Y_S^{O_2: BIO}}{P_V} - m Q_C Y_{N-S}^{O_2: CH} - R_P \quad (2.7)$$

$$\frac{d[CH]}{dt} = D([CH]_{IN} - [CH]) - V_{CH} X P_V \quad (2.10)$$

$$f_s + f_e = 1 \quad (2.S4)$$

$$f_e \Delta G_e^l + f_s \Delta G_{BN} = 0 \quad (2.S9)$$

Table 2.S4C Chemical reactions and corresponding numbers. T-2.S1 indicates Table 2.S1.
Reactions are listed in order of appearance.

Reaction	Chemical equation	Corresponding number
	$N_2 + 8e^- + 8H^+ + 16ATP + 16H_2O \rightarrow 2NH_3 + H_2 + 16ADP + 16P_i$	(2.1)
R_a	$\frac{1}{4}O_2 + H^+ + e^- \rightarrow \frac{1}{2}H_2O$	(T-2.S1-1)
R_{CN}	$\left(\frac{n-c}{d}\right)CO_2 + \left(\frac{c}{d}\right)HCO_3^- + \left(\frac{c}{2d}\right)N_2 + \left(\frac{c+d}{d}\right)H^+ + e^- \rightarrow$ $\left(\frac{1}{d}\right)C_nH_aO_bN_c + \left(\frac{2n-b+c}{d}\right)H_2O + \left(\frac{c}{2d}\right)H_2$	(T-2.S1-2)
	where, $d = 4n + a - 2b + c$	
R_d	$\frac{1}{24}C_6H_{12}O_6 + \frac{1}{4}H_2O \rightarrow \frac{1}{4}CO_2 + H^+ + e^-$	(T-2.S1-3)
R_{py}	$\frac{1}{5}CO_2 + \frac{1}{10}HCO_3^- + H^+ + e^- \rightarrow \frac{1}{10}CH_3COCOO^- + \frac{2}{5}H_2O$	(T-2.S1-4)
R_N	$\frac{1}{8}N_2 + \frac{5}{4}H^+ + e^- \rightarrow \frac{1}{4}NH_4^+ + \frac{1}{8}H_2$	(2.S6)
R_B	$\frac{n-c}{d-4c}CO_2 + \frac{c}{d-4c}NH_4^+ + \frac{c}{d-4c}HCO_3^- + H^+ + e^-$ $\rightarrow \frac{1}{d-4c}C_nH_aO_bN_c + \frac{2n-b+c}{d-4c}H_2O$	(2.S7)

S2.5 Nomenclature

Table 2.S5 Parameters, definitions and units used both in the main text and this supplementary material. The parameters are listed roughly in order of appearance.

Parameter	Definition	Unit
Q_{O_2}	Intra-cellular oxygen	mol O ₂ cell ⁻¹
t	Time	s
P_{O_2}	O ₂ production through photosynthesis	mol O ₂ cell ⁻¹ s ⁻¹
r	Cell radius of the cytoplasm	m cell ⁻¹
κ_{O_2}	Effective diffusion constant of oxygen	m ² s ⁻¹
$[O_2]$	Environmental oxygen concentration	mol O ₂ m ⁻³
$[O_2]_C$	Cellular oxygen concentration	mol O ₂ m ⁻³
R_S	Respiration associated with synthesis	mol O ₂ cell ⁻¹ s ⁻¹
R_m	Respiration associated	mol O ₂ cell ⁻¹ s ⁻¹
R_P	Respiratory protection	mol O ₂ cell ⁻¹ s ⁻¹
μ	Growth rate	s ⁻¹
Q_C	Cellular carbon quota	mol C cell ⁻¹

$Y_S^{O_2: BIO}$	Oxygen consumption : Biomass production in biosynthesis	$\text{mol O}_2 \text{ mol C}^{-1}$
Q_{CH}	Carbohydrate per cell	mol C cell^{-1}
V_{CH}	Carbohydrate uptake rate	$\text{mol C cell}^{-1} \text{ s}^{-1}$
D	Dilution rate (average growth rate)	s^{-1}
$Y_S^{CH: BIO}$	Carbohydrate consumption : Biomass production in biosynthesis	mol C mol C^{-1}
P_V	Vitality ratio	dimensionless
m	Maintenance rate	s^{-1}
$Y_{N-S}^{O_2: CH}$	Oxygen consumption : Carbohydrate consumption in non-synthesis respiration	$\text{mol O}_2 \text{ mol C}^{-1}$
V_{O_2}	Oxygen uptake rate	$\text{mol O}_2 \text{ cell}^{-1} \text{ s}^{-1}$
$\kappa_{O_2}^0$	Diffusivity constant of oxygen in water	$\text{m}^2 \text{ s}^{-1}$
L_g	Cell membrane layer thickness	m cell^{-1}
ε_m	Relative diffusivity of the cell membrane layer to water	dimensionless
$[CH]$	Carbohydrate concentration in the chemostat vessel	mol C m^{-3}

$[CH]_{IN}$	Carbohydrate concentration in the incoming medium	mol C m^{-3}
X	Number density of cells in the chemostat vessel	cell m^{-3}
C_S	Biomass specific carbohydrate consumption rate	$\text{mol C s}^{-1} \text{mol C}^{-1}$
V	Cell volume	$\text{m}^3 \text{cell}^{-1}$
ε	Energy transfer efficiency	dimensionless
$[PR]$	Protein concentration in the chemostat vessel	mol C m^{-3}
$Y^{PR: BIO}$	Cellular protein : biomass	mol C mol C^{-1}
n	Stoichiometric coefficient for C in the biomass equation	dimensionless
a	Stoichiometric coefficient for H in the biomass equation	dimensionless
b	Stoichiometric coefficient for O in the biomass equation	dimensionless
c	Stoichiometric coefficient for N in the biomass equation	dimensionless
d	$d = 4n + a - 2b + c$	dimensionless
R_a	Half reaction for respiratory electron acceptance	-

ΔG_a	Free energy change for R_a	kJ
R_{CN}	Half reaction for biomass synthesis including nitrogen fixation	-
ΔG_{CN}	Free energy change for R_{CN}	kJ
R_d	Half reaction for electron donation	-
ΔG_d	Free energy change for R_d	kJ
R_{py}	Half reaction for pyruvate synthesis	-
ΔG_{py}	Free energy change for R_{py}	kJ
R_e	Respiratory reaction	-
ΔG_e	Free energy production from respiration (energy transfer efficiency not considered)	kJ
R_s	Biomass synthesis reaction including nitrogen fixation	-
ΔG_s	Free energy change for biomass synthesis (energy transfer efficiency not considered)	kJ
R_{cell}	Whole cell reaction	-
f_s	Electron flow to biosynthesis	dimensionless
f_e	Electron flow to respiration	dimensionless

ΔG_n	Free energy required for nitrogen fixation and electron donation	kJ
ΔG_{2ATP}	Free energy produced by 2 ATP consumption	kJ
ΔG_s^l	Free energy required for biomass synthesis with ammonium as a nitrogen source	kJ
j	Modifier for energy transfer efficiency	dimensionless
ΔG_{pc}	Free energy consumption for biomass production with pyruvate as a carbohydrate source and ammonium as a nitrogen source	kJ
ΔG_e^l	Available free energy from respiration	kJ
ΔG_r	Notation used for ΔG_e in Rittmann and McCarty (2001)	kJ
ΔG_p	Notation used for ΔG_{py} in Rittmann and McCarty (2001)	kJ
R_N	Half reaction for nitrogen fixation	-
R_B	Half reaction for biomass synthesis with ammonium as a nitrogen source	-
ΔG_{BN}	Free energy requirement for biomass synthesis including nitrogen fixation	kJ

ε_a	Alginate-layer/water diffusivity ratio	dimensionless
L_a	Thickness of the alginate layer	m cell ⁻¹
l_1	Constant value for ε_a	mol O ₂ m ⁻³
l_2	Power influence for ε_a	dimensionless
L	Cell length based on observation	m cell ⁻¹
W	Cell width based on observation	m cell ⁻¹

S2.6 References

- Alberts B, Bray D, Lewis J, Raff M, Roberts K, Watson JD. (1983). *Molecular Biology of the Cell*. Garland: New York.
- Bühler T, Monter U, Sann R, Kuhla J, Dingier C, Oelze J. (1987). Control of respiration and growth yield in ammonium-assimilating cultures of *Azotobacter vinelandii*. *Arch Microbiol* **148**: 242–246.
- Falkowski PG, Raven JA. (2007). *Aquatic Photosynthesis*. Princeton University Press: Princeton. pp 145.
- Fernandez AC, Phillis GDJ. (1983). Temperature dependence of the diffusion coefficient of polystyrene latex spheres. *Biopolymers* **22**: 593–595.
- Heijnen JJ, Roels JA. (1981). A macroscopic model describing yield and maintenance relationships in aerobic fermentation processes. *Biotechnol Bioeng* **23**: 739–763.
- Jarman TR, Deavin L, Slocombe S, Righelato RC. (1978). Investigation of the effect of environmental conditions on the rate of exopolysaccharide synthesis in *Azotobacter vinelandii*. *J Gen Microbiol* **107**: 59–64.
- Kestin J, Sokolov M, Wakeham WA. (1978). Viscosity of liquid water in the range -8°C to 150°C. *J Phys Chem Ref Data* **7**: 941–948.
- Kuhla J, Oelze J. (1988). Dependency of growth yield, maintenance and K_s -values on the dissolved oxygen concentration in continuous cultures of *Azotobacter vinelandii*. *Arch Microbiol* **149**: 509–514.
- MacDougall JDB, McCabe M. (1967). Diffusion coefficient of oxygen through tissues. *Nature* **215**: 1173–1174.
- McCarty PL. (1971). Energetics and bacterial growth. In: *Organic compounds in aquatic environments*, eds. Faust, SJ, Hunter, JV. 495–529.
- McCarty PL. (2007). Thermodynamic electron equivalents model for bacterial yield prediction: Modifications and comparative evaluations. *Biotechnol Bioeng* **97**: 503–505.
- Oppenheim J, Marcus L. (1970). Correlation of ultrastructure in *Azotobacter vinelandii* with nitrogen source for growth. *J Bacteriol* **101**: 286–291.
- Post E, Golecki JR, Oelze J. (1982). Morphological and ultrastructural variations in *Azotobacter vinelandii* growing in oxygen-controlled continuous culture. *Arch Microbiol* **133**: 75–82.
- Rittmann BE, McCarty PL. (2001). Stoichiometry and bacterial energetics. In: *Environmental Biotechnology: Principles and Applications*. McGraw-Hill: New York. 126–164.
- Sabra W, Zeng AP, Lünsdorf H, Deckwer WD. (2000). Effect of oxygen on formation and structure of *Azotobacter vinelandii* alginate and its role in protecting nitrogenase. *Appl Environ Microbiol* **66**: 4037–4044.

Staal M, Meysman FJR, Stal LJ. (2003). Temperature excludes N₂-fixing heterocystous cyanobacteria in the tropical oceans. *Nature* **425**: 504–507.

van Verseveld, H W. (1979). Influence of environmental factors on the efficiency of energy conservation in *Paracoccus denitrificans*. *PhD-thesis*.

Xiao J, VanBriesen JM. (2005). Expanded thermodynamic model for microbial true yield prediction. *Biotechnol Bioeng* **93**: 110–121.

Chapter 3

On microbial nitrogen fixation in the presence of fixed nitrogen

3.1 Abstract

Nitrogen fixation is vital in global biogeochemical cycles, providing bioavailable nitrogen to the biosphere. The availability of organic carbon provides energy and electrons to fuel nitrogen fixation, while the presence of oxygen and ammonium are known suppresses this process. However, in some environments, such as in soil, benthic sediments, or even surface ocean, active nitrogen fixation is observed under high oxygen and/or ammonium pressure. Here we ask, what are the conditions that allow nitrogen fixation? To understand organic carbon, oxygen and ammonium co-limitation of nitrogen fixation, we have adapted the cell flux model of *Azotobacter vinelandii*, described in Chapter 2, to simulate laboratory experiments where it was grown in the presence of ammonium. We hypothesize that the organism optimizes its nitrogen use strategy (i.e. ammonium and/or nitrogen fixation) so as to maximize population size at a given growth rate in continuous culture. Under this assumption, the model reproduces the growth related parameters and nitrogen fixation rates of *Azotobacter vinelandii* and suggests that even under high pressure of oxygen and/or ammonium, nitrogen fixers will fix nitrogen as long as sufficient carbon is available to protect nitrogenase from oxygen. This simple rule provides useful inferences to the occurrence of nitrogen fixation in various ecosystems, such as soil, benthic sediment and ocean surface. At the same time, the model provides simple and mechanistic framework for studying global nitrogen fixation.

3.2 Introduction

Nitrogen fixers play an important role in both the ocean and terrestrial environments, providing a pathway for reducing stable dinitrogen into bioavailable nitrogen. About 50% of bioavailable nitrogen is due to nitrogen fixation both in land and ocean (Gruber and Galloway, 2008). What controls the rate of nitrogen fixation? One of the major controls is the availability of organic carbon, which provides material for synthesis and energy for nitrogen fixation. Nitrogen fixation requires 16ATP per N₂ fixed (Sohm *et al.*, 2011), and much energy is derived from catabolism of photosynthetically fixed carbon or heterotrophically obtained carbon.

On the other hand, nitrogen fixation can be limited by oxygen (e.g. Wang *et al.*, 1985; Pool and Hill, 1997; Oelze, 2000) and ammonium (e.g. Ohmori and Hattori, 1972; Neilson and Nordlund, 1975; Howarth *et al.*, 1988; Welsh *et al.*, 1997). When the oxygen concentration in the cell is high, an Fe-protein, a Mo-Fe-protein, and other metal co-factors of nitrogenase (nitrogen-fixing enzyme), are oxidized (Gallon, 1981). Once these co-factors are oxidized, the ability of nitrogenase to fix nitrogen is decreased. Thus, oxygen can potentially limit the growth of nitrogen fixers (Robson and Postgate, 1980; Inomura *et al.*, accepted).

The presence of ammonium in the cell suppresses nitrogen fixation both chemically and genetically. Uptake of ammonium causes the electron potential to decrease, which inhibits the flow of reducing equivalent to nitrogenase, hindering nitrogen fixation (Laane *et al.*, 1980). In addition to this direct effect, high intracellular concentration of ammonium leads to downregulation of *nif* genes (Dixon and Kahn, 2004), decreasing the synthesis of the nitrogenase complex.

However, some nitrogen-fixing microbes fix nitrogen when oxygen and/or ammonium is present. In aquatic environments, some major nitrogen-fixing cyanobacteria even fix nitrogen

while undergoing oxygenic photosynthesis (Berman-Frank *et al.*, 2003). The soil bacterium, *Azotobacter vinelandii* is also known to fix nitrogen under high oxygen pressure; as high as air saturation (the ground level air with O₂ mixing ratio of about 21%) (Post *et al.*, 1983), and even at oxygen concentrations 2.5 times higher than ambient air (Hashimoto *et al.*, 2013). To protect nitrogenase from intracellular oxygen, the cells may increase their respiration rate higher than energetically necessary (Kuhla and Oelze, 1988; Inomura *et al.*, accepted; Chapter 2). This, so called Respiratory Protection is known to happen when the cell is fixing nitrogen (Dalton and Postgate, 1969; Poole and Hill, 1997).

While some studies report that ammonium inhibits nitrogen fixation in marine sediments (Howarth *et al.*, 1988), others find nitrogen fixation occurring while ammonium is available (Koike and Hattori, 1978; Bertics *et al.*, 2010). How can we reconcile these contrasting results? Since in benthic sediments, there is a sharp gradient of oxygen, it is possible that oxygen also influences the magnitude of nitrogen fixation together with ammonium. Also, since the sediment also has variation in availability of organic matter, which is important in respiration and nitrogen fixation, the concentration of organic matter may influence the level of nitrogen fixation.

How do carbon, oxygen and ammonium control nitrogen fixation? A chemostat culture study of *Azotobacter vinelandii* by Bühler, *et al.* (1987a, 1987b) provides some hints for ammonium-oxygen-carbon co-limitation of nitrogen fixation. In their study, they varied the C/N ratio (sucrose to ammonium ratio) in the incoming medium of continuous cultures of *Azotobacter*. At the same time, they created four different oxygen concentrations in the medium. Their results show that a high C/N ratio leads to higher nitrogen fixation, and that the nitrogen fixation rate is highest at lowest oxygen concentration (points in Figure 3.1A).

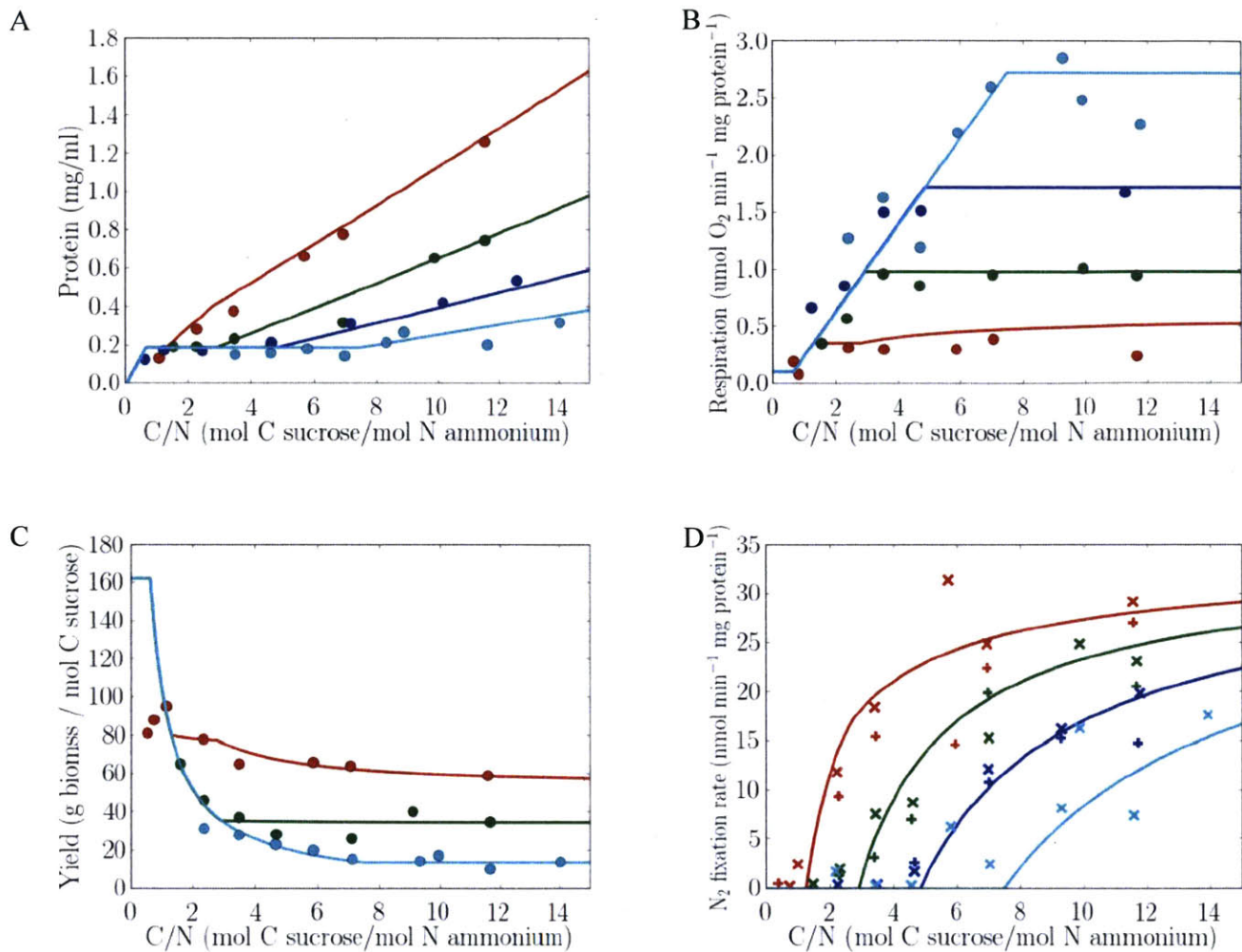


Figure 3.1 Continuous culture of *Azotobacter vinelandii* with observed data (points) redrawn from Bühler *et al.*, 1987a for (A)~(C) and Bühler, *et al.*, 1987b for (D). (A) Protein concentration in the medium. (B) Respiration rate per protein. (C) Yield (Biomass production per sucrose consumption). (D) Nitrogen fixation rate. In (D) “+” are obtained based on acetylene reduction, and “×” are based on the rate of total nitrogen incorporation (Bühler, *et al.*, 1987b). Solid lines are the corresponding simulations from this work. The model reproduces the variation of growth related parameters for different C/N ratios of the incoming medium, and oxygen concentrations: red, O₂=5%; green, O₂=15%; blue, O₂=30%; cyan, O₂=60%. The dilution rate is constant: 0.15 (h⁻¹).

However, their studies do not make clear why the respiration rate stays constant while the C/N ratio (sucrose to ammonium ratio in the incoming medium) increases when *Azotobacter* fixes nitrogen, as can be seen in Figure 3.1B. A mechanistic understanding of why nitrogen fixation happens while ammonium is present has continued to be elusive. Bühler *et al.*'s experiment shows, as the oxygen concentration increases, the C/N ratio at which the nitrogen fixation beginning increases (Figure 3.1D). A quantitative model may provide useful inferences into the control of nitrogen fixation in the presence of oxygen and ammonium.

Finally, there has not yet been a clear understanding of the cell yield (biomass production per carbohydrate sources) based on the C/N ratio and the oxygen concentration in the cell. The yield in Bühler, *et al.*, (1987a) tends to decrease until it reaches a steady level as the C/N ratio increases (Figure 3.1C). The cause of the decreasing yield with the increasing C/N ratio has yet to be well understood. This understanding of the yield can also provide important insight into the control of nitrogen fixation, because the yield coefficient influences the growth of nitrogen fixers, thus, nitrogen fixation of a community.

To mechanistically understand, clarify and interpret these results, we have adapted the cell flux model applied to *Azotobacter vinelandii* (Inomura *et al.*, accepted; Chapter 2). We have assumed that a single cell can combine nitrogen fixation and ammonium uptake, and the cell flexibly changes the ratio of nitrogen fixation and ammonium uptake to maximize the population size at a given growth rate. Based on this assumption, the model predicts many aspects of the laboratory data and provides a mechanistic understanding of carbon-oxygen-ammonium co-limitation of nitrogen fixation.

3.3 Model description

We adapt the previously developed cell flux model (Inomura *et al.*, accepted) to simulate the physiology of *Azotobacter vinelandii* in the presence of oxygen and ammonium. The model is suitable for this study since it captures the fluxes of essential chemical components while it is simple enough to provide the overall understanding of what is happening in the cell. The model describes a simple metabolic flux network in the cell and nutrient uptake by diffusion. The intracellular metabolic fluxes are constrained by mass and electron balance. There are two main pathways: biomass production (including nitrogen fixation) and respiration.

Here, we define critical oxygen concentration as the concentration above which the nitrogen fixation is hindered. When the oxygen concentration is below the critical oxygen concentration, the cell is assumed to respire the minimum amount of carbohydrate to fuel biomass synthesis. When the intracellular oxygen concentration reaches the critical level, the respiration rate is constrained in order to maintain the intracellular oxygen concentration at the critical level. In this case, the cell produces more energy than necessary for biomass production.

We will define f as the ratio of nitrogen fixation to the entire nitrogen source rate, and the ratio of ammonium uptake to the entire nitrogen source becomes $1 - f$. We will assume that the cells optimize f in such a way as to maximize the population in continuous culture (Figure 3.2). Details of the model are provided in the Supplementary Material in this chapter, Chapter 2, and its Supplementary Material. The C/N ratio of the modeled incoming medium is varied within the same range as Bühler *et al.* (1987a, 1987b). There are three cases based on the nutrient limitation and on nitrogen fixation explained as follows.

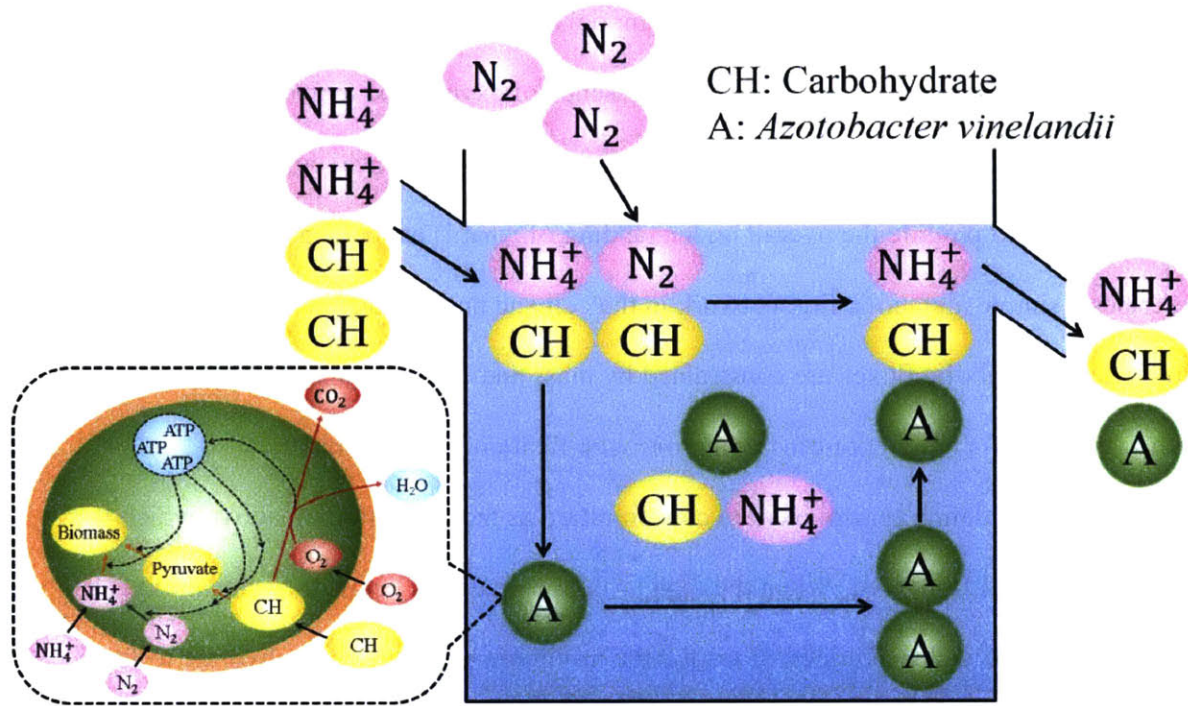


Figure 3.2 Schematic diagram of the steady state chemostat culture box model with carbohydrate and ammonium in the medium. Nutrients are used for the growth and division of cells. Nutrient uptake and cell growth are computed based on the cell flux model (Chapter 2). We assume that the concentration of N_2 is never limiting to nitrogen fixation, since the medium is an open system to the atmospheric nitrogen.

Carbohydrate limited case

At the low range of the C/N ratio, the growth of the cell is limited by the rate of carbohydrate supply. In this case, the population of the cells increases linearly to the C/N ratio when N (ammonium) input is constant. As there is available ammonium in the media, the cell does not

fix nitrogen as this would decrease the average growth efficiency (i.e. decreasing yield due to the high energetic costs), thus maximizing the community production.

Ammonium limited case

As the C/N ratio increases, ammonium becomes the limiting factor. Nitrogen fixation would be an additional source of the nitrogen that can be incorporated into the biomass. However, if the intracellular oxygen concentration is higher than the critical level, nitrogen fixation does not occur. This happens if there is not sufficient excess carbohydrate to reduce intracellular oxygen to the critical level after expenditure on biosynthesis. Thus, the population of the cells is limited by the available ammonium. However, during this phase, we have assumed that the cell respire as much carbohydrate as possible to reduce the intracellular concentration to the lowest possible level (see discussion later).

Nitrogen fixing case

In this case, there is sufficient excess carbohydrate, relative to the needs for biosynthesis, and the oxygen concentration in the cell is reduced to the critical level. The cell consumes virtually all the available ammonium and sufficient carbohydrate is available to eliminate oxygen and to provide electrons and energy to sustain nitrogen fixation. Another way of describing this is to consider that the cell optimizes the f value (the ratio of nitrogen fixation to total nitrogen supply) to maximize community production. It is straightforward to evaluate f which maximizes the standing population in the model (see Supplementary Material 3.S5).

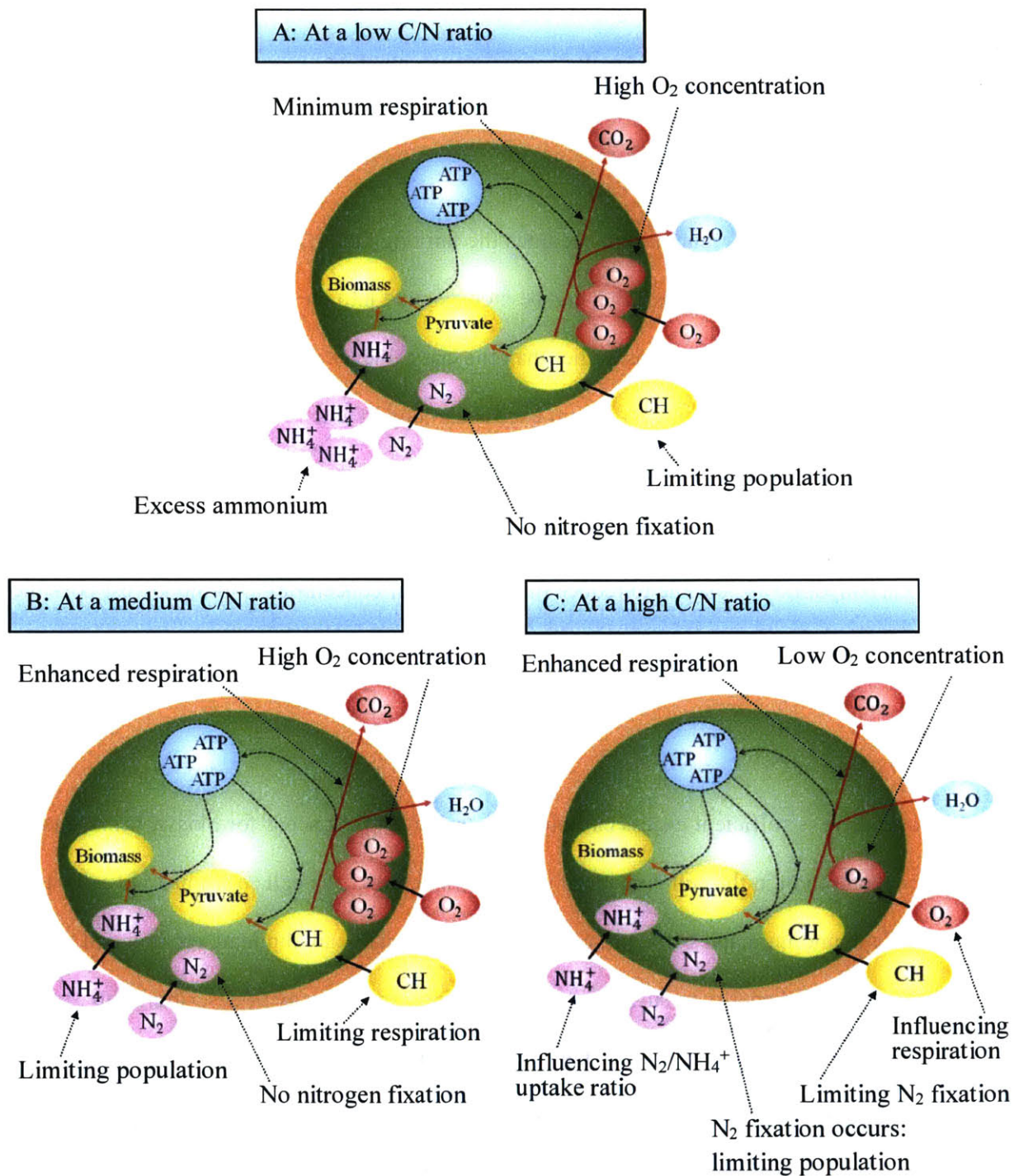


Figure 3.3 The metabolism of the cell changes based on the C/N ratio of the resource in order to maximize the population. As C/N ratio increases the cell metabolism shifts from carbohydrate limited to ammonium limited, and then to nitrogen fixation (Cases A~C in this figure). Unless the oxygen concentration is small, nitrogen fixation requires respiratory protection, which necessitates high C/N ratio.

3.4 Results and discussion

The four graphs in Figure 3.1 compare simulations where the f value is optimized for maximizing biomass concentration, to the laboratory data for growth related parameters: protein concentration in the vessel, respiration rate, molar yield coefficient, and nitrogen fixation rate. We have obtained these parameters for different incoming C/N ratios and at different O₂ concentrations. The protein concentration is stable when ammonium is limiting population, and when the population is carbohydrate limited, it increases with C/N ratio. Respiration rates increase with C/N ratio when ammonium is limiting population but stays constant when the population is limited by carbohydrate. The yield values (the biomass production per carbohydrate sources) vary inversely in relation to the respiration rate. Also, nitrogen fixation rates show a non-linear increase (decreasing slope) with the incoming C/N ratio. Based on the simple assumption that the cell takes the strategy that maximizes the population, the model reproduces the laboratory results in (Bühler *et al.*, 1987a, 1987b). The concordance of model and data demonstrates that the *Azotobacter vinelandii* optimizes the metabolism for each nutrient phase, maximizing population.

Protein concentration

The model shows three distinct phases based on the C/N ratio (Figure 3.1-A): low, medium and high C/N ratio. At low and high C/N ratio, C/N ratio influences protein concentration positively, while at medium C/N ratio it stays constant. Oxygen negatively influences protein concentration especially at high C/N ratio. The model results quantitatively reproduce the experimental data (Bühler *et al.*, 1987a, 1987b).

At low C/N ratio, the protein production is limited by carbohydrate. Thus, as the carbohydrate concentration increases, the protein production increases. In this phase, the cell does not fix nitrogen for several reasons. 1) There is an excess amount of ammonium available in the chemostat vessel. Since in this phase, carbohydrate is the growth limiting factor, even after consuming necessary amount of ammonium, there is still some available ammonium left in the chemostat culture. 2) Using ammonium is more energetically favorable than nitrogen fixation. There is higher energy demand for breaking the triple bond of nitrogen. 3) Fixing nitrogen requires an electron donor. Since N_2 is the more oxidized state than NH_4^+ , the electron supply - thus additional carbohydrate consumption- is necessary. During this phase, the carbohydrate is the growth limiting factor. Thus, the cell optimizes the carbohydrate consumption for the growth by using available ammonium instead of fixing nitrogen. 4) The oxygen concentration in the cell is higher than the critical oxygen concentration. As the cell allocates carbohydrate for the production of biomass to maximize the production, the cell respire the minimum amount to provide just enough energy for the biomass production. Based on the model computation, this minimum respiration is not sufficient to decrease the oxygen concentration enough for the nitrogen fixation.

As the C/N ratio increases to a medium C/N ratio, ammonium becomes the growth limiting factor and the protein concentration stays constant for different C/N ratio. Based on the given biomass elemental ratio, at around the C/N ratio of 0.6, ammonium becomes the growth limiting factor. Since in this model, the ammonium input stays constant, and the production is limited by the nitrogen source, the protein concentration stays constant. During this ammonium limiting phase, the excess carbohydrate is used for the extra respiration to decrease the

intracytoplasmic oxygen concentration. However, the oxygen concentration is still above the critical level. Thus, nitrogen fixation does not occur.

Finally, as the C/N ratio exceeds a certain point, the protein concentration starts to increase as the C/N ratio increases. This increasing protein concentration is caused by increasing nitrogen fixation rate. During this phase, the intracytoplasmic oxygen concentration is decreased to or stays below the critical oxygen concentration, allowing nitrogen fixation. As the C/N ratio increases, there is more carbohydrate available for providing electron for reducing N_2 to NH_4^+ , increasing nitrogen fixation. As nitrogen fixation increases, there is a higher amount of nitrogen available for protein production. Thus, protein concentration increases with f values. For the same amount of ammonium resource, increasing f values leads to higher protein concentration, since it leads to higher amount of nitrogen incorporated into protein. During this nitrogen fixing phase, the cell consumes most ammonium from the environment as it is more energetically favorable. The optimization of the nitrogen source determines the point where the cell uses all the available ammonium and carbohydrate to maximize the production.

As the environmental oxygen concentration increases, the C/N ratio at which nitrogen fixation starts (critical C/N ratio) increases. When the oxygen concentration in the environment increases, the cell needs more carbohydrate to decrease the intra-cytoplasmic oxygen concentration. The environmental oxygen concentration also influences the slope of Figure 3.1A. As the oxygen concentration increases, the slope tends to decrease. This is because each cell consumes more carbon for the same protein production to decrease the intra-cytoplasmic oxygen concentration when the environmental oxygen concentration is high.

Respiration rate

Similar to protein concentration, respiration rates show three distinct phases based on the C/N ratio (Figure 3.1-B). The respiration rates stays constant at low and high C/N ratio and increases during medium C/N ratio. Due to the limiting data points, it is unclear if this constant respiration represents the experimental data. However, the model predicts the magnitude of the experimental data in Bühler, *et al*, (1987a). At medium and high C/N ratio, the model reproduces the data, capturing the slope change in between two phases.

At low C/N ratio, respiration is at the minimum level in order to save carbohydrate. At medium C/N ratio, when ammonium is limiting the population, respiration increases with C/N ratio, using excess carbohydrate. Finally, at high C/N ratio, respiration stays constant at the level where intracellular oxygen concentration is minimum, allowing nitrogen fixation. The model captures overall trend where respiration rate increases with the C/N ratio until the intracellular oxygen concentration is minimized. This result indicates that energetically excess respiration is hard-wired and occurs even when nitrogen fixation does not take place as long as extra carbohydrate is available.

At medium C/N ratio, the cell becomes nitrogen limited with excess carbohydrate. The cells use this excess carbohydrate for respiration, resulting in increasing respiration rate with C/N ratio. This is due to the model assumption that the cell respire all the excess carbon. Concordance with the model result to the laboratory data indicates that this assumption is likely to be true in *Azotobacter*, and respiration is not physiologically down-regulated during nitrogen limited case, possibly showing that the cells are preparing for nitrogen fixation, but unaware whether there is sufficient excess carbohydrate to allow it.

Finally, after nitrogen fixation initiates, respiration stays constant. This constant respiration rate represents the necessary amount of respiration for maintaining the intracytoplasmic oxygen concentration at the critical level.

Yield

The Yield value has an inverse relation to the respiration rate (Figure 3.1C). At low C/N ratio, respiration rate is minimum, leading to the high molar yield coefficient. During the medium C/N ratio, the molar yield coefficient decreases with the C/N ratio, since the respiration rate increases, wasting carbohydrate. At the high C/N ratio, molar yield coefficient stays constant at the lowest level, since the respiration rate is highest during this phase. At the lowest end of the C/N ratio, there is some mismatch between the model and the laboratory data, indicating that some other factors are involved. It might be that the organism cannot achieve the minimum level which is balanced by the energy consumption of other pathways. Also, it is possible that extreme low carbohydrate concentrations in the environment work against the uptake of carbohydrate, decreasing the biomass production. However, in other aspects ($1 < C/N$ in Figure 3.1C), the model matches the data, indicating that the model successfully predicts the carbon metabolism.

Nitrogen fixation rate

The model results show two phases in protein specific nitrogen fixation rates: the low-medium C/N ratio and high C/N ratio (Figure 3.1-D). The specific nitrogen fixation rate is positively influenced by C/N ratio and negatively impacted by O₂ concentration.

In general, C/N ratio positively influences the nitrogen fixation rate since carbon fuels nitrogen fixation providing energy and electron sources. However, at the low-medium C/N ratio,

nitrogen fixation does not occur since the intracellular oxygen concentration is too high. At the high C/N ratio, more carbon is consumed for respiration (more detailed explanation in the later section “Fate of carbohydrate substrate” with Figure 3.6), and oxygen concentration is reduced to the level where nitrogen fixation occurs. During the nitrogen fixation phase, the nitrogen fixation rate increases non-linearly (decreasing slope with increasing C/N ratio), based on the predicted $N_2:NH_4^+$ that optimizes the population (Figure 3.4). This result is based on the assumption that cells choose N_2 or NH_4^+ (i.e. f value) in the ratio that maximizes the population, and the non-linear increase of nitrogen fixation closely reproduces the laboratory data of Bühler *et al.* (1987b) (Figure 3.1D). This concordance of the model to the laboratory data indicates that the observed inhibition of nitrogen fixation by ammonium might be for the cells to preferentially use up ammonium before investing in respiratory protection and nitrogen fixation in order to maximize the population/community production.

O_2 concentration negatively influences the magnitude of the specific nitrogen fixation rate. As O_2 concentration increases, so too does respiration rate. Thus, more carbon is channeled into respiratory protection (more detailed explanation in the later section “Fate of carbohydrate substrate” with Figure 3.6), and nitrogen fixation rate becomes relatively low. Since nitrogen fixation only occurs when intracellular O_2 concentration is low, the C/N ratio where nitrogen fixation initiates, increases with O_2 concentration. When the $O_2 = 5\%$ nitrogen fixation is the major source of nitrogen accounting for about 80% of nitrogen in biomass at a C/N ratio of higher than 8 (Figure 3.4). However, when $O_2=60\%$, most of nitrogen source is ammonium when C/N ratio is lower than 8, and even at C/N ratio=15, only about 50% of biomass nitrogen is based on nitrogen fixation (Figure 3.4).

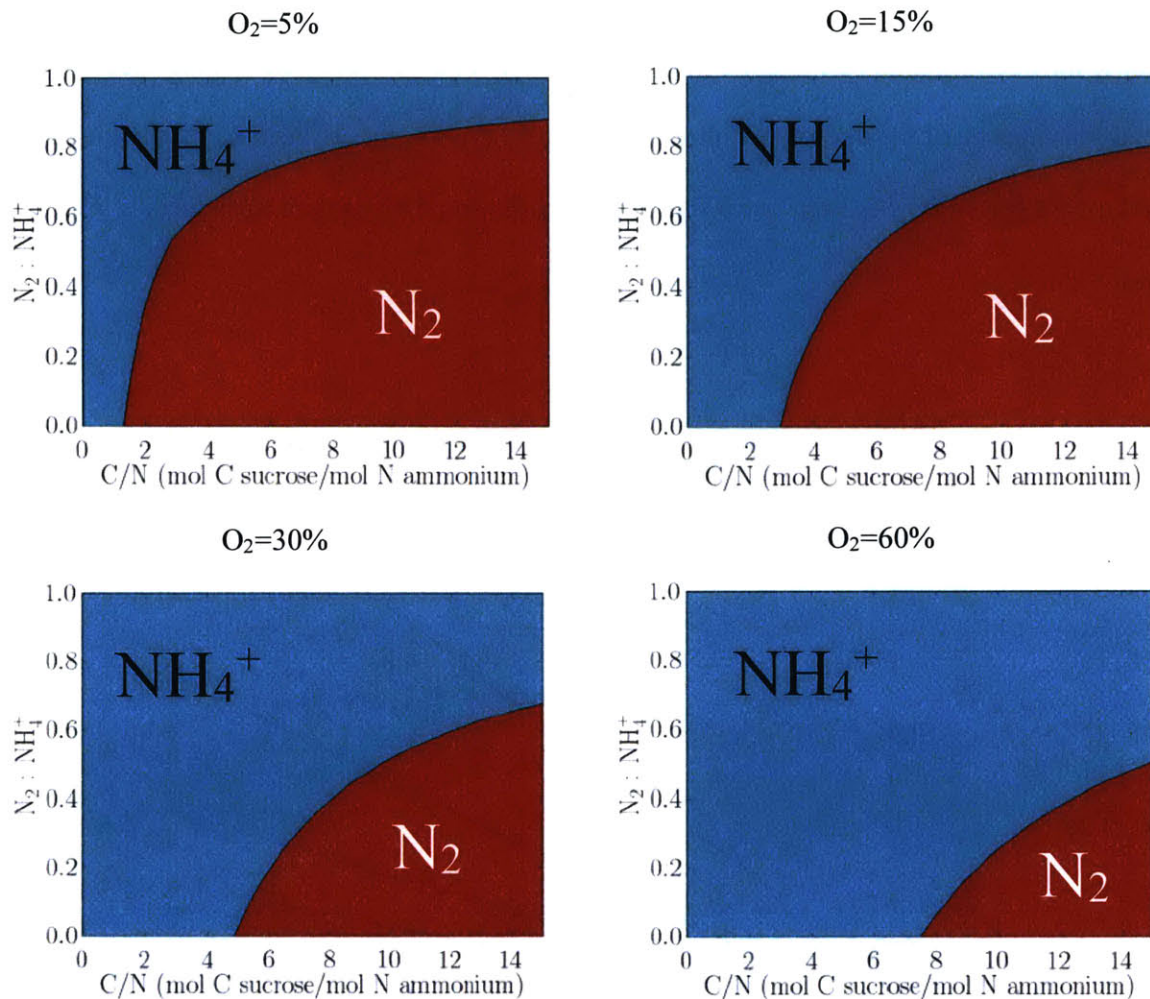


Figure 3.4 The model prediction of nitrogen source ratio ($N_2 : NH_4^+$, i.e. f) for different O_2 concentrations and C/N ratios. Cyan: direct ammonium uptake. Red: nitrogen fixation. The ratio of nitrogen fixation decreases with O_2 concentration, and increases with C/N ratio. Under high O_2 pressure, the cell has to use high carbohydrate resource for respiratory protection. As a result, small proportion of carbohydrate is channeled into nitrogen fixation, which leads to low proportion of nitrogen fixation. However, as C/N ratio increases, more carbohydrate can be channeled into nitrogen fixation, contributing to a higher ratio of nitrogen fixation.

The model predicts the nitrogen fixation rate per culture volume (Figure 3.5). While the specific nitrogen fixation rate increases non-linearly with C/N ratio, nitrogen fixation rate per volume increases linearly. At $C/N=8$, at $O_2=5\%$, the nitrogen fixation is about 25 ($nmol\ min^{-1}\ ml^{-1}$), while at $O_2=60\%$, it is nearly zero. Nitrogen fixation rate per volume is the product of

these values, and oxygen influences the protein concentration (Figure 3.1A), and the protein specific nitrogen fixation rate (Figure 3.1D). Since oxygen influences both values negatively, the negative influence of oxygen on the nitrogen per volume is amplified. As a result the nitrogen fixation rate per volume is even more significantly influenced by oxygen than specific nitrogen fixation rate.

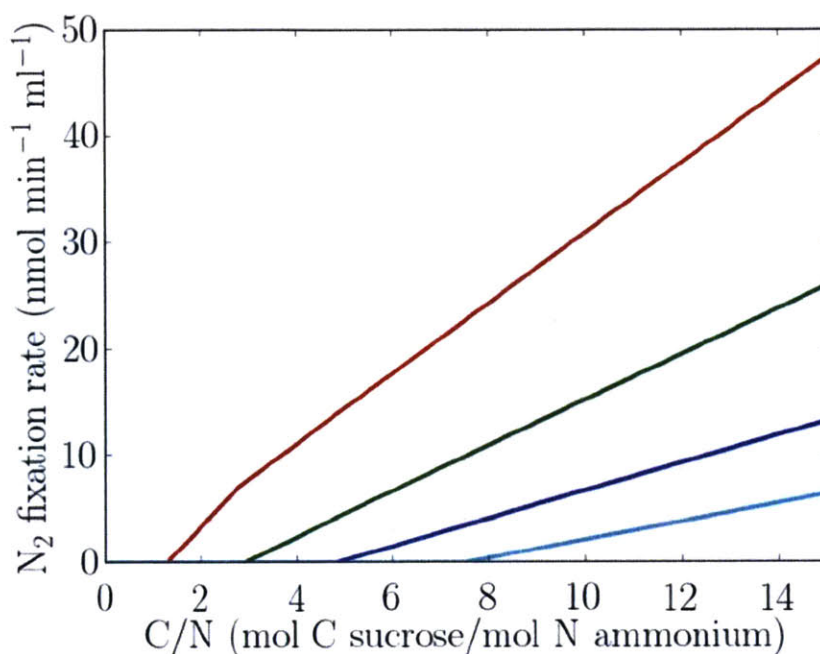


Figure 3.5 The model prediction of nitrogen fixation per volume of the culture; red, $O_2=5\%$; green, $O_2=15\%$; blue, $O_2=30\%$; cyan, $O_2=60\%$. Dilution rate is constant: $0.15 \text{ (h}^{-1}\text{)}$. The influence of the oxygen concentration is more significant in nitrogen fixation per volume of the culture than nitrogen fixation per protein. This is due to the amplifying effect; increasing nitrogen fixation per protein leads to high population, which leads to even higher nitrogen fixation per volume culture.

Fate of carbohydrate substrate

In order to understand $C-O_2-NH_4^+$ co-limitation on the growth, we have computed the fate of carbohydrate (Figure 3.6). In this model, carbohydrate will eventually be used for one of the

following: respiratory protection, respiration for nitrogen fixation, respiration for biomass production, electron donation for nitrogen fixation, and biomass production (Inomura *et al.*, accepted). Respiratory protection is the respiration exclusively for scavenging oxygen. Respiration for nitrogen fixation and biomass provides energy necessary for each purpose. The fate of carbon is influenced by both C/N ratio and oxygen concentration.

As the C/N ratio increases, more carbon is channeled into nitrogen fixation and respiration. Increasing the C/N causes “excess” of carbon. When nitrogen fixation occurs, as the C/N ratio increase, more carbon can be channeled into nitrogen fixing related metabolism (respiration for nitrogen fixation and electron donation for nitrogen fixation), resulting in higher nitrogen fixation. As a result, the ratio of nitrogen fixation for nitrogen source increases. This results in decreased energy efficiency for biomass production, leading to higher respiration for biomass production. As the cell fixes more nitrogen, the protein concentration increases, since nitrogen is essential for protein production especially when fixed nitrogen (NH_4^+ , NO_3^- , etc.) is scarce.

O_2 concentration influences the extra respiration, which indirectly influences nitrogen fixation related carbon use. High oxygen concentration requires high respiratory protection in order to counteract the passive oxygen uptake so that nitrogen fixation occurs. However, at lower C/N ratio, there is not enough carbohydrate source for sufficient respiratory protection. In order for nitrogen fixation to occur, the C/N ratio is higher than a certain level (critical C/N ratio). This critical C/N ratio increases with O_2 concentration, since higher respiratory protection or higher carbon is required when the oxygen concentration is high. In addition, when nitrogen fixation occurs, relatively less carbon is channeled into nitrogen fixation if oxygen concentration is high, due to the higher carbon requirement for respiratory protection. In summary, oxygen

concentration negatively influences the nitrogen fixation related carbon use, and as a result, negatively affects nitrogen fixation.

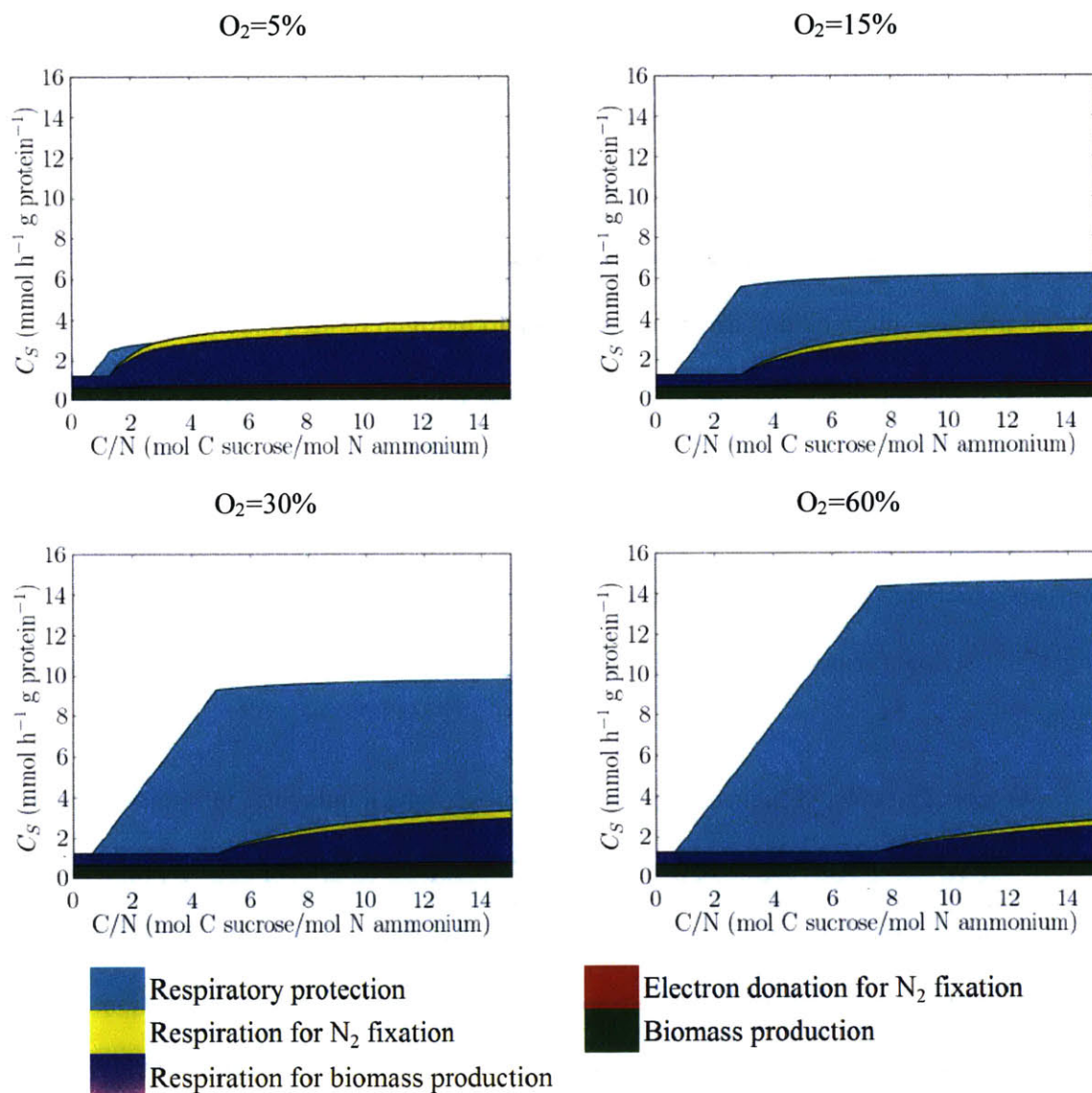


Figure 3.6 Fate of carbohydrate substrate for various O₂ concentration and resource C/N ratios. O₂ concentration increases respiratory protection, while C/N ratio increases nitrogen fixation when the C/N ratio is above the threshold. However, at low C/N ratio below the threshold, increasing C/N ratio does not make any carbohydrate channeled into nitrogen fixation. Instead, increasing carbohydrate is channeled into respiratory protection until the C/N ratio reaches the threshold. Electron donation for N₂ fixation refers to the carbohydrate consumption assuming 100% electron transfer efficiency.

Model prediction in various ammonium resource concentrations

To access the impact of ammonium and oxygen on the growth and nitrogen fixation of nitrogen fixing microbes, we have run the model for different ammonium concentrations in the incoming medium. In this run, the carbohydrate concentration is set at 225 (mol C m^{-3}) and NH_4^+ concentration was varied between 0 and 15 (mol N m^{-3}) in the incoming medium, while in the previous simulation, we have varied sucrose concentration and fixed NH_4^+ concentration. The culture O_2 concentration was set at 5%, 15%, 30% and 60% as in the previous experiment. As the ammonium concentration increases, with some exceptions the model shows three phases in the following order: nitrogen fixation phase, ammonium limiting phase, and carbohydrate limiting phase.

During nitrogen fixation phase higher ammonium suppresses nitrogen fixation, but protein concentration stays almost constant except $\text{O}_2=5\%$ where protein concentration increases with NH_4^+ . The reason for this constancy is stable carbohydrate consumption rate per cell (Figure 3.7). When there is respiratory protection, the total respiration is constrained by oxygen. Although the electron donation for nitrogen fixation decreases with ammonium, as more nitrogen fixation is replaced by direct ammonium uptake, the carbohydrate consumption allocated for this electron donation is limited (Figure 3.7B~D). Therefore, during nitrogen fixation phase, when there is relatively high oxygen concentration, as long as carbohydrate resource is constant, adding more ammonium will not increase the protein concentration significantly. However, when $\text{O}_2=5\%$, at low NH_4^+ input, there is no respiratory protection. In this case, overall carbohydrate consumption per cell decreases with decreasing respiration as more nitrogen fixation is replaced by direct ammonium uptake. As a result, the protein concentration increases.

Thus, during nitrogen fixation phase, it is more advantageous to have higher NH_4^+ when oxygen concentration is low.

The ammonium concentration in the incoming medium influences the protein concentration most when there is no nitrogen fixation and the culture is ammonium limiting. During this phase, as the cells use ammonium as the only nitrogen source for protein production, the protein concentration increases proportionately to ammonium resource concentration. As the ammonium resource concentration increase, respiration rate decreases, since smaller carbohydrate resources are allocated to each cell.

When the respiration rate hits the minimum respiration (the point when respiratory protection become zero in Figure 3.7C~D), the protein concentration becomes carbon limiting, and therefore, constant for the same amount of carbohydrate resources Figure 3.7A. In other words, during carbon limiting phase, the model predicts that ammonium has no influence on protein or nitrogen-fixation rate (Figure 3.7). However, it is possible that the cell stores excess nitrogen in nitrogen rich molecules such as cyanophycin (Saito *et al.*, 2011).

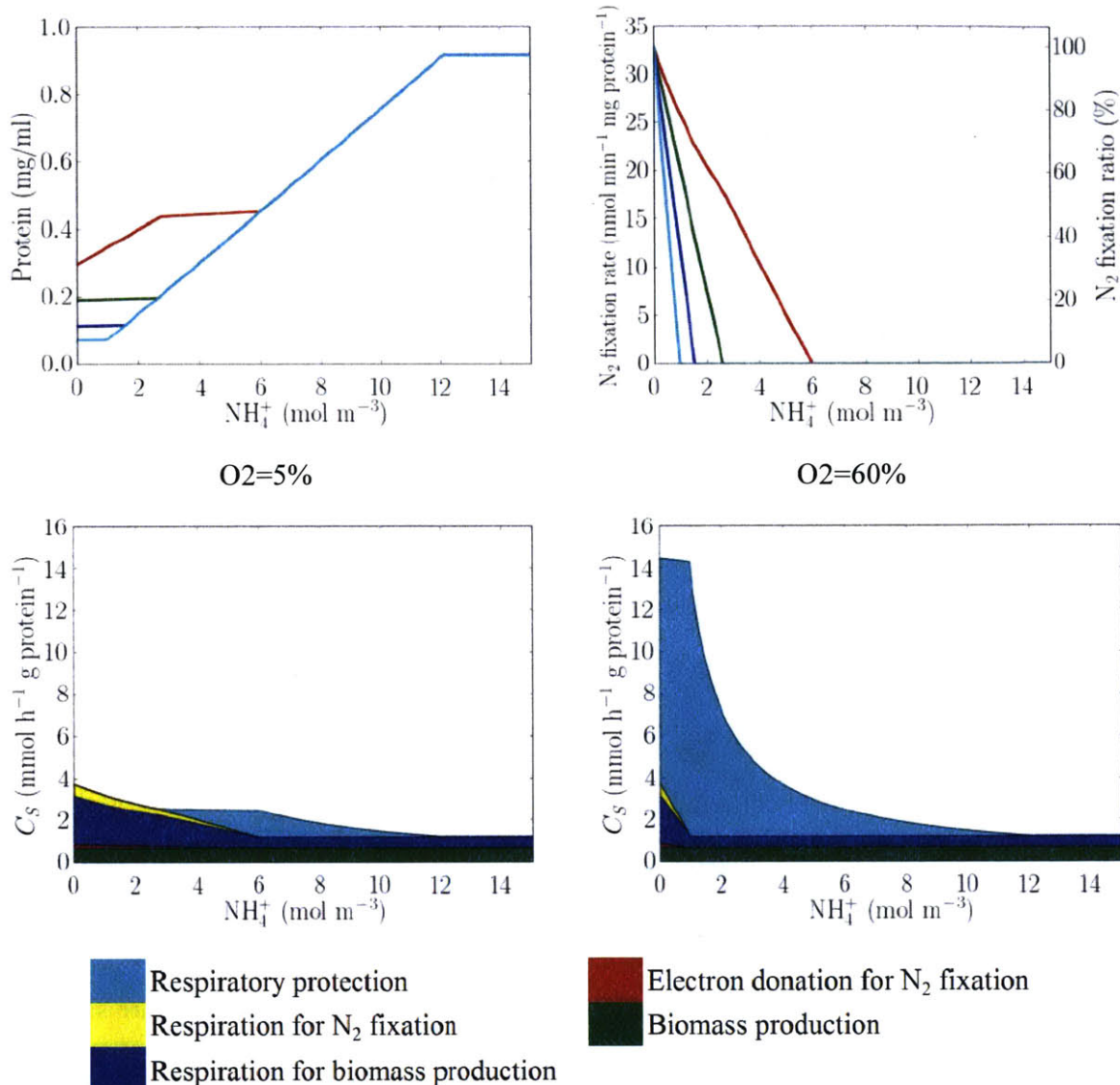


Figure 3.7 Protein concentration, nitrogen fixation rate, and fate of carbon for various oxygen concentrations and ammonium resource concentrations. For the top two diagrams, red, O₂=5%; green, O₂=15%; blue, O₂=30%; cyan, O₂=60%. While increasing ammonium decreases nitrogen fixation rates, it increases the protein concentration until the carbohydrate becomes the growth limiting factor. In this simulation, we have set the sucrose concentration at 7.5 (mol m⁻³). Electron donation for N₂ fixation refers to the carbohydrate consumption assuming 100% electron transfer efficiency.

Nitrate influence on nitrogen fixation

Nitrate is also known to inhibit nitrogen fixation (Nelson and Knowles, 1978; Capone, 1988). However, quantitative understanding of how much nitrate inhibits nitrogen fixation has not been provided. Since nitrate is more abundant than ammonium in some regions (e.g. Woodward and Rees, 2001), understanding the degree of the inhibition can provide important implication in the ecosystem and biogeochemical cycling. Here we provide a brief discussion of nitrate inhibition based on the cell flux model. The model implies the influence of nitrate differs between two cases: when respiratory protection occurs and when not.

When respiratory protection happens, the model implies that the degree of nitrate inhibition is similar to or slightly higher than ammonium inhibition. Since there is extra carbohydrate cost for reducing nitrate to ammonium, there is slightly lower carbohydrate that can be channeled toward nitrogen fixation. This implication coincides with that the threshold concentration of nitrate (the concentration in which nitrogen fixation is inhibited), is slightly higher for nitrate than ammonium (Capone 1988). However, under high oxygen pressure, since the large part of the carbohydrate cost is for respiratory protection, and excess energy is produced (i.e. nitrate reduction is not energy limited), the total carbohydrate costs are similar. Therefore, it is predicted that the degree of inhibition of nitrogen fixation between nitrate and ammonium is similar.

On the other hand, when there is no respiratory protection nitrate inhibition might not be as strong as ammonium inhibition. Since the direct energy cost of nitrogen fixation is relatively small in the cell scale (Inomura *et al.*, accepted) and nitrate reduction requires more electron, if there is no need for respiratory protection (the potentially large cost for nitrogen fixation), the cell may not benefit choosing nitrate over nitrogen fixation. This implication is demonstrated by

heterocystus cyanobacteria *Anabaena cylindrical*. Since *Anabaena*'s heterocysts (nitrogen fixation specialized cells) have a low O₂ diffusive layer, respiratory protection is rarely required (Inomura *et al.*, accepted), and their nitrogen fixation is less strongly inhibited by nitrate (Ohmori and Hattori, 1972).

3.5 Implication for nitrogen fixation under various oxygen-and-ammonium-existing environments

Our model together with the laboratory data of Bühler, *et al.* (1987a, 1987b) indicates that nitrogen fixation happen even in the presence of oxygen and ammonium resources if excess carbon is available. In this section, we discuss nitrogen fixation in various oxygen-and-ammonium-existing environments: soil, benthic sediment, and ocean surface.

Free living soil micro-organisms

Based on the model, we hypothesize that nitrogen fixation occurs at or near the surface. In general, organic carbon decreases with depth (Jobbágy and Jackson, 2000), but oxygen decreases more sharply than organic carbon (Sexstone, *et al.*, 1985; Lüdemann, *et al.*, 2000). The distribution of ammonium is less clear. If we assume the same level of ammonium sources, for nitrogen fixation to occur, low oxygen and high organic matter is required. Since oxygen concentration drops sharply within a few millimeters, while high concentration of organic layer continues up to 1m (Jobbágy and Jackson, 2000), we predict that the optimum condition does not appear right on the surface, but somewhere below the surface but not deeper than 1m. This prediction coincides with the observation by Hanson (1977), where the highest nitrogen fixation

rates are observed below top layer in most cases, and by Högberg and Kvarnström (1982), where the peak of nodule biomass, in which nitrogen fixation occurs, is between 10 and 30cm deep.

Near the root, oxygen concentration is high relatively to surrounding soil (Armstrong *et al.*, 2000), but it is much smaller than atmospheric oxygen concentration (less than 1% of atmospheric pressure in the root in flooded soil (Armstrong *et al.*, 2000). Based on the model, respiratory protection is not needed around near roots. Since root provides organic matter, and some oxygen is necessary for respiration providing energy for biosynthesis and nitrogen fixation, we hypothesize that nitrogen is favored near the root. This hypothesis is supported by the observation that nitrogen fixers colonize on the surface of the roots (Cocking, 2003).

Benthic nitrogen fixers

In benthic sediment in the ocean, similar to the soil, the oxygen and organic carbon decreases with depth (Risgaard-Petersen, *et al.*, 1994; Cai and Sayles, 1996; D'Hondt, 2015). However, in some places organic matter decreases more rapidly than oxygen while in other places the opposite occurs (D'Hondt, *et al.*, 2015). Based on the model, the latter sediment facilitates nitrogen fixation more, since such sediment would provide the sweet spot of high organic carbon and low oxygen below the sediment surface in a similar manner to the soil.

Since model result shows that in the steady state, ammonium concentration is low during nitrogen fixation, it does not explain how nitrogen fixers fix nitrogen in sediment while there is still a high concentration of NH_4^+ in the environment. However, the model indicates that even when the cell assimilate NH_4^+ at a high rate, the excess organic carbon resource may enable nitrogen fixation in the benthic sediment. We hypothesize that since organic carbon is more efficiently exported than organic nitrogen (Hopkinson and Vallino, 2005), the resource for the

benthic sediment has high C/N ratio, contributing to nitrogen fixation even under the presence of ammonium. Also, we predict that due to the high C/N ratio of the organic matter (e.g. Kähler and Koeve, 2001), the deep ocean sediment above which surface water has low nitrogen concentration may have a higher nitrogen fixation rate.

Surface ocean phototrophic nitrogen fixers

In the ocean, One of the most active nitrogen fixers is *Trichodesmium*, that fix 4.8×10^{12} (g) of nitrogen, which is 1/20 of terrestrial and 1/8 of industrial nitrogen fixation (Capone and Carpenter 1982). In a large part of the ocean, ammonium concentration is low as well as nitrate (nanomolar) (Woodward and Rees, 2001). However, since *Trichodesmium* produces O₂ themselves, the cells are under high oxygen pressure. Although the temporal and spatial segregation may help them avoid oxygen during nitrogen fixation (Berman-Frank et al., 2001), the oxygen management mechanism of *Trichodesmium* is not fully understood. However, our model results show that in order to manage such high oxygen pressure, they have to fix a significantly high amount of carbon, favoring moderately high light intensity. This might be one of the reasons why *Trichodesmium* exist at relatively shallow depths of the ocean (e.g. Capone et al., 1997).

3.6 Summary and conclusions

In order to study how carbon, oxygen and ammonium co-limit nitrogen fixation, we have adapted the cell flux model (Inomura *et al.*, accepted) to consider environments where carbon, oxygen and ammonium are supplied/present. The model is based on the assumption that the cell can optimize metabolic fluxes in the way that the population is maximized for a given growth rate. This assumption leads to the three distinct phases of the metabolic fluxes for the different C/N ratio: carbohydrate limiting phase, ammonium limiting phase, and nitrogen fixing phase. The model reproduces the quantitative pattern of growth related parameters and nitrogen fixation rates of *Azotobacter vinelandii* (Bühler, *et al.*, 1987a, 1987b). With this concordance, we hypothesize that nitrogen fixers fix nitrogen when it increases population based on the available resources. Especially, nitrogen fixers fix nitrogen even under high oxygen/ammonium pressure, if they acquire excess carbohydrate.

The model answers the following questions that we asked in the introduction.

How do carbon, oxygen and ammonium co-limit nitrogen fixation?

We provided the detailed mechanism in the result and discussion section, but overall the model showed the following trends. Carbohydrate resources positively influence nitrogen fixation, but have no effect on nitrogen fixation below the threshold C/N ratio due to the high intracellular oxygen concentration. Oxygen negatively influences nitrogen fixation. It increases the threshold C/N ratio and decrease the magnitude of nitrogen fixation. Ammonium suppresses nitrogen fixation, but increases population. The population increase is especially pronounced above the threshold ammonium concentration, above which nitrogen fixation does not occur.

When nitrogen fixation occurs, why does the respiration rate stay constant with increasing C/N ratio?

This constant respiration can be explained by respiratory protection. Except for low oxygen cases, respiratory protection occurs so that the intracellular oxygen concentration is minimized. During this phase, the respiration rate is constrained by the oxygen concentration, since a certain level of respiration is needed to counteract the passive oxygen uptake. Thus, for the same oxygen concentration, the respiration rate stays constant. As the C/N ratio increases, more carbon is available for supporting larger number of cells. This leads to increasing population and protein concentration during nitrogen fixation phase.

What makes the yield coefficient decrease with increasing C/N ratio?

The sharp decrease in the yield coefficient with the increasing C/N ratio is the result of linearly increasing respiration rate during ammonium limited phase. During this phase, increasing carbon resource is channeled into respiratory protection. As the respiratory protection increases, smaller ratio of carbon resource is channeled into biomass production, and yield coefficient decreases.

The model will be useful in simulating nitrogen fixers in the ammonium available ecosystems with various oxygen concentrations. For example, recent ocean ecosystem modes show that nitrogen fixers create niche in the oligotrophic environment (Moore *et al.*, 2004; Monteiro *et al.*, 2010; Monteiro *et al.*, 2011). However, none of them consider the influence of ammonium on the growth of nitrogen fixers, combination of ammonium uptake and nitrogen fixation, or influence of oxygen on nitrogen the fixation rate. Ammonium and oxygen concentration varies by location, and they have an impact on the growth and nitrogen fixation rate. Thus, our simple model can provide more mechanistic and physiology based prediction on global nitrogen fixation.

3.7 References

- Armstrong W, Cousins D, Armstrong J, Turner DW, Beckett PM. (2000). Oxygen distribution in wetland plant roots and permeability barriers to gas-exchange with the rhizosphere: a microelectrode and modelling study with *Phragmites australis*. *Ann Bot* **86**:687–703.
- Berman-Frank I, Lundgren P, Chen Y-B, Küpper H, Kolber Z, Bergman B, *et al.* (2001). Segregation of nitrogen fixation and oxygenic photosynthesis in the marine cyanobacterium *Trichodesmium*. *Science* **294**:1534–1537.
- Berman-Frank I, Lundgren P, Falkowski P. (2003). Nitrogen fixation and photosynthetic oxygen evolution in cyanobacteria. *Res Microbiol* **154**:157–164.
- Bertics VJ, Sohm JA, Treude T, Chow C-ET, Capone DG, Fuhrman JA, *et al.* (2010). Burrowing deeper into benthic nitrogen cycling: the impact of bioturbation on nitrogen fixation coupled to sulfate reduction. *Mar Ecol Prog Ser* **409**:1–15.
- Bühler T, Monter U, Sann R, Kuhla J, Dingier C, Oelze J. (1987). Control of respiration and growth yield in ammonium-assimilating cultures of *Azotobacter vinelandii*. *Arch Microbiol* **148**:242–246.
- Bühler T, Sann R, Monter U, Dingier C, Kuhla J, Oelze J. (1987). Control of dinitrogen fixation in ammonium-assimilating cultures of *Azotobacter vinelandii*. *Arch Microbiol* **148**:247–251.
- Cai W-J, Sayles FL. (1996). Oxygen penetration depths and fluxes in marine sediments. *Mar Chem* **52**:123–131.
- Capone DG. (1988). Benthic nitrogen fixation In *Nitrogen Cycling in Coastal marine Environments*. 85–123.
- Capone DG, Burns J a., Montoya JP, Subramaniam A, Mahaffey C, Gunderson T, *et al.* (2005). Nitrogen fixation by *Trichodesmium spp.*: An important source of new nitrogen to the tropical and subtropical North Atlantic Ocean. *Global Biogeochem Cycles* **19**: GB2024, doi:10.1029/2004GB002331.
- Capone DG, Zehr JP, Paerl HW, Bergman B, Carpenter EJ. (1997). *Trichodesmium*, a globally significant marine cyanobacterium. *Science* **276**:1221–1229.
- Cocking EC. (2003). Endophytic colonization of plant roots by nitrogen-fixing bacteria. *Plant Soil* **252**:169–175.
- D'Hondt S, Inagaki F, Zarikian CA, Abrams LJ, Dubois N, Engelhardt T, *et al.* (2015). Presence of oxygen and aerobic communities from sea floor to basement in deep-sea sediments. *Nat Geosci* **8**:299–304.
- Dalton H, Postgate JR. (1969). Effect of oxygen on growth of *Azotobacter chroococcum* in batch and continuous cultures. *J Gen Microbiol* **54**:463–473.
- Dixon R, Kahn D. (2004). Genetic regulation of biological nitrogen fixation. *Nat Rev Microbiol* **2**:621–631.
- Gallon JR. (1981). The oxygen sensitivity of nitrogenase: a problem for biochemists and micro-organisms. *Trends Biochem Sci* **6**:19–23.

- Gruber N, Galloway JN. (2008). An Earth-system perspective of the global nitrogen cycle. *Nature* **451**:293–296.
- Hanson RB. (1977). Nitrogen fixation (acetylene reduction) in a salt marsh amended with sewage sludge and organic carbon and nitrogen compounds. *Appl Environ Microbiol* **33**:846–852.
- Hashimoto W, Miyamoto Y, Yamamoto M, Yoneyama F, Murata K. (2013). A novel bleb-dependent polysaccharide export system in nitrogen-fixing *Azotobacter vinelandii* subjected to low nitrogen gas levels. *Int Microbiol* **16**:35–44.
- Högberg P, Kvarnström M. (1982). Nitrogen fixation by the woody legume *Leucaena leucocephala* in Tanzania. *Plant Soil* **66**:21–28.
- Hopkinson CS, Vallino JJ. (2005). Efficient export of carbon to the deep ocean through dissolved organic matter. *Nature* **433**:142–145.
- Howarth RW, Marino R, Cole JJ. (1988). Nitrogen fixation in freshwater, estuarine, and marine ecosystems. 2. Biogeochemical controls. *Limnol Oceanogr* **33**:688–701.
- Inomura K, Bragg J, Follows MJ. A quantitative analysis of the direct and indirect costs of nitrogen fixation. Accepted to The ISME Journal.
- Jobbágy EG, Jackson RB. (2000). The vertical distribution of soil organic carbon and its relation to climate and vegetation. *Ecol Appl* **10**:423–436.
- Kähler P, Koeve W. (2001). Dissolved organic matter in the sea: Can its C:N ratio explain carbon overconsumption? *Deep Sea Res I* **48**:49–62.
- Koike I, Hattori a. (1978). Denitrification and ammonium formation in anaerobic coastal sediments. *Appl Environ Microbiol* **35**:278–282.
- Kuhla J, Oelze J. (1988). Dependency of growth yield, maintenance and K_s -values on the dissolved oxygen concentration in continuous cultures of *Azotobacter vinelandii*. *Arch Microbiol* **149**:509–514.
- Laane C, Krone W, Konings W, Haaker H, Veeger C. (1980). Short-term effect of ammonium chloride on nitrogen fixation by *Azotobacter vinelandii* and by bacteroids of *Rhizobium leguminosarum*. *Eur J Biochem* **103**:39–46.
- Lüdemann H, Arth I, Liesack W. (2000). Spatial changes in the bacterial community structure along a vertical oxygen gradient in flooded paddy soil cores. *Appl Environ Microbiol* **66**:754–762.
- Monteiro FM, Dutkiewicz S, Follows MJ. (2011). Biogeographical controls on the marine nitrogen fixers. *Global Biogeochem Cycles* **25**:GB2003.
- Monteiro FM, Follows MJ, Dutkiewicz S. (2010). Distribution of diverse nitrogen fixers in the global ocean. *Global Biogeochem Cycles* **24**:GB3017, doi:10.1029/2009GB003731.
- Neilson AH, Nordlund S. (1975). Regulation of nitrogenase synthesis in intact cells of *Rhodospirillum rubrum*: inactivation of nitrogen fixation by ammonia, L-glutamine and L-asparagine. *J Gen Microbiol* **91**:53–62.

- Nelson LM, Knowles R. (1978). Effect of oxygen and nitrate on nitrogen fixation and denitrification by *Azospirillum brasilense* grown in continuous culture. *Can J Microbiol* **24**:1395–1403.
- Oelze J. (2000). Respiratory protection of nitrogenase in *Azotobacter* species: is a widely held hypothesis unequivocally supported by experimental evidence? *FEMS Microbiol Rev* **24**:321–333.
- Ohmori M, Hattori A. (1972). Effect of nitrate on nitrogen-fixation by the blue-green alga *Anabaena cylindrica*. *Plant Cell Physiol* **13**:589–599.
- Poole RK, Hill S. (1997). Respiratory protection of nitrogenase activity in *Azotobacter vinelandii*-Roles of the terminal oxidases. *Biosci Rep* **17**:303–317.
- Post E, Kleiner D, Oelze J. (1983). Whole cell respiration and nitrogenase activities in *Azotobacter vinelandii* growing oxygen controlled continuous culture. *Arch Microbiol* **134**:68–72.
- Risgaard-Petersen N, Rysgaard S, Nielsen LP, Revsbech NP. (1994). Diurnal variation of denitrification and nitrification in sediments colonized by benthic microphytes. *Limnol Oceanogr* **39**:573–579.
- Robson RL, Postgate JR. (1980). Oxygen and hydrogen in biological nitrogen fixation. *Annu Rev Microbiol* **34**:183–207.
- Saito MA, Bertrand EM, Dutkiewicz S, Bulygin VV, Moran DM, Monteiro FM, *et al.* (2011). Iron conservation by reduction of metalloenzyme inventories in the marine diazotroph *Crocospaera watsonii*. *Proc Natl Acad Sci USA* **108**:2184–2189.
- Sexstone AJ, Revsbech NP, Parkin TB, Tiedje JM. (1985). Direct measurement of oxygen profiles and denitrification rates in soil aggregates. *Soil Sci Soc Am J* **49**:645.
- Sohm JA, Webb EA, Capone DG. (2011). Emerging patterns of marine nitrogen fixation. *Nat Rev Microbiol* **9**:499–508.
- Welsh DT, Bourguès S, De Wit R, Auby I. (1997). Effect of plant photosynthesis, carbon sources and ammonium availability on nitrogen fixation rates in the rhizosphere of *Zostera noltii*. *Aquat Microb Ecol* **12**:285–290.
- Woodward EMS, Rees AP. (2001). Nutrient distributions in an anticyclonic eddy in the northeast Atlantic ocean, with reference to nanomolar ammonium concentrations. *Deep Res Part II Top Stud Oceanogr* **48**:775–793.

Supplementary Material

3.S1 Model details: carbohydrate limiting case

Obtaining cell population and protein concentration for carbohydrate limited case and nitrogen fixation case

In order to obtain the number density of the cell and protein concentration in carbohydrate limited case and nitrogen fixation case, we have used the same method as in Chapter 2. For carbohydrate limited case, we have simply assumed the rate of nitrogen fixation is zero, and computed energy, electron and mass balance accordingly. However, we have assumed a different energy transfer efficiency for the direct ammonium uptake; energy transfer efficiency, $\epsilon=0.45$. For all the cases, we have applied the same parameterizations from Chapter 2 including radius of the cells, fraction of active cells, and diffusivity of the cell membrane.

Obtaining respiration rate, molar yield coefficient and nitrogen fixation rate

Oxygen consumption rate (respiration rate) is computed in the same way as Chapter 2; at low oxygen environment, energy balance controls the respiration, while at high oxygen concentration, respiration is controlled by the passive oxygen uptake.

The molar yield coefficient is represented as follows:

$$Y = \frac{\lambda_S}{V_{CH}} \quad (3.1)$$

where Y (mol C mol C⁻¹) is molar yield coefficient, λ_S (mol C cell⁻¹ s⁻¹) is biomass production rate, V_{CH} is the carbohydrate uptake rate (mol C cell⁻¹ s⁻¹).

3.S2 Model details-ammonium limiting case

Obtaining cell population and protein concentration

In the ammonium limiting case, the growth of the cell is limited by ammonium. In order to compute the number density of cells, we consider the balance of ammonium concentration in the chemostat vessel:

$$\frac{d[NH_4^+]}{dt} = D([NH_4^+]_n - [NH_4^+]) - xV_{NH_4^+} \quad (3.2)$$

where $[NH_4^+]_n$ (mol N m⁻³) is the ammonium concentration in the incoming medium, t (s) is time, D (s⁻¹) is the dilution rate, $[NH_4^+]$ (mol N m⁻³) is the ammonium concentration in the culture, x (cell m⁻³) is the number density of cells, and $V_{NH_4^+}$ is the ammonium uptake rate (mol N cell⁻¹ s⁻¹). In the steady state, the equation becomes as follows along with the assumption that ammonium concentration in the culture is small compared to that in the incoming medium:

$$0 = D[NH_4^+]_n - xV_{NH_4^+} \quad (3.3)$$

From this equation, the number density of cells is obtained as follows:

$$x = \frac{D[NH_4^+]_n}{V_{NH_4^+}} \quad (3.4)$$

Once x is obtained, the protein concentration can be computed through the cellular-protein content used in Chapter 2. In order to compute $V_{NH_4^+}$, we consider the balance of ammonium pool in the cell:

$$\frac{dNH_4^+_{Cell}}{dt} = V_{NH_4^+} - \lambda_S Y_{Bio}^{N:C} \quad (3.5)$$

where $NH_4^+_{Cell}$ (mol N cell⁻¹) is the cellular ammonium quota, and $Y_{Bio}^{N:C}$ (mol N mol C⁻¹) is the N:C ratio of biomass. From this equation in the steady state:

$$V_{NH_4^+} = \lambda_S Y_{Bio}^{N:C} \quad (3.6)$$

3.S3 Model details: nitrogen fixing case

Obtaining population and protein concentration

In this part, two different ways of obtaining population are explained; the population obtained from ammonium limiting perspective, and that obtained from carbohydrate limiting perspective. The population obtained by those different methods are used for optimizing f value to maximize the production (See 3.S5 for more details).

Obtaining population from ammonium limited perspective

During this phase, the cell combines nitrogen fixation and ammonium assimilation. In this model, we use the value “ f ” for the ratio of nitrogen fixation to ammonium assimilation. Thus, from (3.6); .

$$V_{NH_4^+} = \lambda_S Y_{Bio}^{N.C} (1 - f). \quad (3.7)$$

and the number density of cells is obtained from (3.4).

Obtaining population from carbohydrate limited perspective

From the carbohydrate limited perspective, the population of the cell is based on carbohydrate concentrations based on the assumption that the carbohydrate concentration in the chemostat vessel is much smaller than that of the incoming medium. The detailed calculation is described in Chapter 2. Note that we have applied different energy transfer efficiency depending on the f value based on the following equation:

$$\varepsilon = \varepsilon_{NH_4} (1 - f) + \varepsilon_{N_2} f. \quad (3.8)$$

where ε_{NH_4} (dimensionless) is the energy transfer efficiency for direct ammonium uptake, and ε_{N_2} (dimensionless) is that for nitrogen fixation.

3.S4 Determining which case to apply

In this model, it is assumed that the biomass per cell is constant. Thus, maximizing population leads to maximizing the biomass production for the same dilution rate. To maximize population for different oxygen concentration and the C/N ratio in the chemostat vessel, the following method is applied. In order to determine which metabolism is applied, we have considered the lowest possible oxygen concentration in the cell $[O_2]_{Cpot}$ (mol O₂ cell⁻¹) based on the carbohydrate availability and critical oxygen concentration $[O_2]_{cri}$ above which nitrogen fixation does not occur. We have assumed that $[O_2]_{cri}$ is small. $[O_2]_{Cpot}$ is the hypothetical intracellular oxygen concentration based on the assumption that all the available carbohydrate is consumed with no nitrogen fixation.

If $[O_2]_{Cpot} > [O_2]_{cri}$, there is no nitrogen fixation; the growth is either limited by carbon or ammonium. The population for carbohydrate limited case $x_{CHlimited}$ (cell m⁻³) and ammonium limited case $x_{NH_4^+ limited}$ (cell m⁻³) are calculated first and the values are compared to determine what is limiting the growth. When $x_{CHlimited} < x_{NH_4^+ limited}$ the carbohydrate limited case is applied, and when $x_{CHlimited} > x_{NH_4^+ limited}$ the ammonium limited case is applied.

when $[O_2]_{Cpot} < [O_2]_{cri}$, nitrogen fixation can happen. However, if the exclusive consumption of ammonium leads to higher population, nitrogen fixation is assumed to be zero. If $x_{CHlimited} < x_{NH_4^+ limited}$, the carbohydrate limited case is applied since there is available ammonium left in the medium; when there is available ammonium, assimilating ammonium is more

energetically favorable than nitrogen fixation. On the other hand, if $x_{CH\text{limited}} < x_{NH_4^+\text{limited}}$, the nitrogen fixing case is applied.

3.S5 How to optimize f value

The value of f (the ratio of nitrogen fixation to the entire nitrogen assimilate) is determined to maximize the population. To optimize f value, first, the population for nitrogen fixing case is computed for f values covering $0 < f < 1$ with small enough steps. Then, we calculate the population for each case and take the f value that gives maximum population. This f value matches where the population from ammonium limiting perspective matches the population from carbohydrate limiting perspective.

Chapter 4

A macromolecular model of phytoplankton growth under light and nutrient co-limitation

4.1 Abstract

We present a new, steady-state macromolecule-based model to study light-nutrient co-limitation of phytoplankton growth. The model is based on simplified metabolic flux network and resolves key pools of macro-molecules, each of which has different roles for cellular growth. The model is used to predict and interpret the variation of cellular stoichiometry of fresh water *Synechococcus* spp. under different light and nutrient environment over a range of dilution rates (average growth rates) in a steady state culture. The model explains the different response of cellular nitrogen and phosphorus quota to the various light-nutrient environments, predicting protein and RNA as most influential molecules on nitrogen and phosphorus quotas respectively. The model indicates that, though total nitrogen storage is larger than phosphorus storage many times more phosphorus can be stored than required. It accurately predicts the maximum possible growth rate based on the limits of resource allocation within the cell. Finally, the model predicts nutrient-light co-limitation of cell population density under different dilution rates (i.e. rate of nutrient supply). While the concentration of inflowing nutrient in the medium has a direct effect on the population density, light impacts it by modifying the cellular stoichiometry. This steady-state, macromolecule based model provides bases for predicting phytoplankton growth in different dynamic environments.

4.2 Introduction

Marine phytoplankton play an important role in the carbon cycle, accounting for 40~50 % of photosynthesis on the earth (Falkowski, 1994; Field *et al.*, 1998). To predict the phytoplankton abundance and rate of photosynthesis, ocean ecosystem models have been developed over several decades. Fasham *et al.* (1990) built a network model of the surface-ocean ecosystem that encompasses the balance between the growth and grazing of phytoplankton as well as the influence of heterotrophic microbes. The currency of the model was nitrogen, in both inorganic and organic form. Sarmiento *et al.* (1993) combined this ecosystem model to a three-dimensional, regional ocean circulation model with a single phenotype to represent all phytoplankton. During the 21st century, as computational capacities and ecosystem theory develop, ocean ecosystem models which resolve several functional types of phytoplankton have been developed (e.g. Chai *et al.*, 2002; Moore *et al.*, 2002; Le Quéré *et al.*, 2005; Bruggeman and Kooijman, 2007; Follows *et al.*, 2007). A key aspect of predicting the biogeography and biogeochemical impact of phytoplankton is relating their growth rate to the local environment.

The growth of phytoplankton is largely limited by light and nutrient availability (e.g. Laws and Bannister, 1980; Gotham and Rhee, 1982; Cloern, 1999; Moore *et al.*, 2013). In photosynthesis, the light reactions produce energy and a reducing equivalents, which in turn are used for carbon fixation, and biomass synthesis. In biosynthesis, nutrients provide necessary elements for growth.

Light and nutrients co-limit the growth of phytoplankton (e.g. Harrison *et al.*, 1990; North *et al.*, 2007), and the relative importance between light and nutrient changes with environment (Cloern, 1999). Such co-limitation was clearly demonstrated in the chemostat culture of *Synechococcus* spp. discussed by Healey (1985) (Figure 4.1). When irradiance is

around $20 \mu\text{Em}^{-2}\text{s}^{-1}$, both increasing phosphorus and light intensity increases the concentration of biomass in the culture. At around $50 \mu\text{Em}^{-2}\text{s}^{-1}$, however, increasing irradiance has a limited effect while increasing phosphorus has a more significant impact on the biomass concentration. This data set demonstrates that the light and nutrients have dependent effects which are only crudely characterized in current ocean ecosystem models.

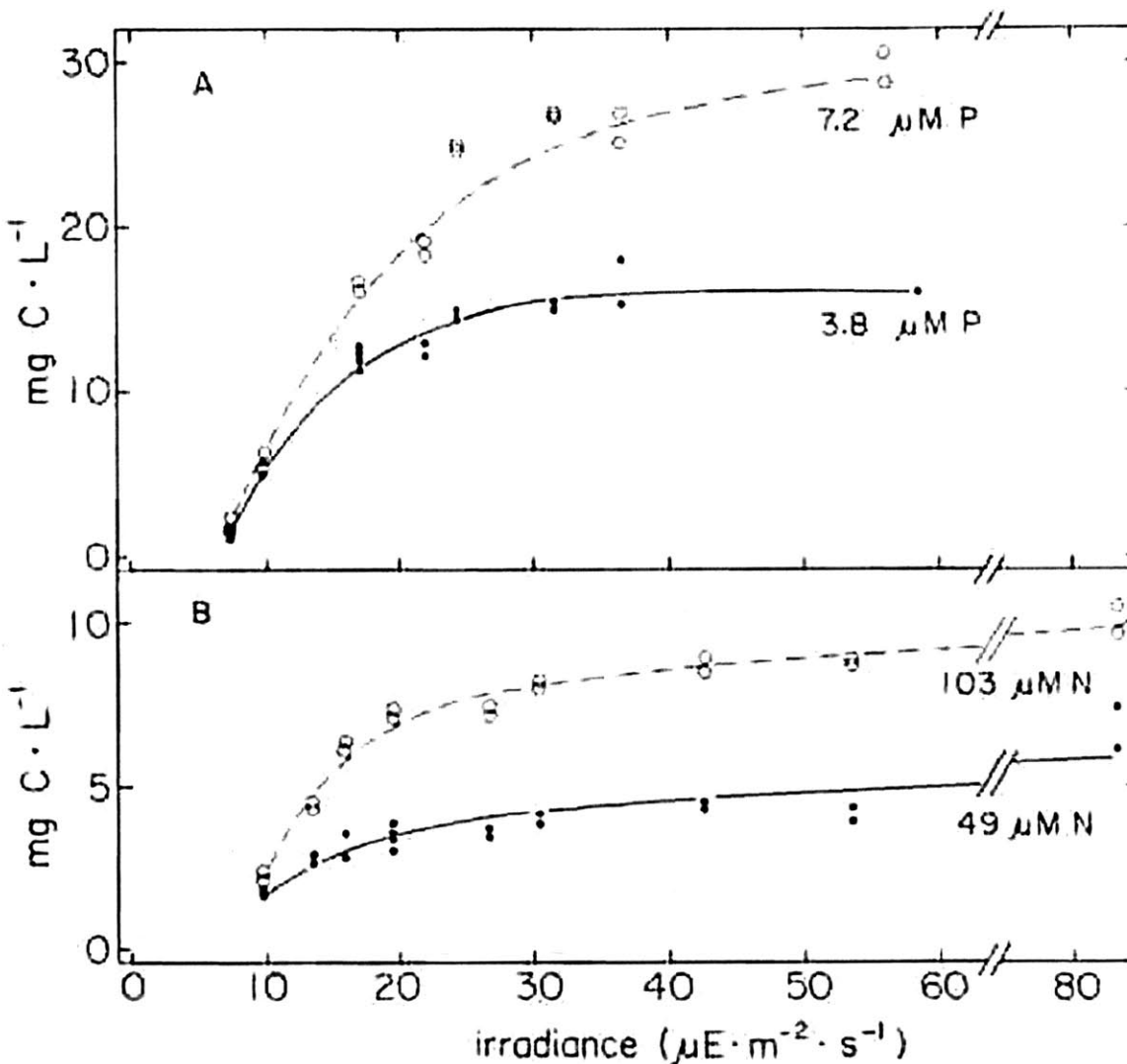


Figure 4.1 Light-nutrient co-limitation on organic carbon in the chemostat culture of *Synechococcus* spp. Y axis is the biomass concentration in carbon, and x axis is the irradiance. (A) Phosphorus limiting culture; white circles: $7.2 \mu\text{M P}$ in the incoming medium; black circles: $3.8 \mu\text{M P}$ (B) Nitrogen limiting culture; white circles: $103 \mu\text{M N}$ in the incoming medium; black circles: $49 \mu\text{M N}$. The figure is taken from Healey (1985) with permission.

The crudeness of the representation of algal physiology in such models has often been justified by a saving in computational costs (Flynn 2003). In most ecological models, the growth of phytoplankton is generally represented as a simple function of external resource concentrations using Monod kinetics (Monod, 1949):

$$\mu = \mu_{max} \frac{[N]}{[N] + K_N} \quad (4.1)$$

where μ is the growth rate, μ_{max} is maximum growth rate, $[N]$ is the external nutrient concentration, and K_N is the half saturation. In order to express nutrient-light co-limitation, μ_{max} is subjected to change depending on the light influence: but how does light influence μ_{max} ? Ocean ecosystem models often assume the independent effect of light and nutrient (e.g. Fasham *et al.*, 1990, Sarmient *et al.*, 1993; Kishi *et al.*, 2007; Follows *et al.*, 2007; Stukel *et al.*, 2014), the growth of phytoplankton is roughly expressed as follows:

$$\mu = \mu_{max}(I) \frac{[N]}{[N] + K_N} \quad (4.2)$$

where I is light intensity. While the equation is analytically transparent, and computationally efficient, light and nutrients should influence each other's effect on growth. For example, if we were to use Monod kinetics, K_N has to vary with the light intensity. Some models use the "affinity" (a) to express the half saturation (e.g. Smith *et al.*, 2009), relating it to a light-dependent maximum growth rate:

$$K_N = \frac{\mu_{max}(I)}{a} \quad (4.3)$$

However, there is limited physiological evidence that half saturation linearly decreases with μ_{max} (I). To better characterize nutrient and light co-limitation of phytoplankton growth, considering cellular physiology is necessary.

One classic and simple improvement that reflects cell physiology is the Droop model (Droop 1968; Caperon 1969; Droop, 1970; Droop, 1973) which decouples uptake and synthesis and expresses the growth rate as a function of the cell quota of the limiting resource:

$$\mu = \mu_{max} \left(1 - \frac{Q_{limiting}^{min}}{Q_{limiting}}\right) \quad (4.4)$$

In most cases, this equation gives satisfactory fits to data on phosphorus limited growth of phytoplankton (e.g. Burmaster, 1979; Auer and Canale, 1982; Garcia *et al.*, 2016), and has been used extensively for ecosystem models (e.g. Ducobu, *et al.*, 1998; Klausmeier, *et al.*, 2004). However, this parameterization often does not provide a good description of nitrogen limited growth. Nitrogen quota often linearly increase with the growth rate (e.g. Laws and Caperon, 1976; Laws and Bannister, 1980; Healey, 1985; Claquin *et al.*, 2002; Flynn, 2008), and in order for to the Droop model to express this trend, μ_{max} has to be infinitely large. This conceptually conflicts with the fact that phytoplankton has finite maximum growth rate.

As for the Monod model, the Droop model is not sufficiently detailed to describe light-nutrient co-limitation (Flynn 2003). The model treats all resources (nitrogen, phosphorus and carbon) equally, but in reality, elements are allocated to different molecules with different physiological purposes. In order to express, light-nutrient co-limitation of the growth, we need to broadly predict the variation of macromolecular components responsible for each cellular process such as photosynthesis and protein synthesis.

Attempts have been made toward resolving macromolecules, yet there are still challenges to overcome. Geider *et al.*, (1996, 1997, 1998) allocated resources (protein) towards three purposes; light harvesting, biosynthesis, energy storage, very effectively describing light and nitrogen co-limitation (Geider *et al.*, 1998). However, since the model does not explicitly resolve protein synthesis and nucleic acids, it could not predict light-phosphorus co-limitation.

Bruggeman and Kooijman (2007) took a similar approach and considered nutrient fluxes allocated towards different functions. However, the model is missing explicit fluxes and reservoirs for biosynthetic apparatus, and it does not predict the relative sizes of macromolecular components. These are the key for predicting light-phosphorus co-limitation, as we will show in this chapter.

To predict light-nitrogen-phosphorus co-limitation of phytoplankton growth, Pahlow and Oschlies (2009) developed a cell quota based model incorporating the influence of cell quota for various nutrient fluxes in and through the cell. However, there is a limited physiological explanation for the flux constraint, and the model has limited predictive capability with regard to N:P ratio and biomass carbon under different dilution rates. In order to predict the light-nutrient co-limitation of phytoplankton growth, we need to breakdown nitrogen and phosphorus quotas into appropriate macromolecules (Follows and Dutkiewicz, 2011) and their influence on chemical fluxes based on the knowledge of biochemistry and cell physiology.

Flynn (2001) has developed a macro-molecular based algal growth, but this model heavily relies on empirically derived parameters as well as tunable parameters, rather than providing concrete macromolecule-flux relations. This model has not yet been extensively applied (Williams and Laurens, 2010), possibly due to its complexity and limited analytical transparency. Similarly, Flux Balance Analysis predicts and resolves a number of reactions within the cell and predicts the reaction rates based on some assumptions such as the optimization of biomass production (e.g. Kauffman *et al.*, 2003; Schuster and Fell, 2007; Orth *et al.*, 2010). However, due to its complexity, FBA has not been broadly used in the ecosystem context. While incorporating many details may improve the fidelity of a model, it can also be obscuring; models

should remain as simple and clear as possible. Simplified approaches are also favorable for a computationally expensive models, such as 3D ocean ecosystem and climate models.

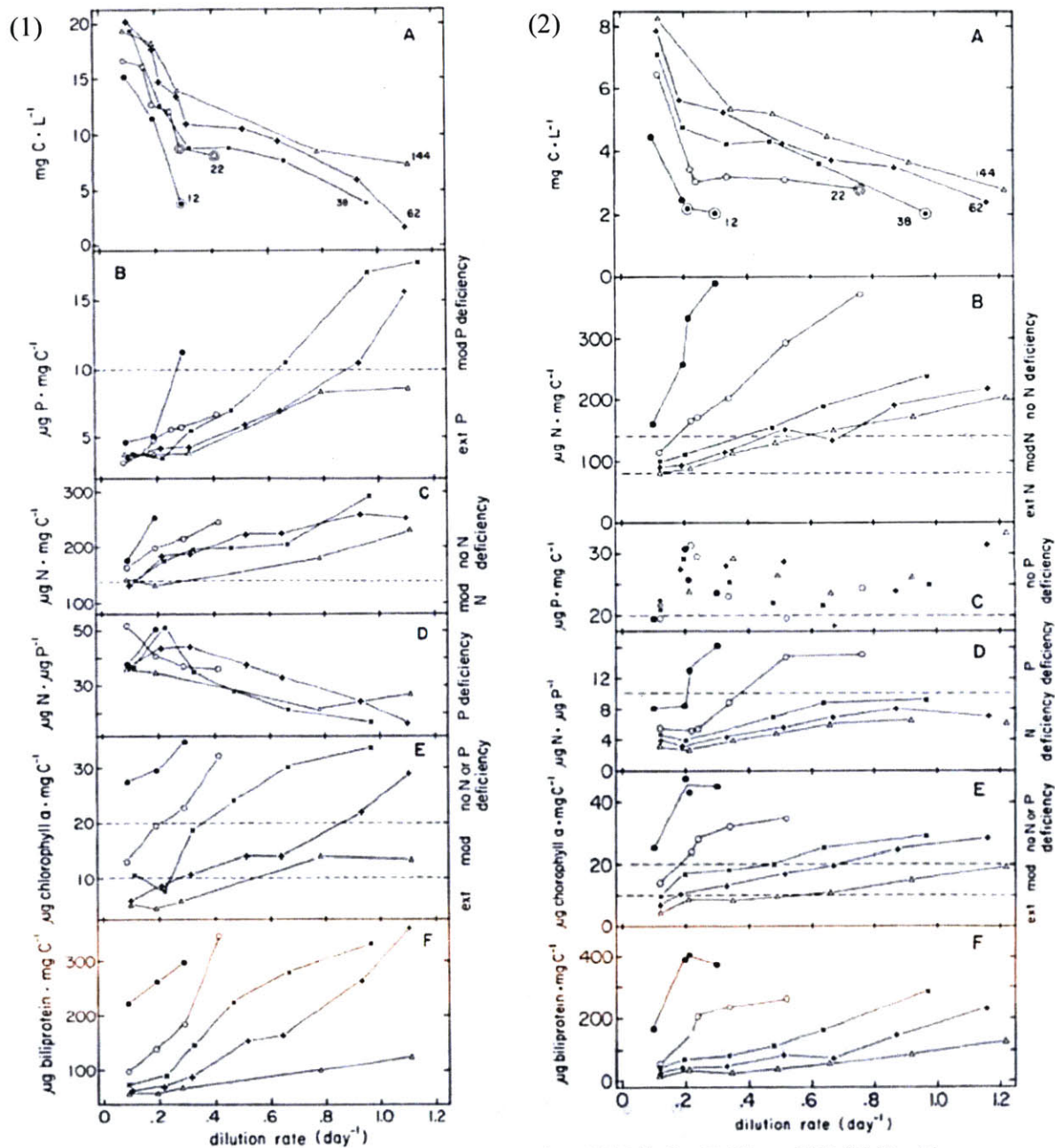


Figure 4.2 Chemostat culture data set from Healey (1985) for P (1) and N (2) limiting conditions for different light intensities: black circles, 12 $\mu\text{E m}^{-2}\text{s}^{-1}$; white circles, 22 $\mu\text{E m}^{-2}\text{s}^{-1}$; x marks, 38 $\mu\text{E m}^{-2}\text{s}^{-1}$; crosses, 62 $\mu\text{E m}^{-2}\text{s}^{-1}$; triangles, 144 $\mu\text{E m}^{-2}\text{s}^{-1}$. (A), biomass carbon

concentration in the culture; (B), P:C ratio; (C), N:C ratio; (D), N:P ratio; (E), Chlorophyll a: C ratio; (F), Biliprotein: C ratio. Circled data in (1-A) and (1-B) indicate presence of extra phosphorus and nitrogen in the culture, respectively. We have obtained the permission for reproducing these figures.

Here, in order to study light-nutrient co-limitation of phytoplankton growth, we have developed a steady state macromolecular model of phytoplankton, the “cell flux model for phytoplankton”. The model is more physiologically detailed than Monod or Droop kinetics, yet simple enough for transparency and computational capability. We have developed and applied the model in describing the characteristics of *Synechococcus* spp. growing in continuous, chemostat culture by Healey (1985) since this paper has one of the most comprehensive steady-state-culture data including biomass carbon concentration, elemental ratios, and pigments to carbon ratios (Figure 4.1).

In the data set of Healey (1985), there are some important features. First, in the P limiting culture, P:C ratio increase non-linearly with dilution rate while N:C ratio increase linearly. The linear trend of N:C ratio is repeatedly observed (e.g. Caperon and Meyer, 1972; Laws and Caperon, 1976; Laws and Bannister, 1980; Healey, 1985; Claquin *et al.*, 2002; Flynn, 2008), while P:C ratio is non-linear in most cases (e.g. Healey, 1985; Claquin *et al.*, 2002; Flynn, 2008). What causes this difference? Second, while N:C ratio shows similar trends in the P and N limiting cases, there are significant differences in P:C ratios between those cases; P:C ratios do not show clear trends in the N limiting culture, and the values are much higher than those in P limiting cases. Can the model explain these differences: differences between N:C and P:C and differences between P:C in P limiting and N limiting cultures? Third, the max chlorophyll content decreases with increasing light intensities, but maximum observed growth rate increases with increasing light intensities. What causes this trend? Fourth, under low light intensity there is

higher P:C ratios and N:C ratios. What macromolecules are responsible for these changes? Finally, increasing dilution rate decreases the biomass carbon while increasing light intensity increase the population. Can we reproduce and mechanistically interpret these trends? In this chapter, we will address all these questions with the cell flux model.

With the model, we predict the size of different macromolecular pools under different light intensities, nutrient resource supplies (nitrogen and phosphorus), and growth rates. The model provides physiological and biochemical explanations of how light and nutrient co-limit the growth of phytoplankton as well as a simple tool for describing and predicting their growth response and elemental composition.

4.3 Methods

Choice of molecular pools and fluxes for the model

To predict light-nutrient co-limitation of the growth as well as macromolecular composition in the cell, we have developed a cell flux model for phytoplankton (Figure 4.3). The model consists of carbon, nitrogen, and phosphorus based molecular pools and fluxes among these pools, creating a simplified flux network. We have selected macromolecular pools that are essential to predict growth and stoichiometry (such as N:C and P:C ratio) of the cell. Those elemental ratios are necessary for predicting the population and standing stock of organic molecules in the steady state culture. In large-scale ocean simulations, these ratios regulate the efficiency of the ocean's carbon pumps and atmospheric CO₂. Hence a simple, practical and flexible description is valuable for climate and carbon cycle modeling.

Carbon metabolism

Resolved, carbon-based molecules are CO₂, carbohydrate (CH), chlorophyll, essential carbon, and other carbon such as lipid/carbohydrate storage (depicted in yellow for molecules and in orange for fluxes in Figure 4.3). CO₂ is essential for photosynthesis, or carbon fixation, which, in this model, provides 100% of carbon necessary for metabolism (anabolism and catabolism). Fixed carbohydrate (CH) is the central carbon metabolism, providing reduced carbon for various molecules, such as proteins, and energy for biosynthesis through respiration. Chlorophyll is essential for light harvesting, which provides energy and reducing equivalents for carbon fixation. We also account for a pool of “other essential carbon”, such as carbon in lipid bilayers in which is significant in restricting the cell volume available for other components. The remainder of the cell’s carbon is considered as stored carbon which is not essential for immediate growth. Protein and nucleic acids contain a substantial amount of carbon, and their carbon pools and fluxes are included in the model with a fixed, assumed C:N and C:P ratio typical of each macromolecular pool. Since they are more influential in nitrogen and phosphorus metabolism, we will discuss them in the following sections.

Nitrogen metabolism

Nitrogen metabolism is strongly influenced by protein, which usually accounts for the largest nitrogen pool in the cell (Nitrogen metabolism is depicted in pink for molecules and in red for fluxes in Figure 4.3). Predicting the amount of protein is essential in predicting growth of the cell, since most reactions related to biosynthesis are constrained by the availability of appropriate enzymes. In this model, we have considered three types of proteins; photosynthesis related proteins, biosynthesis related proteins, and other proteins. This choice is similar to the model by

Geider *et al.*, (1996, 1997, 1998). However, we have included all the proteins necessary for photosynthesis (such as RuBisCo, photosystems, and enzymes for the Calvin Cycle) into photosynthesis related protein, which varies with light intensity, while the model in Geider *et al.*, (1996, 1997, 1998) carbon fixing enzymes are included in biosynthetic apparatus. We have made this decision since not only light harvesting apparatus, but also the amount of enzymes and photosystems must vary depending on the light intensity. Thus, it is essential to separate those light dependent proteins from other biosynthesis related proteins.

By modeling the relative allocation towards these three pools of protein, we can accurately predict the variation of cellular N:C ratio based on light availability and dilution rate. Some other models such as Pahlow and Oschlies (2009) explicitly model the nitrogen allocated in transporters. In this model, however, we have included transporters in other proteins, since the mass of transporters was neither predictable based on the data from Healey (1985), nor was it essential in predicting the cellular N:C ratio. In general, the transporters are small molecules of about 100 kDa, and only cover a part of the cytoplasmic membrane. On the other hand, photosynthesis related protein covers a large area of thylakoid membranes (Szalontai *et al.*, 2000; Kirchhoff *et al.*, 2008), and there are multiple layers of thylakoid membranes (Rast *et al.*, 2015), leading to a large nitrogen quota. Therefore, we assumed that the light-nutrient-growth dependent variation of transporters need not be explicitly resolved. Finally, we have included nitrogen storage (here we assume cyanophycin (e.g. Borzi., 1887; Hai *et al.*, 1999)), since it was necessary to predict the difference in N:C ratios between N-limiting culture and P-limiting culture. Due to nitrogen storage, cells in P-limiting cultures have generally higher N:C ratios than those in N-limiting cultures.

Phosphorus metabolism

To keep the model simple, we have resolved the minimum number of phosphorus pools necessary for the prediction of cellular P:C ratios, and standing stock of biomass. The key aspect of phosphorus metabolism is RNA synthesis, since RNA generally accounts for the largest phosphorus pool in the cell (Geider and La Roche, 2002), and mediates protein synthesis and cell growth significantly. Since DNA can account for a substantial fraction of phosphorus (Bertilsson *et al.*, 2003), we have also explicitly included a DNA pool. The DNA generally increases with dilution rates, since the number of cells with double amount of the DNA increases.

In the process of developing the model, we unexpectedly found that the variation of phosphorus in thylakoid membrane can be important. The P:C data of Healey (1985) shows a higher P:C ratio for the low light conditions. We argue that this variation is due to the increased phosphorus in phospholipid in thylakoid membrane. Low light intensity leads to higher chlorophyll content, but in order to sustain additional chlorophyll, more thylakoid membrane is necessary, since thylakoid membrane is in general significantly dense with proteins and chlorophylls (Szalontai *et al.*, 2000; Kirchhoff *et al.*, 2008).

A high ratio of phospholipids and the size of thylakoid membrane can significantly affect cellular phosphorus quota. About 25% of the lipids used in the thylakoid membrane are phospholipids, which is a larger proportion than in cytoplasmic membrane (Huflejt, 1990). In addition, there are usually many layers of thylakoid membranes (Liberton *et al.*, 2006; Rast *et al.*, 2015) in the cell, leading to a significant amount of phosphorus in total. Therefore, we explicitly model the phosphorus flux to thylakoid membranes, their phosphorus content, and their contribution to the P:C ratio in the cell.

We have accounted for phosphorus storage in order to differentiate the cellular P:C ratio between N-limiting culture and P-limiting culture (Figure 4.2). In N-limiting culture, excess phosphorus is stored in the cell (e.g. Healey, 1985; Kromkamp, 1987), while in P-limiting culture, at steady state, virtually all the phosphorus is actively used for specific purposes. This results in a significant difference in P:C ratio between N-limiting culture and P-limiting culture observed in Healey (1985) with much higher P:C ratio in N-limiting culture. Finally, we have resolved a pool of “other essential phosphorus”, which includes ATP, dissolved phosphate groups, and phospholipids in cytoplasmic membranes. This other essential phosphorus provides the minimum level of phosphorus together with minimum requirement of DNA, RNA and thylakoid membrane phosphorus. This other essential phosphorus pool accounts for a substantial contribution to the total phosphorus budget since, even where minimum phosphorus content is expected (low dilution rate and high light intensity), a substantial amount of intracellular phosphorus is observed (Figure 4.2 (1-B)).

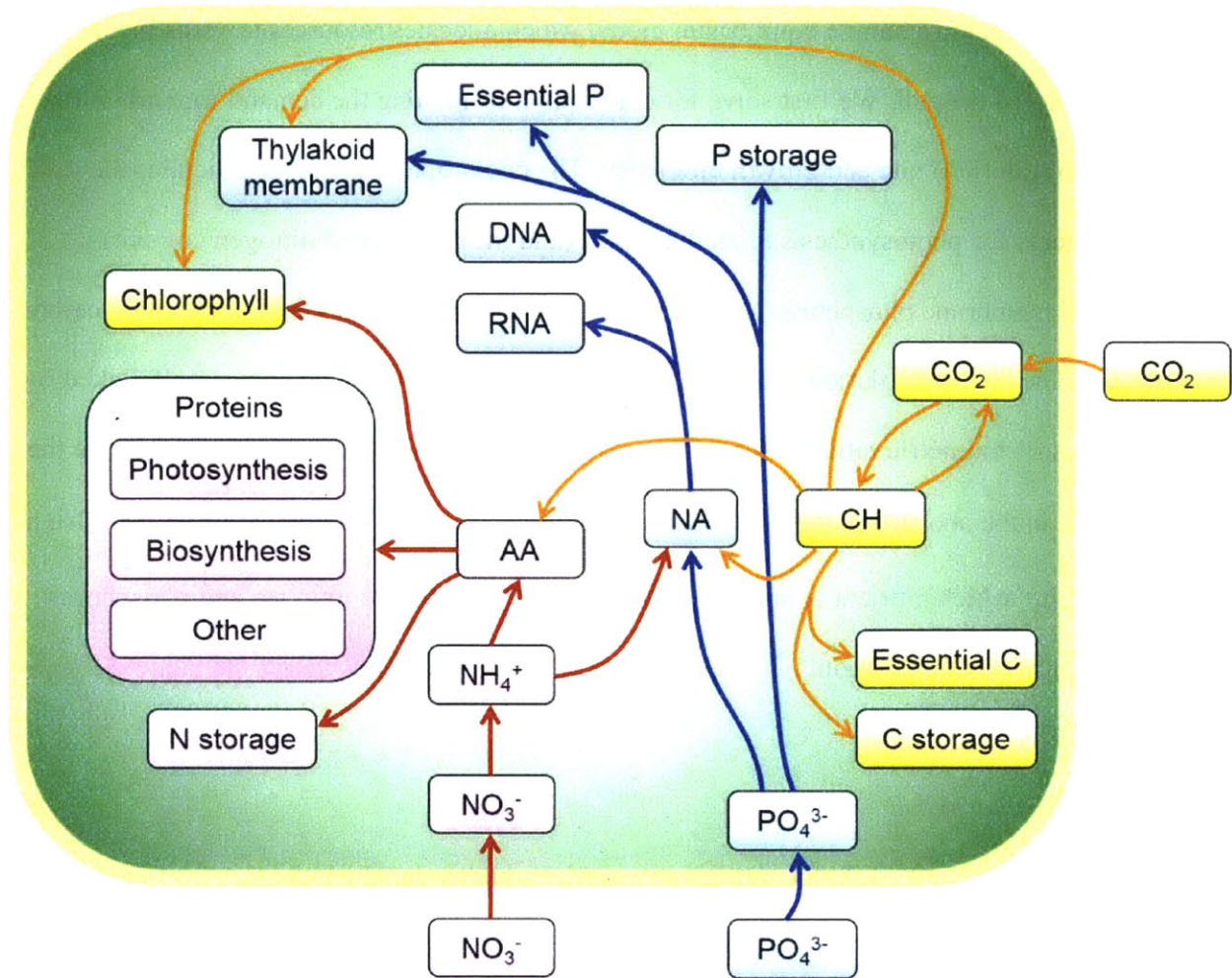


Figure 4.3 Schematic depiction of the cell flux model for phytoplankton. Orange outline, cell membrane layers; Green background, cytoplasm; Pink boxes, nitrogen based compounds; Blue boxes, phosphorus based compounds; Yellow boxes, carbon based compounds; Red arrows, nitrogen fluxes; Blue arrows, phosphorus fluxes; Orange arrows, carbon fluxes.

Model solutions

In order to solve the model for the macro-molecular composition at steady state, we have taken the following steps: solving for chlorophyll (equations (4.6) and (4.7)), solving for nitrogen pools (Table 4.1), solving for phosphorus pools (Table 4.2), solving for cell number density (equation (4.19)) and biomass carbon concentration, solving for stored nutrients, and solving for carbon pools (Table 4.3). Nomenclature with units is provided in Table 4.4.

We develop a simple equilibrium model which allocates resources towards the key components of the cell. We first solve for chlorophyll by relating the demand for carbon fixation to growth (dilution) rate and growth efficiency. The chlorophyll quota then dictates the requirements for photosynthesis related proteins (and their associated nitrogen content), thylakoid membrane phosphorus (and associated phosphorus content), and chlorophyll carbon content. The order of solution order is interchangeable, since N, P and C are simply linked by the imposed stoichiometric ratios of the macromolecular pools. However, we choose to solve the equations in the above order (N→P→C) for simplicity. To solve for population density, we need to determine which nutrient is limiting. Thus, we need to solve for nitrogen and phosphorus before computing population.

Solving for chlorophyll

To obtain cellular chlorophyll content, we consider a budget in which the sources and sinks of carbohydrate CH (see Figure 4.3) are in balance.

$$\frac{dCH}{dt} = ChlP_{Chl} - (1 + E)Q_C D - m \quad (4.5)$$

Definitions and unites for each term is listed in Table 4.4. Based on the assumption that there is no waste of carbon to the external environment, the balance around CH gives one solution for chlorophyll content with high predictive capability. Since in the steady state, the CH production and consumption has to be balanced, we can solve for cellular chlorophyll content:

$$Chl = \frac{(1 + E)Q_C D + m}{P_{Chl}} \quad (4.6)$$

We employ a description of photosynthesis based on “target theory” as used in many other studies (ex. Webb *et al.*, 1974; Platt *et al.*, 1980; Cullen, 1990; Geider *et al.*, 1996, 1997, and 1998):

$$P_{Chl} = P_{Chl}^{max} \left(1 - e^{-A_{pho}I} \right). \quad (4.7)$$

While other parameterizations of photosynthesis might be considered, this form provides a good fit to the data from Healey (1985).

Solving for nitrogen related parameters

To predict the population and growth of phytoplankton, obtaining cellular nitrogen content and its allocation amongst cellular functions is crucial. Here we present the solution for each nitrogen pool (Table 4.1). Nitrogen in chlorophyll N_{Chl} is obtained from chlorophyll content (equation (4.6) above) and an assumed N:C ratio (equation (4.8)). We assume that the quota of photosynthesis related proteins $N_{Protein}^{Photo}$ will vary in proportion to chlorophyll since both are necessary to harvest light and fix carbon. We then evaluate $N_{Protein}^{Photo}$ through a stoichiometric factor $Y^{N_{Photo}:Chl}$. This is not known *a priori*, but can be constrained using the data from Healey (1985). This photosynthetic protein includes proteins in PSI and PSII complexes, RuBisCO, and other photosynthetic proteins. Healey (1985) shows an identical trend between chlorophyll and biliprotein (one of the pigment proteins), indicating that in this particular case, the photo adaptation is not done by increasing the size of antenna, but by increasing the size/number of thylakoid membranes. Given this, the amount of protein in/on thylakoid membranes is proportional to chlorophyll, which in turn support equation (4.9). This assumption is also

supported by the observation that (for plants) there is generally a positive correlation between chlorophyll and RuBisCO (Seemann *et al.*, 1987).

In order to predict the cellular allocation to biosynthesis protein, we linearly relate the amount of biosynthesis protein, $N_{Protein}^{Biosynth}$, to the dilution rate D (equation (4.10)). This is based on the idea that faster growth requires faster production of biomass, which in turn requires higher amount of biosynthetic enzyme. Together, equations (4.9) and (5) anticipate the roughly linear relationship between N:C ratio and dilution rate as is repeatedly observed in laboratory studies (e.g. Caperon and Meyer, 1972; Laws and Caperon, 1976; Laws and Bannister, 1980; Healey, 1985; Claquin *et al.*, 2002; Flynn, 2008). With obtained $N_{Protein}^{Photo}$, $N_{Protein}^{Biosynth}$, and $N_{Protein}^{const}$ (essential protein necessary for cell maintenance; the parameterization described in the Supplementary Material), we can compute the total amount of protein $N_{Protein}$ (equation (4.11)). In general, $N_{Protein}$ accounts for the largest part of cellular nitrogen content. However, nitrogen in nucleic acids (RNA and DNA in this model) also contribute significantly.

We assume that the RNA content is a function of both dilution rate and protein content (equation (4.12)), with a constant part and dilution/growth dependent part. The constant part N_{RNA}^{const} indicates minimum requirement of RNA, perhaps related to protein turnover. The dilution/growth dependent part is influenced by the amount of protein, and dilution rate. We assume a linear relationship between the RNA required to build and maintain a given protein quota and also a linear relationship between the RNA quota and growth rate. Since the protein content is also linearly linked to dilution rate, N_{RNA} in equation (4.12) is a quadratic function of the dilution rate.

We have defined DNA as a linear function of the dilution rate (equation (4.13)). The macromolecular study of *E. coli* (Bremer and Dennis, 1996) shows almost linearly increasing DNA with the dilution rate, since fast growing culture has higher numbers of cells with both new replicated DNA and template DNA, increasing DNA content. However, in this particular study we have assumed that the variation of DNA content with dilution is small since the range of dilution rates of Healey (1985) is much smaller than that of Bremer and Dennis (1996). We define the total essential nitrogen quota, $Q_N^{essential}$, as the sum of allocations to chlorophyll, protein, RNA and DNA in equation (4.14).

Table 4.1 Fundamental relations of cell nitrogen components.

$$N_{Chl} = ChlY_{Chl}^{N:C} \quad (4.8)$$

$$N_{Protein}^{Photo} = ChlY^{Npho:Chl} \quad (4.9)$$

$$N_{Protein}^{Biosynth} = DA_{Biosynth}^N \quad (4.10)$$

$$N_{Protein} = N_{Protein}^{const} + N_{Protein}^{Photo} + N_{Protein}^{Biosynth} \quad (4.11)$$

$$N_{RNA} = N_{RNA}^{const} + N_{Protein} DA_{RNA}^N \quad (4.12)$$

$$N_{DNA} = N_{DNA}^{const} + DA_{DNA}^N \quad (4.13)$$

$$Q_N^{essential} = N_{Chl} + N_{Protein} + N_{RNA} + N_{DNA} \quad (4.14)$$

Solving for phosphorus related parameters

The phosphorus quota for key macromolecules can be obtained from chlorophyll, and nitrogen quotas obtained above (Table 4.2). Specifically, the phosphorus in thylakoid membrane is taken to be linearly related to chlorophyll (equation (4.15)), necessary for complete and functional light

harvesting. To evaluate phosphorus in RNA and DNA, we assume an empirical N:P ratio in these molecules (equation (4.16) and (4.17) and the parameterization in Supplementary Material). In addition there are other essential phosphorus pools including phospholipids in the cytoplasmic membrane and ATP. These are included in the term P_{Other}^{const} , which we assume is constant (the parameterization is described in Supplementary Material). With (4.15)~(4.17) and P_{Other}^{const} we can evaluate the total quota for essential phosphorus, $Q_P^{essential}$ (equation (4.18)).

Table 4.2 Fundamental relations of cell phosphorus components.

$$P_{Thylakoid} = Chl Y_{Thylakoid}^{P:Chl} \quad (4.15)$$

$$P_{RNA} = N_{RNA} Y_{RNA}^{P:N} \quad (4.16)$$

$$P_{DNA} = N_{DNA} Y_{DNA}^{P:N} \quad (4.17)$$

$$Q_P^{essential} = P_{Other}^{const} + P_{Thylakoid} + P_{RNA} + P_{DNA} \quad (4.18)$$

Solving for the cell population density and determining a limited nutrient

In order to obtain the cell population density, we assume that the concentration of limiting nutrient in the medium (at steady state) is small compared to that in the incoming medium. This applies to most cases in Healey (1985) and with this assumption, the cell population density X (cell m^{-3}) is obtained simply by dividing the concentration of limited nutrient $[Nut_{Limiting}]_N$ by the cellular quota of the limited nutrient $Q_{Nut-limiting}^{essential}$:

$$X = \frac{[Nut_{Limiting}]_{IN}}{Q_{Nut-limiting}^{essential}}. \quad (4.19)$$

In this study, the limiting nutrient is either nitrogen or phosphorus. In order to determine which nutrient is limiting, we compute X value based on both phosphorus and nitrogen. The nutrient that leads to the lower X value is assumed to be limiting and the population size is set accordingly. From X and cellular carbon quota Q_C , biomass carbon concentration $[B_C]$ can be obtained as follows:

$$[B_C] = XQ_C. \quad (4.20)$$

Solving for stored nutrients

Phytoplankton can store non-limiting nutrients available in excess. However, the magnitude of nutrient they store differs based on the nutrient. For example, based on the data from Healey (1985), the amount of nitrogen stored is relatively small compared to other nitrogen use. This is implied by the similarity of N:C ratios between N and P limiting cultures to the essential nitrogen use (comparing Figure 4.2 (1-C) and (2-C)), while there is an upper limit of phosphorus for the sum of all the phosphorus quotas in the cell (comparing Figure 4.2 (1-C) and (2-C)). In order to express those differences, we formulate different equations for each nutrient.

First, to evaluate nitrogen storage (in the P-limited case), we first define the maximum nitrogen storage N_{Store}^{max} (the parameterization is in the Supplementary Material), and obtain the maximum potential nitrogen quota based on N_{Store}^{max} :

$$Q_N^{max-Store} = N_{Store}^{max} + Q_N^{essential} \quad (4.21)$$

To account for the availability of excess nitrogen in the medium, we compute the maximum possible nitrogen quota based on the nitrogen concentration in the incoming medium and the population:

$$Q_N^{max-Nin} = \frac{[N]_{IN}}{X_P}. \quad (4.22)$$

If $Q_N^{max-Nin} > Q_N^{max-Store}$, the actual total nitrogen quota $Q_N = Q_N^{max-Store}$ and the actual nitrogen storage $N_{Store} = N_{Store}^{max}$. On the other hand, if $Q_N^{max-Nin} < Q_N^{max-Store}$, $Q_N = Q_N^{max-Nin}$ and N_{Store} is lower than N_{Store}^{max} , and computed from Q_N :

$$N_{Store} = Q_N - Q_N^{essential}. \quad (4.23)$$

When nitrogen is limiting, there is likely phosphorus storage, which is computed in a similar way. Since total phosphorus quota has its maximum based on the data from Healey (1985), we first define the maximum phosphorus quota $Q_P^{max-Cell}$. We compute the potential phosphorus quota from the phosphorus concentration in the incoming media:

$$Q_P^{max-Pin} = \frac{[P]_{IN}}{X_N}. \quad (4.24)$$

If $Q_P^{max-Cell} < Q_P^{max-Pin}$, the actual phosphorus cell quota $Q_P = Q_P^{max-Cell}$, but if $Q_P^{max-Cell} > Q_P^{max-Pin}$, $Q_P = Q_P^{max-Pin}$. In both cases, the phosphorus storage is computed as follows:

$$P_{Store} = Q_P - Q_P^{essential}. \quad (4.25)$$

Solving for carbon related parameters

For molecules that involve phosphorus and nitrogen, we stoichiometrically relate phosphorus or nitrogen quotas to carbon quotas (Table 4.1, equation (4.26)–(4.30)). For essential carbon that

cannot be obtained from phosphorus or nitrogen quotas, we define $C_{Essential}$, which includes lipid membrane and structural carbon products (see Supplementary Material for the parameterization). We assume that the total carbon quota Q_C is constant as Healey (1985) did not find any trends in the carbon quota. We have applied slightly different values for Q_C for phosphorus and nitrogen limited cases based on Healey (1985). With this Q_C and other carbon values, we compute the rest of non-essential stored carbon C_{Store} (equation (4.31)).

Table 4.3 Fundamental relations of cell carbon components.

$$C_{P-lipid}^{Thylakoid} = P_{Thylakoid} Y_{P-lipid}^{C:P} \quad (4.26)$$

$$C_{Protein} = N_{Protein} Y_{Protein}^{C:N} \quad (4.27)$$

$$C_{RNA} = N_{RNA} Y_{RNA}^{C:N} \quad (4.28)$$

$$C_{DNA} = N_{DNA} Y_{DNA}^{C:N} \quad (4.29)$$

$$C_{Nstore} = N_{Store} Y_{Nstore}^{C:N} \quad (4.30)$$

$$C_{Store} = Q_C - Chl - C_{Protein} - C_{RNA} - C_{DNA} - C_{Essential} \quad (4.31)$$

Table 4.4 Symbols, definitions and units used in the model. The symbols are listed in order of appearance.

CH	Cellular intermediate carbohydrate	Mol C cell ⁻¹
t	Time	s
Chl	Cellular chlorophyll	mol C cell ⁻¹
E	CO ₂ production ratio	dimensionless
Q_C	Cellular carbon quota	mol C cell ⁻¹
D	Dilution rate: averaged growth rate	s ⁻¹
m	Maintenance carbon consumption	mol C cell ⁻¹ s ⁻¹
P_{Chl}	Photosynthesis rate per chlorophyll	s ⁻¹
P_{Chl}^{max}	Maximum photosynthesis rate per chlorophyll	s ⁻¹
A_{PHO}	Power coefficient for photosynthesis	μE ⁻¹ m ² s
I	Light intensity	μE m ⁻² s ⁻¹
N_{Chl}	Cellular nitrogen in chlorophyll	mol N cell ⁻¹
$Y_{Chl}^{N:C}$	N:C ratio in chlorophyll	mol N mol C ⁻¹
$N_{Protein}^{Photo}$	Cellular nitrogen in photosynthetic protein	mol N cell ⁻¹
$Y^{Npho:Chl}$	$N_{Protein}^{Photo} : Chl$	mol N mol C ⁻¹
$N_{Protein}^{Biosynth}$	Cellular nitrogen in biosynthesis protein	mol N cell ⁻¹
$A_{Biosynth}^N$	Biosynthesis protein coefficient	mol N cell ⁻¹ s
$N_{Protein}$	Total cellular nitrogen in protein	mol N cell ⁻¹

$N_{Protein}^{const}$	Cellular nitrogen in other protein	mol N cell ⁻¹
N_{RNA}	Cellular nitrogen in RNA	mol N cell ⁻¹
N_{RNA}^{const}	Cellular nitrogen in constant parts of RNA	mol N cell ⁻¹
A_{RNA}^N	Coefficient for variable cellular nitrogen in RNA	s
N_{DNA}	Cellular nitrogen in DNA	mol N cell ⁻¹
N_{DNA}^{const}	Cellular nitrogen in constant parts of DNA	mol N cell ⁻¹
A_{DNA}^N	Coefficient for variable cellular nitrogen in DNA	mol N cell ⁻¹ s
$Q_N^{essential}$	Cellular nitrogen quota	mol N cell ⁻¹
$P_{Thylakoid}$	Cellular phosphorus in thylakoid membranes	mol P cell ⁻¹
$Y_{Thylakoid}^{P:Chl}$	$P_{Thylakoid} : Chl$	mol P mol C ⁻¹
P_{RNA}	Cellular phosphorus in RNA	mol P cell ⁻¹
$Y_{RNA}^{P:N}$	P-N ratio in RNA	mol P mol N ⁻¹
$Y_{DNA}^{P:N}$	P-N ratio in DNA	mol P mol N ⁻¹
$Q_P^{essential}$	Essential cellular phosphorus quota	mol P cell ⁻¹
X	Number density of cells	cell m ⁻³
$[Nut_{Limiting}]_{IN}$	Concentration of growth limiting nutrient in the incoming medium	mol m ⁻³
$Q_{Nut-limiting}^{essential}$	Cellular quota of growth limiting nutrient	mol cell ⁻¹
$[B_C]$	Biomass carbon concentration in the culture	mol C m ⁻³

$Q_N^{max-Store}$	Maximum cellular quota of nitrogen based on nitrogen storage	mol N cell ⁻¹
N_{Store}^{max}	Maximum cellular nitrogen storage	mol N cell ⁻¹
$Q_N^{max-Nin}$	Maximum cellular quota of nitrogen based on nitrogen concentration in the incoming medium	mol N cell ⁻¹
$[N]_{IN}$	Nitrogen concentration in the incoming medium	mol N m ⁻³
X_P	Number density of cells in the phosphorus limited culture	cell m ⁻³
Q_N	Cellular nitrogen quota	mol N cell ⁻¹
N_{Store}	Cellular nitrogen storage	mol N cell ⁻¹
$Q_P^{max-Cell}$	Maximum cellular quota of phosphorus based on cellular capacity of holding phosphorus	mol P cell ⁻¹
$Q_P^{max-Pin}$	Maximum cellular quota of phosphorus based on phosphorus concentration in the incoming medium	mol P cell ⁻¹
$[P]_{IN}$	Phosphorus concentration in the incoming medium	mol P m ⁻³
X_N	Number density of cells in the nitrogen limited culture	cell m ⁻³
Q_P	Cellular phosphorus quota	mol P cell ⁻¹
P_{Store}	Cellular phosphorus storage	mol P cell ⁻¹
$C_{P-lipid}^{Thylakoid}$	Cellular carbon in phospholipids in thylakoid membranes	mol C cell ⁻¹
$Y_{P-lipid}^{C:P}$	C-P ratio in phospholipids	mol C mol P ⁻¹
$C_{Protein}$	Cellular carbon in protein	mol C cell ⁻¹

$Y_{Protein}^{C:N}$	C:N ratio in protein	mol C mol N ⁻¹
C_{RNA}	Cellular carbon in RNA	mol C cell ⁻¹
$Y_{RNA}^{C:N}$	C:N ratio in RNA	mol C mol N ⁻¹
C_{DNA}	Cellular carbon in DNA	mol C cell ⁻¹
$Y_{DNA}^{C:N}$	C:N ratio in DNA	mol C mol N ⁻¹
$C_{Essential}$	Essential cellular carbon	mol C cell ⁻¹
C_{Store}	Other cellular carbon	mol C cell ⁻¹

4.4 Results and discussions

The model described above reproduces the data of Healey (1985) by tuning 12 parameters (parameterizations are described in the supplementary material). The same parameter set qualitatively and quantitatively captures the key features of the laboratory cultures both in phosphorus and nitrogen limited conditions. (Figure 4.4 ~ Figure 4.6 for phosphorus limited culture, and Figure 4.7 ~ Figure 4.9 for nitrogen limited culture). It identifies the light and dilution rate dependent variation of key parameters, such as chlorophyll, cellular N:C and P:C ratios, and cellular carbon concentrations in the culture. The model explains why the P:C ratio non-linearly increase with dilution rate while N:C ratio increase rather linearly. In addition, by quantifying the allocation of each element (Figure 4.5 ~ Figure 4.6 for phosphorus limited culture, and Figure 4.8 ~ Figure 4.9 for nitrogen limited culture), the model predicts differences between nitrogen and phosphorus storage. In the following discussion, we show that not only have we been able to capture cell stoichiometry and efficiency of nutrient storage, the model also predicts the maximum growth rate. This prediction is enabled by the allocation model and the finite volume of the cell, which is imposed. Allocation beyond this maximum cannot be exceeded, placing a finite limit on growth rates under different conditions. Finally, the model explains that the variation of biomass carbon concentration is indirectly influenced by growth rates, light intensity, through cellular stoichiometry, and directly influenced by nutrient resources.

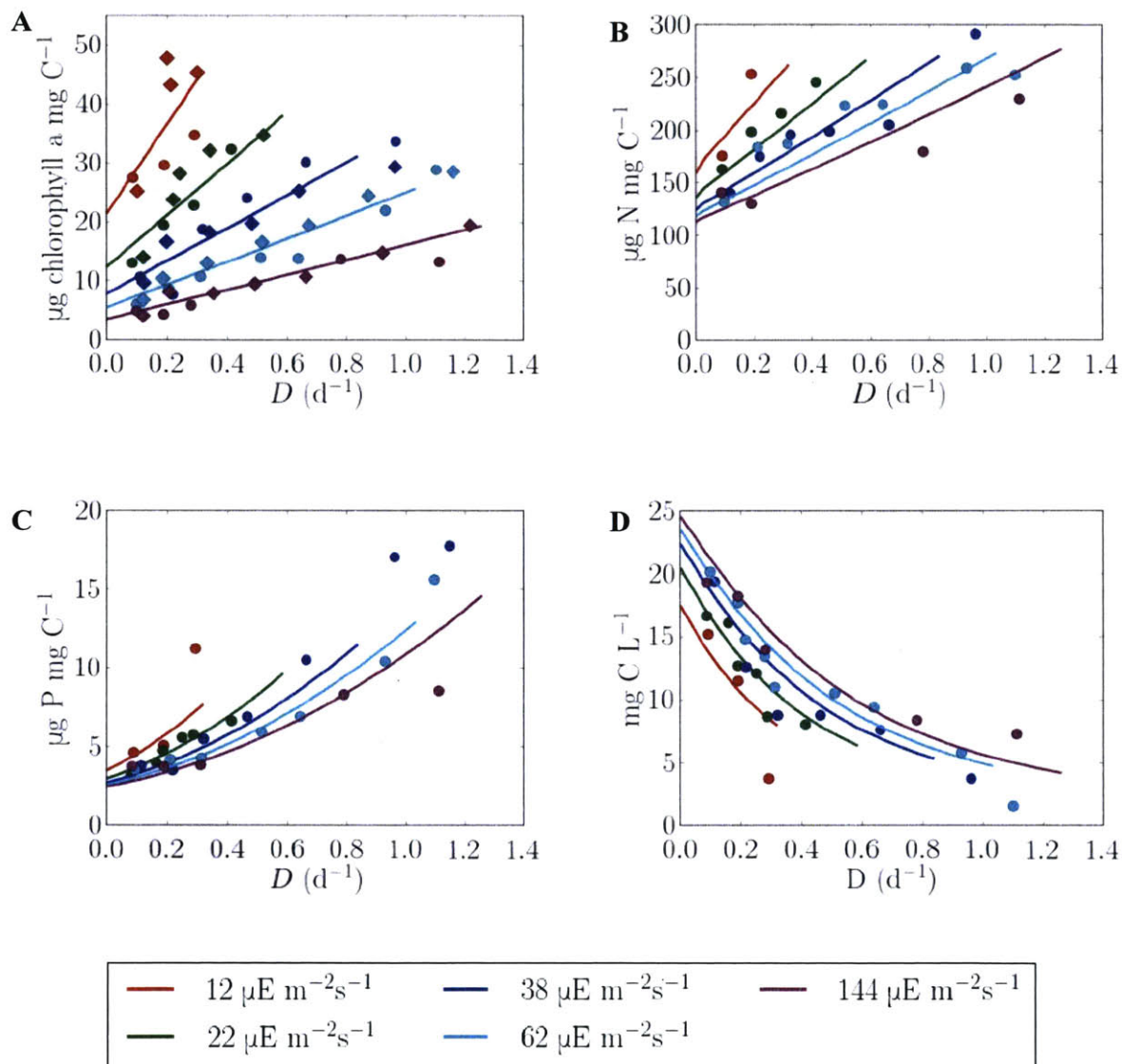


Figure 4.4 Simulation of phosphorus limited continuous culture of *Synechococcus* spp. compared with the laboratory data of Healey (1985). Solid lines are the corresponding simulations from this work. (A) Chlorophyll to carbon ratio. (B) Nitrogen to carbon ratio. (C) Phosphorus to carbon ratio. (D) Cellular carbon concentration in the culture.

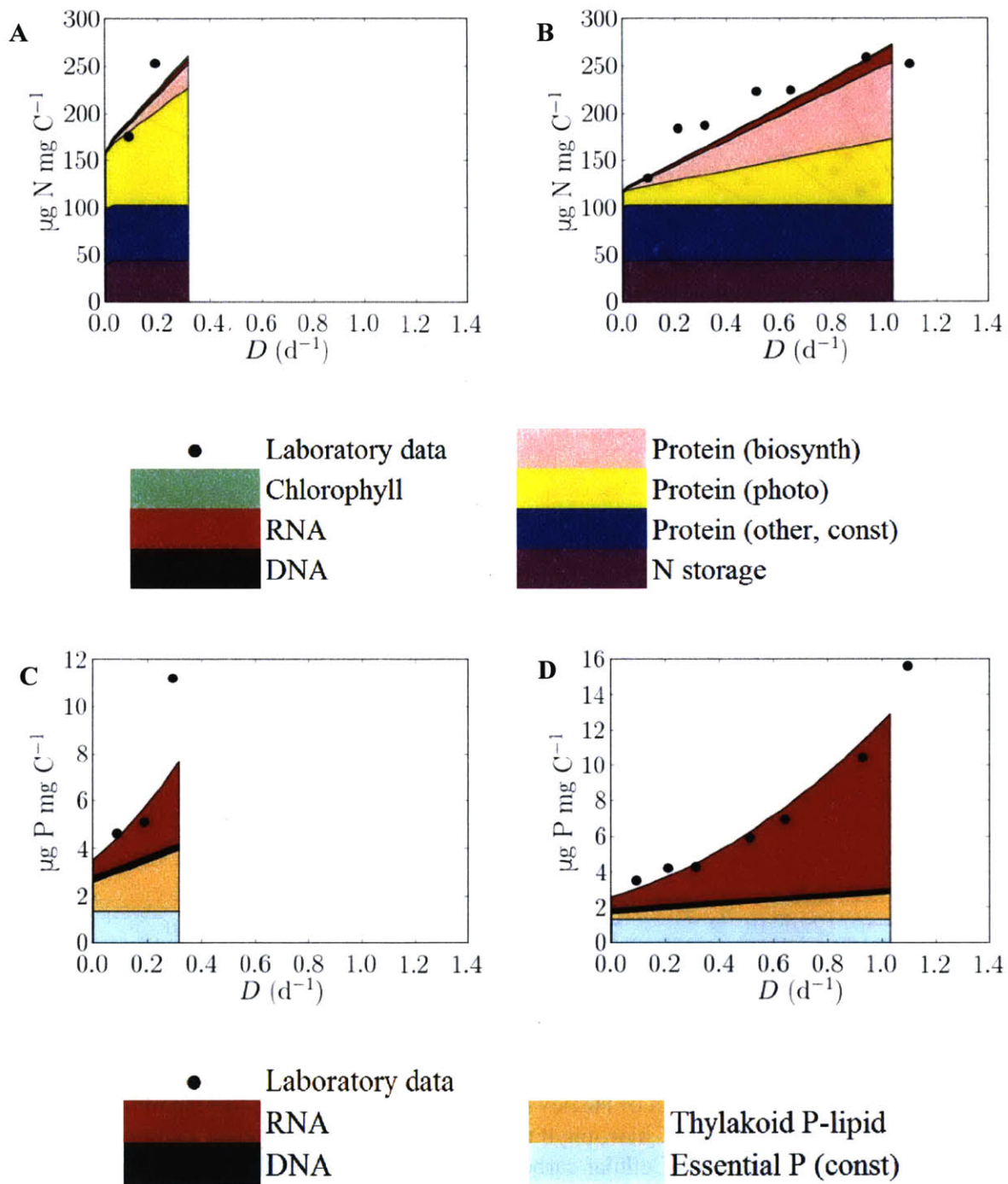


Figure 4.5 Allocation of cellular nitrogen and phosphorus in PHOSPHORUS limited continuous culture in different light intensities. Nitrogen and phosphorus allocation is normalized by cellular carbon. (A) Nitrogen allocation at 12 $\mu\text{E m}^{-2}\text{s}^{-1}$ light intensity. (B)

Nitrogen allocation at $62 \mu\text{E m}^{-2}\text{s}^{-1}$. (C) Phosphorus allocation at $12 \mu\text{E m}^{-2}\text{s}^{-1}$. (D) Phosphorus allocation at $62 \mu\text{E m}^{-2}\text{s}^{-1}$.

Difference between N:C and P:C curves

As discussed in the Introduction, the dependence of N:C and P:C vary differently with respect to dilution rate, and with respect to the limiting resource. The model provides some insight into the controls on those relationships.

We have successfully simulated the difference between N:C and P:C curves ((B) and (C) in Figure 4.4 and Figure 4.7). The key difference is that N:C increases roughly linearly with dilution rate, but when phosphorus is limited, P:C increases non-linearly. This difference is explained by examining what influences the slope of the curve. The slope of the N:C ratio with dilution rate is mostly driven by protein (for biosynthesis and photosynthesis), which increases linearly to the dilution rate to support faster growth and photosynthesis ((A) and (B) in Figure 4.5 and Figure 4.8). On the other hand, the slope of P:C with respect to dilution is mostly influenced by RNA, which increase non-linearly ((A) and (B) in Figure 4.5). This non-linearity is based on equation (4.12) and (4.16) since $N_{Protein}$ increases with dilution rate.

In order to further explain the difference between N:C and P:C curves, we need to consider the N-Storage and P-Storage. The model reveals a clear difference between N-storage (Figure 4.5 (A) and (B)) and P-storage strategies and potential of the cells (Figure 4.8 (C) and (D)). First, as discussed in the method section, nitrogen storage is independent from the total nitrogen in the cell, but the capacity of phosphorus storage varies depending on how much total phosphorus exists in the cell. For example, in Figure 4.8 (C) and (D), as dilution rate increases, more phosphorus is used in RNA, at the expense of P storage.

Second, the cell stores larger amount of nitrogen than phosphorus: about 45 mol $\mu\text{g N mg C}^{-1}$ against 25 $\mu\text{g P mg C}^{-1}$. However, more phosphorus can be stored relative to the requirement for essential macromolecules; at low dilution rate, many times more phosphorus than that necessary is stored (Figure 4.8 (C) and (D)). Such storage is not possible for nitrogen, since it would form much larger fraction of the cellular mass. Considering those differences can be important in studying aquatic ecosystem and biogeochemical cycles.

Here we note that we have assumed that the constant value for the essential P, and we hypothesizes that most essential P is for phospholipids in the cytoplasmic membrane. Although a constant value is assumed due to the limited data, the phosphorus content of the phytoplankton membranes can vary (e.g. Huflejt *et al.*, 1990, Van Mooy *et al.*, 2009, Lepetit *et al.*, 2012). Especially, in the phosphorus limited environment, phospholipids may be replaced by sulfolipids, decreasing phosphorus demand (Van Mooy *et al.*, 2009).

Our model shows that the phosphorus in phospholipids (both in cytoplasmic and thylakoid membranes) accounts for up to about 70% of cellular phosphorus under low irradiance at zero growth rate. This prediction agrees with the observation that more than half of phosphate is allocated to phospholipids (Van Mooy *et al.*, 2006), and supports the idea that replacing the phospholipids to sulfolipids significantly decreases the phosphorus demand (Van Mooy *et al.*, 2006). In addition, our model indicates that the replacement can save phosphorus more significantly in a low light environment, if phospholipids in thylakoid membrane can be replaced by sulfolipids, since thylakoid membrane content is higher under low light intensity.

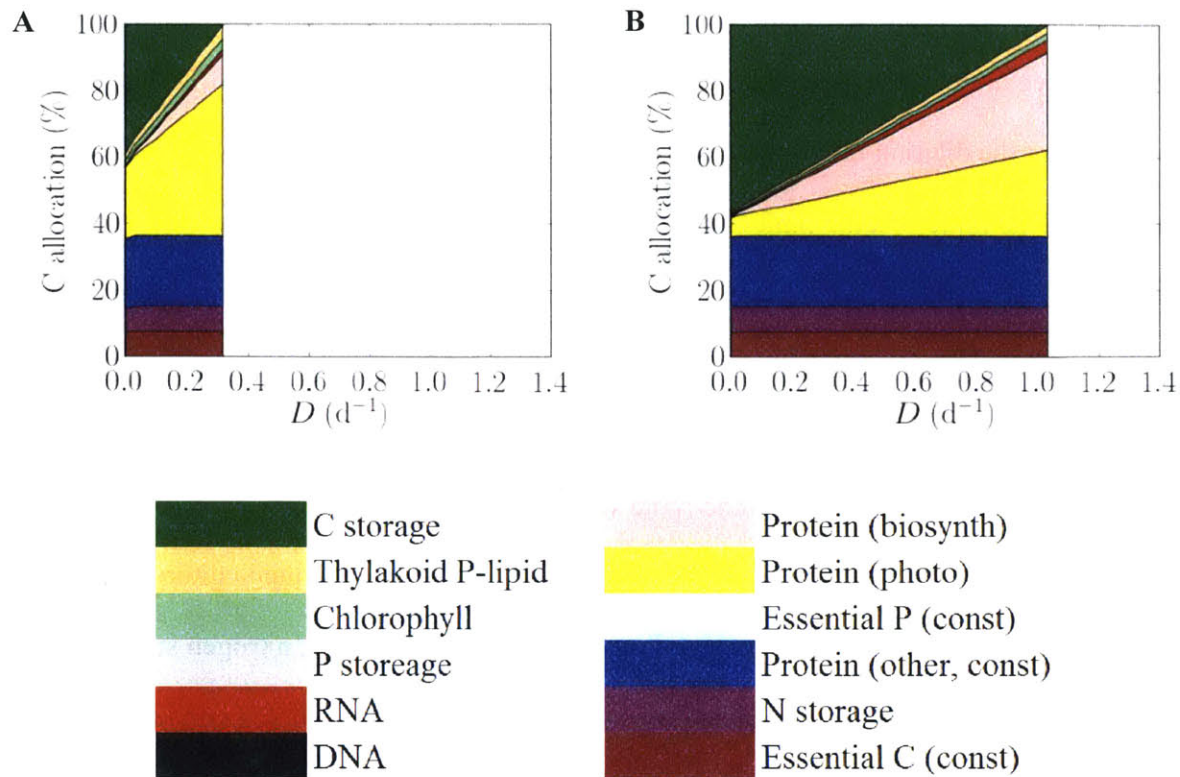


Figure 4.6 Allocation of cellular carbon in phosphorus limited continuous culture in different light intensities. (A) at $12 \mu E m^{-2}s^{-1}$ light intensity. (B) at $62 \mu E m^{-2}s^{-1}$.

Prediction of maximum chlorophyll content as a result of finite cell volume.

The model predicts limits to growth rate and cell composition as a function of its finite volume.

Here we assume a fixed cell volume. (Clearly cells are somewhat variable, but for any given species there will be finite limits). In order for a population to grow faster, cells have to increase their protein and nucleic acid content. However, at some point this is capped by the finite volume of the cell. In order to estimate when the growth is volume limited, we have computed the allocation of cellular carbon as a function of dilution rate and for different light and nutrient conditions (Figure 4.6 and Figure 4.9 for phosphorus and nitrogen limited culture respectively).

When the carbon storage becomes zero due to the carbon allocation for growth related purposes, the growth is limited by volume as represented by the total carbon cell quota. When

photosynthetic and biosynthetic carbon allocation reach the limits allowed by cell volume they cannot produce more of the essential machinery or grow faster. In the chemostat, if this limit is reached before the dilution rate is matched, the cells are flushed away and a population cannot be maintained. This finite volume limit explicitly predicts the maximum growth rate for these cells under different conditions and are represented by the cut-offs of the modeled lines in Figure 4.4~Figure 4.6 and Figure 4.7~Figure 4.9, for both N and P limited cultures respectively. In other words, the lines have not been artificially truncated where the data ends; those terminations represent the end points indicated by the finite volume of the cells.

Notably, the cut-offs are higher in dilution rate in the nitrogen limited culture than in phosphorus limited one. This happens based on the difference in storage; nitrogen storage requires carbon while phosphorus storage does not. Under phosphorus limited condition extra nitrogen is stored, requiring additional carbon. Under nitrogen limited condition, however, excess phosphorus stored, but there is no nitrogen storage. Thus, there is no additional carbon required for storage, leading to a relatively higher cut-offs. This higher cut-off for nitrogen limited culture is supported by the laboratory data by Healey (1985), where they obtained data for generally higher growth rates for nitrogen limited cultures.

Prediction of Biomass carbon concentration for different dilution rate, light intensity, and nutrient resources.

The biomass carbon concentration in the medium decreases with the dilution rate but increases with light intensity (Figure 4.4 and Figure 4.7 (D)). This is explained by the equation for population (equation (4.19)), since under the assumption that the carbon content per cell is constant (which roughly applies to Healey (1985)), the biomass carbon is proportional to the

population (equation (4.19)). Based on equation (4.19), the population is influenced by the cellular quota of limited nutrients. Specifically, in the phosphorus limited culture, the population density is inversely proportional to the total phosphorus quota. This phosphorus quota increase with dilution rate is due to increasing demands for RNA and thylakoid membrane (Figure 4.5 (C) and (D)), which eventually leads to the decreased population, and thus decreased biomass carbon due to equation (4.19).

On the other hand, when nitrogen is limited, the cell population is inversely proportional to the total nitrogen quota. Since this nitrogen quota increases linearly with dilution rate mainly due to increasing biosynthetic and photosynthetic proteins, the population and biomass carbon in the culture decreases with dilution rate.

Light intensity also influences the biomass carbon. However, based on the model, this influence is rather indirect; it occurs through the amount of photosynthesis related macromolecules. For example, when the light intensity is low, the cell contains higher amount of thylakoid membrane, requiring a higher amount of phosphorus for the same dilution rate (comparing Figure 4.5 (C) and (D)). This higher phosphorus quota in turn leads to the lower population (equation (4.19)), thus lower biomass carbon, under phosphorus limited culture. On the other hand, when the light intensity is high, there is smaller amount of thylakoid membrane (comparing Figure 4.5 (C) and (D)), leading to a low phosphorus quota, thus, higher population and biomass carbon in phosphorus limited culture.

In nitrogen limited culture, the light intensity influences the amount of biomass carbon through photosynthetic proteins. As the light intensity decreases, there is a higher amount of photosynthetic protein for the same dilution rate (comparing Figure 4.8 (A) and (B)). This in turn leads to low population and biomass carbon through equation (4.19) . When the light intensity

increases, on the other hand, the photosynthetic protein decreases, which in turn increases the biomass carbon.

Finally, we can simply explain light-nutrient co-limitation of population/biomass carbon through equation (4.19) . Based on this equation, the population increases linearly with the incoming concentration of the limiting nutrient. As explained above, light intensity positively influences population through macromolecules. This understanding of light-nutrient co-limitation of population together with prediction of macromolecular composition for various dilution rates provides the bases for predicting light-nutrient co-limitation of the phytoplankton growth in a dynamic environment.

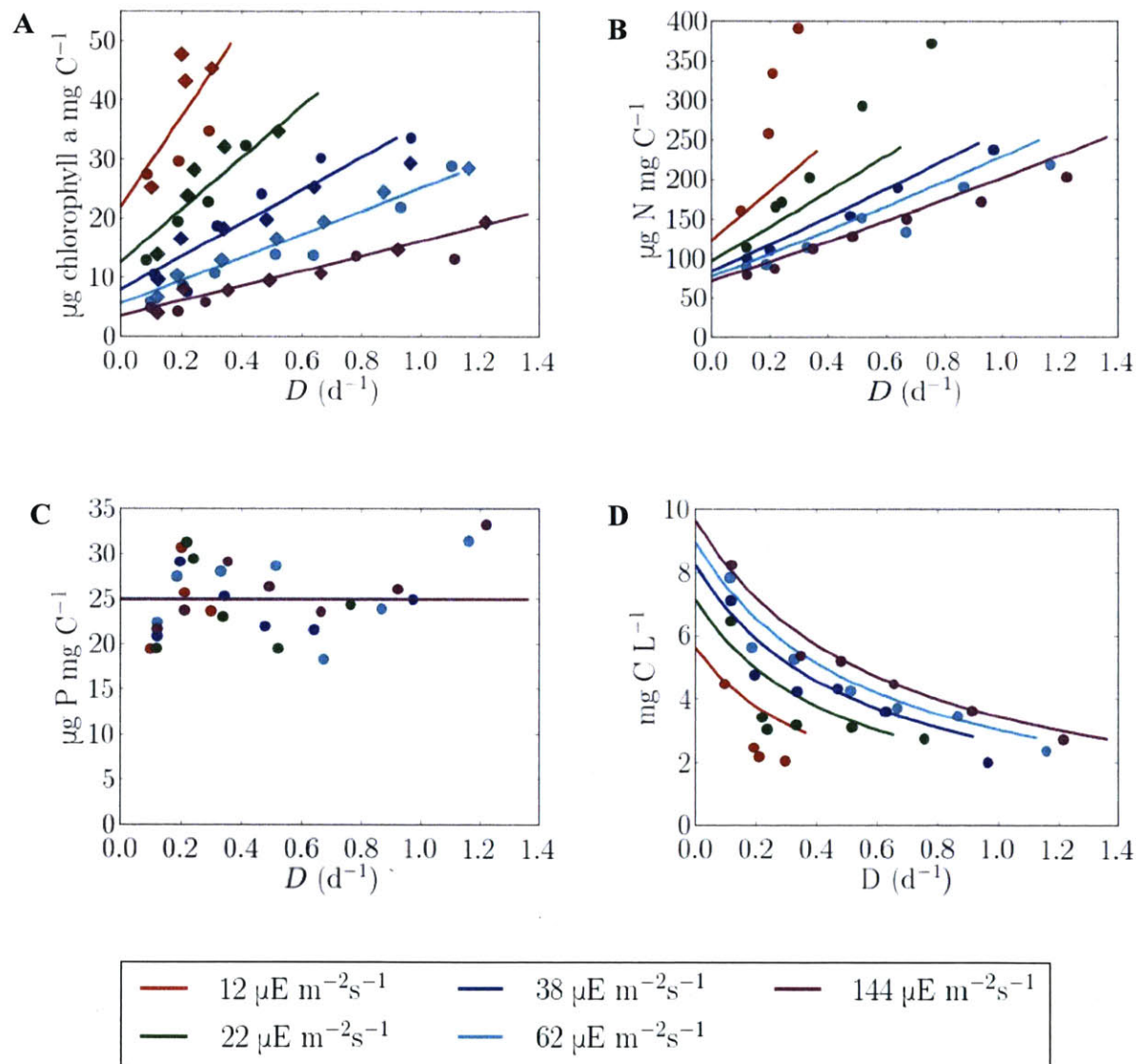


Figure 4.7 Simulation of nitrogen limited continuous culture of *Synechococcus* spp. compared with the laboratory data of Healey (1985). Solid lines are the corresponding simulations from this work. (A) Chlorophyll to carbon ratio. (B) Nitrogen to carbon ratio. (C) Phosphorus to carbon ratio. (D) Cellular carbon concentration in the culture.

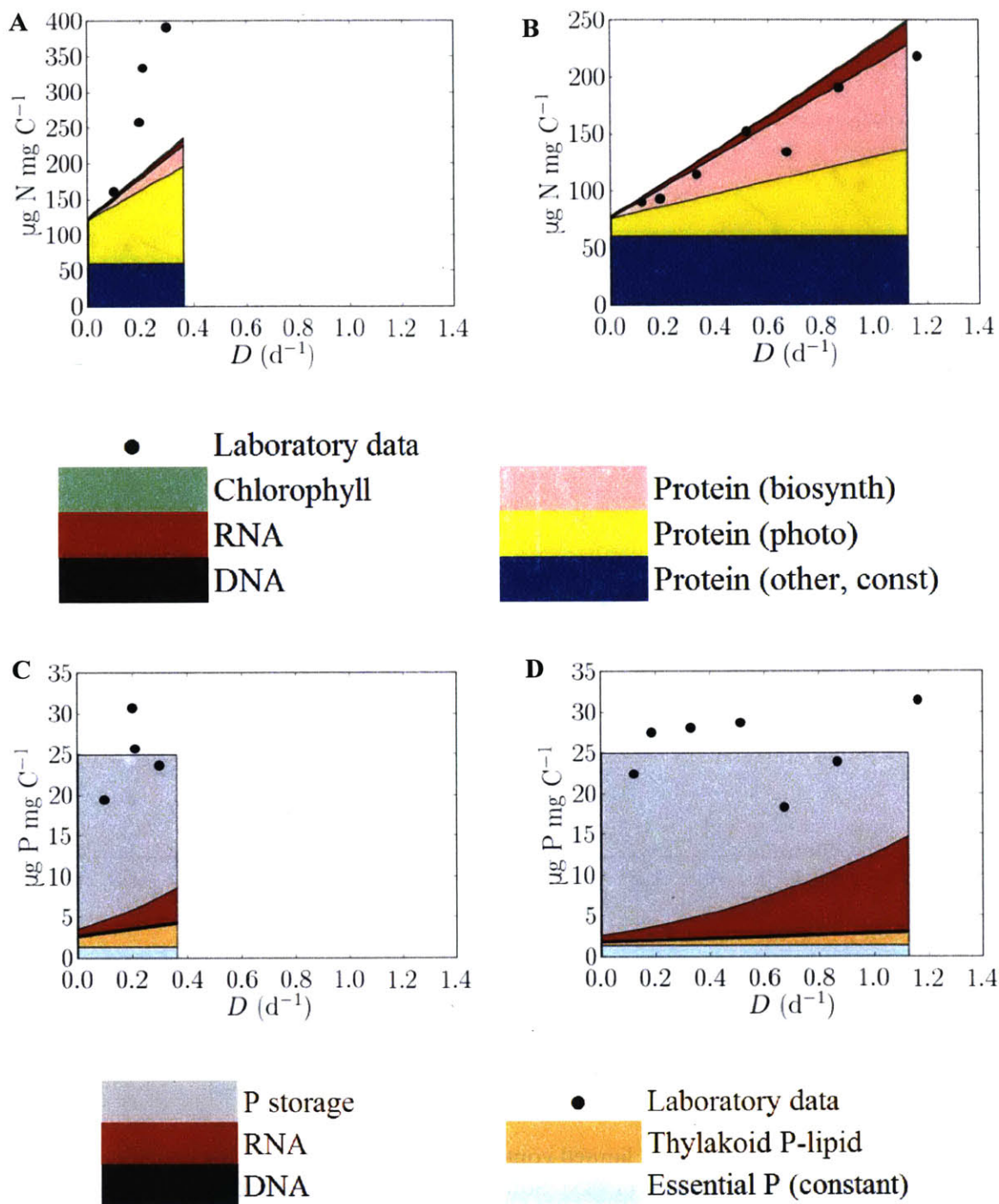


Figure 4.8 Allocation of cellular nitrogen and phosphorus in nitrogen limited continuous culture in different light intensities. Nitrogen and phosphorus allocation is normalized by cellular carbon. (A) Nitrogen allocation at $12 \mu\text{E m}^{-2}\text{s}^{-1}$ light intensity. (B) Nitrogen allocation at $62 \mu\text{E m}^{-2}\text{s}^{-1}$. (C) Phosphorus allocation at $12 \mu\text{E m}^{-2}\text{s}^{-1}$. (D) Phosphorus allocation at $62 \mu\text{E m}^{-2}\text{s}^{-1}$.

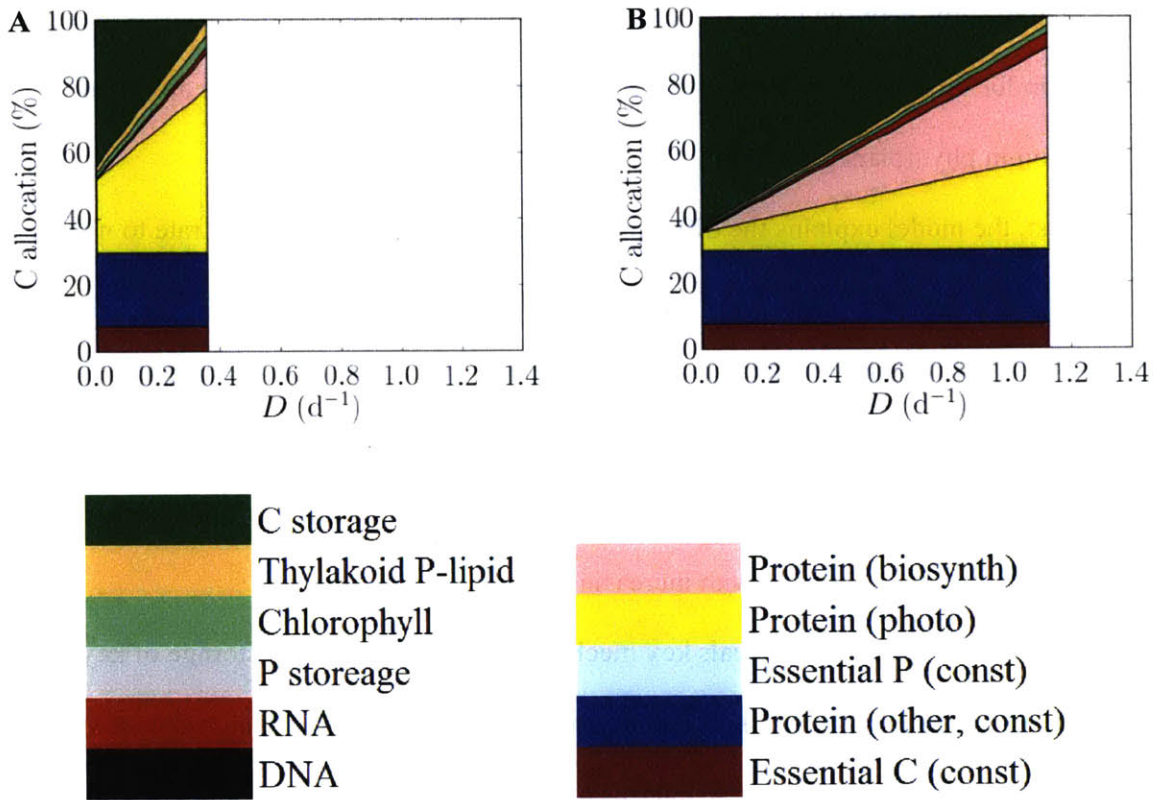


Figure 4.9 Allocation of cellular carbon in nitrogen limited continuous culture in different light intensities. (A) at $12 \mu E m^{-2}s^{-1}$ light intensity. (B) At $62 \mu E m^{-2}s^{-1}$.

4.5 Summary and conclusions

We have developed a cell flux model applied to phytoplankton to study the nutrient and light co-limitation of their growth. By resolving key macromolecular pools which have very different

C:N:P stoichiometries, the model can closely reproduce the experimental dataset of *Synechococcus* spp. in Healey (1985) when a set of 12 key parameters are tuned. Despite the apparently large number of tunable parameters, most values relate to simple (mostly linear) and logical relationships between rates and abundances. The model predicts the macromolecular composition for different light intensity and growth rates, and explains several observed phenomena in phytoplankton growth.

First, the model explains the differences in the relationships of growth rate to nitrogen and phosphorus quotas. Nitrogen quota is significantly influenced by protein, while phosphorus is mainly influenced by RNA. Since increasing dilution rate requires increasing photosynthesis and biosynthesis related protein, nitrogen quota increases roughly linearly with dilution rate. However, phosphorus quota increase quadratically, since RNA, the main influence on phosphorus quota, increases both with increasing protein and dilution rate.

Second, the model also reveals key mechanistic differences in the storage of key resources. While nitrogen storage is independent from other nitrogen use, phosphorus storage is influenced by the amount of other phosphorus quotas, since the maximum quota of total phosphorus is almost constant. Also, the absolute magnitude of nitrogen storage is larger than phosphorus. However, relative to the cellular requirements, much more phosphorus can be stored than nitrogen.

Third, the model indicates that the maximum chlorophyll quota is the result of volume limitation in the cell. In order to grow faster, the cell needs more proteins and other molecules. As the dilution rate in the culture increases, the abundance of such molecules is eventually limited by space, and this point is where chlorophyll shows the maximum value.

Finally, the model provides the basis for predicting population as a function of dilution rate, light intensity, and nutrient inputs. Higher dilution rates require a high cellular quota of limiting nutrient, leading to lower population for the given light and nutrient environment. Higher light intensity leads to lower requirement for the intracellular quota of limiting nutrient, leading to the higher population for a give dilution rate and incoming nutrient concentration. Finally, higher nutrient supply linearly increases population under the same dilution rate and light intensity.

In the future, the model can be applied to various phytoplankton with similar chemostat culture datasets to that in Healey (1985) (e.g. Laws and Bannister 1980; Mougnot *et al.*, 2015; Garcia *et al.*, 2016). We expect that we need different values for most parameters since each phytoplankton species has different metabolisms. However, the model might reveal certain rules in elemental ratios, macromolecular compositions, and other parameters among the same groups of phytoplankton. For example, it would be interesting to test if there are any distinct features among prokaryotes and eukaryotes, and among coastal and open ocean phytoplankton, and to interpret differences between them.

Finally, this simple macromolecular model provides fundamental understanding of phytoplankton growth under different light and nutrient environments. Such understanding will lead to macromolecular based prediction of phytoplankton growth in dynamic state, which in turn can provide new implication for ecosystem dynamics, biogeochemistry and climate. For example, the mechanistic prediction of C:N:P ratios can be applied in the ocean ecosystem models. This may provide more accurate prediction of biological pump, since its efficiency varies with the stoichiometry of the organic matter (Falkowski, *et al.*, 2000).

4.6 References

- Auer MT, Canale RP. (1982). Ecological studies and mathematical modeling of *Cladophora* in lake huron: 3. The dependence of growth rates on internal phosphorus pool size. *J Great Lakes Res* **8**: 93–99.
- Bertilsson S, Berglund O, Karl DM, Chisholm SW. (2003). Elemental composition of marine *Prochlorococcus* and *Synechococcus*: Implications for the ecological stoichiometry of the sea. *Limnol Oceanogr* **48**: 1721–1731.
- Borzi A. (1887). Le comunicazioni intracellulari delle Nostochinee. *Malpighia* **1**: 28–74.
- Bremer H, Dennis P. (1996). Modulation of chemical composition and other parameters of the cell by growth rate. In *Escherichia coli* and *Salmonella typhimurium*. Neidhardt, F (ed) *Washington, DC Am Soc Microbiol Press* 1553–1569.
- Bruggeman J, Kooijman SALM. (2007). A biodiversity-inspired approach to aquatic ecosystem modeling. *Limnol Oceanogr* **52**: 1533–1544.
- Burmester DE. (1979). The continuous culture of phytoplankton: Mathematical equivalence among three steady-state models. *Am Nat* **113**: 123–134.
- Caperon J. (1969). The lag in population growth response of *Isochrysis galbana* to a variable nitrate environment. *Ecology* **50**: 188–192.
- Caperon J, Meyer J. (1972). Nitrogen-limited growth of marine phytoplankton-I. Changes in population characteristics with steady-state growth rate. *Deep Sea Res* **19**: 601–618.
- Chai F, Dugdale RC, Peng T-H, Wilkerson FP, Barber RT. (2002). One-dimensional ecosystem model of the equatorial Pacific upwelling system. Part I: model development and silicon and nitrogen cycle. *Deep Sea Res Part II Top Stud Oceanogr* **49**: 2713–2745.
- Claquin P, Martin-Jézéquel V, Kromkamp JC, Veldhuis MJW, Kraay GW. (2002). Uncoupling of silicon compared with carbon and nitrogen metabolisms and the role of the cell cycle in continuous cultures of *Thalassiosira pseudonana* (Bacillariophyceae) under light, nitrogen, and phosphorus control. *J Phycol* **38**: 922–930.
- Cloern JE. (1999). The relative importance of light and nutrient limitation of phytoplankton growth: A simple index of coastal ecosystem sensitivity to nutrient enrichment. *Aquat Ecol* **33**: 3–16.
- Cullen JJ. (1990). On models of growth and photosynthesis in phytoplankton. *Deep Res* **37**: 667–683.
- Droop MR. (1973). Some thoughts on nutrient limitation in algae. *J Phycol* **9**: 264–272.

- Droop MR. (1970). Vitamin B₁₂ and marine ecology. *Helgoländer wiss Meeresunters* **20**: 629–636.
- Droop MR. (1968). Vitamin B₁₂ and marine ecology. IV. The kinetics of uptake, growth and inhibition in *Monochrysis lutheri*. *J mar biol Ass UK* **48**: 689–733.
- Ducobu H, Huisman J, Jonker RR, Mur LR. (1998). Competition between a prochlorophyte and a cyanobacterium under various phosphorus regimes: Comparison with the droop model. *J Phycol* **34**: 467–476.
- Falkowski PG. (1994). The role of phytoplankton photosynthesis in global biogeochemical cycles. *Photosynth Res* **39**: 235–258.
- Falkowski PG, Scholes RJ, Boyle E, Canadell J, Canfield D, Elser J, *et al.* (2000). The global carbon cycle: a test of our knowledge of earth as a system. *Science* **290**: 291–296.
- Fasham MJR, Ducklow HW, M MS. (1990). A nitrogen-based model of plankton dynamics in the oceanic mixed layer. *J Mar Res* **48**: 591–639.
- Field CB, Behrenfeld MJ, Randerson JT, P F. (1998). Primary production of the biosphere: Integrating terrestrial and oceanic components. *Science* **281**: 237–240.
- Flynn KJ. (2001). A mechanistic model for describing dynamic multi-nutrient, light, temperature interactions in phytoplankton. *J Plankton Res* **23**: 977–997.
- Flynn KJ. (2003). Modelling multi-nutrient interactions in phytoplankton; balancing simplicity and realism. *Prog Oceanogr* **56**: 249–279.
- Flynn KJ. (2008). The importance of the form of the quota curve and control of non-limiting nutrient transport in phytoplankton models. *J Plankton Res* **30**: 423–438.
- Follows MJ, Dutkiewicz S. (2011). Modeling diverse communities of marine microbes. *Ann Rev Mar Sci* **3**: 427–451.
- Follows MJ, Dutkiewicz S, Grant S, Chisholm SW. (2007). Emergent biogeography of microbial communities in a model ocean. *Science* **315**: 1843–1846.
- Garcia NS, Bonachela JA, Martiny AC. (2016). Growth-dependent cell size controls interactions between nutrient supply and cellular elemental stoichiometry of marine *Synechococcus*. *ISME J* doi:10.1038/ismej.2016.50.
- Geider RJ, Macintyre HL, Kana TM. (1996). A dynamic model of photoadaptation in phytoplankton. *Limnol Oceanogr* **41**: 1–15.
- Geider RJ, Macintyre HL, Kana TM. (1998). A dynamic regulatory model of phytoplankton acclimation to light, nutrients, and temperature. *Limnol Oceanogr* **43**: 679–694.

- Geider RJ, Macintyre HL, Kana TM. (1997). Dynamic model of phytoplankton growth and acclimation: responses of the balanced growth rate and the chlorophyll a: carbon ratio to light, nutrient-limitation and temperature. *Mar Ecol Prog Ser* **148**: 187–200.
- Gotham IJ, Rhee G-Y. (1982). Effects of nitrate and phosphate limitation on cyclostat growth of two freshwater diatoms. *J Gen Microbiol* **128**: 199–205.
- Hai T, Oppermann-Sanio FB, Steinbüchel A. (1999). Purification and characterization of cyanophycin and cyanophycin synthetase from the thermophilic *Synechococcus* sp. MA19. *FEMS Microbiol Lett* **181**: 229–236.
- Harrison PJ, Conway HL, Holmes CR, Davis CO. (1990). Effects of nutrients and light on the biochemical composition of phytoplankton. *J Appl Phycol* **2**: 45–56.
- Healey FP. (1985). Interacting effects of light and nutrient limitation on the growth rate of *Synechococcus linearis* (Cyanophyceae). *J Phycol* **21**: 134–146.
- Huflejt ME, Tremolieres A, Pineau B, Lang JK, Hatheway J, Packer L. (1990). Changes in membrane lipid composition during saline growth of the fresh water cyanobacterium *Synechococcus* 6311. *Plant Physiol* **94**: 1512–1521.
- Kauffman KJ, Prakash P, Edwards JS. (2003). Advances in flux balance analysis. *Curr Opin Biotechnol* **14**: 491–496.
- Kirchhoff H, Haferkamp S, Allen JF, Epstein DBA, Mullineaux CW. (2008). Protein diffusion and macromolecular crowding in thylakoid membranes. *Plant Physiol* **146**: 1571–1578.
- Kishi MJ, Kashiwai M, Ware DM, Megrey BA, Eslinger DL, Werner FE, *et al.* (2007). NEMURO-a lower trophic level model for the North Pacific marine ecosystem. *Ecol Modell* **202**: 12–25.
- Klausmeier CA, Litchman E, Levin SA. (2004). Phytoplankton growth and stoichiometry under multiple nutrient limitation. *Limnol Ocean* **49**: 1463–1470.
- Kromkamp J. (1987). Formation and functional significance of storage products in cyanobacteria. *New Zeal J Mar Freshw Res* **21**: 457–465.
- Laws E, Caperon J. (1976). Carbon and nitrogen metabolism by *Monochrysis lutheri*: Measurement of growth-rate-dependent respiration rates. *Mar Biol* **36**: 85–97.
- Laws EA, Bannister TT. (1980). Nutrient- and light-limited growth of *Thalassiosira fluviatilis* in continuous culture, with implications for phytoplankton growth in the ocean. *Limnol Oceanogr* **25**: 457–473.
- Lepetit B, Goss R, Jakob T, Wilhelm C. (2012). Molecular dynamics of the diatom thylakoid membrane under different light conditions. *Photosynth Res* **111**: 245–257.

- Le Quéré C, Harrison SP, Colin Prentice I, Buitenhuis ET, Aumont O, Bopp L, *et al.* (2005). Ecosystem dynamics based on plankton functional types for global ocean biogeochemistry models. *Glob Chang Biol* **11**: 2016–2040.
- Liberton M, Howard Berg R, Heuser J, Roth R, Pakrasi HB. (2006). Ultrastructure of the membrane systems in the unicellular cyanobacterium *Synechocystis* sp. strain PCC 6803. *Protoplasma* **227**: 129–138.
- Monod J. (1949). The growth of bacterial cultures. *Ann Rev Mar Sci* **3**: 371–394.
- Moore CM, Mills MM, Arrigo KR, Berman-Frank I, Bopp L, Boyd PW, *et al.* (2013). Processes and patterns of oceanic nutrient limitation. *Nat Geosci* **6**: 701–710.
- Moore LR, Post AF, Rocap G, Chisholm SW. (2002). Utilization of different nitrogen sources by the marine cyanobacteria *Prochlorococcus* and *Synechococcus*. *Limnol Oceanogr* **47**: 989–996.
- Mouginot C, Zimmerman AE, Bonachela JA, Fredricks H, Allison SD, Van Mooy BAS, *et al.* (2015). Resource allocation by the marine cyanobacterium *Synechococcus* WH8102 in response to different nutrient supply ratios. *Limnol Oceanogr* **60**: 1634–1641.
- North RL, Guildford SJ, Smith REH, Havens SM, Twiss MR. (2007). Evidence for phosphorus, nitrogen, and iron colimitation of phytoplankton communities in Lake Erie. *Limnol Oceanogr* **52**: 315–328.
- Orth JD, Thiele I, Palsson BØ. (2010). What is flux balance analysis? *Nat Biotechnol* **28**: 245–248.
- Pahlow M, Oschlies A. (2009). Chain model of phytoplankton P, N and light colimitation. *Mar Ecol Prog Ser* **376**: 69–83.
- Platt T, Gallegos CL, Harrison WG. (1980). Photoinhibition of photosynthesis in natural assemblages of marine phytoplankton. *J Mar Res* **38**: 687–701.
- Rast A, Heinz S, Nickelsen J. (2015). Biogenesis of thylakoid membranes. *Biochim Biophys Acta* **1847**: 821–830.
- Sarmiento JL, Slater RD, Fasham MJR, Ducklow HW, Toggweiler JR, Evans GT. (1993). A seasonal three-dimensional ecosystem model of nitrogen cycling in the North Atlantic euphotic zone. *Global Biogeochem Cycles* **7**: 417–450.
- Schuster S, Fell D. (2007). Modeling and simulating metabolic networks. In: Lengauer, T. (Ed.), *Bioinformatics: From Genomes to Therapies*. Wiley-VCH: Weinheim. **2**: 755–805.
- Seemann JR, Sharkey TD, Wang J, Osmond CB. (1987). Environmental effects on photosynthesis, nitrogen-use efficiency, and metabolite pools in leaves of sun and shade plants. *Plant Physiol* **84**: 796–802.

- Smith SL, Yamanaka Y, Pahlow M, Oschlies A. (2009). Optimal uptake kinetics: Physiological acclimation explains the pattern of nitrate uptake by phytoplankton in the ocean. *Mar Ecol Prog Ser* **384**: 1–12.
- Stukel MR, Coles VJ, Brooks MT, Hood RR. (2014). Top-down, bottom-up and physical controls on diatom-diazotroph assemblage growth in the Amazon River plume. *Biogeosciences* **11**: 3259–3278.
- Szalontai B, Nishiyama Y, Gombos Z, Murata N. (2000). Membrane dynamics as seen by Fourier transform infrared spectroscopy in a cyanobacterium, *Synechocystis* PCC 6803. *Biochim Biophys Acta* **1509**: 409–419.
- Van Mooy BAS, Fredricks HF, Pedler BE, Dyhrman ST, Karl DM, Koblížek M, *et al.* (2009). Phytoplankton in the ocean use non-phosphorus lipids in response to phosphorus scarcity. *Nature* **458**: 69–72.
- Van Mooy BAS, Rocap G, Fredricks HF, Evans CT, Devol AH. (2006). Sulfolipids dramatically decrease phosphorus demand by picocyanobacteria in oligotrophic marine environments. *Proc Natl Acad Sci USA* **103**: 8607–8612.
- Webb WL, Newton M, Starr D. (1974). Carbon dioxide exchange of *Alnus rubra* A mathematical model. *Oecologia* **17**: 281–291.
- Williams PJLB, Laurens LML. (2010). Microalgae as biodiesel & biomass feedstocks: review & analysis of the biochemistry, energetics & economics. *Energy Environ Sci* **3**: 554–590.

4.7 Supplementary material: model parameterization

We have parameterized the model based on certain clues. There are two types of parameters: tunable parameters and non-tunable parameters. We predict values for tunable parameters based on the laboratory data from Healey (1985). Since each parameter influences distinct features of the data from Healey (1985) (Table 4.5), we expect that the parameter set converges into narrow range in order to equally represent the laboratory data (Table 4.6 for used values). For non-tunable parameters, we have chosen values based on certain information sources (Table 4.7 for sources and for Table 4.8 values).

Parameterizing tunable parameters

Each tunable parameter influences a certain aspect of the data in Healey (1985), such as the y-intercepts (values at $D=0$) of the data, and light dependent variations, and slope of the curves (Table 4.5). In this section, we explain how this specificity helps us parameterize tunable parameters. We discuss the parameters roughly in the order of appearance in the method section.

To begin with, the maintenance m is based on the overall magnitude of y-intercept in Chl/ratio. As can be seen in (Figure 4.2 (1-E) and (2-E)), y-intercept is not zero. This indicates that there has to be minimum chlorophyll in the cell even if the cell is not growing. Why do they need minimum chlorophyll? Here we hypothesize that chlorophyll is necessary to fix carbon, which is used for the cell maintenance. Based on the hypothesis, m gives non-zero y-intercept, whose magnitude is tuned to represent the chlorophyll variation in Healey (1985) together with power coefficient A_{PHO} .

A_{PHO} is parameterized based on light dependent variation in y-intercept in Chl/C ratio (Figure 4.2 (1-E) and (2-E)). Since A_{PHO} controls the slope of the P-I curve (photosynthesis -

light intensity curve), it influences how chlorophyll amount varies based on the light intensity at y-intercept (based on equation (4.6)). Since the data in Healey (1985) shows a certain variation, we can guess an approximate value for A_{PHO} .

P_{Chl}^{max} influences the slope of Chl:C ratio (Figure 4.2 (1-E) and (2-E)). As can be seen in Chl/C ratio - dilution rate curve, the Chl:C ratio increases with the dilution rate. Since P_{Chl}^{max} influences the maximum photosynthesis rate, it influences how much chlorophyll is needed for a certain carbon demand. As the dilution rate increases, the cell grows more quickly requiring a higher amount of carbon. This leads to higher amount of chlorophyll and the increase in chlorophyll is mainly constrained by P_{Chl}^{max} . Thus, by comparing the slope between the model to the data, we can predict an approximate value for P_{Chl}^{max} .

After predicting the values for the chlorophyll related parameters, we next predict the parameter based on elemental ratios such as N:C and P:C ratios (Figure 4.2). By using the N:C ratio in P-limited culture, in a similar way that we predicted three values from chlorophyll to carbon ratio, we can predict $N_{Protein}^{const}$, $Y^{Npho:Chl}$ and $A_{Biosynth}^N$.

To predict $N_{Protein}^{const}$, we use the overall magnitude of y-intercept in N:C ratio in N-limiting case (Figure 4.2 (2-B)). Since $N_{Protein}^{const}$ indicates the minimum requirement of protein in the cell, the value influences all the data points in N:C ratios. Although $Y^{Npho:Chl}$ influences the overall magnitude, the influence is rather limited at y-intercept since at $D=0$, the photosynthesis rate is minimum for a given light intensity.

To predict the ratio between nitrogen photosynthetic protein and chlorophyll $Y^{Npho:Chl}$, we use the light dependent variation in y-intercept in N:C ratio in N-limiting case (Figure 4.2 (2-

B)). Since the N:C ratio is not influenced by the dilution rate at y-intercept (as $D=0$), it is solely influenced by the light intensity through $Y^{Npho:Chl}$. Thus, by comparing the N:C values at y-intercept for five light intensities that Healey (1985), we can predict the value for $Y^{Npho:Chl}$.

Once we predict values for $N_{Protein}^{const}$ and $Y^{Npho:Chl}$, we use the slope of the N:C ratio to estimate $A_{Biosynth}^N$ (Figure 4.2 (1-C) and (2-B)). There are two parameters that significantly influences the slope on N:C ratios: $A_{Biosynth}^N$ and $Y^{Npho:Chl}$. However, since $Y^{Npho:Chl}$ is already constrained at this point, $A_{Biosynth}^N$ can be tuned to add to the slope created by $Y^{Npho:Chl}$. In addition to $A_{Biosynth}^N$ and $Y^{Npho:Chl}$, thus, biosynthesis and photosynthesis protein, Chlorophyll, RNA influences the slope since they all depends on the dilution rates. However, at this point we have obtained the chlorophyll amount. Also, the relative influence of RNA on the nitrogen quota is much smaller than that of proteins. Thus, we can estimate $A_{Biosynth}^N$ with high precision from the slope of N:C ratio.

After using the data of N:C ratios under phosphorus limited cultures, we apply a similar method to P:C ratios in P limiting case (Figure 4.2 (1-B)) in order to estimate another three tunable parameters: P_{Other}^{const} , $Y_{Thylakoid}^{P:Chl}$, and A_{RNA}^N . P_{Other}^{const} is predicted from the overall magnitude of the P/C ratio at y-intercept due to its dominant influence. P_{Other}^{const} is estimated especially by comparing the model-lab values at the high light intensity ($144 \mu\text{Em}^{-2}\text{s}^{-1}$), where P_{Other}^{const} has a dominant influence as a tunable parameter; although the minimum amounts of RNA and RNA has a similar effect to P:C ratios, the values are estimated from certain sources, and thus they are non-tunable.

Then, $Y_{Thylakoid}^{P:Chl}$ is tuned based on the variation in y-intercept of P:C ratios in P-limiting case (Figure 4.2 (1-B)). Since the variation based on the light intensity is exclusively based on $Y_{Thylakoid}^{P:Chl}$, by comparing the model to the laboratory data, we can effectively narrow down the values for $Y_{Thylakoid}^{P:Chl}$.

Once we obtain a descent estimate for the y-intercept of P:C ratios by tuning P_{Other}^{const} and $Y_{Thylakoid}^{P:Chl}$, A_{RNA}^N can be estimated from the non-linear shape of P/C ratios in P-limiting case (Figure 4.2 (1-B)). Since only A_{RNA}^N cause the non-linear shape as can be seen in the experimental data, we can predict A_{RNA}^N with high precision.

After tuning these nine parameters, we will estimate the rest of the tunable parameters N_{Store}^{max} , $Q_P^{max-Cell}$ and $C_{Essential}$ differently from the previous nine parameters. First, N_{Store}^{max} is estimated based on differences in N:C ration between N-limited (Figure 4.2 (2-B)) and P-limited (Figure 4.2 (1-C)) cultures. While there is no nitrogen storage in the N-limited case, but the excess nitrogen is stored in P-limited case. Since this is the only difference between N-limited case and P-limited case, by comparing the model results and the laboratory data for both of them, we can estimate the value for N_{Store}^{max} .

Next, $Q_P^{max-Cell}$ can be predicted from the overall value for the P:C ratio in the N-limited culture (Figure 4.2 (2-C)). Since the laboratory data show about constant values at around 25 ($\mu\text{g P mg C}^{-1}$), which is much higher values than the P-limited case, we predict that this is the maximum amount of phosphorus they can store in the cell, thus $Q_P^{max-Cell}$.

Finally, in order to predict $C_{Essential}$, we compare the maximum dilution rates between the model and the laboratory data for each light intensity (Figure 4.2). We have so far constrained all the other parameters, and only $C_{Essential}$ remains. Depending on how much $C_{Essential}$ the cell has, the maximum dilution rate at which the cell reaches the maximum capacity varies due to the carbon based space limitation. For example, if $C_{Essential}$ is large, the cell reaches the maximum capacity at the low dilution rate since there is only limited space available for other growth related macromolecule. Since the maximum dilution rates are slightly different between N-limited and P-limited cultures based on the existence of nitrogen storage, this difference helps us approximate $C_{Essential}$ as well.

Table 4.5 Influence of each tunable parameter. The parameters are listed in order of appearance in the method section.

Parameter	Influence
m	Overall magnitude in y-intercept in Chl/C ratio
P_{Chl}^{max}	Slope in Chl/C ratio
A_{PHO}	Light dependent variation in y-intercept in Chl/C ratio
$Y^{Npho:Chl}$	Light dependent variation in y-intercept in N/C ratio
$A_{Biosynth}^N$	Slope in N/C ratio
$N_{Protein}^{const}$	Overall magnitude in y-intercept in N/C ratio
A_{RNA}^N	Non-linear shape of P/C ratio
$Y_{Thylakoid}^{P:Chl}$	Light dependent variation in y-intercept in P/C ratio in P-limited case
P_{Other}^{const}	Overall magnitude in y-intercept in P/C ratio in P-limited case
N_{Store}^{max}	Differences in N/C ration between N-limited and P-limited cultures
$Q_P^{max-Cell}$	Overall magnitude in P/C ratio in N-limited case
$C_{Essential}$	Maximum dilution rates (Cut-offs)

Table 4.6 Values used for tunable parameters. The parameters are listed in order of appearance in the method section.

Parameter	Value	Unit
m	5.00×10^{-19}	mol C cell ⁻¹ s ⁻¹
P_{Chl}^{max}	2.63×10^{-3}	s ⁻¹
A_{PHO}	1.25×10^{-2}	μE ⁻¹ m ² s
$Y^{Npho:Chl}$	3.20	mol N mol C ⁻¹
$A_{Biosynth}^N$	5.00×10^{-10}	mol N cell ⁻¹ s
$N_{Protein}^{const}$	4.32×10^{-15}	mol N cell ⁻¹
A_{RNA}^N	6.24×10^3	s
$Y^{P:Chl}_{Thylakoid}$	3.00×10^{-2}	mol P mol C ⁻¹
P_{Other}^{const}	4.50×10^{-17}	mol P cell ⁻¹
N_{Store}^{max}	3.24×10^{-15}	mol N cell ⁻¹
$Q_P^{max-Cell}$	8.07×10^{-16}	mol P cell ⁻¹
$C_{Essential}$	6.66×10^{-15}	mol C cell ⁻¹

Sources for non-tunable parameters

All the non-tunable parameters are based on literature or chemical formula of each compound.

Certain numbers are given to the non-tunable parameters before parameterizing tunable parameters. In this section, we briefly explain each non-tunable parameters roughly in the order of appearance in the method section.

The value of CO₂ production ratio E is estimated from the method in Rittmann and McCarty (2001). In the method, they consider mass, electron and energy budget to compute how much respiration has to occur relative to biomass production. As in Rittmann and McCarty (2001), we approximate E based on the energy transfer efficiency of 0.6 and biomass stoichiometry of C₅H₇O₂N₁, assuming that the variation in the energy requirement caused by stoichiometric change is small. This constant E value leads to the linear curve in Chl:C ratios, which captures the trend in Healey (1985).

The total carbon quota per cell Q_C is based on the averaged value observed in Healey (1985). Although, the author states about $\pm 20\%$ of variation, he did not observe any trend with the dilution rate and irradiance. However, the value for Q_C is slightly different between P-limited and N-limited cases, and we have applied appropriate values for each case.

The constant part of DNA in nitrogen N_{DNA}^{const} is based on the genome size and GC content of *Synechococcus* spp. (NCBI, 2016b). We have used N_{DNA}^{const} and the RNA:DNA ratio of *E. coli* at zero growth estimated from Bremer and Dennis (1996) to obtain the constant part of RNA in nitrogen N_{RNA}^{const} ; we have linearly and polynomially (degree of two) interpolated DNA-growth rate and RNA-growth rate relations, respectively, and we have used the GC content of *E. coli* (NCBI, 2016a) (=50.6 %) for the unit conversion. Also, the value of A_{DNA}^N is assumed small since the range of dilution in Healey (1985) is small compared to that in Bremer and Dennis (1996).

The rest of non-tunable parameters are based on stoichiometry of molecules. $Y_{Chl}^{N:C}$ is based on N/C ratio of Chlorophyll a. RNA and DNA related parameters (N_{RNA}^{const} , N_{DNA}^{const} , $Y_{RNA}^{P:N}$,

$Y_{DNA}^{P:N}$, $Y_{RNA}^{C:N}$, $Y_{DNA}^{C:N}$) are obtained from the stoichiometry of DNA and RNA based on the guanine-cytosine (GC) content of the genome. We have referred to the genome of *Synechococcus* spp. in (NCBI, 2016b) where GC=57.55 %. For $Y_{P-lipid}^{C:P}$ we have used the chemical formula of phosphatidylglycerol (PG) with 16 C fatty acid chains, since this is the most dominant form of phospholipid reported in Huflejt *et al.* (1990). $Y_{Protein}^{C:N}$ is derived from averaged amino acid composition of 16 species of microalgae studied in Brown (1991). $Y_{Nstore}^{C:N}$ is based on the C:N ratio of cyanophycin, key nitrogen storage of *Synechococcus* spp. (e.g. Maheswaran *et al.*, 2006; Ll acer *et al.*, 2008).

Table 4.7 Sources for non-tunable parameters. The parameters are listed in order of appearance in the method section.

Parameter	Source
E	Rittmann and McCarty (2001) (see the text for details)
Q_C	Healey (1985)
$Y_{Chl}^{N:C}$	Based on N/C ratio of Chlorophyll a
N_{RNA}^{const}	Based on GC content of Synechococcus (NCBI, 2016b)
N_{DNA}^{const}	Based on GC content of Synechococcus (NCBI, 2016b)
A_{DNA}^N	Assumed small
$Y_{RNA}^{P:N}$	Based on GC content of Synechococcus (NCBI, 2016b)
$Y_{DNA}^{P:N}$	Based on GC content of Synechococcus (NCBI, 2016b)
$Y_{P-lipid}^{C:P}$	Assuming phosphatidylglycerol (PG) with 16 C fatty acid chains
$Y_{Protein}^{C:N}$	Derived from averaged amino acid composition based on Brown (1991)
$Y_{RNA}^{C:N}$	Based on GC content of Synechococcus (NCBI, 2016b)
$Y_{DNA}^{C:N}$	Based on GC content of Synechococcus (NCBI, 2016b)
$Y_{Nstore}^{C:N}$	Based on C:N ratio of cyanophycin

Table 4.8 Values used for non-tunable parameters. The parameters are listed in order of appearance in the method section.

Parameter	Value	Unit
E	7.74×10^{-1}	dimensionless
Q_C	8.58×10^{-14} for P-limiting and 8.33×10^{-14} for N-limiting culture	mol C cell ⁻¹
$Y_{Chl}^{N:C}$	N:C=4:55	mol N mol C ⁻¹
N_{RNA}^{const}	8.77×10^{-17}	mol N cell ⁻¹
N_{DNA}^{const}	3.34×10^{-17}	mol N cell ⁻¹
A_{DNA}^N	0	mol N cell ⁻¹ s
$Y_{RNA}^{P:N}$	2.64×10^{-1}	mol P mol N ⁻¹
$Y_{DNA}^{P:N}$	2.64×10^{-1}	mol P mol N ⁻¹
$Y_{P-lipid}^{C:P}$	40	mol C mol P ⁻¹
$Y_{Protein}^{C:N}$	4.23	mol C mol N ⁻¹
$Y_{RNA}^{C:N}$	2.81	mol C mol N ⁻¹
$Y_{DNA}^{C:N}$	2.92	mol C mol N ⁻¹
$Y_{Nstore}^{C:N}$	2	mol C mol N ⁻¹

4.8 References for Supplementary Material

Bremer H, Dennis P. (1996). Modulation of chemical composition and other parameters of the cell by growth rate. In *Escherichia coli* and *Salmonella typhimurium*. Neidhardt, F (ed) Washington, DC Am Soc Microbiol Press 1553–1569.

Brown MRR. (1991). The amino-acid and sugar composition of 16 species of microalgae used in mariculture. *J exp mar Biol Ecol* **145**:79–99.

Healey FP. (1985). Interacting effects of light and nutrient limitation on the growth rate of *Synechococcus linearis* (Cyanophyceae). *J Phycol* **21**:134–146.

Huflejt ME, Tremolieres A, Pineau B, Lang JK, Hatheway J, Packer L. (1990). Changes in membrane lipid composition during saline growth of the fresh water cyanobacterium *Synechococcus* 6311. *Plant Physiol* **94**:1512–1521.

Llàcer JL, Fita I, Rubio V. (2008). Arginine and nitrogen storage. *Curr Opin Struct Biol* **18**:673–681.

Maheswaran M, Ziegler K, Lockau W, Hagemann M, Forchhammer K. (2006). P_{II}-regulated arginine synthesis controls accumulation of cyanophycin in *Synechocystis* sp. Strain PCC 6803. *J Bacteriol* **188**:2730–2734.

NCBI, Genome, *Escherichia coli*. MG1655, ID: 167, <http://www.ncbi.nlm.nih.gov/genome/167>, accessed, June 18, 2016a.

NCBI, Genome, *Synechococcus* sp. CC9902, ID: 13522, <http://www.ncbi.nlm.nih.gov/genome/13522>, accessed, June 18, 2016b.

Rittmann BE, McCarty PL. (2001). Stoichiometry and bacterial energetics. In: *Environmental Biotechnology: Principles and Applications*. McGraw-Hill: New York. 126–164.

Chapter 5

The cell flux model indicates multiple oxygen management strategies in *Crocospaera watsonii*

5.1 Abstract

Crocospaera is one of the major nitrogen fixers in the ocean. To avoid the disruption of nitrogenase and nitrogen fixation by oxygen, *Crocospaera* fixes nitrogen during the dark period, temporally segregating it from oxygenic photosynthesis. However, even at night, the surface ocean is saturated in oxygen, requiring additional oxygen management mechanisms, which define the ecological trade-offs for *Crocospaera*. Here we examine oxygen management of *Crocospaera* by developing a simplified metabolic flux network; “the cell flux model”. The model simulates different scenarios based on three oxygen management strategies: respiratory protection, size adaptation, and diffusive protection. Incorporating all of these improves the accuracy of simulations of laboratory cultures, suggesting that *Crocospaera* uses these three oxygen management strategies, and providing a basis for models of *Crocospaera* ecology.

5.2 Introduction

Nitrogen fixers in the ocean account for about 50% of fixed nitrogen input (Gruber and Galloway, 2008). All organisms need nitrogen for proteins and enzymes. Often, fixed nitrogen is the growth-limiting factor for primary producers in the sea (Thomas 1970; Thomas and Owen

1971; Ryther and Dunstan, 1971; Caperon and Meyer, 1972), controlling the flow of carbon through the ecosystem (Falkowski, 1997; Gruber, 2004; Gruber and Galloway, 2008).

Crocospaera watsonii is a major phototrophic nitrogen fixer, which significantly contributes to marine nitrogen fixation in tropical environments (Dyhrman and Haley, 2006).

Crocospaera watsonii usually is found in oligotrophic waters, warmer than 24°C of the western tropical Atlantic and tropical Pacific (JGI, 2013). In those regions, their cell densities may exceed 1,000 cell/ml in the euphotic zone (JGI, 2013). Also, the ecosystem model indicates that *Crocospaera* analogs widely exist in the North Pacific and Equatorial to South Atlantic regions (Saito *et al.*, 2011).

As discussed in Chapter 1, the nitrogen fixing enzyme nitrogenase is sensitive to oxygen and loses its function in the presence of intracellular oxygen (Gallon, 1981). One of the oxygen management strategies that *Crocospaera* uses the temporal separation of nitrogen fixation and oxygenic photosynthesis (Mohr, *et al.*, 2010; Shi *et al.*, 2010; Dron *et al.*, 2012b; Mohr, *et al.*, 2013). This temporal segregation is accompanied by the diurnal intracellular iron cycle (Saito *et al.*, 2011). In the early dark period, *Crocospaera* synthesizes the nitrogenase complex taking iron from the photosystem (Saito *et al.*, 2011). Nitrogen fixation peaks in the middle dark period, and in the late dark period *Crocospaera* decomposes nitrogenase, moving iron back to the photosystem for the next light period (Saito *et al.*, 2011).

However, in the ocean, even at night, the mixed layer is nearly saturated with oxygen (e.g. Robertson *et al.*, 1992; Fransson *et al.*, 2004; de Boyer Montégut, *et al.*, 2004; Yates *et al.*, 2007) due to rapid air-sea oxygen exchange (e.g. Najjar and Keeling, 2000). In such a high oxygen environment, invasion of oxygen into the cell is expected due to passive diffusion. Thus, the temporal segregation of nitrogen fixation from oxygen evolution does not appear to be

sufficient. What other strategies does *Crocospaera* apply to further protect nitrogenase from oxygen? In Chapter 2, we developed a general model of intra-cellular oxygen management:

$$[O_2^{CELL}] = [O_2] - \frac{r^2 \gamma_{TOT}}{3\kappa_{O_2}}. \quad (5.1)$$

Based on this model, there are three strategies which can decrease $[O_2^{CELL}]$: increase the cell size r , increase respiration γ_{TOT} or decrease the oxygen diffusivity in the cell membrane layers κ_{O_2} . *Azotobacter vinelandii*, the unicellular soil-dwelling heterotrophic nitrogen fixer, employs all three strategies (see Chapter 2 and references therein).

Azotobacter and *Crocospaera* are, in some important regards, functionally similar microorganisms. Although they live in different places, are genetically distant, and employ different trophic strategies, they are similar in size, unicellular, and exist in high oxygen environments (*Azotobacters* live in the rhizosphere, and *Crocospaera* live in surface ocean). Also, the energy for nitrogen fixation is not directly derived from photosynthesis; while *Azotobacter* uses external carbohydrate for the energy source for nitrogen fixation, at night *Crocospaera* uses stored carbon for this purpose. Given these similarities, it is possible that *Crocospaera* employs similar strategies to protect the nitrogenase during the dark period.

To better understand the contribution of *Crocospaera* to the global nitrogen cycle, it is important to understand what strategies they apply and how these strategies influence the biogeography of *Crocospaera* and other competing micro-organisms. In chapter two, we have modeled and interpreted the oxygen-management strategies of *Azotobacter*. Here we we further develop the idealized metabolic flux network model (the cell flux model) specifically to consider *Crocospaera*, to study their oxygen-management strategies and to discuss the implication of those strategies in the ecosystem.

5.3 Methods: A metabolic model of *Crocospaera watsonii*

To study the potential oxygen management strategy, we have developed a simplified metabolic flux network model (the cell flux model) for *Crocospaera*. The model resolves the time-dependent concentration of key macromolecular pools, including a general “biomass”, carbon and nitrogen stores, and, pigments, carbohydrates, as well as several inorganic compounds including CO₂, and NH₄⁺ (Figure 5.1A and Figure 5.2A). Those pools are connected by parameterized fluxes, such as nutrient uptake, biomass synthesis, carbon and nitrogen storage production, photosynthesis, and respiration, creating an idealized metabolic network. At the cellular scale, the system is constrained by the mass, electron balance and energy balance, when oxygen concentration is small and respiratory protection is not required. However, when the cell needs respiratory protection, the fluxes are influenced by oxygen and energy balance is ignored as described in Chapter 1.

In addition to including carbon, nitrogen, hydrogen, and oxygen fluxes, the model resolves simplified iron fluxes (Figure 5.1B and Figure 5.2B, C), since the iron allocation to photosystems and nitrogenase has been shown to vary over the diurnal cycle (Saito *et al.*, 2011), moving between photosystems, a buffer, and nitrogenase. Thus, photosynthesis and nitrogen fixation are closely tied to the iron cycle. In order to capture the important diurnal variations, we have developed connected, but somewhat independent metabolic models for the light and dark periods based on the laboratory data from Satio *et al.*, (2011), Mohr *et al.*, (2010), Großkopf and LaRoche, (2012), and Dron *et al.*, (2012b).

In the following sections we first explain schematically the assumptions in the models of light and dark periods (Section 5.3.1). Then, we introduce the time-dependent equations and

mathematical parameterizations of the fluxes which govern the model (Section 5.3.2). The model is then used to simulate laboratory data published by Großkopf and LaRoche, (2012) and sensitivity studies are used to ask whether *Crocospaera* is employing the oxygen management strategies observed in *Azotobacter vinelandii*.

5.3.1 Model overview:

In this section we provide a schematic overview of the processes resolved in the model. We separate this discussion into light, dark, and late-dark periods. The model equations are provided in the next section “Parameterizations and Algorithms”, and Supplementary Material S1 and S2.

Light period

During the light period the key metabolism is photosynthesis, whose rate is constrained by the light intensity and the pigment. Through photosynthesis, *Chrocospaera* fixes carbon in order to support biomass synthesis and to accumulate stored carbon, which fuels the activity of the dark period (Figure 5.1A).

In order to support biomass production, some fixed carbon is also used for respiration during the light period. The rate of biomass production is assumed to depend on the availability of stored nitrogen and the rate of photosynthesis. In this study we have assumed that photo-inhibition does not occur as we model a system at relatively low light intensity. We assume that the nitrogen source for the biomass production during the light period is solely the stored nitrogen fixed during the previous dark period. During the light period, biomass production is accompanied by the carbon storage. In this study, the light intensity is constant, but the model can incorporate dynamic light influence on pigments.

The rate of carbon storage is parameterized as a function of the light intensity, the size of the carbon store, and chlorophyll content. High light intensity and high chlorophyll leads to high carbon storage production, but if the stored carbon accumulates, the carbon storage is down regulated. The energetic cost of carbon storage is assumed to be small compared to biomass production.

The model also resolves the iron fluxes in the cell, which constrains the rate of photosynthesis during the light period. Three iron pools are resolved: photosystem iron, buffer iron, and nitrogenase iron (Figure 5.1B). The allocation of iron to the photosystem is assumed proportional to the chlorophyll content. Thus, high allocation to photosystem iron leads to high carbon fixation, biomass synthesis, and carbon storage production. At the initiation of the light period, the photosystem iron is at the minimum level but is increased at the expense of the buffer.

In order to compute the iron flux to the photosystem, we first compute the ideal photosystem iron requirement based on the potential biomass and carbon storage production. Then, we choose the direction of the iron flux between the buffer and the photosystem based on the difference between the “ideal” and the actual allocation of iron to the photosystem. The magnitude of flux is controlled by the size of the buffer iron pool, and the difference between the ideal and actual photosystem iron allocation. In the dark period, iron is allocated to nitrogenase. During the light period, if there is iron remaining in nitrogenase it is transferred to the buffer iron pool.

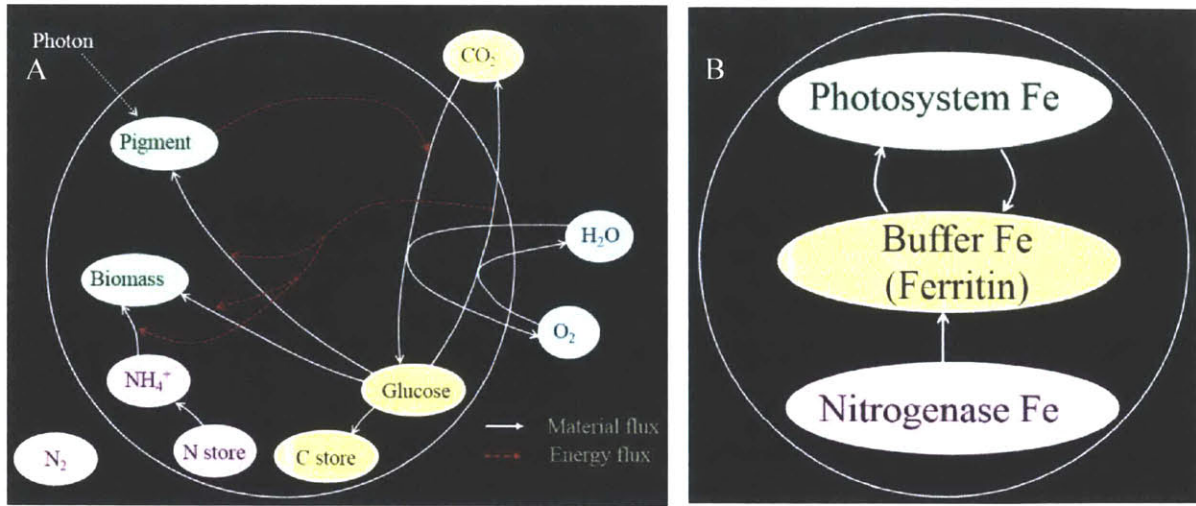


Figure 5.1 Schematic diagrams of the cell flux model for *Chrocosphaera* during the light period. (A) Fluxes other than iron. (B) Iron fluxes.

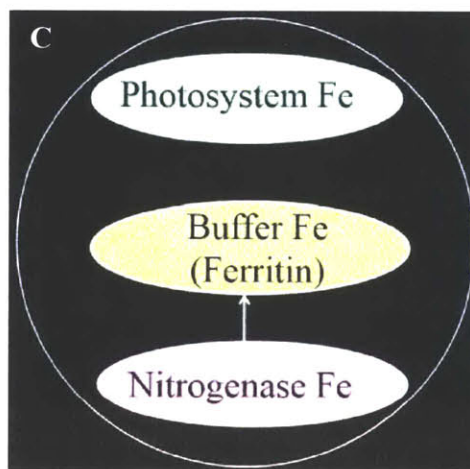
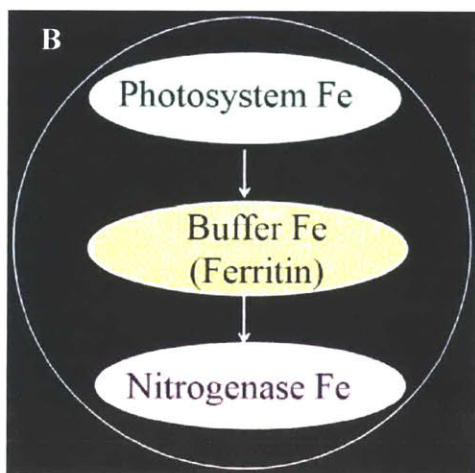
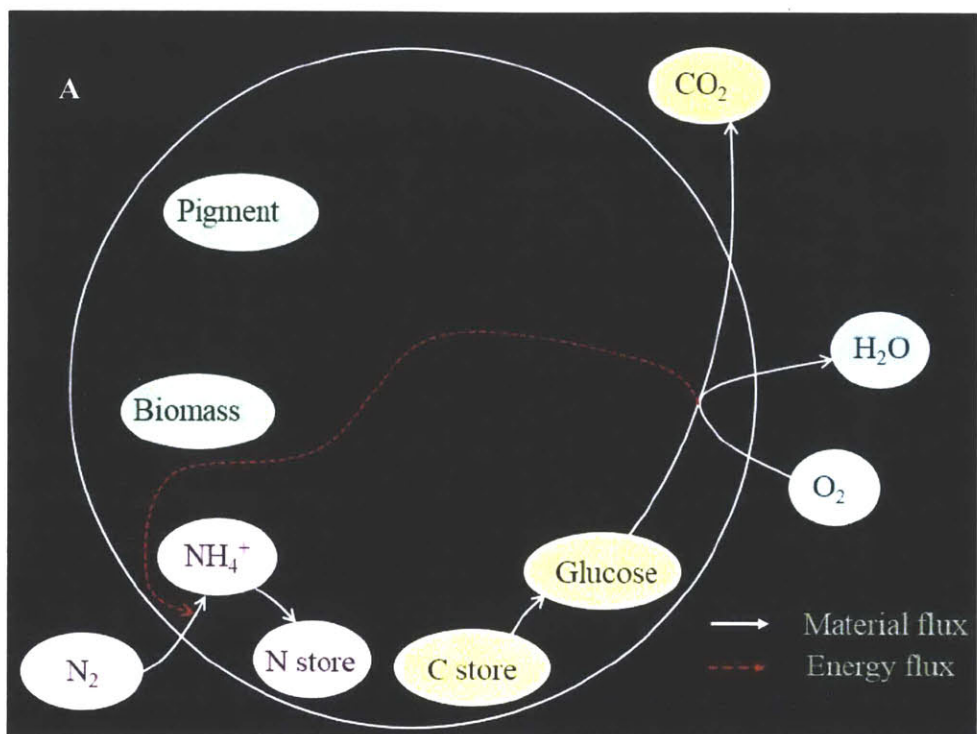


Figure 5.2 Schematics of the model during the dark period. (A) Fluxes other than iron. (B) Iron fluxes during the early dark period. (C) Iron flux during the late dark period.

Dark period

In the dark, the key metabolic processes are nitrogen fixation and storage, which impacts growth in the following light period. Nitrogen fixation is fueled by carbon stored during the previous light period (Figure 5.2A). Respiration provides energy for nitrogen fixation, and is also used to draw down the intracellular oxygen concentration.

The rate of nitrogen fixation is constrained by the amount of stored carbon, the availability of nitrogenase, and the intracellular oxygen concentration. Nitrogenase availability is assumed to be proportional to the allocation of iron. After the dark period initiates, there is a flux of iron from the photosystem to the nitrogenase iron pool through the buffer (Figure 5.2B). The amount of iron in the photosystem and iron buffer controls the flux to the buffer, possibly reflecting an active sensing and regulatory control of intracellular iron pools. In the same way, the flux of iron from the buffer to the nitrogenase is controlled both by the amount of iron in the buffer and the amount of iron in nitrogenase, and the potential nitrogenase production rate. We modeled an increasing capacity of nitrogen fixation with time after the initiation of the dark period in order to reproduce non-linear increase of nitrogen fixation rate observed in several studies (Saito *et al.*, 2011; Mohr *et al.*, 2010; Großkopf and LaRoche, 2012).

Another key feature in the dark period is respiration which influences the intracellular oxygen concentration, which in turn affects the nitrogen fixation rate. The respiration rate is computed based on passive, diffusive oxygen uptake, the respiratory capacity, and the carbon storage availability. In this model, during the dark period, we assume that the cell consumes oxygen as much as possible within the respiratory capacity to keep the intracellular oxygen concentration small relative to the environment. Thus the respiration rate is maintained higher than the level required for energetic demands.

The dark period respiration rate is also regulated by the availability of stored carbon. We also assume that respiratory capacity keeps increasing after the initiation of the dark period based on the hypothesis that adjustment of the metabolic state takes a finite time, so respiratory enzymes for oxygen management are accumulated. The assumption of a finite adjustment time (rather than instantaneous transition from light to dark metabolism) is consistent with experimental data (Mohr *et al.*, 2010; Saito *et al.*, 2011; Großkopf and LaRoche, 2012; Dron *et al.*, 2012b).

Overall, the modeled rate of nitrogen fixation depends on the amount of stored carbon the oxygen concentration in the environment. Although in some cases, the exudation of fixed nitrogen is reported in laboratory studies (e.g. Großkopf and LaRoche, 2012; Masuda, *et al.*, 2013), the magnitude varies and what causes the variation has yet to be well understood. Thus, in this model, it is assumed that all the fixed nitrogen is stored for biomass production in order to keep the model simple.

Late dark period

We also resolve a distinct, late-dark period in which the nitrogen fixing capacity and the respiration rate gradually decrease (Figure 5.2C). These trends are observed in multiple studies (Mohr *et al.*, 2010, Saito *et al.*, 2011, and Großkopf and LaRoche, 2012). We hypothesize that the nitrogen fixation keeps decreasing in order to move iron to the buffer ready for transfer to the photosystem during the next light period. Respiration is also observed to decrease toward the light period during the late dark period (Großkopf and LaRoche, 2012) and we modeled this period dependent decrease of respiration in order to accurately reproduce the observation (See Supplementary Material 5.S3 for more details).

5.3.2 Parameterizations and Algorithms

In this section we describe the algorithms employed to implement the model outlined above. Time dependent equations are written down to describe the rates of change in each of the macromolecular pools (see Table 1 for equations). The fluxes between macro-molecular pools and their dependence on the time of day and current physiological state are parameterized and quantified at each time step. The time dependent equations of Table 1 are stepped forward in finite time-steps, updating the status of the cells.

Here, to clarify the presentation, we discuss the processes and parameterizations of the carbon, nitrogen and oxygen pools first, followed by a discussion of the iron pools. However, the two are tightly coupled. We first describe the equations for time variations of each molecule, and then, we explain how to solve for each term. In order to capture the temporal variations in metabolism of the laboratory datasets of Großkopf and LaRoche (2012) we separate the day into light, dark and late-dark periods, each of which has a different set of metabolic processes and parameterizations at work.

Carbon, nitrogen and oxygen metabolism

Time dependence of molecular pools and cell densities

In order to compute the time variation of carbon, nitrogen and oxygen pools, and cell density, we consider the chemical fluxes that impact them (Table 5.1). The time variation of intermediate carbohydrate pool CH_C (glucose) is based on the balance among photosynthesis P_{lChl} , biomass production λ , CO_2 production $E\lambda$, carbon storage production P_{Cstore} and consumption D_{Cstore} , and excretion Exc , described in equation (5.2). The net flux into the carbon storage C_{Store} is the balance between the production P_{Cstore} and consumption D_{Cstore} of the storage; equation (5.3).

The controls on the photosynthetic apparatus are further discussed in the subsection discussing iron metabolism.

We assume that biomass production is used for the production of new cells, Bio_C in (equation (5.4)), which drives to the time change in population density (equation (5.5)). Biomass production is not only supported by carbon, but also nitrogen. Thus, we consider the time variation of ammonium pool (equation (5.6)), which is the balance between nitrogen fixation N_{2fix} , biomass synthesis λY_{Bio}^{NC} , and production and consumption of nitrogen storage P_{Nstore} and D_{Nstore} respectively. P_{Nstore} and D_{Nstore} influence the amount of nitrogen storage N_{Store} of as well (5.7). Finally, the oxygen budget is based on production of oxygen through photosynthesis P_{O_2} , its consumption through respiration R_{Bio} , and diffusive exchange of oxygen V_{O_2} .

Since the metabolism differs between the light and dark periods, we employ different parameterizations of the fluxes in Table 5.1 at different times of day, as explained in the following subsections. Some terms are specific to particular times of day (if they are not applicable, they are assumed zero). Specifically, $P_l Chl$, λ related terms except $E\lambda$, P_{Cstore} , Exc , P_{Chl} , D_{Nstore} , and P_{O_2} are unique to the light period, and D_{Cstore} , N_{2fix} , and P_{Nstore} are specific to the dark period.

Table 5.1 Fundamental relations of carbon, nitrogen and oxygen based molecules. The definition of each term is listed in Supplementary Material.

$$\frac{dCH_c}{dt} = P_i Chl - \lambda(1 + E) - P_{Cstore} + D_{Cstore} - Exc \quad (5.2)$$

$$\frac{dC_{Store}}{dt} = P_{Cstore} - D_{Cstore} \quad (5.3)$$

$$\frac{dBio_c}{dt} = \lambda \quad (5.4)$$

$$\frac{dX}{dt} = \frac{X\lambda}{Q_c} \quad (5.5)$$

$$\frac{dNH_4^+}{dt} = N_{2fix} - \lambda Y_{Bio}^{N:C} - P_{Nstore} + D_{Nstore} \quad (5.6)$$

$$\frac{dN_{Store}}{dt} = P_{Nstore} - D_{Nstore} \quad (5.7)$$

$$\frac{dO_2}{dt} = P_{O_2} - R_{Bio} + V_{O_2} \quad (5.8)$$

In order to solve the model equations, we have applied a finite-difference method to equation (5.2) ~ (5.7) with a time step of 50 seconds. For the oxygen balance (5.8), we have assumed a pseudo steady state; thus oxygen uptake and oxygen production is always balanced by respiration. For the calculation of fluxes that influences the time variation of each pool, we have considered various factors, such as size of the pools, and light intensities (the details of the flux

calculation are described in the Supplementary Material 5.S1, and parameterization details and nomenclature are provided in 5.S3 and 5.S4 respectively).

Iron metabolism

Time dependence of each iron pool

The rates of carbon and nitrogen fixation both depend on the iron allocation to the enzymes which mediate those processes. Here we model the time dependent allocation to those iron pools. The time-dependent equations for the iron system are given in Table 5.2, and each term is defined in Supplementary Material. We assume that the exchange of iron between photosystem and nitrogenase is mediated by iron buffer (Figure 5.1B, Figure 5.2B, C) (Saito *et al*, 2011). Thus, the time variation of iron in the photosystem is based on its exchange with the buffer iron pool (5.9). The buffer iron pool is influenced not only by the iron from the photosystem, but also by the exchange of iron with nitrogenase (5.10). The iron allocation to nitrogenase results from the balance between the loss to and gain from the buffer (5.11). We have assumed that the chlorophyll to iron ratio (mol C mol Fe^{-1}) is constant, $Y_{Photo}^{Chl:Fe}$, thus, the balance in chlorophyll is proportional to the balance in photosystem iron (5.12).

Table 5.2 Fundamental relations of iron related molecules. The definition of each term is listed in Supplementary Material.

$$\frac{dFe_{Photo}}{dt} = F_{Buffer-Fe}^{Photo-Fe} - F_{Photo-Fe}^{Buffer-Fe} \quad (5.9)$$

$$\frac{dFe_{Buffer}}{dt} = -F_{Buffer-Fe}^{Photo-Fe} + F_{Photo-Fe}^{Buffer-Fe} - F_{Buffer-Fe}^{Nitroge-Fe} + F_{Nitroge-Fe}^{Buffer-Fe} \quad (5.10)$$

$$\frac{dFe_{Nitroge}}{dt} = F_{Buffer-Fe}^{Nitroge-Fe} - F_{Nitroge-Fe}^{Buffer-Fe} \quad (5.11)$$

$$\frac{dChl}{dt} = (F_{Buffer-Fe}^{Photo-Fe} - F_{Photo-Fe}^{Buffer-Fe}) Y_{Photo}^{Chl:Fe} \quad (5.12)$$

In order to calculate the amount of iron pools and chlorophyll, we have applied a finite-difference method to equation (5.9) ~ (5.12) with a time step of 50 seconds. For the computation of iron fluxes, we considered various factors, such as the size of the iron pool of the origin and the destination, time of day, oxygen concentration, and carbohydrate storage (see Supplementary Material 5.S2. for detailed equations, 5.S3 for parameterization, and 5.S4 for nomenclature). Since the metabolism of iron differs between the light and dark period, we define iron fluxes differently between these time periods.

5.4 Results and Discussion: Oxygen management strategies in *Crocospaera*

Using the system of equations and parameterizations defined above, we have simulated time-dependent laboratory cultures of *Crocospaera* published by Großkopf and LaRoche (2012). In a series of sensitivity experiments, we turn on and off various oxygen management strategies in the virtual *Crocospaera*, inspired by the strategies known to be used by *Azotobacter vinelandii* (see Chapter 2). These are respiratory protection, increasing cell radius and producing an extracellular polymeric barrier to oxygen (see equation (1) and Chapter 2). We ask does the presence or absence of each of these strategies qualitatively improve or degrade the veracity of the simulations?

The data set of Großkopf and LaRoche (2012) was particularly valuable for this exercise since the authors quantified various parameters such as the respiration rate, acetylene reduction rate (proxy for nitrogen fixation), and elemental ratios for different oxygen concentrations.

Figure 5.3~Figure 5.5 compare the model and the experimental data from Großkopf and LaRoche (2012); respiration rates, cellular nitrogen contents, and cellular carbon contents respectively. Each figure shows four scenarios (A) With all three oxygen management mechanisms (B) Without respiratory protection but with other two oxygen management mechanisms. (C) Without size variation but with other two oxygen management mechanisms. (D) Without diffusive protection but with other two oxygen management mechanisms. We examine whether missing mechanisms improve/degrade the simulations. An improvement suggests that the process in question may be employed by *Crocospaera* and thus presents a testable hypothesis. All panels show data points from two laboratory experiments, ambient oxygen concentrations equivalent to saturation with 20% and 5% atmospheric mixing ratios, and

four simulations (with/without scenarios for each oxygen concentration). Thus we specifically focus on the investments and adaptations to oxygen management.

The model results show that all the three oxygen management mechanisms considered (increasing respiration, increasing the cell size with oxygen concentration, and low diffusivity), can improve the simulations both qualitatively and quantitatively. We thus hypothesize that *Crocospaera* employs all three strategies.

Examining respiratory protection

We first examine the respiratory protection by comparing the scenario with and without respiratory protection (Figure 5.3~Figure 5.4 (A) for with respiratory protection and (B) without. When respiratory protection is represented, we follow the model developed in Chapter 2 and increase respiration sufficiently to reduce intracellular oxygen concentrations to a very low level during the night-time, nitrogen fixation period. As expected, total respiration is much greater in 20% oxygen than 5% oxygen (Figure 5.3A, Figure 5.4A, and Figure 5.5A). On the other hand, in the scenario without respiratory protection, intracellular oxygen concentration is assumed to have no impact on nitrogen fixation, and the respiration is computed based on the energy balance: there is just sufficient respiration to support night-time nitrogen fixation (Figure 5.3B, Figure 5.4B, and Figure 5.5B). We have set the same nitrogen fixation rate for both cases, so the differences in respiration are entirely due to the relative investments in the protection of nitrogenase.

With respiratory protection, the respiration is three to four times higher in the 20% oxygen environment than the 5% oxygen environment. When the oxygen concentration is 20%, the respiration rate is higher than the energetic demand for biosynthesis and nitrogen fixation.

Thus, the peak respiration rate controlled by the oxygen concentration. However, when the oxygen concentration is 5%, the peak respiration is controlled by the energy requirement for nitrogen fixation. Thus, at low oxygen concentrations, when the nitrogen fixation rate is near the peak, the energetically balanced respiration is sufficient for respiratory protection. These trends in the model match the laboratory data. These results indicate that the cells do employ respiratory protection.

In the model, we have allowed nitrogen fixation even when the respiratory protection is not sufficient to protect nitrogenase in order to compare the respiration rates between respiratory protection and respiration based on nitrogen fixation. Thus, the cellular nitrogen variation in these two cases are similar (Figure 5.4A and B). However, without respiratory protection, nitrogen fixation would not occur or be highly suppressed. This suppression would result in much lower cellular nitrogen content for 20% O₂ than 5% O₂, which is not observed in the laboratory data.

The cellular carbon content is influenced by the magnitude of respiration. With respiratory protection, when the oxygen concentration is 20%, high respiration leads to a high consumption of carbon storage rapidly decreasing the cell carbon during the dark period (Figure 5.5A in red). On the other hand, when the respiration is low/near the energetically balanced level, the decrease in the cell carbon is smaller (Figure 5.5A in black). As a result, the red and black curves cross in Figure 5.5A, as can be seen in the laboratory data points. Cell carbon is higher for the 20% oxygen environment at the initiation of the dark period, but due to the high respiration rate, the cell carbon becomes lower than the 5% oxygen environment during the dark periods. Without respiratory protection, the cell carbon is overestimated for 20% resulting in

having higher values than the 5% oxygen case throughout the dark period, which does not represent the laboratory data, indicating that the cell applies respiratory protection.

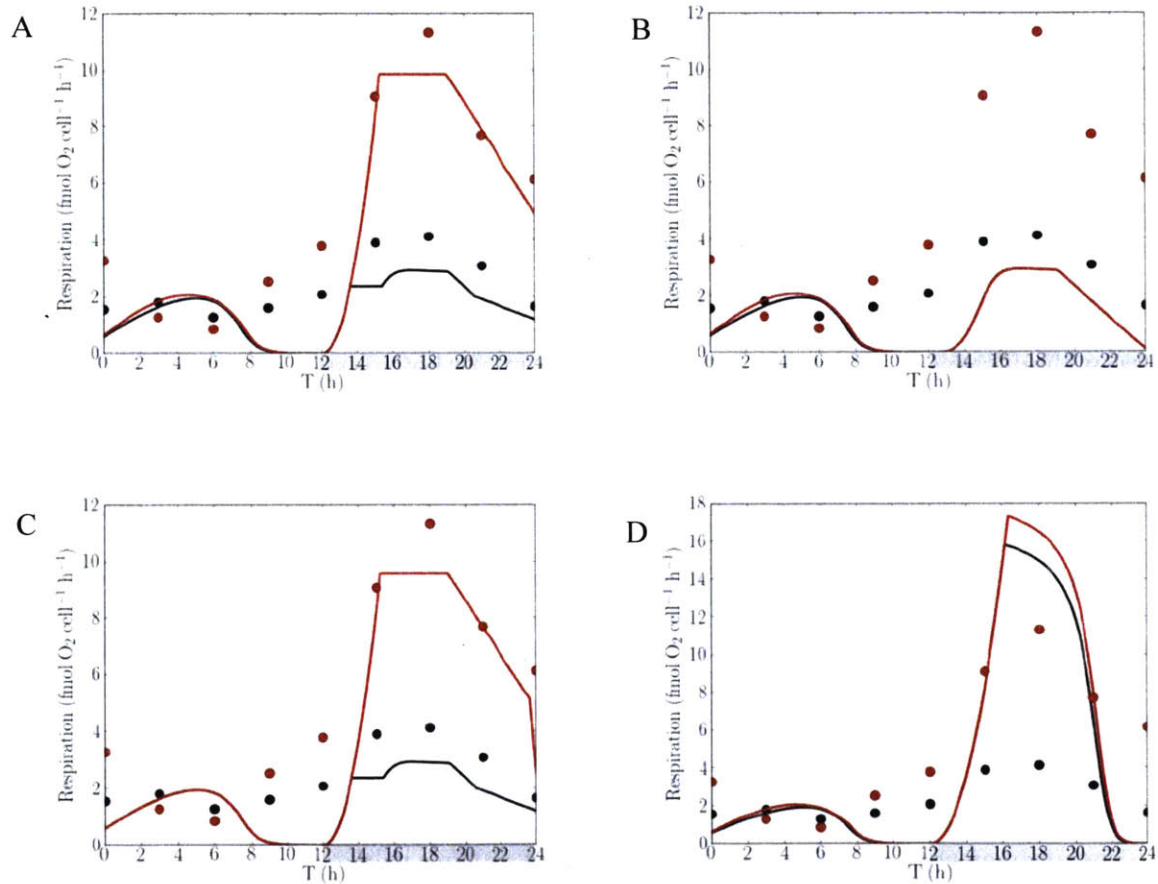


Figure 5.3 Respiration rate for four different scenarios. (A) With all the oxygen management mechanisms (B) Without respiratory protection. (C) Without cell size adaptation. (D) Without diffusive protection. Red: 20% O₂ concentration. Black: 5% O₂ concentration. Dots: laboratory data from Großkopf and LaRoche (2012). Curves: model results from this study. First 12 hours are the light period (no shading) and the later 12 hours are the dark period (gray shading).

Cell size adaptation

Since *Azotobacter vinelandii* (a heterotrophic nitrogen fixer; see Chapter 2) increases its cell size, and reduces oxygen uptake, in high oxygen environments we explored the possibility that *Crocospaera* might employ a similar strategy. Varying the cell size based on the oxygen concentration improves the model results, leading to the testable hypothesis that *Crocospaera* adapt their size in order to regulate oxygen uptake, since a larger cell has low oxygen uptake per volume. In the model with size adaptation, we have used 1.28 (μm) for 5% oxygen, and 1.32 (μm) for 20% oxygen (Figure 5.3A, Figure 5.4A, and Figure 5.5A). On the other hand, for the scenario without size adaptation, we have used 1.28 (μm) for both oxygen concentration (Figure 5.3C, Figure 5.4C, and Figure 5.5C). The respiration rates are similar between two scenarios and both represent the laboratory results in a similar way. Cellular nitrogen and carbon, however, show larger differences between two scenarios. The model results are quantitatively more similar to the laboratory data with size adaptation than without it, supporting this oxygen management mechanism.

Without size adaptation, cellular nitrogen is underestimated for 20% O₂ case (Figure 5.4C). The nitrogen content in the laboratory data shows higher values for most of the time. However, the simulation without size adaptation shows the same values for the light period, and even lower values for the dark period, conflicting with the experimental data. The difference between the laboratory data and the model is especially pronounced during the late dark periods after nitrogen storage is accumulated, suggesting that size adaptation has to be incorporated in the model.

With the size adaptation, we can capture the trend in the laboratory data throughout the both light and dark periods: higher cellular nitrogen for 20% case. In particular, the laboratory data shows larger differences during the light period and smaller difference during the dark period. This trend is also captured by the model with size adaptation. Based on the model, under 5% O₂ condition, the cells fix more nitrogen per cell volume than 20%, since 5% O₂ is favorable for nitrogen fixation than 20% O₂. This leads to the accumulation of higher nitrogen storage for 5% O₂ resulting in higher increase in nitrogen content. However, since the cell size is larger for 20% O₂ case, the cellular nitrogen is still higher for 20% O₂ even during the late dark period as can be seen in the laboratory data. During the light period, there is no nitrogen fixation, and the cellular nitrogen store is consumed for cell growth, resulting in larger difference in nitrogen content between the two oxygen cases.

Incorporating size variation also improves cellular carbon (comparing Figure 5.5 A and C). The laboratory data shows a higher carbon content for 20% O₂ during the light period. With size variation can explain this difference since larger cells generally contains higher carbon. Without size adaptation, however, the model shows the same values in both oxygen cases, conflicting the laboratory data. With size adaptation, the model captures the flip between two lines during the dark periods as can be seen in the laboratory data, which occurs due to higher carbohydrate consumption for respiratory protection for 20% O₂ than 5% O₂, further supporting the hypothesis of size adaptation. This could be tested in the laboratory.

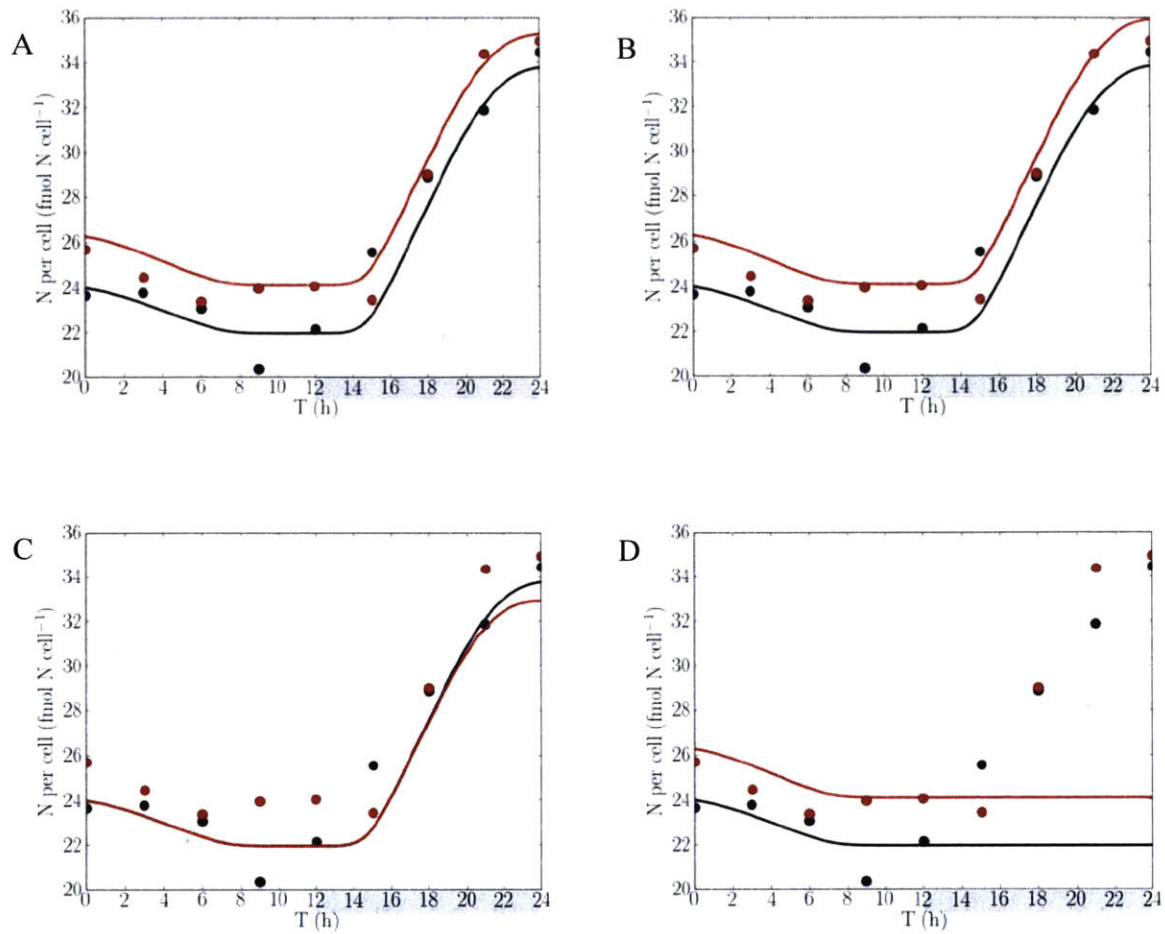


Figure 5.4 Cellular nitrogen content. (A) With all the oxygen management mechanisms (B) Without respiratory protection. (C) Without cell size adaptation. (D) Without diffusive protection. Red: 20% O_2 concentration. Black: 5% O_2 concentration. Dots: laboratory data from Großkopf and LaRoche (2012). Curves: model results from this study. First 12 hours are the light period (no shading) and the later 12 hours are the dark period (gray shading).

Diffusive protection

The model results indicate a significantly low diffusivity of the cell membrane layer. In order to obtain a reasonable match to the experimental data, we must set the relative diffusivity of oxygen through the membrane compared to water at 1.5×10^{-5} , which is about 50 times lower than the value we employed in the *Azotobacter* model in Chapter 1 and Chapter 2 (define this case as “with diffusive protection”). Figure 5.3D, Figure 5.4D, and Figure 5.5D are the results with the diffusivity applied to the *Azotobacter* model for comparison (define this case as “without diffusive protection”). Without diffusive protection, the oxygen flux into the cell is so high that even at 5% oxygen environment leads to an even higher respiratory requirement than 20% case with diffusive protection (comparing Figure 5.3A red curve with Figure 5.3D black curve).

Without diffusive protection, the respiration rate is limited by the carbon storage availability, and is never sufficient for scavenging intracellular oxygen. Also, as carbon storage decreases, respiration rate drops quickly and becomes nearly zero before the end of the dark period (Figure 5.3D). The sharp decrease in the carbon storage is represented in the time variation of the cell carbon both for 5% and 20% case, showing significantly lower values than the experimental data (Figure 5.5D). In the model, due to the high respiration, which is still not enough for the respiratory protection, nitrogen fixation does not occur. This trend is represented by a low cellular nitrogen during the dark periods (Figure 5.4D); while the experimental data show clear accumulation of cell nitrogen in the dark period, the model shows the constant value at the minimum level. These results suggest that to successfully scavenge oxygen, the cell must maintain a significant barrier to oxygen invasion.

Since the predicted diffusivity is significantly low, it might be that *Crocospaera* fix nitrogen with relatively high intracellular O₂ concentration. Although it has been noted that a micro-oxic

environment is required for nitrogen fixation (Dalton and Postgate, 1969; Wang *et al.*, 1985; Poole and Hill, 1997), the intracellular oxygen concentration of the live nitrogen fixers has never been directly measured. If *Crocospaera* can maintain nitrogenase activity in the relatively high intracellular oxygen environment, the actual diffusivity of the cell membrane could be even higher than what we have predicted. However, similar magnitude of O₂ diffusivity is reported for heterocystous nitrogen fixers (Walsby, 1985), and it is certainly possible that *Crocospaera* has a similar level of diffusive protection.

One possibility is that carbohydrate storage may act as oxygen barrier. Figure 2 in Dron *et al.*, (2012a) shows granules accumulated along the cell membrane rather than spreading in the cytoplasm. The granule is made up of starch, relatively rigid and dense hydrophilic molecules, it is possible that they act as a barrier against oxygen during the early night period, before the starch is consumed.

Another possible cause of the low diffusivity is the production of extracellular polymeric substances (EPS). EPS may create a thick hydrophilic layer, where the diffusion of oxygen molecules is reduced. In a batch culture study by Sohm *et al.*, (2011), *Crocospaera* produces EPS roughly proportional to their growth. Also, Dron *et al.*, (2012a) have observed a higher production of EPS during the dark period. In their paper, they mention that the oxygen barrier effect of EPS is hypothesized by Prospero (1994). As described in Chapter I, Sabra *et al* (2000) hypothesize that *Azotobacter vinelnadii* excrete alginate (one kind of EPS) to decrease the passive oxygen uptake to protect nitrogenase. Given the similarity between *Crocospaera* and *Azotobacter* it would not be surprising that *Crocospaera* uses EPS for diffusive protection.

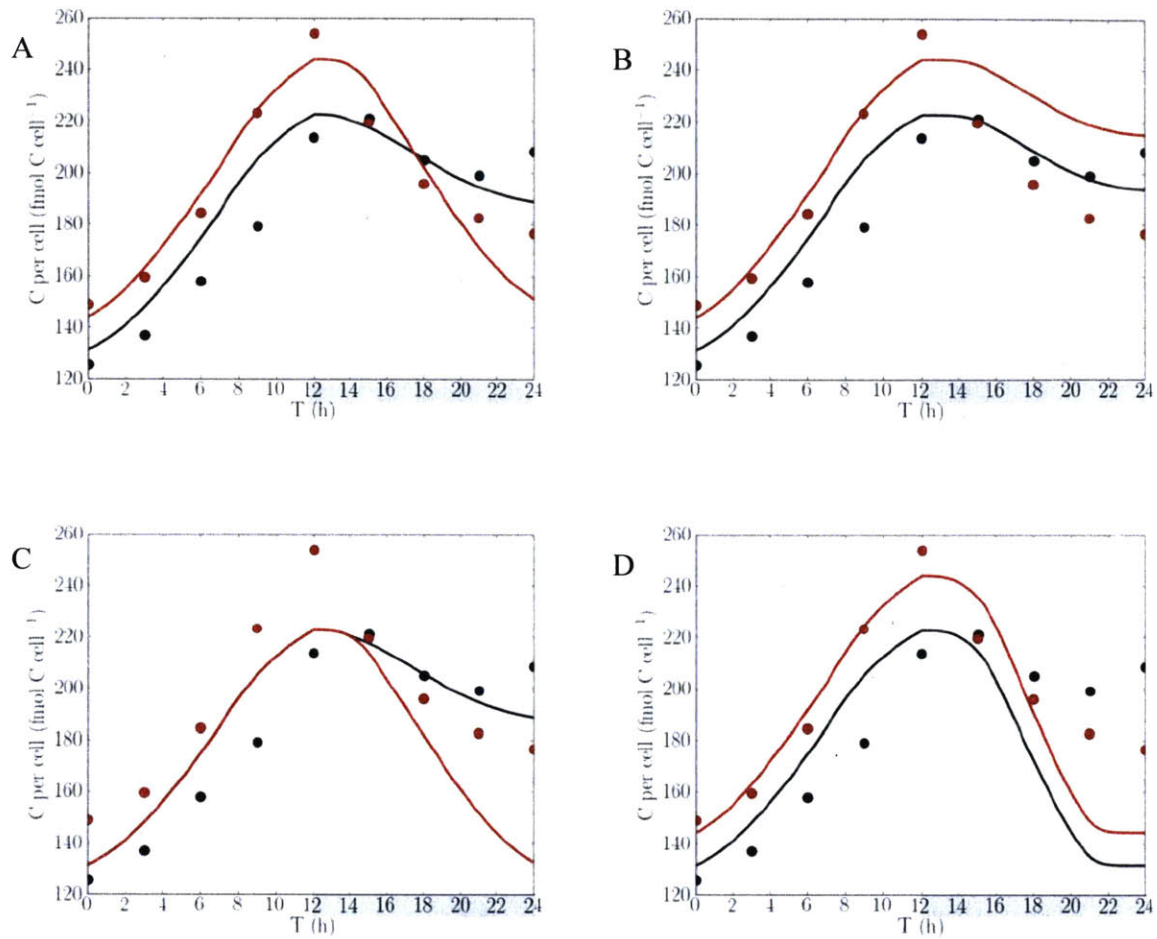


Figure 5.5 Cellular carbon content. (A) With all the oxygen management mechanisms (B) Without respiratory protection. (C) Without cell size adaptation. (D) Without diffusive protection. Red: 20% O₂ concentration. Black: 5% O₂ concentration. Dots: laboratory data from Großkopf and LaRoche (2012). Curves: model results from this study. First 12 hours are the light period (no shading) and the later 12 hours are the dark period (gray shading).

5.5 Implication of these oxygen management mechanisms to the ecosystem

This study indicates three oxygen managements by *Crocospaera*: respiratory protection, size adaptation, and diffusive protection, all of which require a high amount of carbon. Respiratory protection demands higher carbon than energetically balanced respiration, increasing size with oxygen requires carbon, and phosphorus for developing additional cell membranes, and diffusive protection can be based on EPS, which requires significant amount of carbon. Based on this high carbon demand, we hypothesize that *Crocospaera* is adapted to regions where excess carbon fixation occurs relative to other nutrients, such as iron and phosphorus. This hypothesis is supported by observations where high abundance of *Crocospaera* was found in subtropical regions (e.g. Zehr *et al*, 2001; Montoya *et al*, 2004), since in these regions, there is a high irradiance but nutrient is often limited.

Currently, global 3D ocean ecosystem models predict the distribution of nitrogen fixers based on the resource ratio supply to the each computational grid, specifically by P/N and Fe/N supply ratios (Dutkiewicz *et al.*, 2012; Ward *et al.*, 2013; Dutkiewicz *et al.*, 2014). Although this method predicts the distribution of the autotrophic nitrogen fixers as a whole, more information is required for predicting the distribution of different functional types of nitrogen fixers. Based on our study, we may add new constraints to the model based on carbon resources (e.g. C/N, C/Fe, and C/P supply ratios), in order to predict the distribution of *Crocospaera* in the ocean. Since *Crocospaera* has different metabolism and environmental influence than other nitrogen fixers, this new theory will potentially contribute to further understanding of nitrogen and carbon cycles in the ocean.

5.6 Summary and conclusions

In order to study the oxygen management of *Crocospaera*, we have developed the cell flux model applied to *Crocospaera*. The model consists of macromolecules and inorganic reservoirs with fluxes among them, creating a simple flux network. We have also considered the iron flux for computing the capacity of nitrogen fixation and photosynthesis. We have compared the model results with the experimental dataset from Großkopf and LaRoche (2012), and examined what protection mechanisms are necessary for representing the experimental data.

The model results indicate three potential strategies: respiratory protection, size variation with oxygen, and significantly low diffusivity in/around the cell membrane. When oxygen concentration is 20%, the respiration is much higher than the energetically required level, indicating the extra respiration for oxygen scavenging. By incorporating the positive relationship between the size and the oxygen concentration, the model better represents the relation between 5% and 20% oxygen case in the experimental data. Finally, with the given respiration rate, extremely small diffusivity is required for the cell to keep a microoxic environment. These results help us understand the costs and benefits of unicellular nitrogen fixers in the ocean and model the global ocean ecosystem and its biogeochemistry.

5.7 References

- de Boyer Montégut C, Madec G, Fischer AS, Lazar A, Iudicone D. (2004). Mixed layer depth over the global ocean: An examination of profile data and a profile-based climatology. *J Geophys Res* **109**: C12003, doi:10.1029/2004JC002378.
- Caperon J, Meyer J. (1972). Nitrogen-limited growth of marine phytoplankton-I. Changes in population characteristics with steady-state growth rate. *Deep Sea Res* **19**: 601–618.
- Dalton H, Postgate JR. (1969). Effect of oxygen on growth of *Azotobacter chroococcum* in batch and continuous cultures. *J Gen Microbiol* **54**: 463–473.

- Dron A, Rabouille S, Clauquin P, Chang P, Raimbault V, Talec A, *et al.* (2012a). Light:dark (12:12 h) quantification of carbohydrate fluxes in *Crocospaera watsonii*. *Aquat Microb Ecol* **68**: 43–55.
- Dron A, Rabouille S, Clauquin P, Roy B, Talec A, Sciandra A. (2012b). Light-dark (12:12) cycle of carbon and nitrogen metabolism in *Crocospaera watsonii* WH8501: relation to the cell cycle. *Environ Microbiol* **14**: 967–981.
- Dutkiewicz S, Ward BA, Scott JR, Follows MJ. (2014). Understanding predicted shifts in diazotroph biogeography using resource competition theory. *Biogeosciences Discuss* **11**: 7113–7149.
- Dutkiewicz S, Ward BA, Monteiro F, Follows MJ. (2012). Interconnection of nitrogen fixers and iron in the Pacific Ocean: Theory and numerical simulations. *Global Biogeochem Cycles* **26**: 1–16.
- Dyhrman ST, Haley ST. (2006). Phosphorus scavenging in the unicellular marine diazotroph *Crocospaera watsonii*. *Appl Environ Microbiol* **72**: 1452–1458.
- Falkowski PG. (1997). Evolution of the nitrogen cycle and its influence on the biological sequestration of CO₂ in the ocean. *Nature* **387**: 272–275.
- Fransson A, Chierici M, Anderson LG. (2004). Diurnal variability in the oceanic carbon dioxide system and oxygen in the Southern Ocean surface water. *Deep Res Part II Top Stud Oceanogr* **51**: 2827–2839.
- Gallon JR. (1981). The oxygen sensitivity of nitrogenase: a problem for biochemists and microorganisms. *Trends Biochem Sci* **6**: 19–23.
- Großkopf T, LaRoche J. (2012). Direct and indirect costs of dinitrogen fixation in *Crocospaera watsonii* WH8501 and possible implications for the nitrogen cycle. *Front Microbiol* **3**: doi: 10.3389/fmicb.2012.00236.
- Gruber N. (2004). The dynamics of the marine nitrogen cycle and its influence on atmospheric CO₂ variations. In: *The Ocean Carbon Cycle and Climate*, edited by Follows, M. and Oguz, T. Kluwer Academic: Dordrecht. 97–148.
- Gruber N, Galloway JN. (2008). An Earth-system perspective of the global nitrogen cycle. *Nature* **451**: 293–296.
- JGR. Genom Portal, *Crocospaera watsonii* WH8501. <http://genome.jgi-psf.org/crowa/crowa.home.html>. accessed June 4, 2016.
- Masuda T, Furuya K, Kodama T, Takeda S, Harrison PJ. (2013). Ammonium uptake and dinitrogen fixation by the unicellular nanocyanobacterium *Crocospaera watsonii* in nitrogen-limited continuous cultures. *Limnol Oceanogr* **58**: 2029–2036.
- Mohr W, Intermaggio MP, LaRoche J. (2010). Diel rhythm of nitrogen and carbon metabolism in the unicellular, diazotrophic cyanobacterium *Crocospaera watsonii* WH8501. *Environ Microbiol* **12**: 412–421.

- Mohr W, Vagner T, Kuypers MMM, Ackermann M, LaRoche J. (2013). Resolution of conflicting signals at the single-cell level in the regulation of cyanobacterial photosynthesis and nitrogen fixation. *PLOS ONE* **8**: e66060. doi:10.1371/journal.pone.0066060.
- Montoya JP, Holl CM, Zehr JP, Hansen A, Villareal TA, Capone DG. (2004). High rates of N₂ fixation by unicellular diazotrophs in the oligotrophic Pacific Ocean. *Nature* **430**: 1027–1031.
- Najjar RG, Keeling RF. (2000). Mean annual cycle of the air-Sea oxygen flux: A global view. *Global Biogeochem Cycles* **14**: 573–584.
- Poole RK, Hill S. (1997). Respiratory protection of nitrogenase activity in *Azotobacter vinelandii*: Roles of the terminal oxidases. *Biosci Rep* **17**: 303–317.
- Prosperi CH. (1994). A cyanophyte capable of fixing nitrogen under high levels of oxygen. *J Phycol* **30**: 222–224.
- Robertson JE, Watson AJ, Langdon C, Ling RD, Wood JW. (1993). Diurnal variation in surface pCO₂ and O₂ at 60°N, 20°W in the North Atlantic. *Deep Res Part II* **40**: 409–422.
- Ryther JH, Dunstan WM. (1971). Nitrogen, phosphorus, and eutrophication in the coastal marine environment. *Science* **171**: 1008–1013.
- Sabra W, Zeng AP, Lünsdorf H, Deckwer WD. (2000). Effect of oxygen on formation and structure of *Azotobacter vinelandii* alginate and its role in protecting nitrogenase. *Appl Environ Microbiol* **66**: 4037–4044.
- Saito MA, Bertrand EM, Dutkiewicz S, Bulygin V V., Moran DM, Monteiro FM, *et al.* (2011). Iron conservation by reduction of metalloenzyme inventories in the marine diazotroph *Crocospaera watsonii*. *Proc Natl Acad Sci* **108**: 2184–2189.
- Shi T, Ilikchyan I, Rabouille S, Zehr JP. (2010). Genome-wide analysis of diel gene expression in the unicellular N₂-fixing cyanobacterium *Crocospaera watsonii* WH 8501. *ISME J* **4**: 621–632.
- Sohm JA, Webb EA, Capone DG. (2011). Emerging patterns of marine nitrogen fixation. *Nat Rev Microbiol* **9**: 499–508.
- Thomas WH. (1970). On nitrogen deficiency in tropical pacific oceanic phytoplankton: photosynthetic parameters in poor and rich water. *Limnol Oceanogr* **15**: 380–385.
- Thomas WH, Owen RW. (1971). Estimating phytoplankton production from ammonium and chlorophyll concentrations in nutrient-poor water of the eastern tropical Pacific Ocen. *Fish Bull* **69**: 87–92.
- Walsby AE. (1985). The permeability of heterocysts to the gases nitrogen and oxygen. *Proc R Soc B Biol Sci* **226**: 345–366.
- Wang ZC, Burns A, Watt GD. (1985). Complex formation and O₂ sensitivity of *Azotobacter vinelandii* nitrogenase and its component proteins. *Biochemistry* **24**: 214–221.

Ward BA, Dutkiewicz S, Moore CM, Follows MJ. (2013). Iron, phosphorus, and nitrogen supply ratios define the biogeography of nitrogen fixation. *Limnol Oceanogr* **58**: 2059–2075.

Yates KK, Dufore C, Smiley N, Jackson C, Halley RB. (2007). Diurnal variation of oxygen and carbonate system parameters in Tampa Bay and Florida Bay. *Mar Chem* **104**: 110–124.

Zehr JP, Waterbury JB, Turner PJ, Montoya JP, Omoregie E, Steward GF, *et al.* (2001). Unicellular cyanobacteria fix N₂ in the subtropical North Pacific Ocean. *Nature* **412**: 635–638.

Supplementary Material

5.S1 Computation of carbon, nitrogen, and oxygen metabolism

Light period

The rate of photosynthesis dependent on the abundance of chlorophyll, which is dynamic and related to iron allocation (see equation (34), Table 2). We also compute an “ideal” abundance of Chlorophyll; that which would support sufficient carbon fixation to match the demands of nitrogen limited biosynthesis, based on the nitrogen stored. In other words, we can evaluate the ideal chlorophyll concentration as that for which the cell is co-limited by light and nitrogen in the light period. The biomass production rate which determines the ideal chlorophyll concentration ($\text{mol C cell}^{-1} \text{ s}^{-1}$) is thus equal to the nitrogen limited biomass production rate, described as follows by using Michaelis-Menten form:

$$\lambda^{Chl-ideal} = \lambda^{\max} \frac{N_{store}}{N_{store} + K_{Nstore} \frac{Y_{Bio-all}^{N:C}}{Y_{Bio}^{N:C}}} \quad (5.S1)$$

where λ^{\max} ($\text{mol C cell}^{-1} \text{ s}^{-1}$) is the maximum biomass production rate, N_{store} (mol N cell^{-1}) is the nitrogen storage, K_{Nstore} (mol N cell^{-1}) is the nitrogen-storage-half-saturation constant for biomass production, and $Y_{Bio-all}^{N:C}$ and $Y_{Bio}^{N:C}$ (mol N mol C^{-1}) is the N:C ratio of biomass with and without the nutrient storage, respectively.

At the same time, photosynthesis must meet the demands for storage to support night time activity. We compute the rate of carbon storage production based on the current magnitude of carbon storage:

$$P_{Cstore}^{Chl-ideal} = (C_{store}^{\max} - C_{store}) R_{Cstore} \quad (5.S 2)$$

where $P_{C_{store}}^{Chl-ideal}$ (mol C cell⁻¹ s⁻¹) is the ideal carbon storage production rate, C_{store}^{max} (mol C cell⁻¹) is the maximum carbon storage, C_{store} (mol C cell⁻¹) is the carbon storage, and $R_{C_{store}}$ (s⁻¹) is the rate constant for the carbon storage production. If the carbon store is not at maximum capacity, photosynthesis is required to provide a supply at a rate sufficient to keep up with the prescribed storage rate, $R_{C_{store}}$. This is the ideal carbon storage production; that which would be associated with the ideal chlorophyll abundance.

Using (9) and (10) to define the ideal biomass production rate $\lambda^{Chl-ideal}$ and carbon storage production rate $P_{C_{store}}^{Chl-ideal}$, we can use the equilibrium solution of (2) (light period, no excretion) to define the “ideal” chlorophyll concentration Chl^{ideal} (mol C cell⁻¹):

$$Chl^{ideal} = \frac{\lambda^{Chl-ideal} (1 + E) + P_{C_{store}}^{Chl-ideal}}{P_I} \quad (5.S 3)$$

Here, E (dimensionless) is the ratio of the carbohydrate production rate to the biomass production rate based the method on Rittmann and McCarty (2001), and P_I (s⁻¹) is the photosynthesis rate per chlorophyll. For obtaining P_I , we a “target theory” based equation used in many other studies (ex. Webb *et al.*, 1974; Platt *et al.*, 1980; Cullen, 1990; Geider *et al.*, 1996, 1997, and 1998):

$$P_I = P_I^{max} (1 - e^{-A_{PHO} I}). \quad (5.S 4)$$

Since the Chlorophyll concentration is typically not at this ideal state, we parameterize the synthesis terms accordingly. When $Chl^{ideal} > Chl$ where Chl is the actual chlorophyll amount (mol C cell⁻¹), the cell is light limited and carbon storage and biomass synthesis are accordingly reduced from their ideal rates by a factor M_{Chl} (dimensionless):

$$M_{Chl} = \frac{Chl}{Chl^{ideal}} \quad (5.S 5)$$

Alternatively when $Chl^{ideal} \leq Chl$,

$$M_{Chl} = 1. \quad (5.S 6)$$

Hence biomass production rate λ (mol C cell⁻¹ s⁻¹) and the carbon storage production P_{Cstore} are evaluated as calculated as follows:

$$\lambda = \lambda^{Chl-ideal} M_{Chl} \quad (5.S 7)$$

and

$$P_{Cstore} = P_{Cstore}^{Chl-ideal} M_{Chl}. \quad (5.S 8)$$

When $Chl^{ideal} < Chl$, the extra carbon fixed is assumed excreted to the environment at a rate given by:

$$Exc = ChlP_l - \lambda(1 + E) - P_{Cstore}. \quad (5.S 9)$$

Once biomass production rate λ is computed, we can energetically and stoichiometrically relate λ to the biomass production balanced respiration rate R_{Bio} (mol O₂ cell⁻¹ s⁻¹), and to consumption of the nitrogen storage D_{Nstore} (mol N cell⁻¹ s⁻¹) respectively:

$$R_{Bio} = \lambda Y_{SYNTH}^{O_2:Bio} \quad (5.S 10)$$

and

$$D_{Nstore} = \lambda Y_{Bio}^{N:C} \quad (5.S 11)$$

where $Y_{SYNTH}^{O_2: BIO}$ (mol O₂ mol C⁻¹) is the ratio of oxygen production and biomass synthesis, and $Y_{Bio}^{N:C}$ (mol N mol C⁻¹) is the N:C ratio in biomass. Also, we can stoichiometrically relate carbon fixation rate to the photosynthetic oxygen production rate P_{O_2} (mol O₂ cell⁻¹ s⁻¹):

$$P_{O_2} = P_I Chl Y_{NON-SYNTH}^{O_2: CH} \quad (5.S 12)$$

where $Y_{NON-SYNTH}^{O_2: CH}$ (mol O₂ mol C⁻¹) is the O₂/C ratio in the non-synthesis respiration (introduced in Chapter 1). Using these rates, we can step forward in time equations (2)-(7).

We assume that the intracellular oxygen rapidly equilibrates (as is reasonable for small cells). From the respiration rate and the oxygen production rate (equations (17) and (19)), the steady state net oxygen consumption rate, V_{O_2} (mol O₂ cell⁻¹ s⁻¹) can be calculated based on the balance between the respiration and the production:

$$V_{O_2} = R_{Bio} - P_{O_2} \quad (5.S 13)$$

Assuming equilibrium and solving equation (8), the intracellular oxygen concentration [O_2^{CELL}] is obtained as follows:

$$[O_2^{CELL}] = [O_2] - \frac{V_{O_2}}{4\pi r \kappa_{O_2}} \quad (5.S 14)$$

(see Chapter 2 for description of diffusive oxygen uptake and the development of similar solutions).

Dark period

During the dark period, the rates of nitrogen fixation and respiration are influenced by the rate of consumption of stored carbon, which is the electron and energy source for both nitrogen fixation

and respiration. The potential carbon storage decomposition rate (mol C cell⁻¹ s⁻¹) is based on the availability of the carbon storage is represented by the following Michaelis-Menten form:

$$D_{C_{store}}^{potential} = D_{C_{store}}^{max} \frac{C_{store}}{C_{store} + K_{C_{store}}^{Decom}} \quad (5.S 15)$$

where $D_{C_{store}}^{max}$ (mol C cell⁻¹ s⁻¹) is the maximum carbon storage decomposition rate, and $K_{C_{store}}^{Decom}$ (mol C cell⁻¹) is the half saturation constant of the carbon storage for $D_{C_{store}}^{potential}$. This $D_{C_{store}}^{potential}$ imposes the limit of nitrogen fixation and respiration based on the availability of the carbon storage. In addition to that, respiration is limited by the potential oxygen uptake rate and the enzymatically constrained respiratory potential. The potential oxygen uptake (mol O₂ cell⁻¹ s⁻¹) is obtained when the intracellular oxygen concentration is zero:

$$V_{O_2}^{potential} = 4\pi r \kappa_{O_2} [O_2] \quad (5.S 16)$$

where each variable is introduced in Chapter 1. The enzymatically constrained respiratory potential (mol O₂ cell⁻¹ s⁻¹) increases with time after the initiation of the dark period and is represented as follows:

$$R_{enzyme}^{potential} = (t_{dark})^{P3} C_{O_2}^{potential} \quad (5.S 17)$$

where t_{dark} (s) is the time passed since the initiation of the dark period, $P3$ (dimensionless) and

$C_{O_2}^{potential}$ (unit depends on $P3$) are the power factor and the respiratory coefficient for $R_{enzyme}^{potential}$.

We have used this power factor in order to express the observed non-linear time dependence of

respiration during the dark period (Großkopf and LaRoche, 2012). If $V_{O_2}^{potential} > R_{enzyme}^{potential}$, the

potential respiration rate $R_{O_2}^{potential}$ (mol O₂ cell⁻¹ s⁻¹) is equal to $R_{enzyme}^{potential}$, while

$V_{O_2}^{potential} \leq R_{enzyme}^{potential}$, it is equal to $V_{O_2}^{potential}$ (mol O₂ cell⁻¹ s⁻¹). At the same time, $R_{O_2}^{potential}$ must be

larger than the minimum respiration rate for supporting nitrogen fixation. Also, we assume pseudo steady state of cellular oxygen, thus:

$$R_{O_2} = V_{O_2} \quad (5.S 18)$$

and CO₂ production rate $E \lambda$ is computed as follows:

$$E \lambda = \frac{R_{O_2}}{Y_{NON-SYNTH}^{O_2:CH}} \quad (5.S 19)$$

where $Y_{NON-SYNTH}^{O_2:CH}$ (mol O₂ mol C⁻¹) is the ratio of oxygen consumption and carbohydrate consumption in non-synthesis respiration.

The potential nitrogen fixation rate (mol N cell⁻¹ s⁻¹) is constrained by the availability of nitrogenase enzyme:

$$N_{2 \text{ fix}}^{\text{potential}} = Fe_{\text{nitroge}} C_{Fe\text{-nitroge}}^{N_2 \text{ fix}} \quad (5.S 20)$$

where Fe_{nitroge} (mol Fe cell⁻¹) is the amount of iron in nitrogenase, and $C_{Fe\text{-nitroge}}^{N_2 \text{ fix}}$ (mol N mol Fe⁻¹ s⁻¹) is the nitrogen-fixing capacity per nitrogenase iron.

We can ask whether the cell is nitrogen or carbon limited: i.e. whether there is enough carbon stored to meet the demands of potential nitrogen fixation? To do that, we first define the ideal carbon storage decomposition rate $D_{Cstore}^{\text{ideal}}$ (mol C cell⁻¹ s⁻¹) based on those nitrogen fixation and respiration rates:

$$D_{Cstore}^{\text{ideal}} = \frac{N_{2 \text{ fix}}^{\text{potential}} Y_{N_2 \text{ fix}}^{CH:N}}{R_{H_2}} + \frac{R_{O_2}^{\text{potential}}}{Y_{NON-SYNTH}^{O_2:CH}} \quad (5.S 21)$$

where $Y_{N_2 \text{ fix}}^{CH:N}$ (mol C mol N⁻¹) is the ratio of carbohydrate consumption (for electron donation for nitrogen fixation) to nitrogen fixation, and R_{H_2} (dimensionless) is a coefficient for electron recycling from hydrogen molecules. If $D_{Cstore}^{\text{ideal}} < D_{Cstore}^{\text{potential}}$, the decomposition rate of carbon

storage D_{Cstore} is controlled by D_{Cstore}^{ideal} and $N_{2fix} = N_{2fix}^{potential}$. If $D_{Cstore}^{ideal} > D_{Cstore}^{potential}$, $D_{Cstore}^{potential}$

controls the rate D_{Cstore} , and the nitrogen fixation rate is down regulated by $D_{Cstore}^{potential}$:

$$N_{2fix} = \left(\frac{D_{Cstore}^{potential} Y_{NON-SYNTH}^{O2:CH} - R_{O2}^{potential}}{Y_{N2fix}^{CH:N} Y_{NON-SYNTH}^{O2:CH}} \right) R_{H2} \quad (5.S 22)$$

Finally, if $R_{O2}^{potential} > D_{Cstore}^{potential}$, there is no nitrogen fixation and the respiration rate equals

$D_{Cstore}^{potential}$. We assume that all the fixed nitrogen goes to the nitrogen storage, thus,

$$P_{Nstore} = N_{2fix} \quad (5.S 23)$$

and the nitrogen storage amount N_{store} (mol N cell⁻¹) for each time step is computed.

5.S2 Computation of iron metabolism

Light period

We have simulated the translocation of iron among different cellular components; photosystem iron, buffer iron, and nitrogenase iron. Computing iron flux and iron content in each component is essential in predicting photosynthesis and nitrogen fixation. The rate of iron translocation is constrained by the amount of iron in each location.

When $Chl^{ideal} > Chl$ there is translocation of iron from buffer to the photosystem, whose

flux $F_{Buffer-Fe}^{Photo-Fe}$ (mol Fe cell⁻¹ s⁻¹) is represented as follows:

$$F_{Buffer-Fe}^{Photo-Fe} = (Fe_{Photo}^{ideal} - Fe_{Photo}) R_{Buffer-Fe}^{Photo-Fe} \frac{Fe_{Buffer}}{Fe_{Buffer} + K_{FeBuffer}^{Buffer-Photo}} \quad (5.S 24)$$

where Fe_{Photo}^{ideal} (mol Fe cell⁻¹) is the ideal iron mass in the photosystem, Fe_{Photo} (mol Fe cell⁻¹) is

the actual iron mass in the photosystem, $R_{Buffer-Fe}^{Photo-Fe}$ (s⁻¹) is the photosystem production efficiency,

Fe_{Buffer} (mol Fe cell⁻¹) is the iron mass in the buffer, and $K_{FeBuffer}^{Buffer-Photo}$ (mol Fe cell⁻¹) is the buffer iron half saturation constant for $F_{Buffer-Fe}^{Photo-Fe}$. We assume that the amount of the photosystem iron per chlorophyll is constant so that Fe_{Photo}^{ideal} (mol Fe cell⁻¹) is obtained from Chl^{ideal} calculated in equation (5.S 3). $R_{Buffer-Fe}^{Photo-Fe}$ is a function of time in the light period:

$$R_{Buffer-Fe}^{Photo-Fe} = t_{light} C_{Buffer-Fe}^{Photo-Fe} \quad (5.S 25)$$

where $C_{Buffer-Fe}^{Photo-Fe}$ (s⁻²) is a constant value.

When $Chl_{ideal} \leq Chl$, there is a flux of iron from the photosystem to the buffer $F_{Photo-Fe}^{Buffer-Fe}$ (mol Fe cell⁻¹ s⁻¹), represented as follows:

$$F_{Photo-Fe}^{Buffer-Fe} = (Fe_{Photo} - Fe_{Photo}^{ideal}) R_{Photo-Fe}^{Buffer-Fe} \frac{Fe_{Photo}}{Fe_{Photo} + K_{FePhoto}^{Photo-Buffer}} \quad (5.S 26)$$

where $R_{Photo-Fe}^{Buffer-Fe}$ (s⁻¹) is the rate constant for $F_{Photo-Fe}^{Buffer-Fe}$ and $K_{FePhoto}^{Photo-Buffer}$ (mol Fe cell⁻¹) is the photosystem iron half saturation constant for $F_{Photo-Fe}^{Buffer-Fe}$. In addition to the iron transfer between the photosystem and the buffer, there can be a flux of iron from nitrogenase to the buffer $F_{Nitroge-Fe}^{Buffer-Fe}$ (mol Fe cell⁻¹ s⁻¹) if there is still some remaining iron in nitrogenase (this flux tends to occur during the early light period):

$$F_{Nitroge-Fe}^{Buffer-Fe} = Fe_{Nitroge} R_{Nitroge-Fe}^{Buffer-Fe} \frac{Fe_{Nitroge}}{Fe_{Nitroge} + K_{FeNitroge}^{Nitroge-Buffer}} \quad (5.S 27)$$

where $Fe_{Nitroge}$ (mol Fe cell⁻¹) is the amount of iron in nitrogenase, $R_{Nitroge-Fe}^{Buffer-Fe}$ (s⁻¹) is the rate constant for $F_{Nitroge-Fe}^{Buffer-Fe}$, and $K_{FeNitroge}^{Nitroge-Buffer}$ (mol Fe cell⁻¹) is the nitrogenase iron half saturation constant for the nitrogenase-buffer iron transfer. Finally, $F_{Buffer-Fe}^{Nitroge-Fe}$ is assumed to be zero. With

these fluxes, we predict the mass of iron in each cell component. Fe_{Photo} , Fe_{Buffer} and

$Fe_{Nitrogenase}$ are computed based on the balances of the above iron fluxes for each time step.

Dark period

During the early dark period, iron atoms move from the photosystem to the buffer, and the buffer to nitrogenase. The flux of iron from the photosystem to the buffer ($\text{mol Fe cell}^{-1} \text{ s}^{-1}$) is based on the following equation:

$$F_{Photo-Fe}^{Buffer-Fe} = (Fe_{Photo} - Fe_{Photo}^{\min}) R_{Photo-Fe}^{Buffer-Fe} \frac{Fe_{Photo}}{Fe_{Photo} + K_{FePhoto}^{Photo-Buffer}} \quad (5.S 28)$$

where Fe_{Photo}^{\min} (mol Fe cell^{-1}) is the minimum cellular iron in the photosystem and other variables are the same as in equation (5.S 26). Then, the flux of iron from the buffer to nitrogenase ($\text{mol Fe cell}^{-1} \text{ s}^{-1}$) is represented as follows in a similar form:

$$F_{Buffer-Fe}^{Nitrogen-Fe} = (Fe_{Nitrogen}^{ideal} - Fe_{Nitrogen}) R_{Buffer-Fe}^{Nitrogen-Fe} \frac{Fe_{Buffer}}{Fe_{Buffer} + K_{FeBuffer}^{Buffer-Nitrogen}} \quad (5.S 29)$$

where $Fe_{Nitrogen}^{ideal}$ (mol Fe cell^{-1}) is the ideal iron mass in the nitrogenase that fulfills the potential nitrogen fixation rate based on carbon storage availability and oxygen concentration, $R_{Buffer-Fe}^{Nitrogen-Fe}$ (s^{-1}) is the nitrogenase production rate constant, and $K_{FeBuffer}^{Buffer-Nitrogen}$ is the buffer iron half saturation constant for the flux of iron from the buffer to nitrogenase. $R_{Buffer-Fe}^{Nitrogen-Fe}$ is influenced by the oxygen concentration, dark period time t_{dark} (s), and carbon storage:

$$R_{Buffer-Fe}^{Nitrogen-Fe} = C_{Buffer-Fe}^{Nitrogen-Fe} (t_{dark})^{P4} \left([O_2]_{cri}^{nitrogen} - [O_2]^{CELL} \right) \left(\frac{C_{store}}{C_{store} + K_{Cstore}^{nitrogen}} \right)^{P5} \quad (5.S 30)$$

where $C_{Buffer-Fe}^{Nitroge-Fe}$ (unit varies depending on $P4$ and $P5$) is a constant term for $R_{Buffer-Fe}^{Nitroge-Fe}$, $P4$ (dimensionless) is a power factor, necessary to accurately represent repeatedly observed non-linear time dependence of nitrogen fixation (Mohr *et al.*, 2010; Saito *et al.*, 2011; Großkopf and LaRoche, 2012), $[O_2]_{cri}^{nitroge}$ (mol O₂ m⁻³) is a critical oxygen concentration below which nitrogenase can be synthesized (thus, when $[O_2] > [O_2]_{cri}^{nitroge}$, $R_{Buffer-Fe}^{Nitroge-Fe} = 0$), $K_{Cstore}^{nitroge}$ (mol C cell⁻¹) is a half saturation constant of C_{Store} for nitrogenase production, $P5$ (dimensionless) is a power term for carbohydrate-storage influence on nitrogenase synthesis.

$Fe_{Nitroge}^{ideal}$ (mol Fe cell⁻¹) is computed based on the ideal nitrogen fixation rate. First, we compute the ideal nitrogen fixation rate based on the concentration of the nitrogen storage and carbon storage (mol N cell⁻¹ s⁻¹):

$$N_{2\ fix}^{ideal-store} = \frac{N_{store}^{max} - N_{store}}{N_{store}^{max}} N_{2\ fix}^{max} \frac{C_{store}}{C_{store} + K_{Cstore}^{N2\ fix}} \quad (5.S\ 31)$$

where N_{store}^{max} (mol N cell⁻¹) is the nitrogen storage capacity, $N_{2\ fix}^{max}$ (mol N cell⁻¹ s⁻¹) is the maximum possible nitrogen fixation rate, and $K_{Cstore}^{N2\ fix}$ (mol C cell⁻¹) is the Half saturation constant of carbohydrate storage for nitrogen fixation. Then, we compare this value to another ideal nitrogen fixation rate (mol N cell⁻¹), which, this time, is based on the balance between maximum carbon storage decomposition and maximum respiration:

$$N_{2\ fix}^{ideal-balance} = \left(\frac{D_{Cstore}^{max}}{Y_{N2\ fix}^{CH:N}} - \frac{V_{O2}^{potential}}{Y_{NON-SYNTH}^{O2:CH} Y_{N2\ fix}^{CH:N}} \right) R_{H2}, \quad (5.S\ 32)$$

We then take the lower value between $N_{2\text{ fix}}^{\text{ideal-store}}$ and $N_{2\text{ fix}}^{\text{ideal-balance}}$ for the ideal nitrogen fixation rate $N_{2\text{ fix}}^{\text{ideal}}$ (mol N cell⁻¹ s⁻¹). Based on this value, we compute the ideal iron amount in nitrogenase:

$$Fe_{\text{Nitroge}}^{\text{ideal}} = \frac{N_{2\text{ fix}}^{\text{ideal}}}{C_{\text{Fe-nitroge}}^{N_{2\text{ fix}}}}. \quad (5.S 33)$$

Based on the obtained fluxes through the above computations, Fe_{photo} , Fe_{Buffer} and $Fe_{\text{Nitrogenase}}$ (mol Fe cell⁻¹) (cellular iron in photosystems, iron-buffer, and nitrogenase, respectively) are computed for each time step. $F_{\text{Nitroge-Fe}}^{\text{Buffer-Fe}}$ is assumed to be zero, but the flux of iron from nitrogenase to the buffer can occur with a negative value of $F_{\text{Buffer-Fe}}^{\text{Nitroge-Fe}}$.

Late dark period

During the later night time, the cell starts preparing for the photosynthesis during the next light period. The cell starts decomposing nitrogenase to retrieve iron in the buffer, preparing for photosynthesis. Also, during this period, the respiration rate gradually decreases as the nitrogen fixation rate decreases. In this model, we imposed linearly decreasing $F_{\text{Nitrogenase}}^{\text{ideal}}$ and $R_{O_2}^{\text{potential}}$ with time, reaching $F_{\text{Nitrogenase}}^{\text{ideal}} = 0$ and energetically balanced respiration at the initiation of the next light period.

5.S3 Parameterization

Tunable parameters

In order to represent the dataset of Großkopf and LaRoche (2012), we have tuned 27 parameters (Table S3). In addition, we have set that the late dark period starts 7 hours after the initiation of the dark period. After the initiation of the later dark period, $N_{2\text{ fix}}^{\text{ideal}}$ and $V_{O_2}^{\text{potential}}$ (potential maximum oxygen uptake, thus potential maximum respiration in the pseudo steady state) start decreasing linearly and become zero and a half respectively, at the end of the (late) dark period. There can be a significantly different set of parameters that may equally well reproduce the dataset. However, such different parameter set would not change our conclusion that *Crocospaera* employs similar oxygen-management strategies to those of *Azotobacter* will stay same, since diffusivity, cell size, and respiration rate have specific influence on the model results. We have used the same values, K_{Fe} , for $K_{Fe\text{Buffer}}^{\text{Buffer-Photo}}$, $K_{Fe\text{Photo}}^{\text{Photo-Buffer}}$, $K_{Fe\text{Buffer}}^{\text{Buffer-Nitroge}}$, and $K_{Fe\text{Nitroge}}^{\text{Nitroge-Buffer}}$, and we have applied save numbers for $P4$ and $P5$, and $K_{C\text{store}}^{\text{Decom}}$ and $K_{C\text{store}}^{\text{N}_2\text{ fix}}$. For the cellular iron quota, we have used a constant value of 4.87×10^6 molecules per cell based on the maximum value estimated in Saito *et al.*, (2011). For oxygen uptake, we have used equation (2.8) and (2.9) from Chapter 2 with a different value for r and ϵ_m , relative diffusivity of the cell membrane.

Table S3 Values used for tunable parameters. The parameters are for 20% oxygen environment. For 5% oxygen environment, we have used $r=1.28 \times 10^{-6}$ (m) and other per-cell values except for $N_{2\text{ fix}}^{\text{max}}$ are adjusted based on the volume difference between the two oxygen cases.

Parameter	Value	Unit
r	1.32×10^{-6}	m
ϵ_m	1.55×10^{-5}	dimensionless
$Y_{Photo}^{Chl:Fe}$	1.91×10^3	mol C mol Fe ⁻¹
λ^{max}	2.51×10^{-18}	mol C cell ⁻¹ s ⁻¹
N_{Store}	2.21×10^{-15}	mol N cell ⁻¹
(initial value)		
K_{Nstore}	8.83×10^{-16}	mol N cell ⁻¹
$Y_{Bio}^{N:C}$	1 : 6	mol N mol C ⁻¹
C_{store}^{max}	1.19×10^{-13}	mol C cell ⁻¹
R_{Cstore}	6.32×10^{-5}	s ⁻¹
P_I^{max}	2.63×10^{-3}	s ⁻¹
A_{PHO}	5.00×10^{-2}	μE ⁻¹ m ² s
D_{Cstore}^{max}	5.21×10^{-18}	mol C cell ⁻¹ s ⁻¹
K_{Cstore}^{Decom}	6.30×10^{-15}	mol C cell ⁻¹
$P3$	2.00×10^0	dimensionless
$C_{O_2}^{\text{potential}}$	2.00×10^{-26}	unit depends on $P3$

$C_{Fe-nitroge}^{N_2\ fix}$	1.00×10^{-1}	$\text{mol N mol Fe}^{-1} \text{ s}^{-1}$
$C_{Buffer-Fe}^{Photo-Fe}$	2.40×10^{-1}	s^{-1}
K_{Fe}	4.53×10^{-19}	mol Fe cell^{-1}
$R_{Photo-Fe}^{Buffer-Fe}$	5.00×10^{-4}	s^{-1}
$R_{Nitroge-Fe}^{Buffer-Fe}$	3.33×10^{-3}	s^{-1}
$C_{Buffer-Fe}^{Nitroge-Fe}$	2.39×10^{-15}	unit depends on $P4$
$P4$	3.00×10^0	dimensionless
$[O_2^{CELL}]_{cri}^{nitroge}$	3.26×10^{-1}	$\text{mol O}_2 \text{ m}^{-3}$
$K_{Cstore}^{nitroge}$	3.15×10^{-14}	mol C cell^{-1}
N_{store}^{\max}	4.59×10^{-13}	mol N cell^{-1}
$N_{2\ fix}^{\max}$	5.21×10^{-19}	$\text{mol N cell}^{-1} \text{ s}^{-1}$

Non-tunable parameters

In order to constrain other parameters, we have referred to Chapter 2 for the following

parameters; $Y_{SYNTH}^{O_2: BIO}$ ($=Y_{SYNTH}^{O_2: BIO}$ in Chapter 2), $Y_{NON-SYNTH}^{O_2: CH}$ ($=Y_{N-S}^{O_2: CH}$), $Y_{Bio}^{N: C}$ ($=0.2$), and E . We

assume that 100% electron from hydrogen produced from nitrogen fixation, which leads to

$R_{H_2}=4/3$ (Großkopf and LaRoche, 2012). Also, based on the electron balance between nitrogen

fixation and glucose decomposition, $Y_{N_2\ fix}^{CH: N}=1$ (balance between (2.S6) and (T-2.S1-3) in

Supplementary Material in Chapter 2).

5.S4 Nomenclature

Table S4 Parameters, definitions and units used both in the main text and this supplementary material. The parameters are listed roughly in order of appearance in Supplementary Material.

Parameter	Definition	Unit
CH_C	Intermediate carbohydrate pool	mol C cell ⁻¹
t	Time	s
P_I	Photosynthesis rate per chlorophyll	s ⁻¹
Chl	Chlorophyll per cell	mol C cell ⁻¹
λ	Biomass production rate	mol C cell ⁻¹ s ⁻¹
E	CO ₂ production : Biomass production	dimensionless
P_{Cstore}	Rate of carbohydrate storage production	mol C cell ⁻¹ s ⁻¹
D_{Cstore}	Rate of carbohydrate storage decomposition	mol C cell ⁻¹ s ⁻¹
Exc	Rate of carbohydrate excretion	mol C cell ⁻¹ s ⁻¹
C_{Store}	Carbohydrate storage per cell	mol C cell ⁻¹
Bio_C	Biomass per cell	mol C cell ⁻¹
X	Number density of cells	cell m ⁻³
Q_C	Cellular carbon quota	mol C cell ⁻¹
NH_4^+	Cellular ammonium	mol N cell ⁻¹
N_{2fix}	Nitrogen fixation rate	mol N cell ⁻¹ s ⁻¹
P_{Nstore}	Rate of nitrogen storage production	mol N cell ⁻¹ s ⁻¹
D_{Nstore}	Rate of nitrogen storage decomposition	mol N cell ⁻¹ s ⁻¹

N_{Store}	Nitrogen storage per cell	mol N mol C ⁻¹
O_2	O ₂ per cell	mol O ₂ cell ⁻¹
P_{O_2}	O ₂ production rate	mol O ₂ cell ⁻¹ s ⁻¹
R_{Bio}	Respiration rate	mol O ₂ cell ⁻¹ s ⁻¹
V_{O_2}	Oxygen diffusion into the cell	mol O ₂ cell ⁻¹ s ⁻¹
$\lambda^{Chl-ideal}$	Potential biomass production rate under the ideal amount of chlorophyll	mol C cell ⁻¹ s ⁻¹
λ^{max}	Maximum biomass production rate	mol C cell ⁻¹ s ⁻¹
K_{Nstore}	Nitrogen-storage-half-saturation constant for biomass production	mol N cell ⁻¹
$Y_{Bio-all}^{N:C}$	N : C in biomass with nutrient storage	mol N mol C ⁻¹
$Y_{Bio}^{N:C}$	N : C in biomass without nutrient storage	mol N mol C ⁻¹
$P_{Cstore}^{Chl-ideal}$	Potential carbon storage production rate under the ideal amount of chlorophyll	mol C cell ⁻¹ s ⁻¹
C_{store}^{max}	Maximum carbon storage per cell	C mol cell ⁻¹
R_{Cstore}	Rate constant for the production of carbon storage	s ⁻¹
Chl^{ideal}	Chlorophyll per cell	mol C cell ⁻¹
P_I^{max}	Maximum photosynthesis rate per chlorophyll	s ⁻¹
A_{PHO}	Power coefficient for photosynthesis	μE ⁻¹ m ² s
M_{Chl}	$Chl : Chl_{ideal}$	dimensionless

$Y_{SYNTH}^{O_2: BIO}$	Oxygen consumption : Biomass production in biosynthesis	$\text{mol O}_2 \text{ mol C}^{-1}$
$Y_{NON-SYNTH}^{O_2: CH}$	Oxygen consumption : Carbohydrate consumption in non-synthesis respiration	$\text{mol O}_2 \text{ mol C}^{-1}$
$[O_2^{CELL}]$	Cellular oxygen concentration	$\text{mol O}_2 \text{ m}^{-3}$
$[O_2]$	Environmental oxygen concentration	$\text{mol O}_2 \text{ m}^{-3}$
D_{Cstore}^{max}	Maximum rate of carbohydrate storage decomposition	$\text{mol C cell}^{-1} \text{ s}^{-1}$
$D_{Cstore}^{potential}$	Potential rate of carbohydrate storage decomposition based on the storage size	$\text{mol C cell}^{-1} \text{ s}^{-1}$
K_{Cstore}^{Decom}	Half saturation constant of the carbon storage for	mol C cell^{-1}
	$D_{Cstore}^{potential}$	
$V_{O_2}^{potential}$	Potential oxygen uptake rate by diffusion	$\text{mol O}_2 \text{ cell}^{-1} \text{ s}^{-1}$
κ_{O_2}	Effective diffusion constant of oxygen	$\text{m}^2 \text{ s}^{-1}$
$R_{enzyme}^{potential}$	Enzymatically constrained respiratory potential	$\text{mol O}_2 \text{ cell}^{-1} \text{ s}^{-1}$
t_{dark}	Time passed since the initiation of the dark period	s
$P3$	Power factor for $R_{enzyme}^{potential}$	dimensionless
$C_{O_2}^{potential}$	Respiratory coefficient for $R_{enzyme}^{potential}$	unit depends on $P3$
$R_{O_2}^{potential}$	Potential respiration rate	$\text{mol O}_2 \text{ cell}^{-1} \text{ s}^{-1}$
$N_{2\text{ fix}}^{potential}$	Potential rate of nitrogen fixation	$\text{mol N cell}^{-1} \text{ s}^{-1}$

$Fe_{nitroge}$	Nitrogenase iron per cell	mol Fe cell ⁻¹
$C_{Fe-nitroge}^{N_2\ fix}$	Nitrogen-fixing capacity per nitrogenase iron	mol N mol Fe ⁻¹ s ⁻¹
D_{Cstore}^{ideal}	Ideal rate of carbon storage decomposition	mol C cell ⁻¹ s ⁻¹
$Y_{N_2\ fix}^{CH:N}$	Carbohydrate consumption : Nitrogen fixation	mol C mol N ⁻¹
R_{H_2}	Coefficient for electron recycling from hydrogen molecules	(dimensionless)
$Y_{Photo}^{Chl:Fe}$	Chlorophyll to iron ratio	mol C mol Fe ⁻¹
Fe_{Photo}	Iron in the photosystem per cell	mol Fe cell ⁻¹
$F_{Buffer-Fe}^{Photo-Fe}$	Translocation of iron from the buffer to the photosystem	mol Fe cell ⁻¹ s ⁻¹
$F_{Photo-Fe}^{Buffer-Fe}$	Translocation of iron from the photosystem to the buffer	mol Fe cell ⁻¹ s ⁻¹
Fe_{Buffer}	Iron in the buffer per cell	mol Fe cell ⁻¹
$F_{Buffer-Fe}^{Nitroge-Fe}$	Translocation of iron from the buffer to nitrogenase	mol Fe cell ⁻¹ s ⁻¹
$F_{Nitroge-Fe}^{Buffer-Fe}$	Translocation of iron from nitrogenase to the buffer	mol Fe cell ⁻¹ s ⁻¹
$Fe_{Nitroge}$	Iron in nitrogenase per cell	mol Fe cell ⁻¹
Fe_{Photo}^{ideal}	Ideal iron mass in the photosystem	mol Fe cell ⁻¹
$R_{Buffer-Fe}^{Photo-Fe}$	Photosystem production efficiency	s ⁻¹

t_{light}	Time passed since the initiation of the light period	s
$C_{Buffer-Fe}^{Photo-Fe}$	Coefficient for $R_{Buffer-Fe}^{Photo-Fe}$	s^{-2}
$K_{FeBuffer}^{Buffer-Photo}$	Half saturation constant of buffer iron for $F_{Buffer-Fe}^{Photo-Fe}$	$mol\ Fe\ cell^{-1}$
$R_{Photo-Fe}^{Buffer-Fe}$	Rate constant for $F_{Photo-Fe}^{Buffer-Fe}$	s^{-1}
$K_{FePhoto}^{Photo-Buffer}$	Half saturation constant of photosystem iron for $K_{FePhoto}^{Photo-Buffer}$	$mol\ Fe\ cell^{-1}$
$R_{Nitroge-Fe}^{Buffer-Fe}$	Rate constant for $F_{Nitroge-Fe}^{Buffer-Fe}$	s^{-1}
$K_{FeNitroge}^{Nitroge-Buffer}$	Half saturation constant of nitrogenase iron for $F_{Nitroge-Fe}^{Buffer-Fe}$	$mol\ Fe\ cell^{-1}$
Fe_{Photo}^{min}	Minimum iron amount in the photosystem	$mol\ Fe\ cell^{-1}$
$Fe_{Nitroge}^{ideal}$	Ideal iron mass in nitrogenase	$mol\ Fe\ cell^{-1}$
$R_{Buffer-Fe}^{Nitroge-Fe}$	Rate constant for $F_{Buffer-Fe}^{Nitroge-Fe}$	s^{-1}
$K_{FeBuffer}^{Buffer-Nitroge}$	Half saturation constant of the buffer iron for $F_{Buffer-Fe}^{Nitroge-Fe}$	$mol\ Fe\ cell^{-1}$
$C_{Buffer-Fe}^{Nitroge-Fe}$	constant term for	unit depends on $P4$
$P4$	power factor for $R_{Buffer-Fe}^{Nitroge-Fe}$	dimensionless
$[O_2]_{cri}^{nitroge}$	Critical oxygen concentration below which nitrogenase can be synthesized	$mol\ O_2\ m^{-3}$

$K_{C_{store}}^{nitroge}$	Half saturation constant of C_{Store} for nitrogenase production	mol C cell ⁻¹
$P5$	Power term for carbohydrate-storage influence on nitrogenase synthesis	dimensionless
$N_{2\ fix}^{ideal-store}$	Ideal nitrogen fixation rate based on the concentration of the nitrogen storage and carbon storage	mol N cell ⁻¹ s ⁻¹
N_{store}^{max}	Maximum nitrogen storage	mol N cell ⁻¹
$N_{2\ fix}^{max}$	Maximum possible nitrogen fixation rate	mol N cell ⁻¹ s ⁻¹
$K_{C_{store}}^{N2\ fix}$	Half saturation constant of carbohydrate storage for nitrogen fixation	mol C cell ⁻¹
$N_{2\ fix}^{ideal-balance}$	Nitrogen fixation rate based on the balance between maximum carbon storage decomposition and maximum respiration	mol N cell ⁻¹ s ⁻¹
$N_{2\ fix}^{ideal}$	Ideal nitrogen fixation rate	mol N cell ⁻¹ s ⁻¹
r	Cytoplasmic radius	m
ϵ_m	Relative diffusivity of the cell membrane	dimensionless

5.S5 References

- Cullen JJ. (1990). On models of growth and photosynthesis in phytoplankton. *Deep Res* **37**: 667–683.
- Großkopf T, LaRoche J. (2012). Direct and indirect costs of dinitrogen fixation in *Crocospaera watsonii* WH8501 and possible implications for the nitrogen cycle. *Front Microbiol* **3**: doi: 10.3389/fmicb.2012.00236.

Mohr W, Intermaggio MP, LaRoche J. (2010). Diel rhythm of nitrogen and carbon metabolism in the unicellular, diazotrophic cyanobacterium *Crocospaera watsonii* WH8501. *Environ Microbiol* **12**: 412–421.

Platt T, Gallegos CL, Harrison WG. (1980). Photoinhibition of photosynthesis in natural assemblages of marine phytoplankton. *J Mar Res* **38**: 687–701.

Rittmann BE, McCarty PL. (2001). Stoichiometry and bacterial energetics. In: Environmental Biotechnology: Principles and Applications. McGraw-Hill: New York. 126–164.

Saito MA, Bertrand EM, Dutkiewicz S, Bulygin V V., Moran DM, Monteiro FM, *et al.* (2011). Iron conservation by reduction of metalloenzyme inventories in the marine diazotroph *Crocospaera watsonii*. *Proc Natl Acad Sci* **108**: 2184–2189.

Webb WL, Newton M, Starr D. (1974). Carbon dioxide exchange of *Alnus rubra* A mathematical model. *Oecologia* **17**: 281–291.

Chapter 6

Summary and future directions

Throughout this thesis, we have developed the cell flux model and applied it as a tool to interpret traits and trade-offs for several micro-organisms. The model provides an intuitive and quantitative description of key metabolic constraints, growth rates and growth efficiencies of micro-organisms. In each chapter we have adapted the cell flux model in order to answer specific questions, spanning chemoheterotrophic nitrogen fixers, small prokaryotic phytoplankton, and small, unicellular photo-autotrophic nitrogen fixers. The models have provided simple but logical interpretations of the laboratory data sets, and suggested some new interpretations of cell physiology.

In each chapter, we have asked specific questions all of which eventually lead to deeper understanding of nitrogen fixation and nitrogen fixers. In Chapter 2, we have asked what decrease the growth efficiency of nitrogen fixers. In Chapter 3, our question is “How do carbon, oxygen and ammonium co-limit nitrogen fixation?”. In Chapter 4, we have investigated how light and nutrient co-limit phytoplankton growth. In Chapter 4, we have asked how *Crocospaera* manage oxygen during the dark period. In order to answer these questions, we have developed and adapted the cell flux model for each microorganism we have studied.

In the future, the model will be further developed and applied to a wider variety of microorganisms, or even macroorganisms, as a tool to describe and interpret cell physiology. At the same time, the model will be plugged into various ecosystem models, increasing the biological resolution, and providing higher flexibility.

6.1 Chapter Summary

In Chapter 2, we have developed the cell flux model for chemoheterotrophic nitrogen fixers to study what makes their growth inefficient. The model has been brought into consistency with the data of *Azotobacter vinelandii* (Kuhla and Oelze, 1988) quantifying the cost of nitrogen fixation. In a high oxygen environment, carbohydrate expenditure is dominated by the indirect cost of respiratory protection, far outweighing the direct cost of nitrogen fixation. At low oxygen concentrations the costs associated with biomass production becomes more important. We have demonstrated that the observed, non-linear increase of carbohydrate consumption with increasing oxygen concentration can be attributed to increasing cell size or decreasing the diffusivity of the cell membrane layers. Either of these strategies is less costly than respiratory protection alone. Finally, the model is informative about the oxygen management strategies of other nitrogen fixers, such as *Crocospaera*, heterocystus cyanobacteria, and *Trichodesmium*.

In Chapter 3, we have incorporated direct ammonium uptake into the cell flux model for chemoheterotrophic nitrogen fixers to study when and how much ammonium suppresses nitrogen fixation. Assuming that the organisms optimize metabolism in order to maximize the population provides good simulations and a clear explanation leading to a good fit between model and the experimental data for *Azotobacter vinelandii* (Bühler *et al.*, 1987a, 1987b). The study provides a quantitative approach for modeling nitrogen fixation in the presence of fixed nitrogen.

In Chapter 4, we have adapted the cell flux model for photo-autotrophy to study light-nitrogen-phosphorus-co-limited growth of phytoplankton. Although in the previous chapters we have

consider a stoichiometrically defined, bulk “biomass” as the end product of biosynthesis, in this chapter we have resolved classes of macromolecules including proteins with different functions, phospholipids in thylakoid membranes, DNA, RNA and different nutrient storages in order to simulate and interpret the chemostat culture data in Healey (1985). By expressing various macromolecules, the model provides new insights into the growth and physiology of phytoplankton. The model provides an interpretation for the repeatedly observed differences between growth-rate-dependence on nitrogen and phosphorus quotas. It encapsulates the quantitative differences between nitrogen and phosphorus storage capacities. The model indicates that the cellular chlorophyll maximum and maximum growth rates under different light intensities are the result of a spatial constraint: despite some flexibility, cells of a given size eventually run out of room for additional machinery. Finally, the model predicts the biomass concentration for various culture conditions and provide the basis for a mechanistic and quantitative representation of light-nutrient co-limitation of phytoplankton growth in dynamic environments.

In Chapter 5, we have adapted the cell flux model to simulate the unicellular-photoautotrophic-nitrogen-fixer *Crocospaera* and to examine how this organism manages oxygen. The model is based on that for *Azotobacter vinelandii* (Chapters 2 and 3) combined with a representation of photo-autotrophy similar to that described for *Synechococcus spp.* (Chapter 4). In addition, we have resolved a diurnal iron exchange between nitrogenase and photosystems. In this study, we hypothesize that *Crocospaera* has a similar oxygen-management strategy to that of *Azotobacter*, which are (1) respiratory protection, (2) size adaptation, and (3) the production of extracellular oxygen barriers. Simulations of the batch culture studies from Großkopf and

LaRoche (2012) are qualitatively and quantitatively improved when incorporating these three oxygen management strategies. We hypothesize that *Crocospaera* manages oxygen with similar strategies to *Azotobacter*.

Significance of this thesis

Through this thesis, we have quantitatively demonstrated that the oxygen is an important factor in nitrogen fixation and the growth of nitrogen fixers. In Chapter 2, the model shows that oxygen management accounts for a large fraction of the carbohydrate budget for nitrogen fixers, especially at high oxygen concentrations. In Chapter 2, the model has shown that not only oxygen influences the magnitude of nitrogen fixation, but also it influences the minimum carbohydrate : ammonium ratio of the resource at which nitrogen occurs. In Chapter 3, the model implies that marine unicellular nitrogen fixers apply similar oxygen management mechanisms to the terrestrial unicellular nitrogen fixers, indicating that the costs of oxygen management is universal.

The model that we have developed throughout this thesis is simple, but it captures the important processes of cells, such as respiration, biomass production, photosynthesis, storage production/decomposition and nitrogen fixation. Since the model is flexible, it can be applied to other organisms, such as diatoms and calcifiers, or potentially express symbiosis such as Diatom Diazotroph Associations. In addition, because the model is computationally efficient, it can be applied to a wide range of studies, including cellular physiology, ecology, and biogeochemistry. In the next section, we describe the application of the model to various problems.

6.2 Future directions

Our future projects are roughly separated into two parts: the further development of the cell flux model and the application of the cell flux model. In this thesis, we have developed the cell flux model for some functional types of nitrogen fixers and phytoplankton. However, the microbial community is much more diverse, and we aim to adapt the cell flux model to describe and model other micro-organisms such as diatoms and calcifiers. The knowledge from developing the cell flux model can also be implemented into, and improve, current generation marine ecosystem models. For example, based on the knowledge, we can express more diverse nitrogen fixers in the ocean ecosystem models. In addition, we can adapt the macromolecular scale cell flux model for phytoplankton to the dynamic environment. This dynamic model will be simple enough to be adapted to various functional types of micro-organisms, which in turn can be applied to/incorporated into ecosystem models such as the Darwin model in MITgcm.

Short term goals

Developing the cell flux model for diatoms

To apply the cell flux model to diatom species, we adopt Raven's (1983) hypothesis that diatoms grow efficiently partially due to the low cost associated with the production of silica frustule, relative to a carbon based cell structure. Although there is a certain maintenance cost for silica frustule as suggested in Hecky *et al.*, (1973) and Raven (1983), the cost for the production of silica frustule is much smaller than the production of organic biomass (Raven, 1983). We can quantitatively explore this hypothesis in our cell flux model.

We will modify the phytoplankton cell flux model by incorporating the production of silica frustules, which also involves an organic component providing a protective skin to prevent

the frustule dissolving (Figure 6.1). We have two potential strategies for modeling the production of silica shells. The first strategy is to assign an average elemental composition of the silica shells, and based on this elemental composition, we will build appropriate half reactions. The challenge here is that we have yet to find such laboratory data. Also, the explicit energetics of the production of the organic material in silica frustule has yet to become available.

The alternative strategy is to separate the organic skin production and silica frustule, and include the organic skin part in the biomass pool. This will enable us to only think about the energy difference before and after the dehydration synthesis of silicic acid. Although we still have to estimate what “n” is in silica frustule $\text{SiO}_2 \cdot n\text{H}_2\text{O}$, this strategy makes the system simpler than the first strategy. We will start from this second solution, while we keep investigating the availability of data for the elemental ratio of the diatom shell.

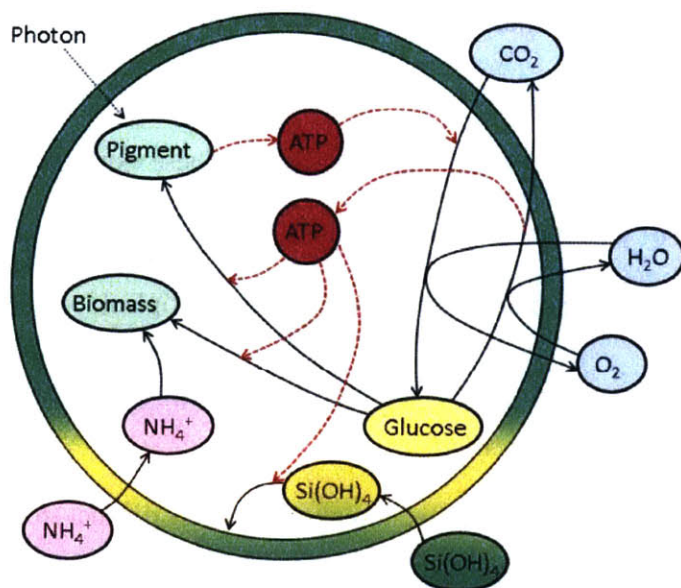


Figure 6.1 Cell flux model applied for Diatoms. Black solid arrows and red dashed arrows represent elemental and energy fluxes, respectively. The green layer represents the silica frustule.

For the uptake of nutrient, there are different mechanisms for each species of diatom. Some species, such as *Thalassiosira eccentrica*, have column shaped silica frustule, and the uptake of nutrient occurs through the bottom and top parts with different diffusivities (Mitchell *et al.*, 2013). Thus we may explore and model these geometric and structural differences.

We will first approximate with a complete sphere, thus applying the diffusion uptake model based on (Staal *et al.*, 2003). Depending on the different shape or diffusivity of the membrane of diatom, we can systematically adjust the diffusion efficiency term. Although this is a highly idealized approximation, it simplifies the model parameterization.

We can also consider the eddy transport of nutrient for large diatom species. The size of diatom varies between a few tens of microns to over one hundred microns. For the large diatom species, not only molecular diffusion, but eddy diffusion can influence the uptake of the nutrient (Barton *et al.*, 2014). We could adjust the eddy diffusivity depending on the dilution rate of chemostat culture. Also, we will replace the silica frustule to the appropriate amount of organic membrane and compare the difference in the growth cost. These explorations will provide a quantitative indication of whether, and by how much, silicification represents an energy saving for the diatom compared to a similarly sized, non-diatom phytoplankton.

Developing the cell flux models for calcifiers

To model calcifiers, we hypothesize that what makes calcifiers distinct from other functional types is the calcium carbonate shells and the production of the shells require certain concentration of calcium ions in the coccolith vesicle (Paasche, 2002) (thus, the growth can be

limited by the investment in controlling the internal chemistry (analogous to the oxygen control in nitrogen fixers)). Also, calcium carbonate liths influences the nutrient uptake.

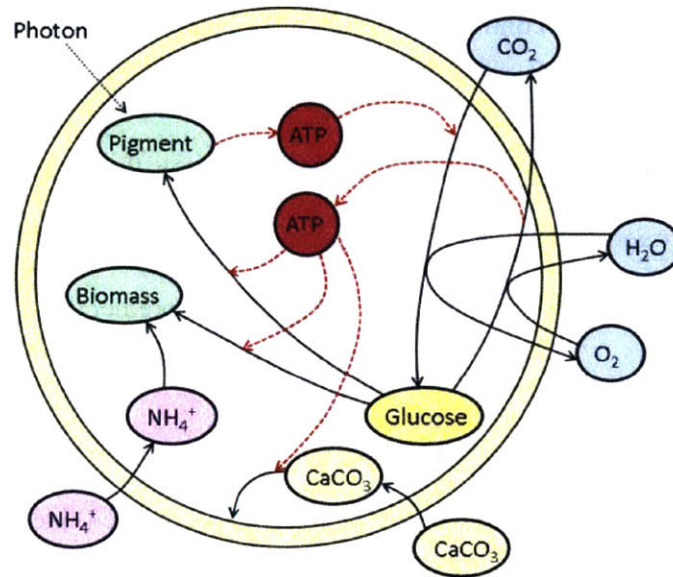


Figure 6.2 Cell flux model applied for Calcifiers. Black solid arrows and red dashed arrows represent elemental and energy fluxes, respectively. The cream layer represents the calcium carbonate shell.

For the uptake of nutrient, there can be an impedance of nutrient flow due to the shell. The simplest way to deal with this impedance is to add a layer of calcium carbonate outside of the cell membrane and adjust the diffusion efficiency. We will build two types of uptake model: porter uptake with calcium carbonate layer impedance, and diffusion uptake with calcium carbonate layer impedance. We will choose a model to use depending on whether the molecule is transported through the inner membrane by diffusion or by transporters.

Modeling the biogeography of nitrogen fixers in the global ocean

Efforts have been made to develop predictive models for the biogeography and activity of nitrogen fixers in the ocean (Moore *et al.*, 2002, 2004; Coles and Hood, 2004, 2007; Monteiro *et al.*, 2010, 2011; Saito *et al.*, 2011; Dutkiewicz *et al.*, 2012; Stukel *et al.*, 2014; Dutkiewicz *et al.*, 2015). While these models have contributed to the overall understanding in traits-tradeoffs and biogeography of nitrogen fixers, nitrogen fixers are more diverse than modeled so far (Riemann *et al.*, 2010; Zehr *et al.*, 2011; Sohm *et al.*, 2011). What controls the distribution of different functional types of nitrogen fixers? Since different nitrogen fixers influence the ecosystem and biogeochemistry in unique ways, it is essential to express and predict the distribution of different functional types of nitrogen fixers in the ocean.

In this project, we will extend the models of Monteiro *et al.*, (2011) and Dutkiewicz *et al.*, (2012) in order to express six distinct functional types of nitrogen fixers based on the knowledge of the cell flux model in this thesis. Those six functional types are *Trichodesmium*, uni-cellular photoautotrophic nitrogen fixer with intracellular iron recycling (e.g. *Crocospaera* (Saito *et al.*, 2011), uni-cellular photoautotrophic nitrogen fixer without intracellular iron recycling (e.g. possibly *Cyanothece*), endosymbiotic diatom-diazotroph association (DDA) (e.g. *Hemiaulus-Richelia* symbioses (e.g. Foster *et al.*, 2011)), exosymbiotic diatom-diazotroph association (e.g. *Chaetoceros-Richelia* symbioses (e.g. Gómez *et al.*, 2005; Foster *et al.*, 2011)), UCYN-A-prymnesiophyte association (e.g. Thompson *et al.*, 2012). In this project, we aim to reproduce a similar pattern of these different functional types of nitrogen fixers to the general pattern described in literature (e.g. Sohm *et al* 2011).

We differentiate these functional types by giving different parameters for each functional type. For example, we can differentiate *Trichodesmium* from endosymbiotic and exosymbiotic DDA by giving DDA higher maximum growth rates and growth limitation by

silica. Similarly, we can differentiate unicellular photoautotrophic nitrogen fixer from UCYN-A-prymnesiophyte association by giving the association higher maximum growth rate but higher half saturation constants for iron and phosphorus due to the simpler metabolism of UCYN-A but larger phosphorus and iron requirements for prymnesiophyte. We also plan to incorporate oxygen's influence on the growth rate based on this thesis. We will use the model to simulate and interpret the distribution of different nitrogen fixers, which in turn contributes our understanding in physiological and ecological control of nitrogen fixation in the global ocean.

Modeling dynamic growth of phytoplankton

Although studying phytoplankton in the steady state culture is extremely informative constraining the costs and benefits of phytoplankton growth under different light and nutrient environment (Chapter 4), the growth of phytoplankton more typically occurs in dynamic environments in the ocean. Thus, in order to incorporate the cell flux model for phytoplankton in the dynamic ecosystem models, we need to adapt the model to the dynamic environment and dynamic growth. In the process of making the model dynamic, we need to address the following questions.

- How do different nutrient concentrations influence the cellular macromolecular compositions?
- How do macromolecular compositions fluctuate with the light-dark cycle?
- How does light influence the macro-molecular compositions in dynamic nutrient environment?

We will address these questions based on what we have learned in Chapter 4. We aim to maintain the model simple and fast enough to be compatible with a global ocean ecosystem models.

Long term goal: application of the cell flux model to global scale ocean ecosystem modeling

As introduced in Chapter 1 and 4, the growth of phytoplankton is highly idealized in current ecosystem models. In order to address more diverse phytoplankton community, the model needs to incorporate more detailed physiology than Monod or Droop types of models (Monod, 1949; Droop, 1968, respectively). Thus, we aim to incorporate the cell flux model to Ocean ecosystem models such as the Darwin model (Follows *et al.*, 2007; Dutkiewicz *et al.*, 2009) with MITgcm physical framework (Marshall *et al.*, 1997a, 1997b). In this project, we need to address following challenges.

- Despite the advance in computational capacity, in order to be run in the 3D ocean ecosystem models, the model still needs to be computationally light and efficient.
- Most current ecosystem models do not include diurnal cycles.

In order to address the first challenge, the cell flux model has to avoid any loops or complex algorithms. In addition, the model has to be kept as simple as possible. The cell flux model is a part of a few loops (e.g. loop for the time, space, plankton species, etc.), the length of the model programming linearly influences the computational time. In order to be make the model as efficient as possible, we may need to further simplify and streamline the cell flux model.

For addressing the second challenge, we can either incorporate the diurnal cycles in the ecosystem model, or adapt the cell flux model to the “averaged” light intensity during the day. While the former strategy is more challenging and needs collaboration with the ocean dynamists,

the latter one is relatively simple and it can be done by developing a calibration method based on the laboratory data and the model output.

This cell flux-ocean ecosystem coupled model will provide link between physiology and the growth/competition of phytoplankton in the ocean. In other words, It will be the tool to connect cell biology and biochemistry to the ecosystem and biogeochemistry in the global ocean more explicitly than ever before.

With the coupled model, we can address new questions; for example:

- What is the impact of *Prochlorococcus* having a large proportion of sulfolipid on the ocean biogeography?
- How much does *Prochlorococcus* having low GC content in their DNA and RNA help them propagate in the ocean?
- Why is there no super-bug in the ocean? (We may address this question from the view point of space and energy limitation in the cell).
- Why are heterocystous cyanobacteria mostly symbiotic in the ocean? (We can address this question by incorporating solitary heterocystous cyanobacteria analogue of the cell flux model)
- How does having silica frustule help diatoms acquire their niche?
- How does changing ocean pH influence the photosynthesis and biogeography of calcifiers?

6.3 References

- Barton AD, Ward BA, Williams RG, Follows MJ. (2014). The impact of fine-scale turbulence on phytoplankton community structure. *Limnol Oceanogr Fluids Environ* **4**: 34–49.
- Bühler T, Monter U, Sann R, Kuhla J, Dingier C, Oelze J. (1987a). Control of respiration and growth yield in ammonium-assimilating cultures of *Azotobacter vinelandii*. *Arch Microbiol* **148**: 242–246.
- Bühler T, Sann R, Monter U, Dingier C, Kuhla J, Oelze J. (1987b). Control of dinitrogen fixation in ammonium-assimilating cultures of *Azotobacter vinelandii*. *Arch Microbiol* **148**: 247–251.
- Coles VJ, Hood RR. (2007). Modeling the impact of iron and phosphorus limitations on nitrogen fixation in the Atlantic Ocean. *Biogeosciences* **4**: 455–479.
- Coles VJ, Hood RR, Pascual M, Capone DG. (2004). Modeling the impact of *Trichodesmium* and nitrogen fixation in the Atlantic ocean. *J Geophys Res C Ocean* **109**: C06007, doi:10.1029/2002JC001754.
- Droop MR. (1968). Vitamin B₁₂ marine ecology. IV. The kinetics of uptake, growth and inhibition in *Monochrysis lutheri*. *J Mar Biol Assoc United Kingdom* **48**: 689–733.
- Dutkiewicz S, Follows MJ, Bragg JG. (2009). Modeling the coupling of ocean ecology and biogeochemistry. *Global Biogeochem Cycles* **23**: GB4017, doi:10.1029/2008GB003405.
- Dutkiewicz S, Hickman AE, Jahn O, Gregg WW, Mouw CB, Follows MJ. (2015). Capturing optically important constituents and properties in a marine biogeochemical and ecosystem model. *Biogeosciences* **12**: 4447–4481.
- Dutkiewicz S, Ward BA, Monteiro F, Follows MJ. (2012). Interconnection of nitrogen fixers and iron in the Pacific Ocean: Theory and numerical simulations. *Global Biogeochem Cycles* **26**: GB1012, doi:10.1029/2011GB004039.
- Follows MJ, Dutkiewicz S, Grant S, Chisholm SW. (2007). Emergent biogeography of microbial communities in a model ocean. *Science* **315**: 1843–1846.
- Foster RA, Kuypers MMM, Vagner T, Paerl RW, Musat N, Zehr JP. (2011). Nitrogen fixation and transfer in open ocean diatom-cyanobacterial symbioses. *ISME J* **5**: 1484–1493.
- Gómez F, Furuya K, Takeda S. (2005). Distribution of the cyanobacterium *Richelia intracellularis* as an epiphyte of the diatom *Chaetoceros compressus* in the western Pacific Ocean. *J Plankton Res* **27**: 323–330.
- Großkopf T, LaRoche J. (2012). Direct and indirect costs of dinitrogen fixation in *Crocospaera watsonii* WH8501 and possible implications for the nitrogen cycle. *Front Microbiol* **3**: doi: 10.3389/fmicb.2012.00236.
- Healey FP. (1985). Interacting effects of light and nutrient limitation on the growth rate of *Synechococcus linearis* (Cyanophyceae). *J Phycol* **21**: 134–146.
- Hecky RE, Mopper K, Kilham P, Degens ET. (1973). The amino acid and sugar composition of diatom cell-walls. *Mar Biol* **19**: 323–331.
- Kuhla J, Oelze J. (1988). Dependency of growth yield, maintenance and K_s -values on the

- dissolved oxygen concentration in continuous cultures of *Azotobacter vinelandii*. *Arch Microbiol* **149**: 509–514.
- Marshall J, Adcroft A, Hill C, Perelman L, Heisey C. (1997a). A finite-volume, incompressible Navier Stokes model for studies of the ocean on parallel computers. *J Geophys Res* **102**: 5753–5766.
- Marshall J, Hill C, Perelman L, Adcroft A. (1997b). Hydrostatic, quasi-hydrostatic, and nonhydrostatic ocean modeling. *J Geophys Res* **102**: 5733–5752.
- Mitchell JG, Seuront L, Doubell MJ, Losic D, Voelcker NH, Seymour J, *et al.* (2013). The role of diatom nanostructures in biasing diffusion to improve uptake in a patchy nutrient environment. *PLOS ONE* **8**: e59548.
- Monod J. (1949). The growth of bacterial cultures. *Ann Rev Mar Sci* **3**: 371–394.
- Monteiro FM, Dutkiewicz S, Follows MJ. (2011). Biogeographical controls on the marine nitrogen fixers. *Global Biogeochem Cycles* **25**: GB2003.
- Monteiro FM, Follows MJ, Dutkiewicz S. (2010). Distribution of diverse nitrogen fixers in the global ocean. *Global Biogeochem Cycles* **24**: GB3017, doi:10.1029/2009GB003731.
- Moore JK, Doney SC, Kleypas JA, Glover DM, Fung IY. (2002). An intermediate complexity marine ecosystem model for the global domain. *Deep Res II* **49**: 403–462.
- Moore JK, Doney SC, Lindsay K. (2004). Upper ocean ecosystem dynamics and iron cycling in a global three-dimensional model. *Global Biogeochem Cycles* **18**: GB4028, doi:10.1029/2004GB002220.
- Raven J. (1983). The transport and function of silicon in plants. *Biol Rev* **58**: 179–207.
- Riemann L, Farnelid H, Steward GF. (2010). Nitrogenase genes in non-cyanobacterial plankton: Prevalence, diversity and regulation in marine waters. *Aquat Microb Ecol* **61**: 235–247.
- Saito MA, Bertrand EM, Dutkiewicz S, Bulygin V V, Moran DM, Monteiro FM, *et al.* (2011). Iron conservation by reduction of metalloenzyme inventories in the marine diazotroph *Crocospaera watsonii*. *Proc Natl Acad Sci USA* **108**: 2184–2189.
- Sohm JA, Webb EA, Capone DG. (2011). Emerging patterns of marine nitrogen fixation. *Nat Rev Microbiol* **9**: 499–508.
- Staal M, Meysman FJR, Stal LJ. (2003). Temperature excludes N₂-fixing heterocystous cyanobacteria in the tropical oceans. *Nature* **425**: 504–507.
- Stukel MR, Coles VJ, Brooks MT, Hood RR. (2014). Top-down, bottom-up and physical controls on diatom-diazotroph assemblage growth in the Amazon River plume. *Biogeosciences* **11**: 3259–3278.
- Thompson AW, Foster RA, Krupke A, Carter BJ, Musat N, Vaultot D, *et al.* (2012). Unicellular cyanobacterium symbiotic with a single-celled eukaryotic alga. *Science* **337**: 1546–1550.
- Zehr JP. (2011). Nitrogen fixation by marine cyanobacteria. *Trends Microbiol* **19**: 162–173.